

**Aims and Scope:** The "Cell Journal (Yakhteh)" is a peer review and monthly English publication of Royan Institute of Iran. The aim of the journal is to disseminate information through publishing the most recent scientific research studies on exclusively Cellular, Molecular and other related topics. **Cell J**, has been certified by the Ministry of Culture and Islamic Guidance since 1999 and also accredited as a scientific and research journal by HBI (Health and Biomedical Information) Journal Accreditation Commission since 2000 which is an open access journal. **This journal holds the membership of the Committee on Publication Ethics (COPE).**

### 1. Types of articles

The articles in the field of Cellular and Molecular can be considered for publications in **Cell J**. These articles are as below:

#### A. Original articles

Original articles are scientific reports of the original research studies. The article consists of English Abstract (structured), Introduction, Materials and Methods, Results, Discussion, Conclusion, Acknowledgements, Author's Contributions, and References (**Up to 40**).

#### B. Review articles

Review articles are the articles written by well experienced authors and those who have excellence in the related fields. The corresponding author of the review article must be one of the authors of at least three published articles appearing in the references. The review article consists of English Abstract (unstructured), Introduction, Conclusion, Author's Contributions, and References (**Up to 70**).

#### C. Systematic Reviews

Systematic reviews are a type of literature review that collect and critically analyzes multiple research studies or papers. The Systematic reviews consist of English Abstract (unstructured), Introduction, Materials and Methods, Results, Discussion, Conclusion, Acknowledgements, Author's Contributions, and References (**Up to 70**).

#### D. Short communications

Short communications are articles containing new findings. Submissions should be brief reports of ongoing researches. The short communication consists of English Abstract (unstructured), the body of the manuscript (should not hold heading or sub-heading), Acknowledgements, Author's Contributions, and References (**Up to 30**).

#### E. Case reports

Case reports are short discussions of a case or case series with unique features not previously described which make an important teaching point or scientific observation. They may describe novel techniques or use equipment, or new information on diseases of importance. It consists of English Abstracts (Unstructured), Introduction, Case Report, Discussion, Acknowledgements, Author's Contributions, and References (**Up to 30**).

#### F. Editorial

Editorials are articles should be written in relevant and new data of journals' filed by either the editor in chief or the editorial board.

#### G. Imaging in biology

Images in biology should focus on a single case with an interesting illustration such as a photograph, histological specimen or investigation. Color images are welcomed. The text should be brief and informative.

#### H. Letter to the editors

Letter to the editors are in response to previously published **Cell J** articles, and may also include interesting cases that do not meet the requirement of being truly exceptional, as well as other brief technical or clinical notes of general interest.

#### I. Debate

Debates are articles which show a discussion of the positive and negative view of the author concerning all aspect of the issue relevant to scientific research.

### 2. Submission process

It is recommended to see the guidelines for reporting different kinds of manuscripts. This guide explains how to prepare the

manuscript for submission. Before submitting, we suggest authors to familiarize themselves with **Cell J** format and content by reading the journal via the website ([www.celljournal.com](http://www.celljournal.com)). The corresponding author ensures that all authors are included in the author list and agree with its order, and they must be aware of the manuscript submission.

### A. Author contributions statements

It is essential for authors to include a statement of responsibility in the manuscript that specifies the contribution of every one of them. This participation must include conception and design of the manuscript, data acquisition or data analysis and interpretation, drafting of the manuscript and/or revising it for critically important intellectual content, revision and final approval of the manuscript and statistical analysis, obtaining funding, administrative, technical, or material support, or supervision. Authors who do not meet the above criteria should be acknowledged in the **Acknowledgments section**.

### B. Cover letter and copyright

Each manuscript should be accompanied by a cover letter, signed by all authors specifying the following statement: "The manuscript has been seen and approved by all authors and is not under active consideration for publication. It has neither been accepted for publication nor published in another journal fully or partially (except in abstract form). **Also, no manuscript would be accepted in case it has been pre-printed or submitted to other websites.** I hereby assign the copyright of the enclosed manuscript to **Cell J**." Corresponding author must confirm the proof of the manuscript before online publishing. Also, it is needed to suggest three peer reviewers in the field of their manuscript.

### C. Manuscript preparation

Authors whose first language is not English encouraged to consult a native English speaker in order to confirm his manuscripts to American or British (not a mixture) English usage and grammar. It is necessary to mention that we will check the plagiarism of your manuscript by iThenticate Software. The manuscript should be prepared in accordance with the "International Committee of Medical Journal Editors (ICMJE)". Please send your manuscript in two formats word and PDF (including: title, name of all the authors with their degree, abstract, full text, references, tables and figures) and also send tables and figures separately in the site. The abstract and text pages should have consecutive line numbers in the left margin beginning with the title page and continuing through the last page of the written text. Each abbreviation must be defined in the abstract and text when they are mentioned for the first time. Avoid using abbreviation in the title. Please use the international and standard abbreviations and symbols

It should be added that an essential step toward the integration and linking of scientific information reported in published literature is using standardized nomenclature in all fields of science and medicine. Species names must be italicized (*e.g.*, *Homo sapiens*) and also the full genus and species written out in full, both in the title of the manuscript and at the first mention of an organism in a paper.

It is necessary to mention that genes, mutations, genotypes, and alleles must be indicated in italics. Please use the recommended name by consulting the appropriate genetic nomenclature database, *e.g.*, HUGO for human genes. In another words; if it is a human gene, you must write all the letters in capital and italic (*e.g.*, *OCT4*, *c-MYC*). If not, only write the first letter in capital and italic (*e.g.*, *Oct4*, *c-Myc*). **In addition, protein designations are the same as the gene symbol but are not italicized.**

**Of note, Cell J** will only consider publishing genetic association study papers that are novel and statistically robust. Authors are advised to adhere to the recommendations outlined in the STREGA statement (<http://www.strega-statement.org>). The following criteria must be met for all submissions:

1. Hardy-Weinberg Equilibrium (HWE) calculations must be carried out and reported along with the P-values if applicable [see Namipashaki et al. 2015 (Cell J, Vol 17, N 2, Pages: 187-192) for a discussion].
2. Linkage disequilibrium (LD) structure between SNPs (if multiple SNPs are reported) must be presented.
3. Appropriate multiple testing correction (if multiple independent SNPs are reported) must be included.

Submissions that fail to meet the above criteria will be rejected before being sent out for review.

Each of the following manuscript components should begin in the following sequence:

**Authors' names** and order of them must be carefully considered (full name(s), highest awarded academic degree(s), email(s), and institutional affiliation(s) of all the authors in English. Also, you must send mobile number and full postal address of the corresponding author).

**Changes to Authorship** such as addition, deletion or rearrangement of author names must be made only before the manuscript has been accepted in the case of approving by the journal editor. In this case, the corresponding author must explain the reason of changing and confirm them (which has been signed by all authors of the manuscript). If the manuscript has already been published in an online issue, an erratum is needed.

**Title** is providing the full title of the research (do not use abbreviations in title).

**Running title** is providing a maximum of 7 words (no more than 50 characters).

**Abstract** must include Objective, Materials and Methods, Results, and Conclusion (no more than 300 words).

**Keywords**, three to five, must be supplied by the authors at the foot of the abstract chosen from the Medical Subject Heading (MeSH). Therefore; they must be specific and relevant to the paper.

The following components should be identified after the abstract:

**Introduction:** The Introduction should provide a brief background to the subject of the paper, explain the importance of the study, and state a precise study question or purpose.

**Materials and Methods:** It includes the exact methods or observations of experiments. If an apparatus is used, its manufacturer's name and address should be stipulated in parenthesis. If the method is established, give reference but if the method is new, give enough information so that another author can perform it. If a drug is used, its generic name, dose, and route of administration must be given. Standard units of measurements and chemical symbols of elements do not need to be defined.

**Statistical analysis:** Type of study and statistical methods should be mentioned and specified by any general computer program used.

**Ethical considerations:** Please state that informed consent was obtained from all human adult participants and from the parents or legal guardians of minors and include the name of the appropriate institutional review board that approved the project. It is necessary to indicate in the text that the maintenance and care of experimental animals complies with National Institutes of Health guidelines for the humane use of laboratory animals, or those of your Institute or agency.

**Clinical trial registration:** All of the Clinical Trials performing in Iran must be registered in Iranian Registry of Clinical Trials ([www.irct.ir](http://www.irct.ir)). The clinical trials performed abroad, could be considered for publication if they register in a registration site approved by WHO or [www.clinicaltrials.gov](http://www.clinicaltrials.gov). If you are reporting phase II or phase III randomized controlled trials, you must refer to the CONSORT Statement for recommendations to facilitate the complete and transparent reporting of trial findings. Reports that do not conform to the CONSORT guidelines may need to be revised before peer-reviewing.

**Results:** They must be presented in the form of text, tables, and figures. Take care that the text does not repeat data that are presented in tables and/or figures. Only emphasize and summarize the essential features of the main results. Tables and figures must be numbered consecutively as appeared in the text and should be organized in separate pages at the end of the manuscript while their location should be mentioned in the main text.

**Tables and figures:** If the result of your manuscript is too short, it is better to use the text instead of tables & figures. Tables should have a short descriptive heading above them and also any footnotes. Figure's caption should contain a brief title for the whole figure and continue with a short explanation of each part and also the symbols used (no more than 100 words). All figures must be prepared based on cell journal's guideline in color (no more than 6 Figures and Tables) and also in TIF format with 300 DPI resolution.

**Of Note: Please put the tables & figures of the result in the results section not any other section of the manuscript.**

**Supplementary materials** would be published on the online version of the journal. This material is important to the understanding and interpretation of the report and should not repeat material within the print article. The amount of supplementary material should be limited. Supplementary material should be original and not previously published and will undergo editorial and peer review with the main manuscript. Also, they must be cited in the manuscript text in parentheses, in a similar way as when citing a figure or a table. Provide a caption for each supplementary material submitted.

**Discussion:** It should emphasize the present findings and the variations or similarities with other researches done by other researchers. The detailed results should not be repeated in the discussion again. It must emphasize the new and important aspects of the study.

**Conclusion:** It emphasizes the new and important aspects of the study. All conclusions are justified by the results of the study.

**Acknowledgements:** This part includes a statement thanking those who contributed substantially with work relevant to the study but does not have authorship criteria. It includes those who provided technical help, writing assistance and name of departments that provided only general support. You must mention financial support in the study. Otherwise; write this sentence "There is no financial support in this study".

**Conflict of interest:** Any conflict of interest (financial or otherwise) and sources of financial support must be listed in the Acknowledgements. It includes providers of supplies and services from a commercial organization. Any commercial affiliation must be disclosed, regardless of providing the funding or not.

**Of Note:** If you have already any patent related to the subject of your manuscript, or you are going to apply for such a patent, it must be mentioned in this part.

**References:** The references must be written based on the Vancouver style. Thus the references are cited numerically in the text and listed in the bibliography by the order of their appearance. The titles of journals must be abbreviated according to the style used in the list of Journals Indexed in PubMed. Write surname and initials of all authors when there are six or less. In the case of seven or more authors, the names of the first six authors followed by "et al." must be listed. You can download Endnote file for Journal references style: endnote file

The reference of information must be based on the following order:

**Article:**

Surname(s) and first letter of name & middle name(s) of author(s). Manuscript title. Journal title (abbr). publication date (year); Volume & Issue: Page number.

Example: Manicardi GC, Bianchi PG, Pantano S, Azzoni P, Bizzaro D, Bianchi U, et al. Presence of endogenous nicks in DNA of ejaculated human spermatozoa and its relationship to chromomycin A3 accessibility. *Biol Reprod.* 1995; 52(4): 864-867.

**Book:**

Surname(s) and first letter of name & middle name(s) of author(s). Book title. Edition. Publication place: publisher name; publication date (year); Page number.

Example: Edelman CL, Mandle CL. Health promotion throughout the lifespan. 2<sup>nd</sup> ed. ST Louis: Mosby; 1998; 145-163.

**Chapter of book:**

Surname(s) and first letter of name & middle name(s) of author(s). Chapter title. In: Surname(s) and first letter of name & middle name(s) of editor(s), editors. Book title. Edition. Publication place: publisher name; publication date (year); Page number.

Example: Phillips SJ, Whisnant JP. Hypertension and stroke. In: Laragh JH, Brenner BM, editors. Hypertension: pathophysiology, diagnosis, and management. 2<sup>nd</sup> ed. New York: Raven Press; 1995; 465-478.

**Abstract book:**

Example: Amini rad O. The antioxidant effect of pomegranate juice on sperm parameters and fertility potential in mice. *Cell J.* 2008;10 Suppl 1:38.

**Thesis:**

Name of author. Thesis title. Degree. City name. University. Publication date (year).

Example: Eftekhari Yazdi P. Comparison of fragment removal and co-culture with Vero cell monolayers on development of human fragmented embryos. Presented for the Ph.D., Tehran. Tarbiyat Modarres University. 2004.

**Internet references**

**Article:**

Example: Jahanshahi A, Mirnajafi-Zadeh J, Javan M, Mohammad-Zadeh M, Rohani M. Effect of low-frequency stimulation on adenosine A1 and A2A receptors gene expression in dentate gyrus of perforant path kindled rats. *Cell J.* 2008; 10 (2): 87-92. Available from: <http://www.celljournal.org>. (20 Oct 2008).

**Book:**

Example: Anderson SC, Poulsen KB. Anderson's electronic atlas of hematology.[CD-ROM]. Philadelphia: Lippincott Williams & Wilkins; 2002.

**D. Proofs** are sent by email as PDF files and should be checked and returned within 72 hours of receipt. It is the authors' responsibility to check that all the text and data as contained in the page proofs are correct and suitable for publication. **We are requested to pay particular attention to author's names and affiliations as it is essential that these details be accurate when the article is published.**

**E. Pay for publication:** Publishing an article in **Cell J** requires Article Processing Charges (APC) that will be billed to the submitting author following the acceptance of an article for publication. For more information please see [www.celljournal.org](http://www.celljournal.org).

**F. Ethics of scientific publication:** Manuscripts that have been published elsewhere with the same intellectual material will refer to duplicate publication. If authors have used their own previously published work or work that is currently under review, as the basis for a submitted manuscript, they are required to cite the previous work and indicate how their submitted manuscript offers novel contributions beyond those of the previous work. Research and publication misconduct is considered a serious breach of ethics.

The Journal systematically employs iThenticate, plagiarism detection and prevention software designed to ensure the originality of written work before publication. Plagiarism of text from a previously published manuscript by the same or another author is a serious publication offence. Some parts of text may be used, only where the source of the quoted material is clearly acknowledged.

### 3. General information

**A.** You can send your manuscript via online submission system which is available on our website. If the manuscript is not prepared according to the format of **Cell J**, it will be returned to authors.

**B.** The order of article appearance in the Journal is not demonstrating the scientific characters of the authors.

**C.** **Cell J** has authority to accept or reject the manuscript.

**D.** The received manuscript will be evaluated by associate editor. **Cell J** uses a single-blind peer review system and if the manuscript suits the journal criteria, we select the reviewers. If three reviewers pass their judgments on the manuscript, it will be presented to the editorial board of **Cell J**. If the editorial board has a positive judgment about the manuscript, reviewers' comments will be presented to the corresponding author (the identification of the reviewers will not be revealed). The executive member of journal will contact the corresponding author directly within 3-4 weeks by email. If authors do not receive any reply from journal office after the specified time, they can contact journal office. Finally, executive manager will respond promptly to authors' request.

### The Final Checklist

The authors must ensure that before submitting the manuscript for publication, they have to consider the following parts:

1. The first page of manuscript should contain title, name of the author/coauthors, their academic qualifications, designation & institutions they are affiliated with, mailing address for future correspondence, email address, phone, and fax number.
2. Text of manuscript and References prepared as stated in the "guide for authors" section.
3. Tables should be on a separate page. Figures must be sent in color and also in JPEG (Jpg) format.
4. Cover Letter should be uploaded with the signature of all authors.
5. An ethical committee letter should be inserted at the end of the cover letter.

*The Editor-in-Chief: Ahmad Hosseini, Ph.D.*

*Cell Journal* (Yakhteh)

*P.O. Box: 16635-148, Iran*

*Tel/Fax: + 98-21-22510895*

*Emails: info@celljournal.org*

*journals@celljournal.org*





## IN THE NAME OF GOD

Gone But not Forgotten

In the memory of the late Director of Royan Institute,  
Founder of Stem Cells Research in Iran and Chairman of  
*Cell Journal* (Yakhteh). May he rest in peace.

**Dr. Saeed Kazemi Ashtiani**

### OWNED:

Royan Institute, Iranian Academic Center for Education Culture and Research (ACECR)

### CHAIRMAN:

Hamid Gourabi, Ph.D., (Professor, Royan Institute, Tehran, Iran)

### EDITOR IN CHIEF:

Ahmad Hosseini, Ph.D., (Professor, Shahid Beheshti Medical University, Tehran, Iran)

### EDITOR ASSOCIATE:

Saeid Abroun, Ph.D., (Professor, Tarbiat Modares University, Tehran, Iran)

### EDITORIAL BOARD:

Saeid Abroun, Ph.D., (Professor, Tarbiat Modares University, Tehran, Iran)

Kamran Alimoghadam, M.D., (Associate Professor, Tehran Medical University, Tehran, Iran)

Alireza Asgari, Ph.D., (Professor, Baghyatallah University, Tehran, Iran)

Mohammad Kazem Aghaee Mazaheri, D.D.S., (Assistant Professor, ACECR, Tehran, Iran)

Mohamadreza Baghaban Eslaminejad, Ph.D., (Professor, Royan Institute, Tehran, Iran)

Gila Behzadi, Ph.D., (Professor, Shahid Beheshti Medical University, Tehran, Iran)

Hossein Baharvand, Ph.D., (Professor, Royan Institute, Tehran, Iran)

Marzieh Ebrahimi, Ph.D., (Professor, Royan Institute, Tehran, Iran)

Mary Familiar, Ph.D., (Senior Lecturer, University of Melbourne, Melbourne, Australia)

Hamid Gourabi, Ph.D., (Professor, Royan Institute, Tehran, Iran)

Jurgen Hescheler, M.D., (Professor, Institute of Neurophysiology of University Zu Koln, Germany)

Ghasem Hosseini Salekdeh, Ph.D., (Professor, Agricultural Biotechnology Research Institute, Karaj, Iran)

Esmail Jabbari, Ph.D., (Associate Professor, University of South Carolina, Columbia, USA)

Suresh Jesuthasan, Ph.D., (Associate Professor, National University of Singapore, Singapore)

Bahram Kazemi, Ph.D., (Professor, Shahid Beheshti Medical University, Tehran, Iran)

Saadi Khochbin, Ph.D., (Professor, Inserm/Grenoble University, France)

Ali Khademhosseini, Ph.D., (Professor, Harvard Medical School, USA)

Kun Ping Lu, M.D., Ph.D., (Professor, Harvard Medical School, Boston, USA)

Navid Manuchehrabadi, Ph.D., (Angio Dynamics, Marlborough, USA)

Hossein Ali Mehrani, Ph.D., (Professor, Baghyatallah University, Tehran, Iran)

Marcos Meseguer, Ph.D., (Clinical Embryology Laboratory IVI Valencia, Valencia, Spain)

Seyed Javad Mowla, Ph.D., (Professor, Tarbiat Modares University, Tehran, Iran)

Mohammad Hossein Nasr Esfahani, Ph.D., (Professor, Royan Institute, Tehran, Iran)

Toru Nakano, M.D., Ph.D., (Professor, Osaka University, Osaka, Japan)

Donald Newgreen, Ph.D., (Professor, Murdoch Children Research Institute, Melbourne, Australia)

Mojtaba Rezazadeh Valojerdi, Ph.D., (Professor, Tarbiat Modares University, Tehran, Iran)

Mohammad Hossein Sanati, Ph.D., (Associate Professor, National Institute for Genetic Engineering and Biotechnology, Tehran, Iran)

Eimei Sato, Ph.D., (Professor, Tohoku University, Sendai, Japan)

Andreas Serra, M.D., (Professor, University of Zurich, Zurich, Switzerland)

Abdolhossein Shahverdi, Ph.D., (Professor, Royan Institute, Tehran, Iran)

Michele Catherine Studer, Ph.D., (Institute of Biology Valrose, IBV University of Nice Sophia-Antipolis, France)

Peter Timashev, Ph.D., (Sechenov University, Moscow, Russia)

Daniela Toniolo, Ph.D., (Head, Unit of Common Disorders, San Raffaele Research Institute, Milano, Italy)

Christian van den Bos, Ph.D., Managing Director MARES Ltd, Greven, Germany

Catherine Verfaillie, Ph.D., (Professor, Katholie Universiteit Leuven, Leuven, Belgium)

Gianpaolo Zerbini, M.D., Ph.D., (San Raffaele Scientific Institute, Italy)

Shubing Zhang, Ph.D., (Associate Professor, Central South University, China)

Daniele Zink, Ph.D., (Institute of Bioengineering and Nanotechnology, Agency for Science Technology & Science, Singapore)

**EXECUTIVE MANAGER:**

Farideh Malekzadeh, M.Sc., (Royan Institute, Tehran, Iran)

**EXECUTIVE BOARD:**

Parvaneh Afsharian, Ph.D., (Royan Institute, Tehran, Iran)  
Reza Azimi, B.Sc., (Royan Institute, Tehran, Iran)  
Reza Omani-Samani, M.D., (Royan Institute, Tehran, Iran)  
Elham Amirchaghmaghi, M.D., Ph.D., (Royan Institute, Tehran, Iran)  
Leila Daliri, M.Sc., (Royan Institute, Tehran, Iran)  
Mahdi Lotfipanah, M.Sc., (Royan Institute, Tehran, Iran)  
Faezeh Shekari, Ph.D., (Royan Institute, Tehran, Iran)

**ENGLISH EDITOR:**

Mitra Amiri Khabooshan, Ph.D., (Monash University, Victoria, Australia)  
Sima Binaafar, M. Sc., (Royan Institute, Tehran, Iran)  
Saman Eghtesad, Ph.D., (Royan Institute, Tehran, Iran)  
Jane Elizabeth Ferrie, Ph.D., (University College of London, London, UK)  
Vahid Ezzatizadeh, Ph.D., (Royan Institute, Tehran, Iran)  
Kiana Kakavand, Ph.D., (University of Melbourne, Melbourne, Australia)  
Farnaz Shapouri, Ph.D., (Memphasys Limited, NSW, Australia)  
Kim Vagharfard, M.Sc., (Royan Institute, Tehran, Iran)  
Maryam Vatani, M.Sc., (University of Calgary, Canada)

**GRAPHICS:**

Laleh Mirza Ali Shirvani, B.Sc., (Royan Institute, Tehran, Iran)

**PUBLISHED & SPONSORED BY:**

Publication of Royan Institute (ACECR)

**Indexed in:**

1. Thomson Reuters (ISI)
2. PubMed
3. PubMed Central (PMC)
4. National Library Medicine (NLM)
5. Biosis Preview
6. Index Medicus for the Eastern Mediterranean Region (IMEMR)
7. Regional Information Center for Sciences and Technology (RICeST)
8. Index Copernicus International
9. Cambridge Scientific Abstract (CSA)
10. EMBASE
11. Scopus
12. Cinahl Database
13. Google Scholar
14. Chemical Abstract Service (CAS)
15. Proquest
16. Directory of Open Access Journals (DOAJ)
17. Open Academic Journals Index (OAJI)
18. Directory of Research Journals Indexing (DRJI)
19. Scientific Information Database (SID)
20. Iranmedex
21. Islamic World Science Citation Center (ISC)
22. Magiran
23. Science Library Index
24. Biological Abstracts
25. Essential Science Indicators
26. EuroPub

**ACECR****Copyright and license information:**

The **Cell Journal**<sup>(Yakhteh)</sup> is an open access journal which means the articles are freely available online for any individual author to download and use the providing address. The journal is licensed under a Creative Commons Attribution-Non Commercial 3.0 Unported License which allows the author(s) to hold the copyright without restrictions that is permitting unrestricted non-commercial use, distribution, and reproduction in any medium provided the original work is properly cited.

**Editorial Office Address (Dr. Ahmad Hosseini):**

Royan Institute, P.O.Box: 16635-148,  
Tehran, Iran  
Tel & Fax: (+9821)22510895  
Website: [www.celljournal.org](http://www.celljournal.org)  
Emails: [info@celljournal.org](mailto:info@celljournal.org)  
[journals@celljournal.org](mailto:journals@celljournal.org)

**Printing Company:**

Naghshe e Johar Co.  
No. 103, Fajr alley, Tehranpars Street,  
Tehran, Iran.



CONTENTS

**Original Articles**

- **Assessment of Cytotoxicity and Odontogenic/Osteogenic Differentiation Potential of Nano-Dentine Cement Against Stem Cells from Apical Papilla**  
 Eshagh Ali Saberi, Narges Farhad Mollashahi, Fatemeh Ejeian, Marzieh Nematollahi, Omolbanin Shahraki, Arezoo Pirhaji, Mohammad Hossein Nasr-Esfahani ..... **637**
- **Colchicine of *Colchicum autumnale*, A Traditional Anti-Inflammatory Medicine, Induces Apoptosis by Activation of Apoptotic Genes and Proteins Expression in Human Breast (MCF-7) and Mouse Breast (4T1) Cell Lines**  
 Elham Adham Foumani, Shiva Irani, Yalda Shokoohinia, Ali Mostafaie ..... **647**
- **PRDX1 Influences The Occurrence and Progression of Liver Cancer by Inhibiting Mitochondrial Apoptosis Pathway**  
 Hong-hua Sun, Yang-long Li, Hao Jiang, Xiang-hua Yin, Xing-lin Jin ..... **657**
- **Long Non-Coding RNA CASC2 Functions as A Tumor Suppressor in Colorectal Cancer via Modulating The *miR-18a-5p/BTG3* Pathway**  
 Liumin Kang, Jie Sun, Jie Liu, Feng Xu, Qilin Zhu, Xiaohua Shi..... **665**
- **MiR-140-3p Ameliorates The Inflammatory Response of Airway Smooth Muscle Cells by Targeting HMGB1 to Regulate The JAK2/STAT3 Signaling Pathway**  
 Jun Meng, Yingxia Zou, Li Hou, Limin He, Yuanjuan Liu, Menghan Cao, Chunjie Wang, Junying Du ..... **673**
- **Ferulic Acid Ameliorates Cell Injuries, Cognitive and Motor Impairments in Cuprizone-Induced Demyelination Model of Multiple Sclerosis**  
 Mojtaba Ghobadi, Babak Arji, Maryam Yadegari, Mansour Esmailidehaj, Farshad Homayouni-Moghadam, Mohammad Ebrahim Rezvani ..... **681**
- **Human Umbilical Cord Mesenchymal Stem Cells-Derived Small Extracellular Vesicles Can Be Considered as Cell-Free Therapeutics for Angiogenesis Promotion**  
 Somayeh Divband, Nooshin Tasharofi, Saeid Abroun, Mina Soufi Zomorrod ..... **689**
- **Effect of PLGA Nanoparticle-Mediated Delivery of miRNA 503 on The Apoptosis of Ovarian Endometriosis Cells**  
 Shahla Chaichian, Abolfazl Mehdizadeh Kashi, Kobra Tehermanesh, Vahid Pirhajati Mahabadi, Sara Minaeian, Neda Eslahi ..... **697**
- **Front page of Cell Journal<sub>(Yakhteh)</sub>: Figure 3, Page: 661**

# Assessment of Cytotoxicity and Odontogenic/Osteogenic Differentiation Potential of Nano-Dentine Cement Against Stem Cells from Apical Papilla

Eshagh Ali Saberi, M.D.S.<sup>1</sup>, Narges Farhad Mollashahi, M.D.S.<sup>1</sup>, Fatemeh Ejeian, M.Sc.<sup>2</sup>, Marzieh Nematollahi, M.Sc.<sup>2</sup>, Omolbanin Shahraki, Ph.D.<sup>3</sup>, Arezoo Pirhaji, M.D.S.<sup>4\*</sup>, Mohammad Hossein Nasr-Esfahani, Ph.D.<sup>2\*</sup>

1. Department of Endodontics, Faculty of Dentistry, Oral and Dental Diseases Research Center, Zahedan University of Medical Sciences, Zahedan, Iran
2. Department of Animal Biotechnology, Cell Science Research Center, Royan Institute for Biotechnology, ACECR, Isfahan, Iran
3. Pharmacology Research Center, Zahedan University of Medical Sciences, Zahedan, Iran
4. Department of Endodontics, Faculty of Dentistry, Zahedan University of Medical Sciences, Zahedan, Iran

\*Corresponding Addresses: P.O.Box: 9817699693, Department of Endodontics, Faculty of Dentistry, Zahedan University of Medical Sciences, Zahedan, Iran

P.O.Box: 8159358686, Department of Animal Biotechnology, Cell Science Research Center, Royan Institute for Biotechnology, ACECR, Isfahan, Iran

Emails: arezoo.pirhaji.ap@gmail.com, mh.nasr-esfahani@royaninstitute.org

Received: 04/July/2021, Accepted: 24/January/2022

## Abstract

**Objective:** Assessment of the cytotoxicity of novel calcium silicate-based cement is imperative in endodontics. This experimental study aimed to assess the cytotoxicity and odontogenic/osteogenic differentiation potential of a new calcium silicate/pectin cement called Nano-dentine against stem cells from the apical papilla (SCAPs).

**Materials and Methods:** In this experimental study, the cement powder was synthesized by the sol-gel technique. Zirconium oxide was added as opacifier and Pectin, a plant-based polymer, and calcium chloride as the liquid to prepare the nano-based dental cement. Thirty-six root canal dentin blocks of human extracted single-canal premolars with 2 mm height, flared with #1, 2 and 3 Gates-Glidden drills were used to prepare the cement specimens. The cement, namely mineral trioxide aggregate (MTA), Biodentine, and the Nano-dentine were mixed according to the manufacturers' instructions and applied to the roots of canal dentin blocks. The cytotoxicity and odontogenic/osteogenic potential of the cement were evaluated by using SCAPs.

**Results:** SCAPs were characterized by the expression of routine mesenchymal cell markers and differentiation potential to adipocytes, osteoblasts, and chondrocytes. Cement displayed no significant differences in cytotoxicity or calcified nodules formation. Gene expression analysis showed that all three types of cement induced significant down-regulation of *COLA1*; however, the new cement induced significant up-regulation of *RUNX2* and *SPP1* compared to the control group and MTA. The new cement also induced significant up-regulation of *TGFB1* and inducible nitric oxide synthase (iNOS) compared with Biodentine and MTA.

**Conclusion:** The new Nano-dentine cement has higher odontogenic/osteogenic potential compared to Biodentine and MTA for differentiation of SCAPs to adipocytes, osteoblasts, and chondrocytes.

**Keywords:** Biodentine, Calcium Silicate, Mineral Trioxide Aggregate, Stem Cells

Cell Journal (Yakhteh), Vol 24, No 11, November 2022, Pages: 637-646

**Citation:** Saberi EA, Farhad Mollashahi N, Ejeian F, Nematollahi M, Shahraki O, Pirhaji A, Nasr-Esfahani MH. Assessment of cytotoxicity and odontogenic/osteogenic differentiation potential of nano-dentine cement against stem cells from apical papilla. Cell J. 2022; 24(11): 637-646. doi: 10.22074/cellj.2022.8126. This open-access article has been published under the terms of the Creative Commons Attribution Non-Commercial 3.0 (CC BY-NC 3.0).

## Introduction

Different types of cement have been traditionally applied for sealing the pulp cavity and preventing bacterial leakage as an efficient vital pulp therapy (1). Although, there is still high demand for applying advanced materials in the apical region of the root canal through endodontic regeneration procedures in the hope of improving the healing process of periodontal tissues. The ultimate goal of developing novel biomaterials is to enhance their capability for inducing differentiation of mesenchymal stem cells (MSCs) to odontoblast-like cells and stimulating hard tissue formation. Indeed, the biocompatibility of these types of cement is of great importance regarding their direct contact with live tissues (2).

Currently, mineral trioxide aggregate (MTA) is known as the most commonly used capping biomaterial in

clinical studies (1), which is composed of tiny hydrophilic particles that are allowed to set in aqueous/moisture conditions (3). MTA presents suitable biocompatibility, radiopacity, and strength, which provides significant advantages in contrast to amalgam and super-EBAn (4). The optimum working time for MTA is around 5 minutes, with a setting time of 2.45 to 4 hours. Based on the literature, its cementogenesis property is attributed to the release of calcium ions reacting with phosphate groups in interstitial fluid and forming hydroxyapatite on the surface (5). However, long setting time, low compressive strength, and low flowability are considered the significant drawbacks of MTA (6). Furthermore, the ability of MTA to support the adhesion, proliferation, and anchoring of human MSCs has been previously investigated (7).

The other extensively used compound applied as

a restorative dentin replacement is Biodentine (8). It has notable superiorities over MTA, including easy manipulation, compatibility, and appropriate setting time. The major components of Biodentine are tri- and di-calcium silicate, which are incorporated with calcium carbonate, oxide fillers, and iron oxide to confer optimal color. Also, it contains calcium chloride as an accelerator, a water-soluble polymer as a dehydrator, and zirconium oxide (in some instances) as an opacifier. The preparation process of Biodentine includes a primary setting time of around 6 min and a final setting time of 10-12 minutes, which are shorter than glass ionomer and MTA (9). Over its suitable biocompatibility, Biodentine has been known as a bioactive material which promotes osteogenic differentiation and mineralization of different MSC types. It also possesses a suitable potential for inducing odontogenic differentiation and changing the equilibrium from inflammation to regeneration via decreasing the expression and activity level of TNF-induced transient receptor potential ankyrin1 (TRPA1) (10).

On the other hand, Youssef et al. (11) provided significant evidence for the cytotoxic effect of Emdogain, MTA, Biodentine, and calcium hydroxide against human dental pulp stem cells. In addition, another calcium silicate-based material (TheraCal) showed decreased proliferation rate in pulp fibroblasts and stimulated the release of IL-8 as a pro-inflammatory cytokine (12). Indeed, Saberi et al. (13) showed that the viability of stem cells from the apical papilla (SCAPs) treated with Biodentine was decreased over time.

Despite the remarkable merits of Biodentine, its high cost leads scientists to develop new inexpensive cement with improved sealability, minimized cytotoxicity, and higher osteoinductivity. In this regard, we take advantage of nano-calcium silicate and pectin biopolymer to overcome physical and chemical shortcomings faced by traditional calcium silicate cement. In addition, it was endorsed that nanomaterials revealed a higher antibacterial effect and better root canal filling (14).

Regarding the relatively low cost, renewability, diverse structures, and different physical properties, biomaterials reached many interests for use in a wide range of pharmaceutical and biomedical applications. Notably, some influential biopolymers have been developed recently with suitable applications in wound healing. They revealed a good potential for absorbing a high volume of water from the inflamed tissues when applied in dry form and providing the required water for the tissue when used in hydrated format (15). In particular, Pectin is known as a biopolymer with a wide range of biomedical activities, including B-lymphocyte activation and inducing the release of pro-inflammatory cytokines (such as IL-1B) from macrophages. Also, pectin-based materials were extensively used in traditional wound healing/dressing products, according to their noteworthy physico-chemical characteristics (16). Namely, Pectin have a suitable hydrophilicity, allowing exudate removal from the inflamed tissues (17). Also, Pectin can potentially preserve the

wound site's acidic pH, which serves as a barrier against bacteria and fungi. Moreover, it could bond to various active molecules and protect them against degradation (18). Although, it is worth mentioning that there is some evidence showing the remarkable cytotoxicity of Pectin at high concentrations (19).

Despite the promising potential of Pectin as a part of the capping agent, there is no report on the evaluation of cytotoxicity and odontogenic/osteogenic differentiation potential of pectin-containing materials. So, in this research, we introduced a new calcium silicate-based cement containing pectin polymer and aimed to assess its cytotoxicity and odontogenic/osteogenic differentiation potential over SCAPs through *in vitro* condition

## Materials and Methods

### Synthesis and preparation of the new cement

The new cement was composed of a powder phase and a liquid phase. Generally, the powder contained 80% tri- and di-calcium silicate, 14.9% calcium carbonate (Merck, Germany) as the filler, and 5% zirconium oxide (Merck, Germany) as the opacifier, and 0.1% pectin (Sigma Aldrich, Steinheim, Germany). The tri- and di-calcium silicate was synthesized by the sol-gel technique. For this purpose, 8.48 ml of tetraethyl orthosilicate (pure TEOS, FlukaMerck, Germany) was dissolved in double distilled water, and the pH of the solution was adjusted to 4.5 by nitric acid. Then 26.58 g calcium nitrate tetrahydrate (Merck, Germany) was gradually added to the solution during continuous stirring. Next, the solution was heated at 70°C for 24 hours to form a gel (20), and the obtained gel was then heated at 120°C for 24 hours for drying. Finally, the obtained compound was heated at 1500°C for 2 hours for calcination (21). The final liquid contained, the cement was prepared by mixing the powder (0.3 g) and liquid (calcium chloride (Merck, Germany) in a capsule using an amalgamator.

### Characterization of the nano-dentine

The morphological feature of raw new cement was analyzed by using scanning electron microscopy (SEM, KYKY, EM-3900M, China). Also, the crystalline structure of nano-dentine was characterized using X-Ray diffraction (XRD, Bruker D8 Advance Diffractometer) with the 2-theta method (range 5° -80°, step size 0.02°, 1 s/step). Peaks were compared with standard XRD profiles obtained from the powder diffraction file (PDF) database. ATR-FTIR spectra of cement have been collected with a Bruker Tensor II FTIR System (Bruker Optics, Ettlingen, Germany) over wavelengths between 400 cm<sup>-1</sup> and 4000 cm<sup>-1</sup> with a resolution of 1.5 cm<sup>-1</sup>. To analyze Nano-dentine's degradation rate, the modified ANSI/ADA Specification Number 9 was applied. Briefly, hardened samples with 10 mm diameter and 1 mm thickness (n=5) were immersed in 50 ml of HPLC grade water and incubated at 37°C for 5 and 30 days. At each time point, cement were removed, and water left to evaporate

at 80°C following an overnight at 110°C. Finally, the residual materials were collected, and the weight loss percentage was calculated based on the formulation of  $\Delta W\% = [(W2-W1)/W1] * 100$ , through which W1 indicating the weight of the initial dried material and W2 referred to the material weight at the end of incubation time points.

### Application of cement into root canal dentine blocks

Human single-rooted premolars were taken from teeth extracted for various clinical reasons (as part of prosthetic, periodontal, or orthodontic treatment) following obtaining written informed consent from the patients. The study was approved by the ethics committee of Zahedan University of Medical Sciences (IR.ZAUMS.REC.1398.353). All teeth underwent digital periapical radiography in buccolingual and mesiodistal directions. The teeth had mature apices, one straight canal, no history of previous endodontic treatment, and no defects such as calcification, resorption, or cracks were picked for further experiments. The hard and soft tissue residues were removed from the tooth surface using an ultrasonic scaler. After primary disinfection of the teeth with 5.5% sodium hypochlorite for 10 minutes, and subsequent rinse with saline, they were stored in 0.9% saline until use. The teeth were then decoronated at their cemento-enamel junction by a carbon disc and surgical handpiece under water coolant. A #20 K-file was used to negotiate the canal orifice. To standardize the internal canal space to have 1.5 mm diameter, #1, 2 and 3 Gates-Glidden drills were used orderly for primary flaring of the canal. Subsequently, final root canal preparation was performed using #2, 3, 4, and 5 peeso reamers.

Afterward, 36 roots were sectioned into dentine blocks with 2 mm height by a carbon disc and surgical handpiece under water coolant. The specimens were then stored in 0.9% saline, randomly divided into 3 groups (n=12 for each), and sterilized at 121°C and 2 bar pressure for 20 minutes. MTA and Biodentine were prepared according to the manufacturers' instructions in aseptic conditions and packed in the root canal of the dentine block. Briefly, the powder and liquid were homogeneously mixed in 1:3 ratios to prepare MTA. For Biodentine, five drops of the liquid part were added to each capsule and underwent trituration in an amalgamator at 4000 rpm for 30 seconds to achieve a paste-like consistency. In the case of new cement, six drops of the liquid were added to each capsule and mixed in an amalgamator at 4000 rpm for 15 seconds until obtaining a paste-like consistency. Finally, all specimens were incubated in a moist environment for 15 minutes for the primary setting. The sample preparation procedure was schematically presented in Figure 1A.

### Cell isolation and culture

As previously reported, the SCAPs were harvested and characterized from healthy immature human third molar teeth (22). The teeth were extracted for other medical issues after obtaining informed consent from volunteers. Briefly,

the apical tissue was rinsed with phosphate buffered saline (PBS, Bio-Idea, Tehran, Iran) supplemented with penicillin-streptomycin (2X Penicillin-Streptomycin, Gibco, Paisley, UK). For enzymatic digestion, first, the apical tissue was diced into pieces by a surgical scalpel, and the pieces were exposed to 3 mg/mL of collagenase type I and 4 mg/mL dispase (both from Gibco, Paisley, UK) for 30 to 45 minutes at 37°C. Next, the obtained cell suspension was filtered through a 70- $\mu$ m filter mesh and centrifuged for 8-10 minutes at 1800 rpm. The collected cells were cultured in minimum essential Eagle's medium (a-MEM, Sigma, Munich, Germany), supplemented with 15% fetal bovine serum (FBS, Gibco, Paisley, UK), 1% Glutamax, 1% penicillin/streptomycin, 250  $\mu$ g/mL amphotericin B (PAA, Cölbe, Germany), and gentamycin (Gentamicin Sulfate, Sigma, Munich, Germany), then incubated (Labotec C200) at 37°C and 5% CO<sub>2</sub> and filling the dish, the cells were passaged after reaching confluence condition.

### Characterization of isolated cells

To evaluate the stemness of the isolated cells, expression of CD105, CD45, CD146, CD73, STRO-1, and CD90 surface markers was measured by flow cytometry. For this purpose, after counting the cells, they were fixed in 4% paraformaldehyde at 4°C for 30 minutes and permeabilized using 0.2% Triton-X100 for 30 minutes. The fixed cells were then rinsed with PBS and incubated in primary antibodies (all from Merck Millipore, Billerica, MA, USA) diluted in 10 mg/mL BSA overnight. Finally, the following incubation with appropriate secondary antibodies at 37°C for 2 hours, the expression analysis was performed by a FACS Calibur cytometer (Becton Dickinson, San Jose, CA, USA) and analyzed by WinMDI 2.9 software.

Next, their three-lineage differentiation potential was evaluated. For this purpose, after reaching over 95% confluence, the culture medium was replaced with an osteogenic medium (including 0.1  $\mu$ M dexamethasone, 50  $\mu$ g/mL ascorbic acid-2 phosphate, and 10 mM  $\beta$ -glycerophosphate), and adipogenic medium (containing 0.1  $\mu$ M dexamethasone, 50  $\mu$ g/mL ascorbic acid-2 phosphate and 50  $\mu$ g/mL indomethacin). To induce chondrogenic differentiation, cells were centrifuged at 300 g for 5 minutes and incubated in a basic culture medium supplemented with a specific chondrogenic medium containing 0.1  $\mu$ M dexamethasone, 50  $\mu$ g/mL ascorbic acid-2 phosphate, 10 ng/mL transforming growth factor B (TGFB1), and 1% ITS. The medium was refreshed every 3 days for 21 days. At the end of the differentiation period, specific staining was carried out for the assessment of osteogenic differentiation (Alizarin Red S staining), chondrogenic differentiation (Toluidine Blue staining), and adipogenic differentiation (Oil Red-O staining).

### *In vitro* osteogenic/odontogenic differentiation assay

To assess the odontogenic/osteogenic differentiation of SCAPs in the presence of different blocks, cells

were cultured with a density of  $2.1 \times 10^5$ . After reaching 90% confluency, the culture medium was replaced with an odontogenic/osteogenic medium, as previously described in section 3.3. The efficiency of odontogenic/osteogenic differentiation was evaluated by Alizarin Red staining and analyzing the expression level of specific markers by quantitative real-time polymerase chain reaction (qRT-PCR). Each test was performed in three independent experiments, and the values were reported as mean values  $\pm$  SEM.

### Cytotoxicity assay

To assess the potential cytotoxicity of cement in direct contact with the SCAPs, cultured cells were faced with dentine blocks filled with cement placed on top of 6.5-mm diameter, 0.4  $\mu$ m pore size transwell inserts wholly covered with the culture medium. The cultured cells without cement were evaluated as the control group. Also, the indirect cytotoxicity of cement was evaluated following incubation of cells with a medium conditioned with dentine blocks for 10 days through culture conditions.

After 1, 3, 5, 7, and 10 days, the cells' metabolic activity and proliferation rate was measured with an MTS assay using the MTS kit (Promega, USA), based on the manufacturer's instruction. Briefly, the dentine blocks were removed from the wells after 3.5 hours' incubation with MTS/PMS. The product absorbance was measured at 490 nm by a microplate reader (Fluostar Optima, BMG Lab Technologies, Germany). Each test was performed in three independent experiments, and the values were reported as mean values  $\pm$  SEM.

### Alizarin Red staining

After 21 days, the cells were rinsed with PBS, fixed with 96% ethanol, and stained with 0.2% Alizarin Red (pH=6.4) for 1 hour at room temperature. Eventually, cells were immersed in a solution of 20% methanol and 10% citric acid for 15 minutes. Then, the conditioned solution was transferred to 96-well plates, and their optical density was read at 450 nm using a microplate reader (Fluostar Optima, BMG Lab Technologies, Germany).

### RNA extraction, cDNA synthesis, and quantitative real-time polymerase chain reaction analysis

The SCAPs were rinsed with PBS and collected in Trizol reagent (Sigma, Munich, Germany), following the differentiation process. Total RNA extraction was carried out using the phenol-chloroform method. To eliminate possible DNA contamination, the extracted samples were treated with DNase1, and cDNA was synthesized according to the protocol provided by the kit (Fermentas, CA, USA). Next, the qRT-PCR analysis was performed for specific osteogenic markers (*COL1A1*, *SPPI/OPN*, and *RUNX2*) as well as well-known inflammatory-related genes (*TNF-alpha*, *TGFBI*, and *iNOS*) using ABI device (Applied Biosystems, USA). Detailed information for the primers is provided in Table 1. The relative expression of the target genes was calculated through the delta-delta-Ct (ddCt) method compared to the untreated cells before differentiation induction.

**Table 1:** Information on primers used in quantitative real-time polymerase chain reaction

Gene symbol	Primer sequence (5'-3')	Accession number
<i>rh.B.actin</i>	F: AGATGCGTTGTACAGGAAG R: TGTGTGGACTTGGGAGAG	NM_001101.3
<i>rh.COL1A1</i>	F: TAGTCTGCTCCTGCGTCCTCTG R: TTTTGCTTCCTCCCACCCCTA	NM_000088.3
<i>rh.SPPI</i>	F: TTCGCAGACCTGACATCCA R: CCAATCAACTCCTCGCTTTCC	NM_001251830.1
<i>rh.TNF-alpha</i>	F: TAAGAGGGAGAGAAGCAACT R: CAGTATGTGAGAGGAAGAGAAC	NM_000594.3
<i>rh.RUNX2</i>	F: TCACTGCCTCTCACTTGCCA R: TACACACATCTCCTCCCTTC	NM_001015051.4
<i>rh.TGFBI</i>	F: ACAATTCCTGGCGATACCTCA R: GTGAACCCGTTGATGTCCACT	NM_000660.5
<i>rh-iNOS</i>	F: GTCCCTTTCTACTACTATC R: CTGATTTCTGTCTCTGTC	NM_000625.4

### Statistical analysis

The data were analyzed using SPSS version 16 (Inc., Chicago, USA) via one-way ANOVA and t test.  $P < 0.05$  were considered significant.

## Results

### Characterization of new cement

The macroscopic appearance of new cement revealed a white powder (Fig.1A) composed of relatively homogeneous grain size, as shown in SEM images (Fig.1B, C). Moreover, the X-ray diffraction peaks for the Nano-dentine has properly matched the standard graphs for  $\text{Ca}_3\text{SiO}_5$  (reference ID: 14-0693) and  $\text{Ca}_2\text{SiO}_4$  (reference ID: 31-0297), which confirmed the presence of the crystalline form of calcium silicates, as the main component of the Nano-dentine (Fig.1D, E).

The transmission spectrum of nano-dentine cement showed a peak at  $512 \text{ cm}^{-1}$  attributed to the vibration bending of calcium silicate anhydrate ( $\text{SiO}_4^{2-}$ ), which was also observed in biodentine and MTA spectrum (Fig.1F). For both nano-dentine and biodentine, the strong band around  $1460 \text{ cm}^{-1}$  could be assigned to the aromatic ring, and the weak peak at  $712 \text{ cm}^{-1}$  ascribed to the  $\text{V}_4$  vibrations of  $\text{CO}_3$ . Moreover, the sharp peak around  $870 \text{ cm}^{-1}$  in all types of cement is associated with the C-O group. The biodegradation assay revealed an increasing rate of degradation, through which the mean cumulative weight loss (%) of Nano-dentine after 5 and 30 days were  $6.16\% \pm 0.47$  and  $11.13\% \pm 0.75$ , respectively.

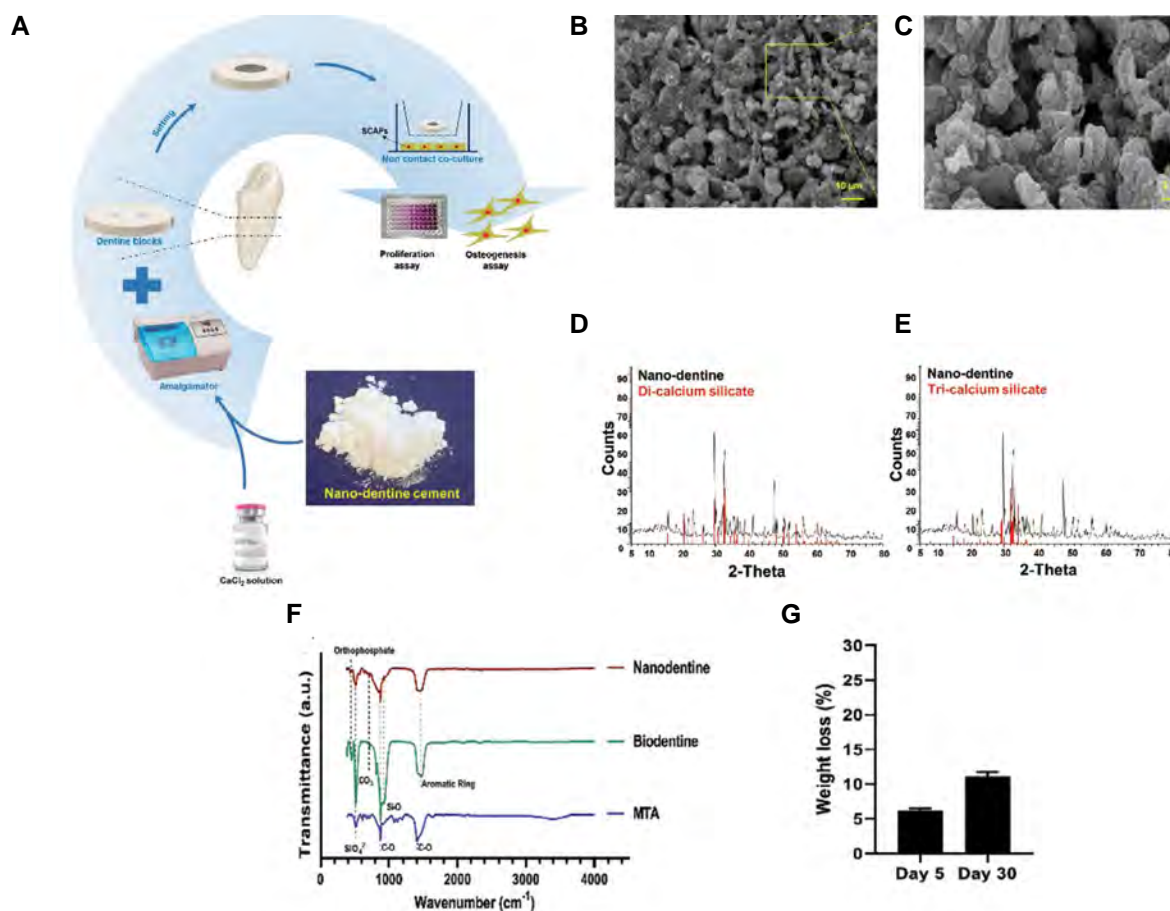


**Fig.1:** Characterization of Nano-dentine cement. **A.** The schematic presentation of experimental design. Scanning electron microscopic images of the cement at the magnification of **B.** 100X, and **C.** 500X. XRD diffraction pattern of Nano-dentine compared to the standard patterns of **D.** Di-calcium silicate and **E.** Tri-calcium silicate. **F.** FTIR spectrum of three MTA, Biodentine, and Nano-dentine in the wave range of 400-4000  $\text{cm}^{-1}$ . **G.** The weight loss percentage of Nano-dentine cement over five and 30 days. Results from three independent experiments are expressed as means  $\pm$  SEM. XRD; X-ray diffraction, FTIR; Fourier transform infrared, and MTA; Mineral trioxide aggregate.

### Isolation of SCAPs

After 48 hours from the primary seeding, adhered cells colonies appeared, which covered almost 70% of the culture plate following 10 days' incubation in normal culture conditions (Fig.2A). The cells resembled fibroblast-like morphology and grew as a monolayer after the first passage (Fig.2B). After the three passages, we reached a relatively homogenous population of stem cells used for further characterization.

### Assessment of the expression of mesenchymal stem cell markers by flow cytometry

The expression of specific mesenchymal stem cell markers, including CD146, STRO-1, CD105, CD90, and CD73, and a hematopoietic stem cell marker (CD45) at passage 4 revealed a substantial expression of all MSC-related markers. Figure 2C exhibited a representative histogram for each protein approved that over 95% of the cells expressed mesenchymal cell markers (CD73, CD90, CD105), and around 90% of the cells expressed dental stem cell markers (CD146, STRO-1). However, the cells did not express CD45 as a prominent hematopoietic stem cell marker (0.45%).

### Assessment of differentiation potential of cells into three mesenchymal cell lines

Staining with Oil Red, Alizarin Red, and toluidine blue after 21 days of treatment in the specific media confirmed the differentiation potential of isolated cells to adipocytes, osteoblasts, and chondrocytes, respectively (Fig.2D-F). The lipid particles formed in adipocytes colored red after Oil Red staining (Fig.2D). Also, calcium-phosphate deposits released from osteoblasts completely covered the cell surface and appeared in the form of red nodules after Alizarin Red staining (Fig.2E). After sectioning the formed cartilaginous masses and their staining with toluidine blue, the underlying collagen in the ECM of chondrocytes in lacuna-shaped structures confirmed the formation of cartilage-like tissue (Fig.2F).

### Assessment of proliferation and viability of SCAPs

Assessment of proliferation rate of the cells directly or indirectly faced with different dentine blocks via MTS assay revealed no significant difference in cell viability during 10 days. The results indicated an increasing profile in metabolic activity for all experimental groups over time. When the cells were directly treated with Nano-dentine, they showed maximum cell viability and proliferation rate on the day 7,

similar to the control group. However, MTA and Biodentine groups reached maximum absorbance after 10 days (Fig.3A). Although the MTA-conditioned medium caused higher

cellular metabolic activity in all time points, significant differences were only observed against Biodentine on day 3 and day 10, as well as Nanodentine on day 3 (Fig.3B).

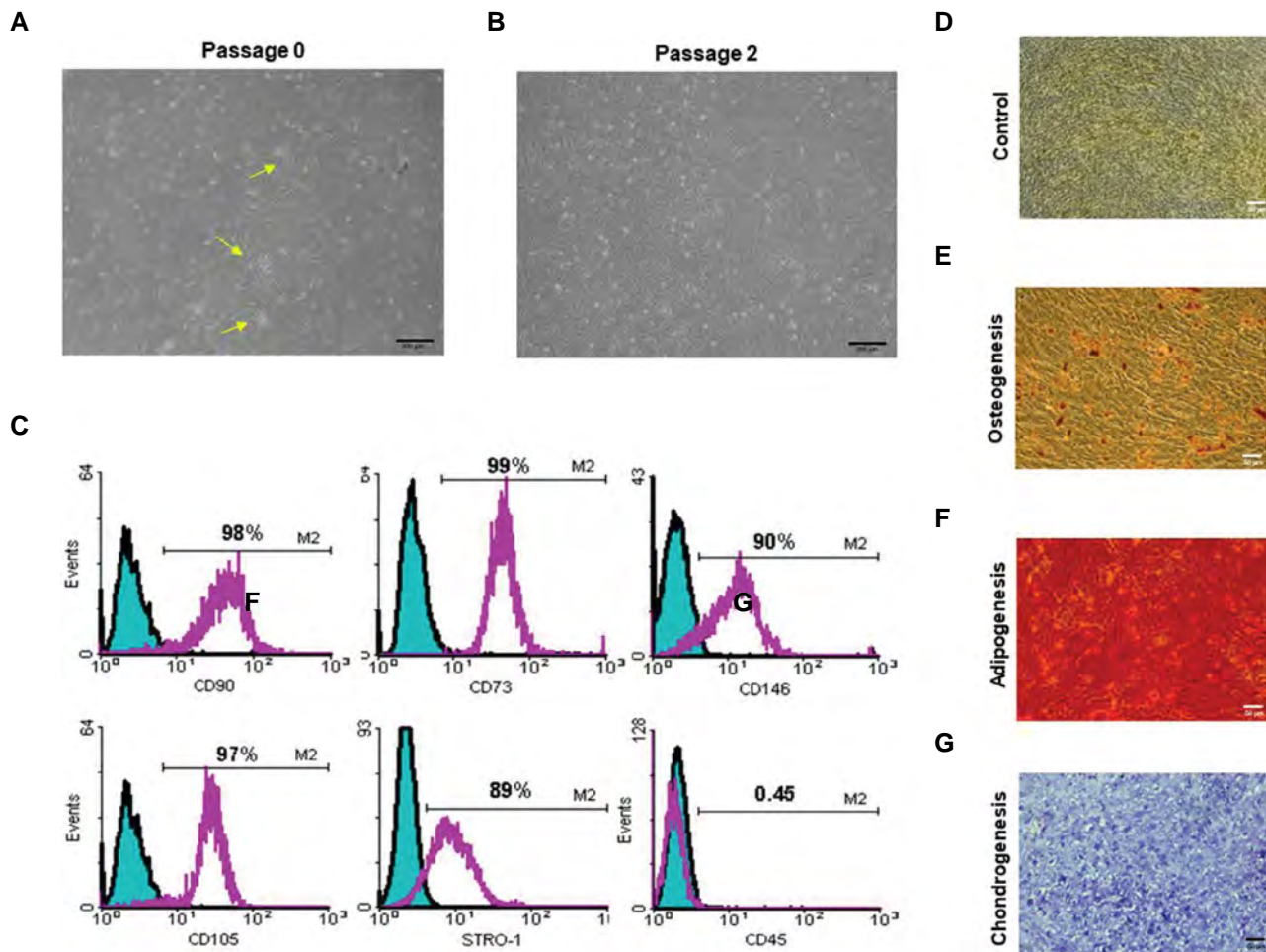


**Fig.2:** Characterization of harvested cells from apical papilla. Inverted microscopic photographs of the morphology of SCAPs. **A.** 10 days after primary culture. Colonies formed in the primary culture are marked with yellow arrows, **B.** After the second passage (scale bar=200 µm). **C.** Representative histogram of the expression of CD105, CD90, CD73, CD146, STRO-1, and CD45. Green histogram indicates cell fluorescence with the control antibody (isotype control), and a purple histogram indicates cell fluorescence with the respective antibody. **D.** Control cells following 21 days of cultivation under normal culture conditions. Assessment of multilineage differentiation potential of isolated cells to **E.** Adipocytes, **F.** Osteoblasts, and **G.** Chondrocytes after 21 days of treatment in specific media, and stained with Oil Red, Alizarin Red, and toluidine blue, respectively. SCAPs; Stem cells from apical papilla.

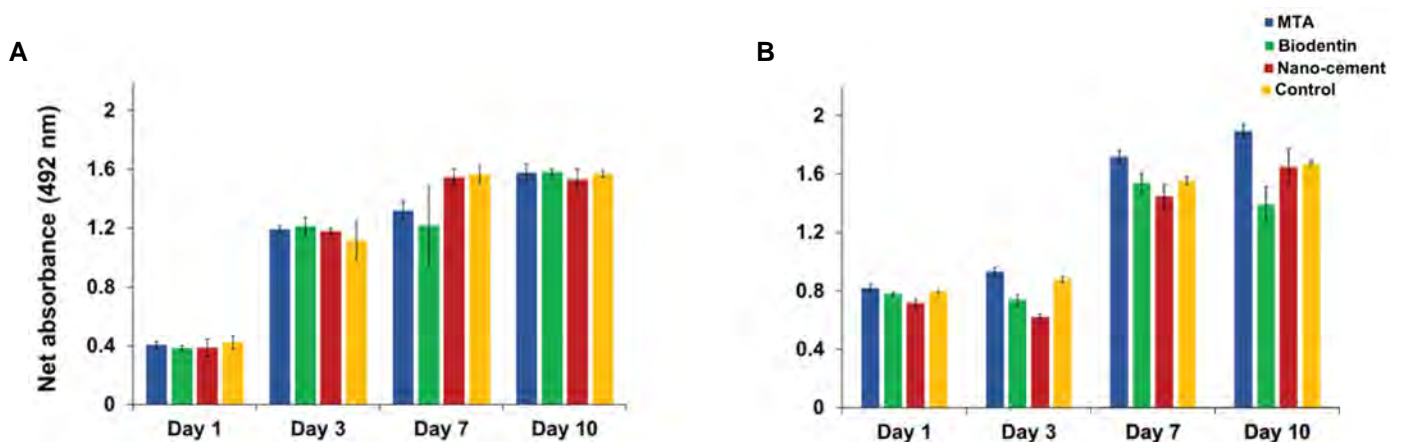


**Fig.3:** Assessment of the viability of SCAPs using the MTS assay. The absorbance of formazan at 492 nm wavelength at 1, 3, 7, and 10 days after culture indicated the activity and viability of cells **A.** Directly or **B.** Indirectly treated with the Nano-dentine cement, MTA and Biodentine, compared with the no-cement control groups. Data are presented as the mean value of three independent experiments ± SEM. SCAPs; Stem cells from apical papilla, MTS; 3-(4,5-dimethylthiazol-2-yl)-5-(3-carboxymethoxyphenyl)-2-(4-sulfophenyl)-2H-tetrazolium, and MTA; Mineral trioxide aggregate.

### Assessment of odontogenic/osteogenic differentiation by real-time qRT-PCR

Analyzing the expression value of odontogenic/osteogenic markers at the mRNA level in the treated cells, compared with pre-incubation cells revealed significant down-regulation of *COLA1* simultaneous with significant up-regulation of *RUNX2* and *SPP1* as indicators of bone specification and osteoblast maturation, respectively, in all samples. Significant up-regulation of these markers was particularly noted in the new cement group, compared with the control and MTA groups ( $P=0.01$ , Fig.4A-C).

### Assessment of osteogenic differentiation by Alizarin Red staining

Semi-quantitative analysis of Alizarin Red S accumulation revealed no significant differences ( $P>0.05$ )

in calcium deposition between SCAPs exposed to different cements after 21 days treatment with osteogenic medium. In addition, neither the Nano-dentine nor the commercial counterparts (Biodentine and MTA) showed significant difference compared with the control group (Fig.4D, E).

### Assessment of the expression of markers involved in inflammation by real-time qRT-PCR

No sign of up-regulation of pro-inflammatory markers (inducible nitric oxide synthase (iNOS) and TNF-alpha) was observed after 21 days of treatment with Biodentine and MTA in comparison to control. However, SCAPs exposed to the new cement showed relative up-regulation of both markers. On the other hand, expression of TGF $\beta$ 1 increased in all experimental groups, particularly in the new cement group (Fig.5).

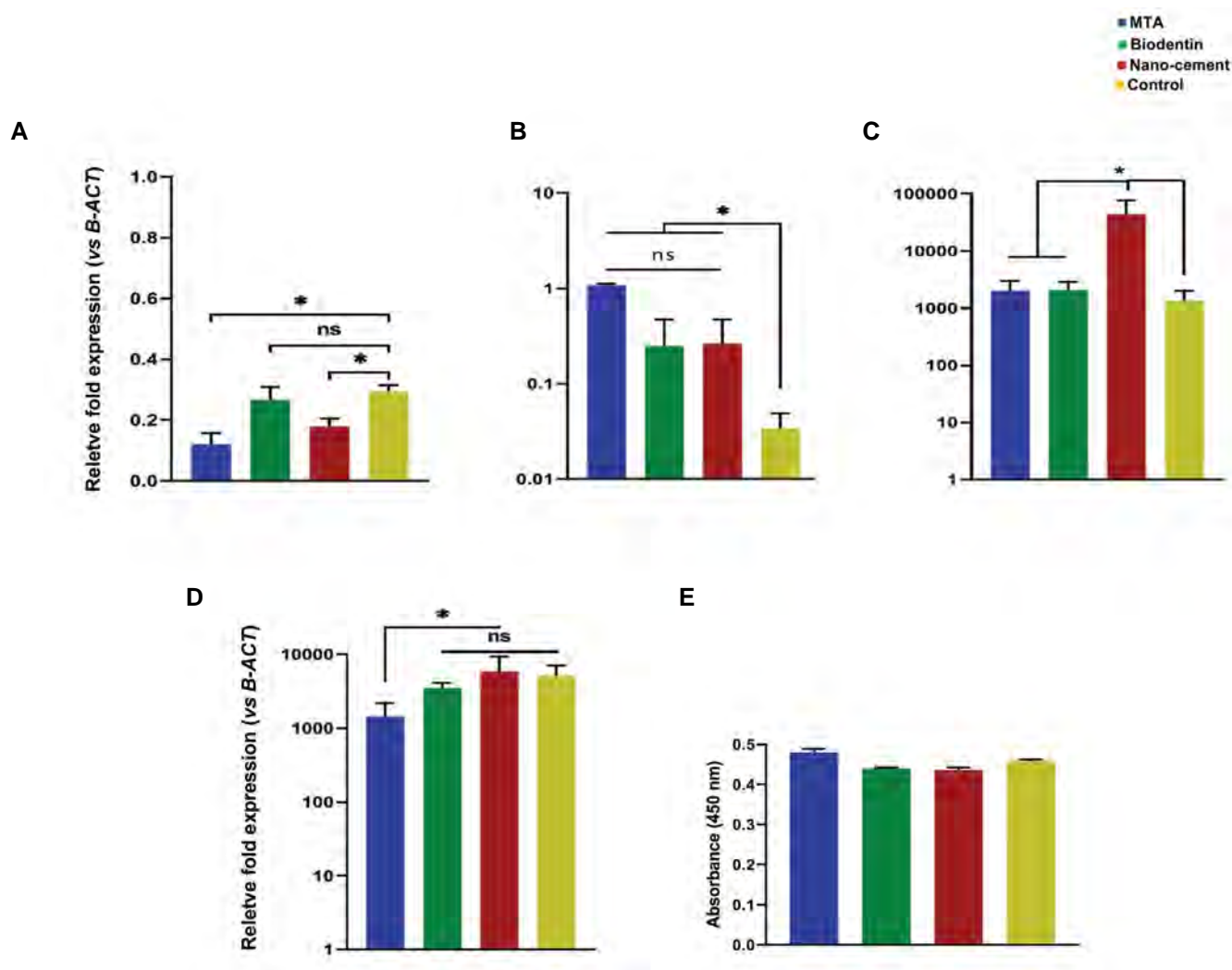


**Fig.4:** Assessment of the osteogenic potential in the presence of dental materials. Analysis of the mRNA expression level of **A.** *ALP*, **B.** *COLA1*, **C.** *RUNX2*, and **D.** *SPP1* as the indicators of early, intermediate, and maturation phase of osteoblasts compared with their expression before induction of differentiation (day 0). Data are presented as the mean value of three independent experiments  $\pm$  SEM. **E.** Semi-quantitative analysis of Alizarin Red staining in different groups using spectrophotometry at 450 nm wavelength. Data are presented as the mean value of three independent experiments  $\pm$  SEM. \*; Indicates a significant difference with  $P<0.05$  and ns; Non significant change.

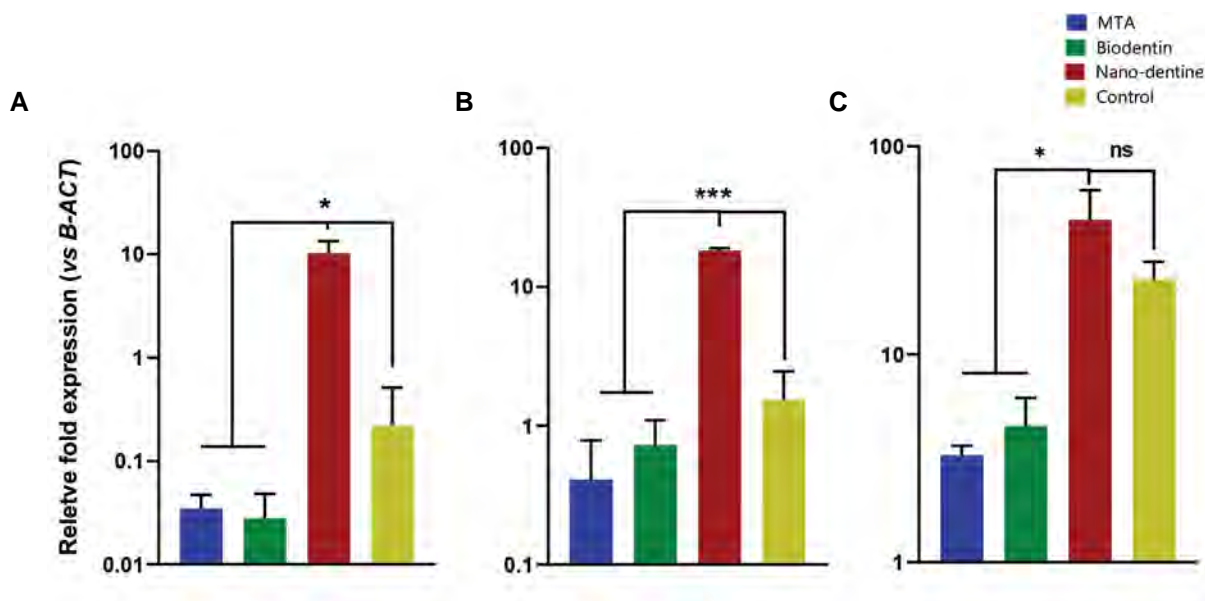


**Fig.5:** Expression of markers involved in inflammation at the mRNA level. Expression of **A.** TNF-alpha and **B.** iNOS as markers of Inflammation, and **C.** TGFB1 as an anti-inflammatory marker, compared with their expression before induction of differentiation (day 0). Data are presented as the mean value of three independent experiments  $\pm$  SEM. \* indicates a significant difference with \*;  $P < 0.5$ , \*\*\*;  $P < 0.005$ , TNF; Tumor necrosis factor, iNOS; Inducible nitric oxide synthase, and ns; Non significant change.

## Discussion

In this study, we introduced Nano-dentine as a novel calcium silicate-based material and assessed its bio-functionality against SCAPs. We found that SCAPs could survive and proliferate in the presence of dentine blocks filled with the Nano-dentine similar to the control group and the commercial counterpart (MTA and Biodentine). The SCAPs have reached a steady state after seven days, while maximum cell proliferation in MTA and Biodentine groups were reported on day ten post treatment. The higher proliferation rate of cells in the presence of Nano-dentine is likely attributed to the pectin component. Pectin is a natural water-soluble polymer, which is widely used in food and drink manufacturing industries as a concentrating, reinforcing, and gelation reagent. In addition, there are numerous reports on the significant antiproliferative effect of Pectin on cancer cells via inducing apoptosis or regulating cell signaling pathways (23). It is evident that Pectin only has an inhibitory effect on cells that express the galectin receptor, especially in high concentrations (24). Intravenous injection of Pectin also triggered coagulation in a shorter time which would be beneficial for controlling hemorrhage and local bleeding (25). Pectin's physicochemical properties highlighted its relevance for wound dressing and elimination of exudates from the wound site (17).

In addition, Pectin can prevent the colonization of bacteria and fungi by providing the acidic pH in the environment and protecting biomaterials against degradation via binding active sites (18). Nano-dentine revealed a suitable degradation rate after one week (7.33%) comparable to Portland cement as well as gray and white MTA (26).

Furthermore, our findings align with previous reports on reasonable cytotoxicity of Biodentine and MTA over

SCAPs (13, 27). Although Nano-dentine group showed a higher level of *RUNX-2* and *SPPI* expression, *COL1A1* was expressed in a similar way in all experimental groups, which was probably due to the high primary level of *COL1A1* in dental-related stem cells (28). It is evident that the expression level of *ALP*, as an early marker of osteogenesis, was reduced in all groups at the end of treatment time. This finding is in harmony with the highly overexpression of *SPPI*, as a late osteogenic marker, and confirms the maturity of osteoblasts. In this way, alizarin red staining confirmed the functional osteoblast differentiation in all experimental groups, which is consistent with the previous report on the remarkable calcification induced by MTA and Biodentine due to the release of calcium hydroxide and deposition of hydroxyapatite (27).

*RUNX2* is a key transcriptional modulator for osteoblastic differentiation, which plays a critical role in the maturation and homeostasis of osteoblasts during embryogenesis and regeneration (29). Indeed, *SPPI* (osteopontin) which is known as the critical non-collagenous bone matrix phospho-glycoprotein, reveals a high affinity to hydroxyapatite and acts as a chemo-attachment for osteoclasts (30). Hence, it is directly and actively involved in the process of bone resorption by osteoclasts (31, 32).

Moreover, the SCAPs showed a significantly higher expression level of TNF-alpha, TGFB1, and iNOS after exposure to Nano-dentine compared to Biodentine and MTA. This effect may be attributed to the positive impact of Pectin on the expression/activation of SMAD3 as the main effector of the TGFB signaling pathway (33). Additionally, Amorim et al. (34) showed that this biopolymer increases NOS expression. A different

line of studies has asserted that in natural dentine tissue, odontoblast express pro- and anti-inflammatory cytokines having paracrine/autocrine effect (35). A complex orchestration of inflammatory mediators seems to be required for the regeneration process. In this way, Saber et al. (27) reported a significant increase in the expression of TNF-alpha after 3 and 7 days of treatment with MTA and Biodentine, respectively. It has been documented that TGFβ1 plays a fundamental role in the migration and differentiation of stem cells to odontoblast-like cells (36). Also, FGF2 and TGFβ1 play critical roles in the induction, specification, and morphogenesis of stem cells during odontogenesis (37).

Nitric oxide is a free radical produced from L-arginine guanidino-nitrogen in three isoforms [endothelial NOS (eNOS), neural NOS (nNOS), and iNOS], depending on the tissue origin and their physiological role (38). In particular, iNOS and eNOS are expressed by the stromal bone marrow cells, osteoblasts, osteocytes, and osteoclasts, whereas the expression of nNOS is limited to osteolineages. Although all three NOS isoforms play an important role in bone healing, iNOS is considered the main factor (39). The substantial overexpression of iNOS in Nano-dentine supports this material's higher potential for osteo-induction.

## Conclusion

Getting all together, we introduce dentine blocks as a novel method for simulating the natural clinical condition. The Nano-dentine cement showed comparable results to Biodentine and MTA in the preservation of cell viability and formation of calcified nodules. Nano-dentine's sensible odontogenic/osteogenic potential was approved via up-regulation of *RUNX2*, *SPP1*, *iNOS*, *TNF-alpha*, and *TGFβ1* markers, which seems to depend on the presence of Pectin in its formulation. Moreover, Nano-dentine showed some superiorities over the other materials because of easy manipulation, less setting time, and low price. These advantages lead Nano-dentine to find a broad application in vital pulp therapy (direct and indirect pulp capping, partial and cervical pulpotomy), apexification, endodontic regeneration, repair of root perforations, and root-end filling.

## Acknowledgements

The authors thank all members of the Royan Institute for preparing facilities and an outstanding scientific environment during this project. There is no financial support and conflict of interest in this study.

## Authors' Contributions

E.A.S., F.E., A.P.; Participated in conception and design, data evaluation, and statistical analysis. M.N., A.P.; Contributed to experimental study and data collection. O.Sh.; Performed material preparation and characterization. E.A.S.; Drafted the manuscript. F.E., N.F.M.; Analysed the results and critically revised the manuscript. A.P., M.H.N.-E.; Took the lead in writing

the manuscript and supervised the research. All authors performed editing and approved the final version of this paper for submission.

## References

- Holliday R, Alani A. Traditional and contemporary techniques for optimizing root canal irrigation. *Dental Update*. 2014; 41(1): 51-61.
- Gomes-Filho JE, Watanabe S, Bernabé PFE, de Moraes Costa MT. A mineral trioxide aggregate sealer stimulated mineralization. *J Endod*. 2009; 35(2): 256-260.
- Shojaee NS, Sahebi S, Karami E, Sobhnamayan F. Solubility of two root-end filling materials over different time periods in synthetic tissue fluid: a comparative study. *J Dent (Shiraz)*. 2015; 16(3): 189-194.
- Song M, Yoon TS, Kim SY, Kim E. Cytotoxicity of newly developed pozzolan cement and other root-end filling materials on human periodontal ligament cell. *Restor Dent Endod*. 2014; 39(1): 39-44.
- Roberts HW, Toth JM, Berzins DW, Charlton DG. Mineral trioxide aggregate material use in endodontic treatment: a review of the literature. *Dent Mater*. 2008; 24(2): 149-164.
- Silva E, Senna P, De-Deus G, Zaia A. Cytocompatibility of Biodentine using a three-dimensional cell culture model. *Int Endod J*. 2016; 49(6): 574-580.
- D'Antò V, Di Caprio MP, Ametrano G, Simeone M, Rengo S, Spagnuolo G. Effect of mineral trioxide aggregate on mesenchymal stem cells. *J Endod*. 2010; 36(11): 1839-1843.
- Luo Z, Kohli MR, Yu Q, Kim S, Qu T, He W-x. Biodentine induces human dental pulp stem cell differentiation through mitogen-activated protein kinase and calcium/calmodulin-dependent protein kinase II pathways. *J Endod*. 2014; 40(7): 937-942.
- Malkondu Ö, Karapinar Kazandağ M, Kazazoğlu E. A review on biodentine, a contemporary dentine replacement and repair material. *Biomed Res Int*. 2014; 2014: 160951.
- Saber E, Farhad-Mollashahi N, Saber M. Interaction of intracanal medicaments with apical papilla stem cells: quantitative cytotoxicity assessment by methyl thiazolyl tetrazolium, trypan blue and lactate dehydrogenase. *Minerva Stomatol*. 2019; 68(1): 36-41.
- Youssef AR, Emara R, Taher MM, Al-Allaf FA, Almalki M, Almasri MA, et al. Effects of mineral trioxide aggregate, calcium hydroxide, biodentine and emdogain on osteogenesis, Odontogenesis, angiogenesis and cell viability of dental pulp stem cells. *BMC Oral Health*. 2019; 19(1): 133.
- Jeanneau C, Laurent P, Rombouts C, Giraud T, About I. Light-cured tricalcium silicate toxicity to the dental pulp. *J Endod*. 2017; 43(12): 2074-2080.
- Saber EA, Karkehabadi H, Mollashahi NF. Cytotoxicity of various endodontic materials on stem cells of human apical papilla. *Iran Endod J*. 2016; 11(1): 17-22.
- Hamouda IM. Current perspectives of nanoparticles in medical and dental biomaterials. *J Biomed Res*. 2012; 26(3): 143-151.
- Smith AM, Moxon S, Morris G. Biopolymers as wound healing materials. *Wound Healing Biomaterials*, Elsevier; 2016: 261-287.
- Inngjerdigen M, Inngjerdigen KT, Patel TR, Allen S, Chen X, Rolstad B, et al. Pectic polysaccharides from *Biophytum pendens* Klotzsch, and their activation of macrophages and dendritic cells. *Glycobiology*. 2008; 18(12): 1074-1084.
- Munarin F, Tanzi MC, Petrini P. Advances in biomedical applications of pectin gels. *Int J Biol Macromol*. 2012; 51(4): 681-689.
- Jáuregui KMG, Cabrera JCC, Ceniceros EPS, Hernández JLM, Ilyina A. A new formulated stable papin-pectin aerosol spray for skin wound healing. *Biotechnol Bioprocess Eng*. 2009; 14(4): 450-456.
- Chittasupho C, Jaturanpinyo M, Mangmool S. Pectin nanoparticle enhances cytotoxicity of methotrexate against hepG2 cells. *Drug Deliv*. 2013; 20(1): 1-9.
- de Souza Balbinot G, Leitune VCB, Nunes JS, Visioli F, Collares FM. Synthesis of sol-gel derived calcium silicate particles and development of a bioactive endodontic cement. *Dent Mater*. 2020; 36(1): 135-144.
- Lee BS, Lin HP, Chan JCC, Wang WC, Hung PH, Tsai YH, et al. A novel sol-gel-derived calcium silicate cement with short setting time for application in endodontic repair of perforations. *Int J Nano-medicine*. 2018; 13: 261-271.
- Karamali F, Esfahani MHN, Hajian M, Ejeian F, Satarian L, Baharvand H. Hepatocyte growth factor promotes the proliferation of human embryonic stem cell derived retinal pigment epithelial cells. *J Cell Physiol*. 2019; 234(4): 4256-4266.

23. Bergman M, Djaldetti M, Salman H, Bessler H. Effect of citrus pectin on malignant cell proliferation. *Biomed Pharmacother.* 2010; 64(1): 44-47.
24. Abdel-Massih R, Hawach V, Boujaoude MA. The cytotoxic and anti-proliferative activity of high molecular weight pectin and modified citrus pectin. *Funct Foods Health Dis.* 2016; 6(9): 587-601.
25. Kadajji VG, Betageri GV. Water soluble polymers for pharmaceutical applications. *Polymers.* 2011; 3(4): 1972-2009.
26. Alqedairi A, Muñoz-Viveros CA, Pantera EA, Campillo-Funollet M, Alfawaz H, Abou Neel EA, et al. Superfast set, strong and less degradable mineral trioxide aggregate cement. *Int J Dent.* 2017; 2017: 3019136.
27. Saberi E, Farhad-Mollashahi N, Aval FS, Saberi M. Proliferation, odontogenic/osteogenic differentiation, and cytokine production by human stem cells of the apical papilla induced by biomaterials: a comparative study. *Clin Cosmet Investig Dent.* 2019; 11: 181-193.
28. Sollazzo V, Palmieri A, Girardi A, Zollino I, Brunelli G, Spinelli G, et al. Osteopontin acts on stem cells derived from peripheral blood. *J Indian Soc Periodontol.* 2010; 14(1): 12-17.
29. Ducky P, Starbuck M, Priemel M, Shen J, Pinero G, Geoffroy V, et al. A Cbfa1-dependent genetic pathway controls bone formation beyond embryonic development. *Genes Dev.* 1999; 13(8): 1025-1036.
30. Ohtsuki C, Kamitakahara M, Miyazaki T. Bioactive ceramic-based materials with designed reactivity for bone tissue regeneration. *J R Soc Interface.* 2009; 6 Suppl 3: S349-S360.
31. Dodds RA, Connor JR, James IE, Lee Rykaczewski E, Appelbaum E, Dul E, et al. Human osteoclasts, not osteoblasts, deposit osteopontin onto resorption surfaces: an in vitro and ex vivo study of remodeling bone. *J Bone Miner Res.* 1995; 10(11): 1666-1680.
32. Bailey S, Karsenty G, Gundberg C, Vashishth D. Osteocalcin and osteopontin influence bone morphology and mechanical properties. *Ann N Y Acad Sci.* 2017; 1409(1): 79-84.
33. Cao Y, Gao X, Zhang W, Zhang G, Nguyen AK, Liu X, et al. Dietary fiber enhances TGF- $\beta$  signaling and growth inhibition in the gut. *Am J Physiol Gastrointest Liver Physiol.* 2011; 301(1): G156-G64.
34. Amorim JC, Vriesmann LC, Petkowicz CL, Martinez GR, Noleto GR. Modified pectin from *Theobroma cacao* induces potent pro-inflammatory activity in murine peritoneal macrophage. *Int J Biol Macromol.* 2016; 92: 1040-1048.
35. Park M, Pang NS, Jung IY. Effect of dentin treatment on proliferation and differentiation of human dental pulp stem cells. *Restor Dent Endod.* 2015; 40(4): 290-298.
36. Smith AJ, Matthews JB, Hall RC. Transforming growth factor- $\beta$ 1 (TGF- $\beta$ 1) in dentine matrix: Ligand activation and receptor expression. *Eur J Oral Sci.* 1998; 106(S1): 179-184.
37. He H, Yu J, Liu Y, Lu S, Liu H, Shi J, et al. Effects of FGF2 and TGF $\beta$ 1 on the differentiation of human dental pulp stem cells in vitro. *Cell Biol Int.* 2008; 32(7): 827-834.
38. Wang FS, Kuo YR, Wang CJ, Yang KD, Chang PR, Huang YT, et al. Nitric oxide mediates ultrasound-induced hypoxia-inducible factor-1 $\alpha$  activation and vascular endothelial growth factor-A expression in human osteoblasts. *Bone.* 2004; 35(1): 114-123.
39. Wimalawansa SJ. Nitric oxide and bone. *Ann N Y Acad Sci.* 2010; 1192(1): 391-403.

# Colchicine of *Colchicum autumnale*, A Traditional Anti-Inflammatory Medicine, Induces Apoptosis by Activation of Apoptotic Genes and Proteins Expression in Human Breast (MCF-7) and Mouse Breast (4T1) Cell Lines

Elham Adham Foumani, Ph.D.<sup>1</sup>, Shiva Irani, Ph.D.<sup>1</sup>, Yalda Shokoohinia, Ph.D.<sup>2</sup>, Ali Mostafaie, Ph.D.<sup>3\*</sup>

1. Department of Biology, Science and Research Branch, Islamic Azad University, Tehran, Iran

2. Department of Pharmacognosy and Biotechnology, School of Pharmacy, Kermanshah University of Medical Sciences, Kermanshah, Iran

3. Medical Biology Research Center, Kermanshah University of Medical Sciences, Kermanshah, Iran

\*Corresponding Address: P.O.Box: 6714869914, Medical Biology Research Center, Kermanshah University of Medical Sciences, Kermanshah, Iran  
Email: amostafaie@kums.ac.ir

Received: 25/September/2021, Accepted: 15/May/2022

## Abstract

**Objective:** Breast cancer is one of the major causes of mortality among women. Due to many side effects of the existing chemotherapeutic agents, the research of anti-cancer drugs, including natural products, is still a big challenge. Here, we investigated the effects of colchicine on apoptosis of two breast cancer cell lines (human MCF-7 and mouse 4T1).

**Materials and Methods:** In this experimental study, we evaluated the apoptotic effects of colchicine on (MCF-7) and (4T1), as well as a human cancer-associated fibroblast cell line as a control group. Extraction and chromatographic techniques were applied to isolate colchicine from *Colchicum autumnale* L. To compare the isolated colchicine with pure standard colchicine, we used the H-NMR technique. The methyl thiazolyl tetrazolium (MTT) assay, quantitative reverse transcriptase-polymerase chain reaction, Western blotting and annexin V/PI staining were used to evaluate the apoptotic effects of the isolated and standard colchicine.

**Results:** Similar to standard colchicine, the isolated colchicine inhibited cell proliferation significantly in cancer cell lines. Colchicine inhibited proliferation and induced apoptosis on a dose-dependent manner. The medicine modified the expression of genes-related to apoptosis by up-regulation of *P53*, *BAX*, *CASPASE-3*, *-9* and down-regulation of *BCL-2* gene, which led to an increase in the *BAX/BCL-2* ratio.

**Conclusion:** We showed that isolated colchicine from *Colchicum autumnale* and pure standard colchicines modulate the expression levels of several genes and therefore exerting their anticancer effects on both human (MCF-7) and mouse (4T1) breast cancer cells. Based on these results, we suggest that colchicine can be a potential candidate for prevention and treatment of breast cancer.

**Keywords:** Apoptosis, Breast Cancer Cell, Colchicine, *Colchicum autumnale*, Toxicity

Cell Journal (Yakhteh), Vol 24, No 11, November 2022, Pages: 647-656

**Citation:** Adham Foumani E, Irani Sh, Shokoohinia Y, Mostafaie A. Colchicine of *colchicum autumnale*, a traditional anti-inflammatory medicine, induces apoptosis by activation of apoptotic genes and proteins expression in human breast (MCF-7) and mouse breast (4T1) cell lines. Cell J. 2022; 24(11): 647-656. doi: 10.22074/cellj.2022.8290.

This open-access article has been published under the terms of the Creative Commons Attribution Non-Commercial 3.0 (CC BY-NC 3.0).

## Introduction

As the most common cancer among women, breast cancer is a major public health problem around the world, in both developed and developing countries. Based on World Health Organization (WHO), over 502,000 women die annually from breast cancer and it also results in more than \$7 billion medical costs per year, worldwide. Unfortunately, the mortality rate due to this type of cancer has dramatically increased in the past decade in Iran (1, 2). Recently, chemotherapy and radiotherapy (lonely or in combination) are the common treatments for breast and other types of cancers as well. But besides their therapeutic effects, they induce wide undesired effects on healthy cells as well (3).

Colchicine is a tropane alkaloid, widely used for its anti-gout and anti-inflammatory activities (4-6). Colchicine by binding to the tubulins and interfering with their polymerization, results in disruption of

mitosis. It also leads to the inhibition of leukocytes and migration of other inflammatory cells (7, 8). Besides, colchicine increases the cellular free tubulins to limit the mitochondrial metabolism in cancer cells by blocking voltage-dependent anion channels of the mitochondrial membrane (9). Other studies have also reported the antiproliferative and anticarcinogenic properties of colchicine in different cell lines and animal models. Additionally, recent studies in this area have shown that colchicine as an anticancer agent, has a high potential to induce apoptosis in cancer cells. This is evidenced by its growth inhibitory effect on certain types of tumor cell lines both *in vitro* and *in vivo*, such as gastric cells (10, 11), hepatocellular carcinoma (12), liver cells (13), and cholangiocarcinoma (14). Colchicine at high doses is extremely toxic, which limits its use in therapy on human cells (10). Apoptosis is a highly regulated process that begins by activation of various molecules in this pathway.

Therefore, the activations of these molecules in the apoptosis pathway offer promising approaches towards cancer therapy. However, the exact cytotoxic mechanism of colchicine is still unknown due to the certain anti- and pro-apoptotic signaling pathways in different cell types. Since colchicine is extremely toxic at high doses (15), the amount of it that may be used on cells is limited, and thus it is a big challenge to determine the mechanism behind its apoptotic effects on breast cancer cells.

In this study, we evaluated the cytotoxic and growth inhibitory effects of isolated colchicine from *C. autumnale* L., and investigated its effects on apoptotic genes and proteins in human (MCF-7) and mouse (4T1) breast cancer cell lines.

## Materials and Methods

### Extraction and purification of colchicine from *Colchicum autumnale* L. corms

This report is on an experimental study, in which the corms of *Colchicum* were collected from Kermanshah, Iran, between October and November 2014. Corms were further identified and confirmed by the Department of Agricultural College (Voucher number: 2770, deposited in Herbarium of Razi University, director: Dr. S. M. Maassoumi). Extraction was performed according to Alali et al. (16) with slight modifications. Briefly, the bulbs were crushed and dried out in the dark and then powdered with a laboratory grinder. One weight of the powder was extracted two times with 50 volumes of ether while shaking for 2 hours, followed by filtration. The solid residues were air-dried and extracted with dichloromethane (DCM) at room temperature for 30 minutes by shaking. Then, 10% ammonia solution was added to the mixture with intense shaking for 10 minutes and the mixture was left undisturbed for the next 60 minutes. Right after the break, 250 ml of DCM was added and the mixture was immediately filtered. The residue was washed twice with 250 ml of DCM and then pooled with the filtrate. The solution was allowed to evaporate to dry.

Column chromatography was performed on silica gel (Merck, Darmstadt, Germany; 63-200 µm particle size) that was already slurry-packed with DCM. The dried extract from the previous step dissolved in DCM and was applied to the column. The column was eluted by using chloroform-methanol solution (5:95). The eluted fractions were evaluated through thin layer chromatography (TLC) and then visualized by ultraviolet (UV) at 254 nm. In the eluted fractions colchicines were identified by TLC and classified into five groups based on the band intensity. Each of the five groups was evaporated to dryness. In the next step, the content of each group was evaluated by TLC and compared to the pure standard colchicine powder from Alexis (Nottingham, East Midlands, UK). Two fractions that showed the highest similarity to the standard control colchicine were further tested for their effectiveness.

For quantitative analysis of the isolated colchicine, we used the UV spectroscopy method (Bioaquarius, Cecile,

UK) with the standard control colchicine as the reference. Moreover, a known amount of colchicine was dissolved in methanol and checked for its  $\lambda_{ref}$  value with UV spectroscopy. In order to run Fourier-transform infrared (FTIR) spectroscopy (PerkinElmer- M-15 model), the sample was prepared according to the protocol and the results were analyzed by SHIMADZU (IR Prestige-21 model).

Finally, the H-NMR method was used to determine the similarity of the isolated colchicine from *C. autumnale* L. to the standard control colchicine. The H-NMR spectra in the experiment were recorded on a 500 MHz (Bruker, Germany) instrument, with chloroform ( $CDCl_3$ ) as the solvent.

### Cultivation of cell lines

Human (MCF-7) and mouse (4T1) breast cancer cell lines were obtained from Pasteur Institute of Iran and human fibroblast cells were isolated from normal-healthy skin used as the control [all experimental procedures were carried out in accordance with the Ethical Principles and the National Norms and Standards for Conducting Medical Research in Iran (IR.KUMS.REC.1397.941)]. Informed consent was obtained from all individual participants included in the study. The human and mouse breast cancer cells (MCF-7, 4T1) were cultured in Dulbecco's Modified Eagle's Medium (DMEM) supplemented with 10% fetal bovine serum (FBS), 100 units/ml penicillin, and 100 µg/ml streptomycin. Incubation was carried out at 37°C with 5%  $CO_2$ .

### Cytotoxicity assay

MCF-7, 4T1, and fibroblast cells were cultured in 96-well plates in DMEM containing 10% fetal calf serum (FCS), at 37°C and 5%  $CO_2$  and were allowed to reach 70-80% confluency. Culture medium after 24 to 48 hours (by cell type) was replaced with 300 µl fresh medium containing 5% FCS. The wells were treated with different concentrations of isolated and standard colchicine and some wells were assigned as controls (untreated). After 24 hours, cells were detached from the plate using trypsin-EDTA and resuspended in a 100 µl of culture medium after centrifugation. The suspension was well dispersed and then the viability of the cells was evaluated after adding trypan blue (0.4% in PBS) to the test and control wells. The following formula was applied to calculate the viability at different time intervals:

$$\text{Viability}\% = [1.00 - (\text{Number of blue cells} \div \text{Number of total cells})] \times 100.$$

### Growth inhibition using MTT assay

Human (MCF-7) and mouse (4T1) breast cancer cell lines and normal human fibroblasts were seeded (5000 cells/wells) in 96-well plates and incubated in a serum-containing medium, as mentioned above, for 48 hours. Then, cells were treated with various concentrations of purified and isolated colchicine (1-400 ng/ml)

while control wells remained untreated. The cells were incubated for an additional 48 hours, thereafter 200  $\mu$ l of MTT solution (5 mg/ml, filtered) was added to each well and the cells were incubated for another 3-4 hours. Dimethyl sulfoxide (DMSO) was added (150  $\mu$ l) to each well after removal of the medium and the absorbance was measured in a microplate reader at 570 nm.

### Quantitative analysis of reverse transcriptase-polymerase chain reaction

Total RNA was extracted by RNeasy Mini Kit (Qiagen, Hilden, Germany) according to the manufacturer's instructions. The high-capacity cDNA RT kit (Applied Biosystems, Foster City, CA) was used to synthesize cDNA. To prevent the formation of primer-dimers and non-specific products during real-time polymerase chain reaction (PCR), melt curve analysis and PCR were also done. Gene expression was assessed by real-time quantitative PCR using the Real-Time PCR system (Rotor-Gene 6000 Cyler, Qiagen, Germany) and the Power SYBR Green PCR master mix. Primers were selected for each cell line and for the target genes *BAX*, *BCL-2*, *P53* and  $\beta$ -*ACTIN* (MCF-7 cell line), *Bax*, *Bcl-2*, *p53* and  $\beta$ -*Actin* (4T1 cell line) based on the nucleotide sequences downloaded from the Pre Primer software. Furthermore, the specificity of the primers was checked by the National Center for Biotechnology Information data bank. To ensure the absence of singly nucleotide polymorphism (SNP), these primers were reviewed on the site of the NCBI checker.

The real-time PCR for relative quantification of the target genes was performed in a total volume of 20  $\mu$ l comprised of 10  $\mu$ l SYBR® Premix Ex Taq™ master mix (Takara, Japan), 0.5  $\mu$ l of each forward and reverse primer, 0.08  $\mu$ l diluted ROX, and 2  $\mu$ l DNA template, under following conditions: an initial denaturation of templates at 95°C for 10 minutes, followed by 35 cycles of denaturation at 95°C for 10 seconds and annealing/extension at 60°C for 30 seconds. The reaction was ended after the final extension at 75°C for 15 seconds. A melt curve analysis was performed to assess the formation of primer-dimer or non-specific products during the amplification. Accordingly, at the last step of the amplification, the reaction was continued by heating at 95°C for 15 seconds, a temperature gradient of 60-95°C for 1 minute, and 95°C for 15 seconds. The relative expression genes (both cell line) in the treated and control mice was calculated by using the formula  $2^{-\Delta\Delta Ct}$  presented below.

### Western blot

To detect changes in apoptosis-related proteins (p53, Bcl-2, Bax, caspase-3 and caspase-9), MCF-7 and 4T1 cells ( $1 \times 10^7$  cells) were seeded in 10cm<sup>2</sup> dishes and treated with 0.5 and 1  $\mu$ g/ml of isolated colchicine and 0.2 and 0.4  $\mu$ g/ml of pure standard colchicine. After 24 hours, the cells were harvested and lysed using a lysis buffer (50 mM Tris-HCL, pH=8, 8 M urea, 2 M thiourea and 0.1 mM PMSF). The protein concentration of the cell lysates

was quantified according to the method of Bradford with BSA as the standard. Total protein (35  $\mu$ g) was run onto a 12% sodium dodecyl sulfate-polyacrylamide gel electrophoresis (SDS-PAGE) for 60 minutes. Then, the protein bands were transferred to a polyvinylidene difluoride membrane (PVDF, Roche, Germany). The membranes were blocked with PBS containing Tween 0.5% and BSA 2% for 20 minutes and incubated overnight at 4°C with the following primary antibodies (Santa Cruze): anti-p53 (1:300), anti-Bcl-2 (1:300), anti-Bax (1:300), anti-b-actin (1:1000) anti-caspase-3 (1:500), and anti-caspase-9 (1:500). After washing the membrane in PBS containing Tween 0.05% (PBS-T) four times, the membrane was incubated with horseradish peroxidase (HRP) conjugated secondary antibody for detection. After washing in PBS-T (four times), the reactive bands were visualized using 3,3'-diaminobenzidine (DAB) and H<sub>2</sub>O<sub>2</sub> substrate solution. Finally, the reactive bands were analyzed by Image J software (LOCI, U.S). The relative fold-difference was calculated by the integration of the normalized to the intensity of the  $\beta$ -actin band.

### Annexin-V/PI staining assay

The PI and annexin V-FITC double-binding assay was applied to detect apoptotic cells by annexin V-FITC/PI kit. Cells were seeded in 6-well plates containing complete medium for 24 hours and then in a 24-hours treatment, MCF7 and 4T1 cells were exposed to the isolated (0.5 and 1  $\mu$ g/ml) and control (0.2 and 0.4  $\mu$ g/ml) colchicine. As stated in the kit manual, we harvested the cells, rinsed twice with PBS and gently resuspended in annexin V binding buffer and incubated with annexin V-FITC/PI in the dark for 10 minutes. Ultimately, the cells were evaluated by fluorescence microscopy (Ts100, Nikon, Tokyo, Japan) with at least  $1 \times 10^6$  cells per sample. The investigation was repeated 3 times for each group.

### Statistical analysis

Statistical analysis was performed using SPSS 21.0 for Windows (SPSS, Chicago, IL, USA), where the data is reported as means  $\pm$  standard error (SE). Differences between the isolated colchicine treated, standard colchicine treated and control groups (untreated) were analyzed by one-way analysis of variance (ANOVA) followed by Tukey's test for multiple comparisons. Significance levels were determined by the Student t test.  $P < 0.05$  was considered statistically significant.

## Results

### Physicochemical characters of colchicine from *C. autumnale*

The isolated colchicine from *C. autumnale* L. was compared to standard colchicine (Nottingham, East Midlands, UK) using Fourier Transform Infrared Spectroscopy (FTIR), Proton Nuclear magnetic resonance spectroscopy (H-NMR) and UV spectroscopy to determine the purity and similarity of the isolated colchicines.

The results of FTIR and H-NMR confirmed the same molecular structure in both types of colchicines. The results of the UV scan determined a  $\lambda$  max value of 243.5 and 350 nm for pure standard colchicine; completely similar to what is stated in previous studies. Isolated colchicine also had a maximum absorption of approximately 200-400 nm, which is about the same as the standard colchicine. Therefore, in this study, isolated colchicine from *C. autumnale* L. has been used as an anti-cancer agent on MCF-7, 4T1 cells.

### Cytotoxic effects of colchicine on MCF-7 and 4T1 cells

Trypan Blue exclusion test was applied for investigation of the cytotoxic effects of colchicine on human and mouse breast cancer cells, as well as on fibroblasts. The results from MCF-7 cells exposed to various concentrations (0.002-8  $\mu$ g/ml) of the standard and isolated colchicine during a 24 hours period are shown in Figure 1A. The cytotoxic effect was significant, indicated by the uptake of trypan blue dye, at the concentrations of greater than or equal to 0.1  $\mu$ g/ml and 0.5  $\mu$ g/ml for isolated and standard colchicine, respectively ( $P < 0.05$ ). Additionally, 50% Cytotoxicity Concentrations (CC<sub>50</sub>) of the isolated and standard colchicines on MCF-7 cells were 2  $\mu$ g/ml and 1  $\mu$ g/ml, respectively (Fig.1A). For further investigations, concentrations close to the CC<sub>50</sub> values (0.5 and 1  $\mu$ g/ml) were selected.

The results from treating the 4T1 cell line with various concentrations (1-800  $\mu$ g/ml) of standard and isolated colchicine for a 24 hours period are shown in Figure 1B. Cytotoxicity of both compounds on mouse breast cancer cells was significant at concentrations  $\geq 10$   $\mu$ g/ml ( $P < 0.05$ ). Furthermore, the CC<sub>50</sub> for both compounds was similar (300  $\mu$ g/ml, Fig.1B). We observed significant cytotoxic activity on human fibroblast cells when using concentrations above 0.1  $\mu$ g/ml for isolated and 0.4  $\mu$ g/ml for standard colchicine ( $P < 0.05$ ). The CC<sub>50</sub> of colchicine for human fibroblast was 6  $\mu$ g/ml (Fig.1C).

### The growth inhibitory effect of colchicine on MCF-7 and 4T1 cells

Growth inhibitory activity of colchicine on human and mouse breast cancer cells and human fibroblasts was evaluated after treating the cells with either form of colchicine for 48 hours. Thereafter, the viability of the cells was estimated using MTT assay. The MCF-7, 4T1 and fibroblast cells that were exposed to standard and isolated colchicine showed a significant decrease in cell growth in a dose-dependent manner. The inhibitory effects of the two colchicines on MCF-7 cells was remarkable at concentrations  $\geq 8$  ng/ml ( $P < 0.001$ ). Finally, 50% inhibitory concentration (IC<sub>50</sub>) of both isolated and standard colchicines were 8 ng/ml and 4 ng/ml, respectively (Fig.2A).

In the case of 4T1 cells, the effective inhibitory

concentrations of the isolated and standard colchicine started from  $\geq 20$   $\mu$ g/ml and  $\geq 100$   $\mu$ g/ml, respectively ( $P < 0.05$ ). But the IC<sub>50</sub> value for both colchicines on 4T1 cells was 200  $\mu$ g/ml (Fig.2B).

The significant growth inhibitory effect of the isolated and standard colchicines on fibroblast cells started from 0.4  $\mu$ g/ml ( $P < 0.001$ ). The IC<sub>50</sub> of both colchicines on fibroblast cells was 2  $\mu$ g/ml (Fig.2C).

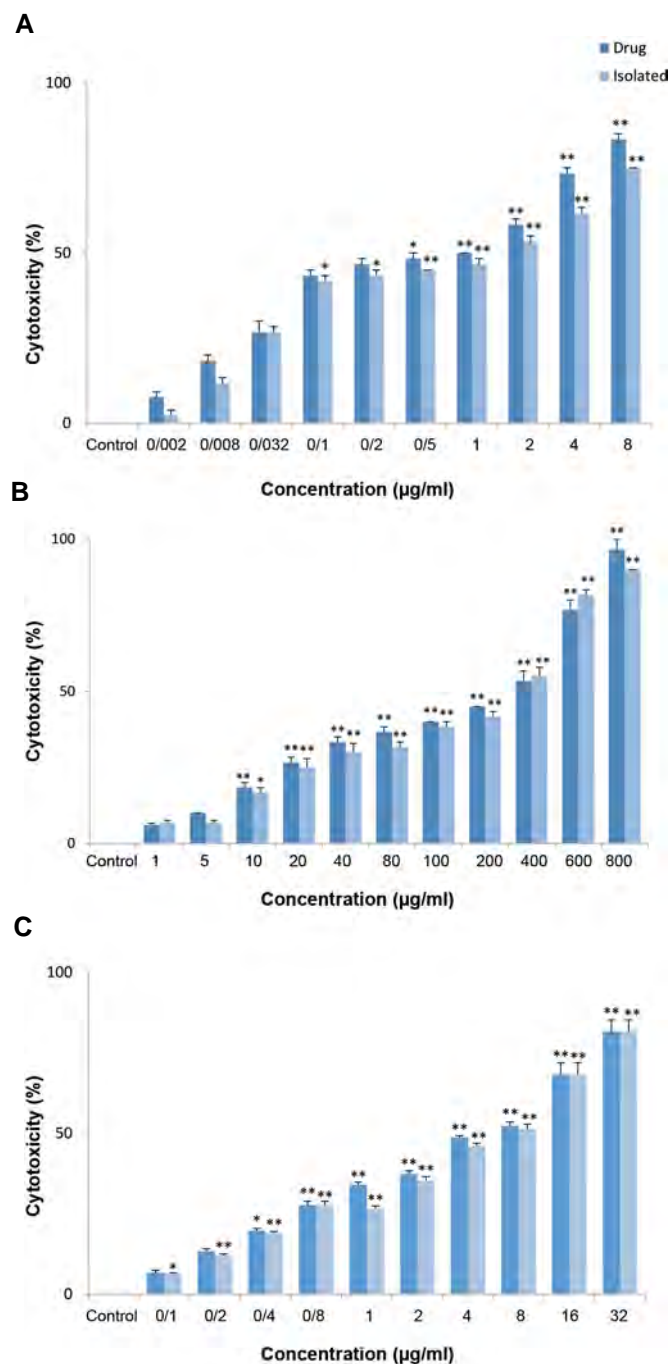


**Fig.1:** Cytotoxic effects of different concentrations of standard (drug) and isolated colchicine after 24-hours of treatment. **A.** On MCF-7 cells, **B.** On 4T1 cells, and **C.** On fibroblast cells. Data are given as mean  $\pm$  SE for each point of three separate experiments, \*,  $P < 0.05$ , \*\*,  $P < 0.001$  vs. control.

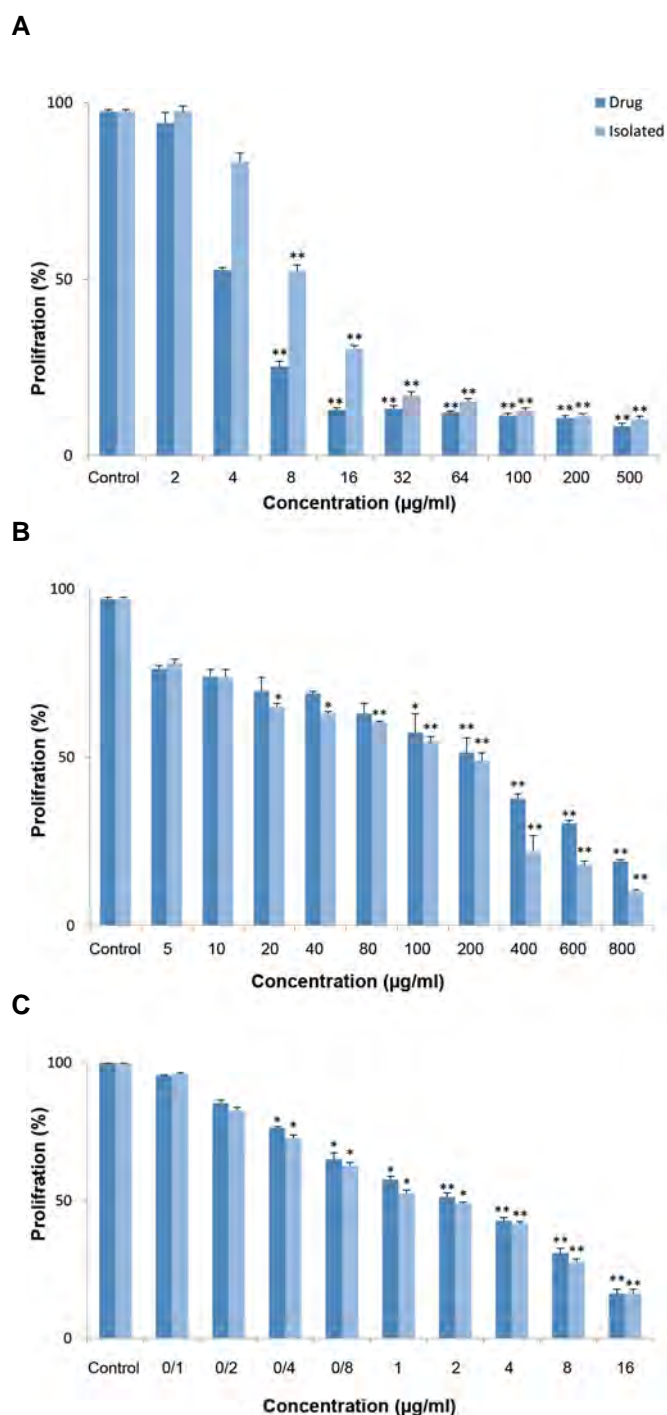


**Fig.2:** The growth inhibitory effect of different concentrations of isolated and standard colchicine (drug) after 48 hours. **A.** On MCF-7 cells, **B.** 4T1 cells, and **C.** Fibroblast cells. Data are given as mean  $\pm$  SE for each point of three separate experiments, \*;  $P < 0.05$  and \*\*;  $P < 0.001$  vs. control.

### The effects of colchicine on the expression of *P53*, *BAX* and *BCL-2* genes

The effects of isolated and standard colchicine on expression of the three mentioned genes *P53*, *BAX* and *BCL-2* in MCF-7 cells was examined by quantitative RT-PCR. Both compounds induced an up-regulation of *P53* gene (2.75-folds and 1.22 folds at 0.5  $\mu\text{g/ml}$ ,

and 1.68 folds and 2.47 folds at 1  $\mu\text{g/ml}$ , respectively) and *BAX* gene (5-folds and 2.07-folds at 0.5  $\mu\text{g/ml}$ , 1.61-folds and 2-folds at 1  $\mu\text{g/ml}$ , respectively). However, both colchicines down-regulated *BCL-2* gene (0.74-fold and 0.59-fold at 0.5  $\mu\text{g/ml}$ , and 0.7-fold and 0.53-fold at 1  $\mu\text{g/ml}$ , respectively). Additionally, significantly different gene expression levels were observed between the two cell types when using equal concentrations of the standard and the isolated colchicine (\* $P < 0.01$ , \*\* $P < 0.05$ , and \*\*\* $P < 0.001$ ). This significant difference was also observed when using different concentrations (0.5 and 1  $\mu\text{g/ml}$ ) of the two colchicines (Fig.3A, \* $P < 0.01$ , \*\* $P < 0.05$ , and \*\*\* $P < 0.001$ ).

Investigating the expression levels of *P53*, *Bax* and *Bcl-2* genes in 4T1 cells treated with isolated and standard colchicine at 200-400  $\mu\text{g/ml}$  concentrations demonstrated an up-regulation in the expression of *P53* gene (1.07-folds and 1.29-folds at 200  $\mu\text{g/ml}$ , 2.73-folds and 2.04-folds at 400  $\mu\text{g/ml}$  of the isolated and standard colchicine, respectively) and *Bax* gene (6.27-folds and 4.43-folds at 200  $\mu\text{g/ml}$ , 1.72-folds and 1.44-folds at 400  $\mu\text{g/ml}$  of both compounds, respectively) but a down-regulation of *Bcl-2* gene (0.21-fold and 0.43-fold at 200- $\mu\text{g/ml}$ , 0.61-fold and 0.18-fold at 400  $\mu\text{g/ml}$  of the isolated- and standard-colchicine, respectively). Similar to MCF-7 cells, significantly different effects on gene expression levels in the 4T1 cells were observed using equal concentration of the isolated and the standard colchicine (\* $P < 0.01$ , \*\* $P < 0.05$ , and \*\*\* $P < 0.001$ ). Significant differences in the effects of our treatments on gene expression levels at two different concentrations (200 and 400  $\mu\text{g/ml}$ ) of standard and the isolated colchicine was found as well (Fig.3B, \* $P < 0.01$ , \*\* $P < 0.05$ , and \*\*\* $P < 0.001$ ).

*BCL-2* superfamily plays an important role in cell apoptosis. Two members of the *BCL-2* family are anti-apoptotic *BCL-2* and pro-apoptotic *BAX*. Isolated colchicine increased the *BAX/BCL-2* ratio (as an index of apoptosis) in MCF-7 at the concentrations of 0.5 and 1  $\mu\text{g/ml}$  and in 4T1 cells at 200 and 400  $\mu\text{g/ml}$ . Isolated colchicine raised the *BAX/BCL-2* ratio up to 4.5 fold and 1.3 fold at the concentrations of 0.5 and 1  $\mu\text{g/ml}$ , respectively in the MCF-7 cells compared to the control group. Standard colchicine also lead to the same outcome but in different amounts (1.6 fold and 1 fold at 0.5 and 1  $\mu\text{g/ml}$ , respectively). In the 4T1 cells, standard colchicine increased this ratio up to 2.9 fold and 2.8 fold at concentrations of 200 and 400  $\mu\text{g/ml}$ , respectively. Besides that, isolated colchicine caused a more remarkable increase in *BAX/BCL-2* ratio, which was 10.8 fold and 8 fold at the concentrations of 200 and 400  $\mu\text{g/ml}$ , respectively (Fig.3C).

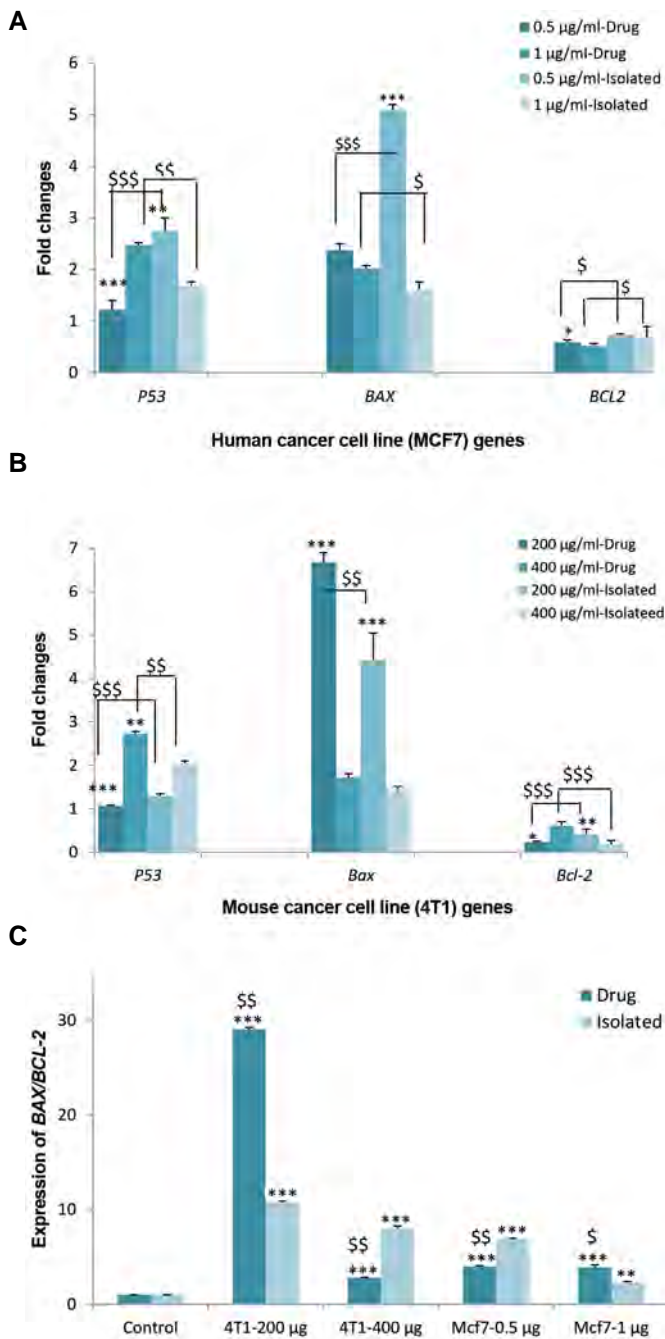


**Fig.3:** mRNA expression of pro-apoptotic and anti-apoptotic genes. **A.** *P53*, *BAX*, *BCL-2* in MCF-7 cells, **B.** *p53*, *Bax*, *Bcl-2* in 4T1 cells. The expression of pro-apoptotic and anti-apoptotic genes in both cell lines was determined by measuring mRNA levels using real-time polymerase chain reaction (PCR). Data are given as mean  $\pm$  SE for each point of three separate experiments, \*,  $P < 0.01$ , \*\*,  $P < 0.05$ , \*\*\*,  $P < 0.001$ , between equal concentrations of colchicine and \$;  $P < 0.01$ , \$\$;  $P < 0.05$ , \$\$\$;  $P < 0.001$ , between different concentrations of colchicine. **C.** Colchicine effects on the expression of *BAX/BCL-2* in MCF-7 and 4T1 cells. Data are given as mean  $\pm$  SE for each point of three separate experiments. \*,  $P < 0.01$ , \*\*,  $P < 0.05$ , \*\*\*,  $P < 0.001$  vs. control and \$;  $P < 0.01$ , \$\$;  $P < 0.05$ , \$\$\$;  $P < 0.001$  vs. equal concentrations of isolated and standard colchicine (drug).

### The effect of colchicine on the level of apoptosis-related proteins

In this experiment, the effect of colchicine-induced apoptosis on MCF-7 and 4T1 cells was investigated, the constitutive expression of typical apoptosis-related

proteins of P53, Bax, Bcl-2, Caspase-3, Caspase-9 and  $\beta$ -Actin (as the reference protein) by Western blot method. The results showed that after 24 hours of treatment, the levels of pro-apoptotic proteins (P53 and Bax) increased, while the expression of anti-apoptotic proteins of the Bcl-2 family decreased (Fig.4A).

Compared to the controls (untreated group), treating MCF-7 cells with 0.5  $\mu\text{g/ml}$  of standard colchicine led to an 82% decrease in pro-apoptotic protein Bax level (Fig.4B). The isolated colchicine also induced the same effect on Bax level (85%) in these human cells. However, at higher concentrations of both standard and isolated colchicine (1  $\mu\text{g/ml}$ ), 27% and 5% increases were seen in Bax level, respectively. The expression level of the anti-apoptotic protein Bcl-2 in the treated cells with 0.5  $\mu\text{g/ml}$  of the standard colchicine significantly decreased (94%) but isolated colchicine at the same concentration increased the Bcl-2 level by 2.7%. On the other hand, 1  $\mu\text{g/ml}$  of the standard colchicine caused a 13% decrease in Bcl-2 level, but the isolated colchicine induced a 1.5% increase in Bcl-2 expression level.

The level of pro-apoptotic protein, Bax, in the case of 4T1 cells showed an 87% decrease and 83% increase after exposure to 200  $\mu\text{g/ml}$  of the standard and the isolated colchicine, respectively (Fig.4C). But at a higher concentration (400  $\mu\text{g/ml}$ ), the standard and isolated colchicine had opposite effects (64% increase and 7% decrease, respectively). The expression level of the anti-apoptotic protein of Bcl-2 in 4T1 cells treated with 200  $\mu\text{g/ml}$  of the standard and the isolated colchicine was decreased by 55% and 41%, respectively. This is while at 400  $\mu\text{g/ml}$ , the standard and isolated colchicines induced 42% and 44% decrease in Bcl-2 expression level, respectively.

### The effect of colchicine on Caspase-3, -9 activities in MCF-7 and 4T1 cells

Based on the results, which are presented in Figures 4B, C, the expression levels of Caspase-3, -9 protein decreased compared to the controls. By considering that our used antibodies detected the pre-caspases, reduction in the pre-caspases level can be due to their turnover into active caspases in the apoptosis pathway.

### Apoptotic effect of colchicine on MCF-7 and 4T1 cells

100 treated and 100 untreated cells were counted from MCF-7 and 4T1 cell lines under the fluorescence microscope after Annexin-V/PI staining to determine the early and late apoptosis (Figs.5, 6). After 24-hours of treatment with the isolated and standard colchicine, the early apoptosis percentage of the treated MCF-7 cells at the dose of 0.5  $\mu\text{g/ml}$  were 20% and 24% and at the dose of 1  $\mu\text{g/ml}$  were 14% and 18%, respectively. These results showed a significant apoptotic effect compared to the controls (\* $P < 0.05$  and \*\* $P < 0.001$ ).

A significant difference was also observed between the late and early apoptosis at the same concentration of the isolated and standard colchicine ( $^{\$}P<0.05$  and  $^{\$\$}P<0.001$ , Fig.5F).

In the case of 4T1 cells treated with the isolated and standard colchicines, the early apoptosis percentage was determined as 12% and 30% at 200  $\mu\text{g/ml}$  and 6% and 8% at 400  $\mu\text{g/ml}$ , respectively (Fig.6F). That means a significant apoptotic effect of both colchicines ( $^*P<0.05$  and  $^{**}P<0.001$ ). Additionally, a significant difference was also observed between the late and early apoptosis with equal concentrations of the isolated and standard colchicines ( $^*P<0.05$  and  $^{**}P<0.001$ , Fig.6F).

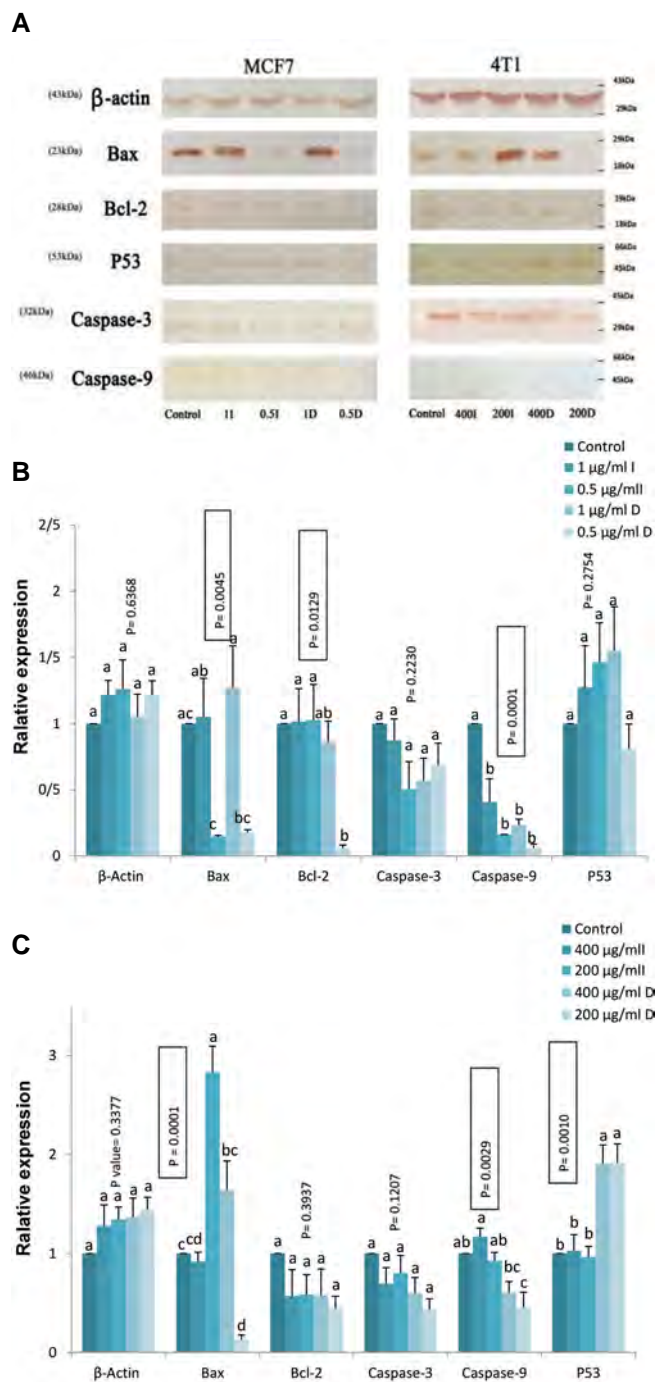


**Fig.4:** Expression of pro-apoptotic and anti-apoptotic proteins and densitometric analysis. **A.** The effects of colchicine on the expression of pro-apoptotic and anti-apoptotic proteins in MCF-7 and 4T1 cells. Cells were exposed to the isolated and standard colchicine (drug) at 0.5 and 1  $\mu\text{g/ml}$  and 200 and 400  $\mu\text{g/ml}$ , respectively for 24 hours. The protein expression of P53, Bax, Bcl-2, caspase-3 and -9 was determined by Western blotting against controls, **B.** Densitometry analysis of P53, Bax, Bcl-2, Caspase-3 and -9 proteins in MCF-7 cell line, and **C.** Densitometry analysis in 4T1 cell line. Data are given as mean  $\pm$  SE for each point of three separate experiments. Different letters indicate a significant difference ( $P<0.05$ ) and the same characters indicate a non-significant difference between the treatments ( $P>0.05$ ). I; Isolated and D; Drug.

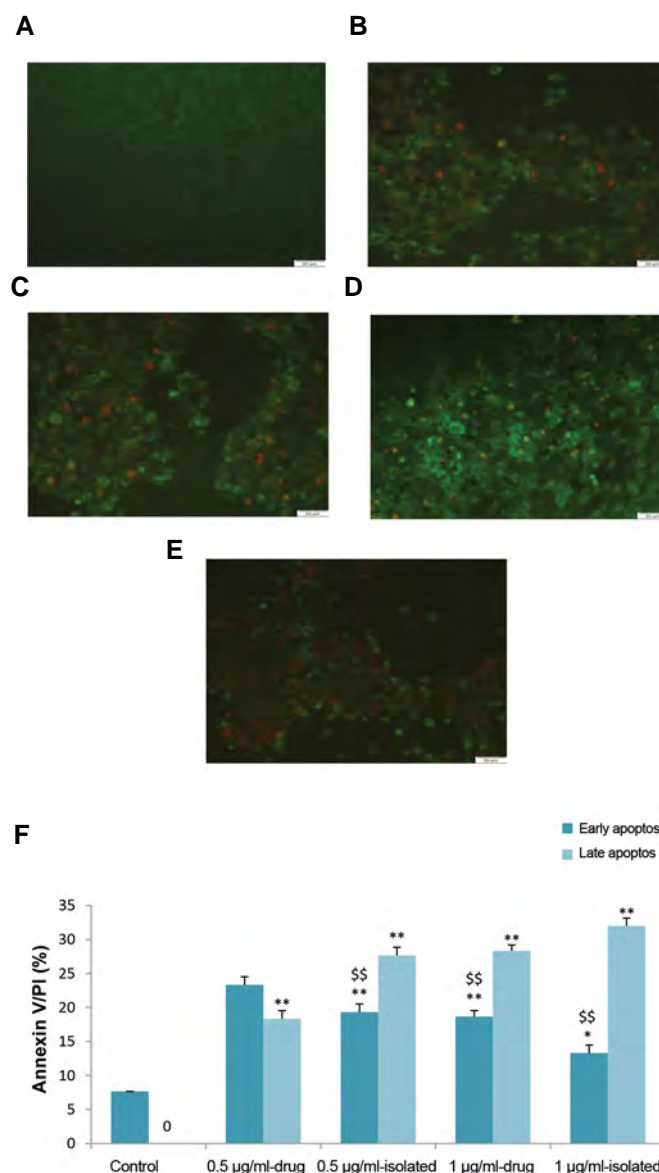


**Fig.5:** Results of Fluorescence Microscope image and early and late apoptosis of MCF-7 cells. **A.** Untreated cells as the control group, **B.** Treated cells with 0.5  $\mu\text{g/ml}$  of standard colchicine (drug), **C.** Treated cells with 1  $\mu\text{g/ml}$  of standard colchicine (drug), **D.** Treated cells with 0.5  $\mu\text{g/ml}$  of isolated colchicine (scale bar: 50  $\mu\text{m}$ ), and **E.** Treated cells with 1  $\mu\text{g/ml}$  of isolated colchicine (scale bar: 50  $\mu\text{m}$ ), and **F.** The results of early and late apoptosis in MCF-7 cells determined by Annexin V-PI method.  $^{**}$ ;  $P<0.001$  vs. control, and  $^{\$}$ ;  $P<0.001$  vs. equal concentrations of isolated and standard colchicine (drug).

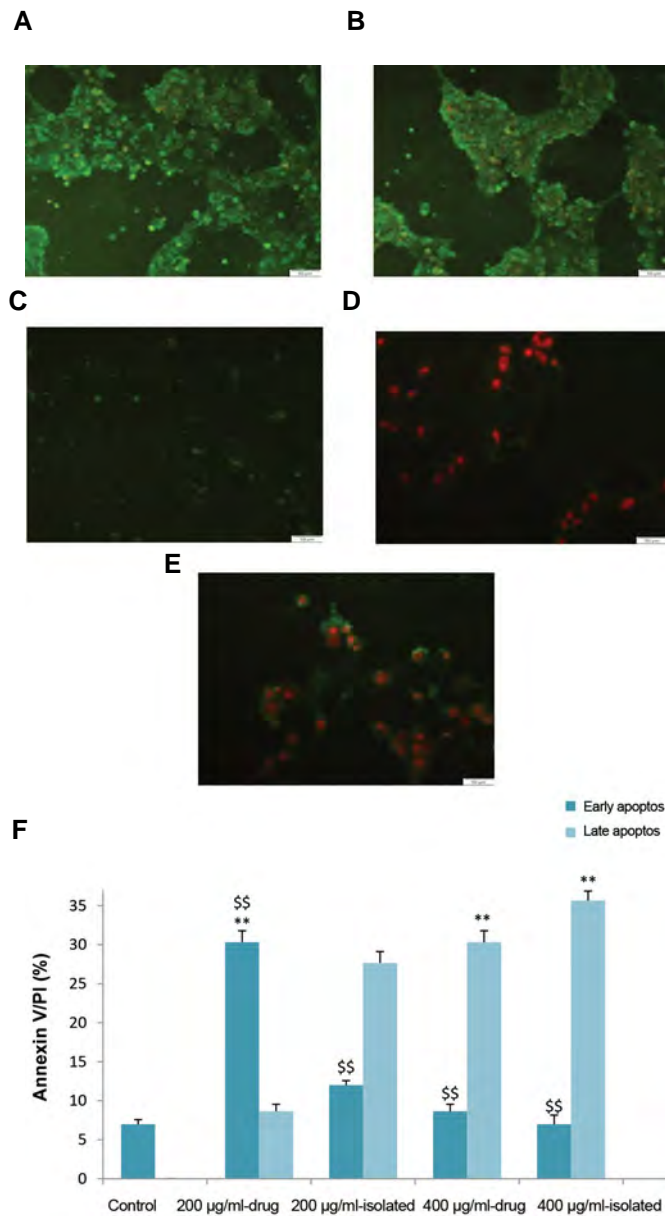


**Fig.6:** Results of Fluorescence Microscope image and early and late apoptosis of 4T1 cells. **A.** Untreated cells as control group, **B.** Treated cells with 200 µg/ml of standard colchicine, **C.** Treated cells with 400 µg/ml of standard colchicine (drug), **D.** Treated cells with 200 µg/ml of isolated colchicine, **E.** Treated cells with 400 µg/ml of standard colchicine (drug) (scale bar: 50 µm), and **F.** Results of early and late apoptosis in 4T1 cells determined by Annexin V-PI method. \*\*; P<0.001 vs. control and \$\$; P<0.001 vs. same concentration of isolated and standard colchicine (drug).

## Discussion

Herein, for the first time, we try to uncover some possible effects of isolated colchicine of *Colchicum autumnale* on MCF-7 and 4T1 cell cycle, growth and apoptosis. The isolated colchicine, which was (compared to standard colchicine) induced cytotoxic effects on MCF-7 and 4T1 cells in a dose-dependent manner. Our results revealed that low concentrations of colchicine (1-2 µg/ml) had a significant cytotoxic effect on the MCF-7 cell line compared to healthy human fibroblast cells (6 µg/ml). In contrast, the cytotoxic effect of colchicine on 4T1 cell line was observed at a concentration of 300 µg/ml (vs. 6 µg/

ml on fibroblasts). Purified and standard colchicines both appear to reduce the growth of cancer cells at much lower concentrations (4-8 ng/ml) compared to the cytotoxic concentrations. This suggest that at low concentration, colchicine has an antiproliferative effect on these cancer cells, while at high concentrations it turns out to be cytotoxic. This is a very crucial factor to consider in chemotherapy planning when choosing a suitable anti-cancer agent. However, these *in vitro* results need to be confirmed by *in vivo* investigation.

The cytotoxic and growth inhibition effects of colchicine on mouse breast cancer cells, however, were observed at 300 and 200 µg/ml, respectively. Previous studies have revealed that colchicine at the concentrations of 2 ng/ml, 4 ng/ml, 6 ng/ml and 0.04-4 µg/ml, has a significant anti-proliferative effect on cholangiocarcinoma, hepatocellular carcinoma (HCC), neuronal cells, gastric cancer cells and healthy liver cells (L-02), which can confirm our results (10-14). These results indicated that various cell types have different susceptibility and sensitivity to colchicine toxicity. Therefore, we believe that this remarkable concentration difference of colchicine to induces an anti-proliferative effect between these two cell lines can be possibly due to mutations in *p53* gene or other unknown mutations in the mouse breast cancer cells (4T1).

The cell cycle could be an appropriate target for anti-cancer drugs to induce apoptosis (17-19). Colchicine is a natural alkaloid that binds to tubulin, inhibits the formation of microtubules in mitotic spindles and therefore prevents cell division to finally be recognized as a well-known anti-cancer agent (5, 7, 20-22). Here, we have shown that both isolated and standard colchicine lead to different expression levels of several genes that have anti-cancer effects on human (MCF-7) and mouse (4T1) breast cancer cells.

Apoptosis, as a gene-controlled process, can be mediated through two pathways: mitochondrial (intrinsic) pathway or death receptor (extrinsic) pathway (23). More than 100 different genes have been identified to be involved in cell survival. It is revealed that two families of caspases and the *BCL-2* gene directly involved in apoptosis (24). The intrinsic pathway is initiated due to the release of mitochondrial proteins, for instance cytochrome c, which further binds to Apaf-1 and converts procaspase-9 to active caspase-9, leading to activation of caspase-3 and finally inducing apoptosis (25-27). It is well known that the balance between replication and apoptosis is interrupted in cancer cells, therefore apoptosis plays the key role in inhibition of their growth and proliferation. Accordingly, there is a reverse relationship between expression of the apoptosis-related genes and cancerous process.

In this study, the expression levels of apoptosis-related proteins including P53, Bax, Bcl-2, caspase-3 and caspase-9 activities were investigated to help us in understanding the molecular mechanisms of colchicine's anticancer and apoptosis-inducing effects. The results

indicated a dose-dependent up-regulation of P53 and Bax proteins, down-regulation of Bcl-2 and activation of caspase-3 and -9 as well. These results are consistent with the findings in other types of malignancies (28-31).

Several studies have demonstrated that apoptosis is mainly regulated by the Bcl-2 family members; either through activation of Bax or inhibition Bcl-2 (32). As it is revealed, during apoptosis the levels of Bcl-2 family proteins are significantly reduced while, the level of Bax is increased remarkably (33). Our results indicated that colchicine-induced apoptosis relates to an augmented level of Bax and down-regulated Bcl-2, which finally lead to apoptosis of human and mouse breast cancer cells. In a study by Gundamaraju et al. (34), the effect of colchicine on the expression levels of *BAX* and *BCL-2* genes was evaluated in some mammalian cells. Their results showed a significant increase in the *BAX* gene expression level, while the *BCL-2* gene expression was unaffected. In our study, the level of *BAX* gene expression increased significantly, while in some cases the expression level of the *BCL-2* gene was not affected. The balance between *BCL-2* (anti-apoptotic) and *BAX* (pro-apoptotic) is the most critical parameter determining a cell's fate in response to extracellular stimuli.

This clearly suggests that increasing *BAX/BCL-2* ratio might be the means by which colchicine induces apoptosis. In many studies the apoptotic Mechanism of action of colchicine of colchicine has been assessed on neurons and liver cancer cells, but its exact mechanism of action, especially in breast cancer, is still unclear. In this study, the apoptotic features of colchicine are very similar to the results from other studies. These data indicate an increased expression level of Bax and p53 proteins, decreased expression of Bcl-2, and activated caspases-3 and -9. Therefore, based on the evidence and despite the lack of examination on the release of cytochrome c from mitochondria, it can be suggested that colchicine induces apoptosis in MCF-7 and 4T1 cells through the mitochondrial pathway (intrinsic pathway).

There are many questions yet to be answered that will require investigations beyond evaluating gene expressions. It has been demonstrated that protein production level is not quite in proportion to its mRNA level. Likewise, mRNA level is not often an exact indicator of protein expression, since they may contain multiple copies of one or a certain number of proteins (35, 36). In this regard, our results also showed that in our studied cell lines, there is no definite relationship between mRNA level and protein production of *P53*, *BCL-2* and *BAX* genes. However, the analysis of proteins involved in apoptosis clearly showed that both types of colchicine induce apoptosis (through increasing Bax and P53 and decreasing Bcl2 expressions) and interestingly, isolated colchicine was found as effective as the standard one.

## Conclusions

In summary, we isolated colchicine from *C. autumnale*

*L.* with physicochemical and biological characteristics similar to standard colchicine. We showed that the apoptotic effects of the isolated colchicine from *C. autumnale* *L.* were as strong as the standard colchicine or even better in some cases, due to the tropolone alkaloids compounds. Further investigation is required to evaluate this combination for therapy. Moreover, appropriate *in vivo* (animal cancer models and then human) studies are needed in order to uncover additional possible colchicine's mechanisms of action.

## Acknowledgements

The authors thank our colleagues at Medical Biology Research Center of Kermanshah University of Medical Sciences for their assistance and valuable suggestions throughout the project. This work was financially supported by Kermanshah University of Medical Sciences under Grant 92100. There is no conflict of interest in this study.

## Authors' Contributions

A.M.; Conceived the first idea of the project, planned the experiments, and performed the final revision. A.M., Sh.I.; Supervised the project. E.A.F.; Acquisition of the experimental data and written the first draft of the manuscript. A.M., Y.Sh., Sh.I.; Performed the analysis and interpretation of the data. All authors read and approved the final manuscript.

## References

1. Sung H, Ferlay J, Siegel RL, Laversanne M, Soerjomataram I, Jemal A, et al. Global cancer statistics 2020: GLOBOCAN estimates of incidence and mortality worldwide for 36 cancers in 185 countries. *CA Cancer J Clin.* 2021; 71: 209-249
2. Ferlay J, Colombet M, Soerjomataram I, Mathers C, Parkin DM, Piñeros M, et al. Estimating the global cancer incidence and mortality in 2018: GLOBOCAN sources and methods. *Int J Cancer.* 2019; 144(8): 1941–1953.
3. Le Saux O, Ripamonti B, Bruyas A, Bonin O, Freyer G, Bonnefoy M, et al. Optimal management of breast cancer in the elderly patient: current Perspectives. *Clin Interv Aging.* 2015; 10: 157-174.
4. Capistrano R, Vangestel C, Wouters A, Dockx Y, Pauwels P, Stroobants S, et al. Efficacy screening of *Gloriosa superba* extracts in a murine pancreatic cancer model using (18)F-FDG PET/CT for monitoring treatment response. *Cancer Biother Radiopharm.* 2016; 31(3): 99–109.
5. Dasgeb B, Kornreich D, McGuinn K, Okon L, Brownell I, Sackett DL. Colchicine: an ancient drug with novel applications. *Br J Dermatol.* 2018; 178(2): 350–356.
6. Toplan GG, Gurer C, Mat A. Importance of *Colchicum* species in modern therapy and its in Turkey. *J Fac Pharm Ist.* 2016; 46(2): 129–144.
7. Kumar A, Sharm PR, Mondhe DM. Potential anticancer role of colchicine-based derivatives: an overview. *Anticancer Drugs.* 2017; 28(3): 250–262.
8. Forkosh E, Kenig A, Ilan Y. Introducing variability in targeting the microtubules: Review of current mechanisms and future directions in colchicine therapy. *Pharmacol Res Perspect.* 2020; 8(4): e00616.
9. Slobodnick A, Shah B, KrasnoKutsky S: Update on colchicine, 2017. *Rheumatology (Oxford).* 2018; 57 Suppl 1: i4-i11.
10. Lin ZY, Kuo CH, Wu DC, Chuang WL. Anticancer effects of clinically acceptable colchicine concentrations on human gastric cancer cell lines. *Kaohsiung J Med Sci.* 2016; 32(2): 68-73.
11. Zhang T, Chen W, Jiang X, Liu L, Wei K, Du H, et al. Anticancer effects and underlying mechanism of Colchicine on human gastric cancer cell lines in vitro and in vivo. *Biosci Rep.* 2019; 39(1):

- BSR20181802.
12. Lin ZY, Yeh ML, Huang CI, Chen SC, Huang CF, Huang JF, et al. Potential of novel colchicine dosage schedule for the palliative treatment of advanced hepatocellular carcinoma. *Kaohsiung J Med Sci.* 2021; 37(7): 616-623.
  13. Chen XM, Liu J, Wang T, Shang J. Colchicine-induced apoptosis in human normal liver L-02 cells by mitochondrial mediated pathways. *Toxicol In Vitro.* 2012; 26(5): 649-655.
  14. Wu CC, Lin ZY, Kuoc CH, Chuang WJ. Clinically acceptable colchicine concentrations have potential for the palliative treatment of human cholangiocarcinoma. *Kaohsiung J Med Sci.* 2015; 31(5): 229-234.
  15. Leung YY, Yao Hui LL, Kraus VB. Colchicine--Update on mechanisms of action and therapeutic uses. *Semin Arthritis Rheum.* 2015; 45(3): 341-350.
  16. Alali FQ, Tawaha K, El-Elimat T. Determination of (–)-demecolcine and (–)-colchicine content in selected Jordanian Colchicum species. *Pharmazie.* 2007; 62(10): 739–742.
  17. Abaza MS, Orabi KY, Al-Quattan E, Al-Attayah RJ. Growth inhibitory and chemo-sensitization effects of naringenin, a natural flavanone purified from *Thymus vulgaris*, on human breast and colorectal cancer. *Cancer Cell Int.* 2015; 15: 46.
  18. Hauck L, Grothe D, Billia F. p21(CIP1/WAF1)-dependent inhibition of cardiac hypertrophy in response to Angiotensin II involves Akt/MyoD and pRb signaling. *Peptides.* 2016; 83: 38–48.
  19. Cheng W, Yang Z, Wang S, Li Y, Wei H, Tian X, Kan Q. Recent development of CDK inhibitors: An overview of CDK/inhibitor co-crystal structures. *Eur J Med Chem.* 2019; 164: 615–639.
  20. Pierens GK, Venkatachalam TK, Reutens DC. NMR and DFT investigations of structure of colchicine in various solvents including density functional theory calculations. *Sci Rep.* 2017; 7: 5605.
  21. Borys F, Tobiasz P, Poterała M, Krawczyk H. Development of novel derivatives of stilbene and macrocyclic compounds as potent of anti-microtubule factors. *Biomed Pharmacother.* 2021; 133: 110973.
  22. Johnson L, Goping IS, Rieger A, Mane JY, Huzil T, Banerjee A, et al. Novel colchicine derivatives and their anti-cancer activity. *Curr Top Med Chem.* 2017; 17(22): 2538-2558.
  23. Fuchs Y, Steller H. Live to die another way: modes of programmed cell death and the signals emanating from dying cells. *Nat Rev Mol Cell Biol.* 2015; 16(6): 329–344.
  24. Vervliet T, Parys JB, Bultynck G. Bcl-2 proteins and calcium signaling: complexity beneath the surface. *Oncogene.* 2016; 35(39): 5079–5092.
  25. Lopez J, Tait SW. Mitochondrial apoptosis: killing cancer using the enemy within. *Br J Cancer.* 2015; 112(6): 957–962.
  26. Cao K, Tait SWG. Apoptosis and cancer: force awakens. phantom menace, or both? *Int Rev Cell Mol Biol.* 2018; 337: 135–152.
  27. Galluzzi L, López-Soto A, Kumar S, Kroemer G. Caspases connect cell-death signaling to organismal homeostasis. *Immunity.* 2016; 44(2): 221–231.
  28. Daley-Brown D, Oprea-Ilie GM, Lee R, Pattillo R, Gonzalez-Perez RR. Molecular cues on obesity signals, tumor markers and endometrial cancer. *Horm Mol Biol Clin Investig.* 2015; 21(1): 89–106.
  29. Labi V, Erlacher M. How cell death shapes cancer. *Cell Death Dis.* 2015; 6(3): e1675.
  30. Hou Z, Cui Y, Xing H, Mu X. Down-expression of poly(ADP-ribose) polymerase in p53-regulated pancreatic cancer cells. *Oncol Lett.* 2018; 15(2): 1943–1948.
  31. Watanabe G, Ishida T, Furuta A, Takahashi S, Watanabe M, Nakata H, et al. Combined immunohistochemistry of PLK1, p21, and p53 for predicting TP53 status: An independent prognostic factor of breast cancer. *Am J Surg Pathol.* 2015; 39(8): 1026–1034.
  32. Kale J, Osterlund EJ, Andrews DW. BCL-2 family proteins: changing partners in the dance towards death. *Cell Death Differ.* 2018; 25(1): 65-80.
  33. Hata AN, Engelman JA, Faber AC. The BCL2 Family: Key mediators of the apoptotic response to targeted anticancertherapeutics. *Cancer Discov.* 2015; 5(5): 475-487.
  34. Gundamaraju R, Vemuri R, Chong WC, Geraghty DP, Eri R. Cell stress signaling cascades regulating cell fate. *Curr Pharm Des.* 2018; 24: 3176-3183.
  35. Koussounadis A, Langdon SP, Um IH, Harrison DJ, Smith VA. Relationship between differentially expressed mRNA and mRNA-protein correlations in a xenograft model system. *Sci Rep.* 2015; 5: 10775–10775.
  36. Liu Y, Beyer A, Aebersold R. On the dependency of cellular protein levels on mRNA abundance. *Cell.* 2016; 165(3): 535-550.

# PRDX1 Influences The Occurrence and Progression of Liver Cancer by Inhibiting Mitochondrial Apoptosis Pathway

Hong-hua Sun, M.D.<sup>1</sup>, Yang-long Li, M.D.<sup>1</sup>, Hao Jiang, M.D.<sup>1</sup>, Xiang-hua Yin, M.D.<sup>1</sup>, Xing-lin Jin, M.D.<sup>2\*</sup>

1. Department of Oncology, Yanbian University Hospital (Yanbian hospital), Yanji, China  
2. Department of Hepatobiliary Surgery, Yanbian University Hospital (Yanbian hospital), Yanji, China

\*Corresponding Address: Department of Hepatobiliary Surgery, Yanbian University Hospital (Yanbian hospital), Yanji, China  
Email: jinxinglin\_yuh@126.com

Received: 04/August/2021, Accepted: 09/March/2022

## Abstract

**Objective:** The aim of this study is to elucidate the role of *PRDX1* in hepatocellular carcinoma using hepatoma cells.

**Materials and Methods:** In this experimental study, we elucidated role of *PRDX1*, using hepatoma cell lines.

**Results:** *PRDX1* was upregulated in different types of cancers, including lung adenocarcinoma, breast cancer and liver cancer reported by several studies. nevertheless, mechanism of inducing liver cell death by *PRDX1* remains largely unknown. Here, we showed that *PRDX1* expression is enhanced in different cell lines. Here, we used western blot, quantitative real time polymerase chain reaction (qRT-PCR) and different biochemical assays to explore the role of *PRDX1*. We observed that overexpression of *PRDX1* significantly enhanced proliferation of hepatoma cell lines, while knock-down of this gene showed significant inhibitory effects. We found that knock-down of *PRDX1* activated cleaved caspase-3, caspase-9 proteins and Poly [ADP-ribose] polymerase 1 (PARP-1), which further executed apoptotic process, leading to cell death. We found that *PRDX1* knock-down significantly produced mitochondrial fragmentation. We showed that silencing *PRDX1* led to the loss of B-cell lymphoma 2 (Bcl-2) and activated Bcl-2-like protein 11 (Bim) which further induced Bax activation. Bax further released cytochrome c from mitochondria and induced apoptotic proteins, suggesting a significant role of *PRDX1* knock-down in apoptosis. Finally, we showed that knock-down of *PRDX1* significantly activated expression of Dynein-related protein 1 (Drp1), fission 1 (Fis1) and dynamin-2 (Dyn2) suggesting a crucial role of *PRDX1* in mitochondrial fragmentation and apoptosis conditions. This study highlighted an important role of *PRDX1* in regulating proliferation of hepatoma cells and thus future studies are required to validate its effect on hepatocytes.

**Conclusion:** We propose that future works on *PRDX1* inhibitors may act as a therapeutic candidate for treatment of liver cancer.

**Keywords:** Hepatocellular Carcinoma, Liver Cancer, Peroxiredoxins, *PRDX1*

Cell Journal (Yakhteh), Vol 24, No 11, November 2022, Pages: 657-664

**Citation:** Sun Hh, Li Yi, Jiang H, Yin Xh, Jin Xi. *PRDX1* influences the occurrence and progression of liver cancer by inhibiting mitochondrial apoptosis pathway. Cell J. 2022; 24(11): 657-664. doi: 10.22074/cellj.2022.8159.

This open-access article has been published under the terms of the Creative Commons Attribution Non-Commercial 3.0 (CC BY-NC 3.0).

## Introduction

Human hepatocellular carcinoma (HCC) is one of the most common types of liver cancer, which accounts for more than 70% of total liver cancer. It is known for the high mortality rate (>8%) worldwide. Peroxiredoxins are a large family of antioxidant enzymes that play an essential role in antioxidant defense and peroxide detoxification. *PRDX1* is a multifunctional protein involved in cell growth, differentiation and apoptosis (1). *PRDX1* is reported in different types of cancer, including lung adenocarcinoma, breast cancer, soft tissue sarcomas (2), colorectal cancer and prostate cancer. Most studies reported elevated level of *PRDX1* in pathological conditions.

However, Fang et al. (3) showed the lower *PRDX1* expression in HCC cells. *PRDX1* is upregulated in cervical cancers and enhanced proliferation, migration and invasion by inhibiting apoptosis (4). Analysis of a disease model represented higher *PRDX1* expression level in brain, while it is associated with toll like

receptor-4 (TLR-4) inflammation and apoptosis. Several studies reported its expression in tumor tissues of the liver (3). However, the cellular role of *PRDX1* in hepatocellular carcinoma and mechanism of this association with related protein remains unknown. Caspases are essential proteins. They are activated when cell death is required (5). Poly ADP-ribose polymerase 1 (PARP-1) has multiple functions involved in DNA repair, cell death and transcriptions of some essential genes involved in inflammatory processes (6). It is a well-known substrate of caspase proteins (7). Caspase-3 cleaves PARP-1 upon activation and therefore prevents PARP-1 from repairing the damage (8). It has been demonstrated that overexpression of human Mitochondrial fission 1 protein (hFis1) induced apoptosis, which may suggest a role of mitochondrial fission in apoptosis. Dynein-related protein 1 (Drp1) expression is upregulated in HCC cells and involved in autophagy (9).

Here, in this study, we elucidated role of *PRDX1*

in hepatocellular carcinoma using hepatoma cells. The role of *PRDX1* on hepatocytes cells was poorly known. We reported for the first time that the mechanism by which *PRDX1* acts on HCC cells via B-cell lymphoma 2 (Bcl-2).

## Materials and Methods

### RNA sequencing database

In this experimental study, the RNA sequencing data from more than 350 patients of liver cancer were obtained from TCGA database. The expression of *PRDX1* mRNA were analyzed using the database. The Kaplan-Meier and Cox regression survival analysis was performed to see the relationship between *PRDX1* levels and patient survival.

### Cell culture

HCC cells were obtained from ATCC (Virginia, USA). Cell culture media and supplements were purchased from Gibco (Sigma, USA). HCC cells were cultured in DMEM high glucose medium supplemented with 2 mM glutamine, 100 units/ml penicillin (both from Gibco, USA), 10 % fetal calf serum (ThermoFisher, USA) and 100 lg/ml, streptomycin (Gibco, USA). Cells were grown at 37°C in the presence of 5% CO<sub>2</sub>. Cells were grown for 2-3 days. Following the confluency, the cells were proceeded for analysis of mRNA or protein expressions.

### Quantitative reverse transcription polymerase chain reaction

Extraction of total RNA was done by Trizol reagent (Ambion, USA). Synthesis of cDNA was done by RevertAid cDNA Synthesis Kit (Thermo Fisher Scientific, USA) for that 1 µg of total RNA of each sample was used. The cDNA samples were kept at -20°C for quantitative reverse transcriptipn PCR (qRT-PCR). The SYBR green dye (Invitrogen, USA) was used to bind to double stranded DNA and emit green light (λ<sub>max</sub>=520 nm), in terms of quantifying cDNA. For qRT-PCR, the master mix was used as the manufacturer's instruction. Specific primers of *PRDX1* and *GAPDH* were used (Table 1). Data was acquired and analyzed using comparative CT method.

**Table 1:** Primer information

Gene name	Primer sequence (5'-3')
<i>PRDX1</i>	F: GCACCATTGCTCAGGATTATG
	R: GCCAACAGGGAGGTCATTTAC
<i>GAPDH</i>	F: GGTGTGAACCATGAGAAGTATGA
	R: GAGTCCTCCACGATACCAAG

### Cells transfection

The *PRDX1*-siRNA are 5'GCACCAUUGCUCAG-GAUUATT3' which was synthesized by GenePharma (Shanghai, China). HepG2 Cells were seeded and transfected using Lipofectamine 2000 reagent (Invitrogen, USA) following manufacturer's instructions. 3×10<sup>4</sup> cells were seeded and allowed to 70-90% confluency. Transfection mixture was prepared with 50 ng, 25 µl DNA dilution and 25 µl opti-MEM (Gibco, USA) dilution. Mixing Lipofectamine 2000 diluent and DNA diluent was performed in a centrifuge tube with a capacity of 1.5 ml, followed by 15 minutes incubation in hood. Optimum medium was removed and DNA/lipofectamine 2000 mixture was gently added dropwise into cells.

### Western blotting

Lysis buffer (200 µl/well) was used to lyse HepG2 cells. Lysis buffer was composed of Triton X-100 (1%), Tris (50 mM, pH=7.6) and NaCl (150 mM), with inhibitors of phosphatases and proteases. sodium dodecyl sulfate polyacrylamide gel electrophoresis (SDS-PAGE, 7.5%) was used to separate 40 µg of the total extracted protein. Then Western blotting was done as demonstrated by Moeschel et al. (10). Following the application of antibodies for western blotting anti-*PRDX1* (ab109498), anti-beta actin (ab115777), anti caspase-3 (ab13847 and ab32042), anti-cleave caspase-9 (ab202068 and ab25758), anti-PARP-1 (ab191217), anti-Bim (ab7888), anti-Fis1 (ab189846), anti-APaf-1 (ab254248), anti-cytochrome c (ab133504), anti-Bcl-2 (ab182858), anti-Bax (ab3191), anti-DRP1 (ab184247) and anti-Dyn2 (ab65556; all purchased from AbCam, UK). Nitrocellulose was blocked using skimmed milk (5%) or BSA (2%, both from Merck, Germany) for two hours. Subsequently, membranes were incubated with primary antibodies at 4°C overnight. Before incubation with secondary antibody, washing was performed (four times for 10 minutes), followed by appropriate conjugated secondary incubation for one hour. For visualizing expression level of proteins, enhanced chemiluminescence was performed.

### Cell counting assay

For detecting proliferation, the number of living cells was determined with CCK-8 kit (ab228554, AbCam, UK), according to the manufacturer's instructions. In 96-well plate HepG2 cells were cultivated (five thousands cells in each well). In the incubator, the cells were seeded for 24, 48 and 72 hours. After that, four hours incubation was performed on the cells containing CCK-8 reagent (10 µl). Lastly, optical density was determined at wave length of 450 nm.

### Annexin V-FITC-PI staining analysis

HepG2 Cells were stained with Annexin V-FITC/PI

(ab14085, AbCam, UK), following the manufacturer's guidelines. Firstly HCC cells were harvested via trypsinization, then washed with PBS buffer. Centrifugation was done and pellet was collected. The cells were re-suspended with binding buffer. Incubation was performed with annexin V-FITC and propidium iodide (PI) for 10 minutes on ice in dark environment. For detection of apoptotic cells flow cytometry was performed. Binding buffer (150  $\mu$ l) was added to the sample tubes before analysis on flow cytometry. Data was generated on FACS (Becton Dickinson, USA). Then Cell-Quest software (Becton Dickinson) was used for analyzing or processing the given data.

### Clone formation assay

Clone forming assay is an *in vitro* assay which enable single cell to form a colony. Suspension of single cell was made by digesting cells in culture media with (0.25%) or EDTA (0.02%) during logarithm stage. HepG2 Cells were counted via counting chamber in 10  $\mu$ l suspension using inverted microscope and equal amount of cells were plated in 6-well culture plate. Each well was covered by sterile cover slips. Until formation of colonies, medium was changed every four days. After fixation of colonies with methanol, staining was performed by using crystal violet (1%). Differences in colony formation was observed in the all groups.

### Confocal microscopy

MitoTracker red staining was used to analyze mitochondrial filamentous morphology of cells. MitoTracker probes was diluted to 1 mM by adding DMSO. Staining procedure with MitoTracker Red (M22425) and CMXRos (E-max 599 nm; both from ThermoFisher) was performed as described earlier by Harwig et al. (11). Fifty nM MitoTracker™ was used for cells and incubated for 30 minutes at 37°C and. The cells were next washed with FluoroBrite DMEM medium (Gibco, USA), supplemented with 10% fetal cow serum (FCS). Additionally, HepG2 cells were stained with DAPI targeting DNA in nucleus. After staining, the cells were observed under confocal microscope.

### Statistical analysis

All experiments were performed three times. Represented data were analyzed by using GraphPad Prism (Graphpad software, Inc., San Diego, CA). Multiple groups differences were analyzed using one-way ANOVA.  $P < 0.05$  was considered to be statistically significant.

## Results

### *PRDX1* is upregulated in liver cancers cells

Given the role of *PRDX1* as an antioxidant system and regulating oxidation reductions, its expression level is critical. Higher-level expression was reported by several

studies in different malignancies, including lung (12), cervical (13), prostate (14) and liver cancers (4). However, limited studies reported *PRDX1* expression in human specimens. Significant difference in *PRDX1* expression using TCGA public database was observed, we found that transcripts of *PRDX1* had a significant differences between cancerous and paracancerous tissues of liver cancer patients (Fig.1A). *PRDX1* mRNA expression was found to have a higher expression of 1.3 fold in cancerous tissues compared to control (15). *PRDX1* transcript and protein expression levels were significantly higher in different cancerous cell lines (HepG2, Huh-7, Hep-3B) compared to control cells (Fig.1B-D), which are consistent with the other studies. The highest *PRDX1* mRNA and protein level were found in HepG2 cells with 3-fold higher expression compared to control.

### *PRDX1* knock-down induced apoptosis in hepatoma cells

Based on the higher expression of *PRDX1* in most of the cancerous tissues and cells, we were interested to see its cellular role. We overexpressed the *PRDX1* construct in HCC cells and tested the efficiency of transfection. We found almost 3-fold higher mRNA and protein expression of *PRDX1* using hepatoma cells, while using siRNA against *PRDX1* (si-*PRDX1*) significantly inhibited its expression (Fig.2A, 2B). Figure 2C shows relative expression level of *PRDX1*, in the presence of si-RNA. Cell counting kit-8 (CCK-8) is a widely used colorimetric-based assay used to measure cells viability. We wanted to test the effect of *PRDX1* on HCC cell proliferations. We found that knock-down of *PRDX1* significantly decreased half maximal inhibitory concentration ( $IC_{50}$ ) value of HCC cells, suggesting that Knock-down of *PRDX1* possesses great anti-tumor activity (Fig.2D). This was further confirmed by clonal formation assay, which was used to assess effect of *PRDX1* expression on the proliferation of hepatoma cells. *PRDX1* overexpression significantly enhanced proliferation of hepatoma cells (Fig.2E, middle panel) compared to control cells, while knock-down of *PRDX1* showed significant inhibitory effects and reduced cell proliferations. Next, we were interested to see its effect on caspase proteins. Interestingly, we found that knock-down of *PRDX1* induced cell death via activation of cleaved and active caspase-3 and caspase-9, which further executed an apoptotic process, leading to cell death and inhibited proliferation of hepatoma cells (Fig.2F, G). As overexpression of *PRDX1* played a role in cellular proliferation, it regulated PARP-1 to inhibit apoptosis, while knock-down of *PRDX1* greatly increased PARP-1 expression, suggesting depletion of  $NAD^+$  levels, thereby induced cellular death (Fig.2G). Figure 2H represents statistical analysis of western blot protein. These results suggested that *PRDX1* knock-down inhibited cell proliferation and induced cell death via activation of caspase proteins.

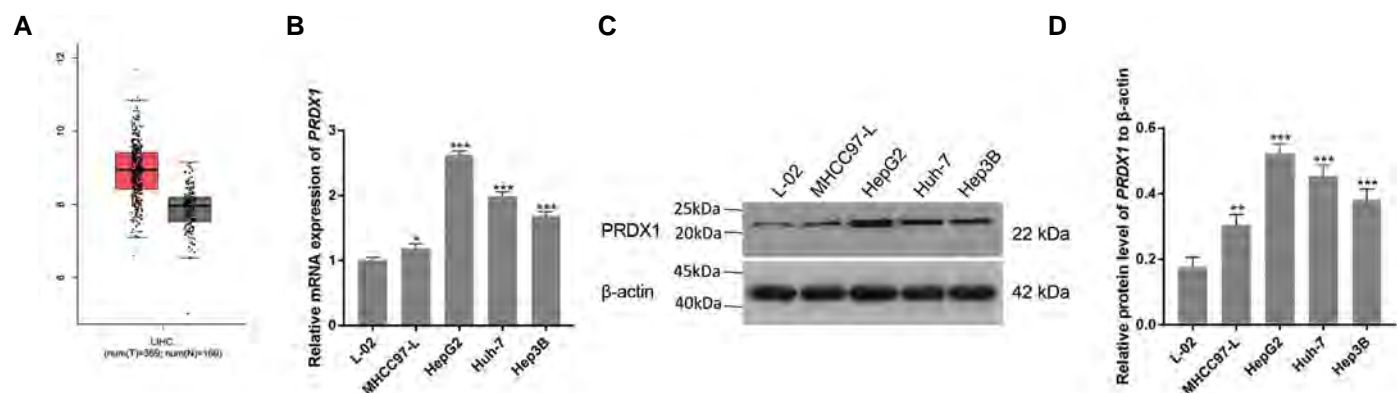


**Fig.1:** Expression of peroxiredoxin 1 (*PRDX1*) in different cell lines of liver cancers. **A.** Box diagram of *PRDX1* expression, with significant difference between cancerous and paracancerous tissues of liver cancer patients. **B.** *PRDX1* mRNA expression was significantly higher in cancerous cells. **C.** Western blot results showed an increased expression of *PRDX1* protein in cancerous cells, with the highest expression level observed in hepatoma (HepG2) cells. **D.** Quantifications of protein levels. The experiment was repeated three times. Data represent mean  $\pm$  SEM. \*,  $P < 0.05$ , \*\*,  $P < 0.01$ , and \*\*\*,  $P < 0.001$ .

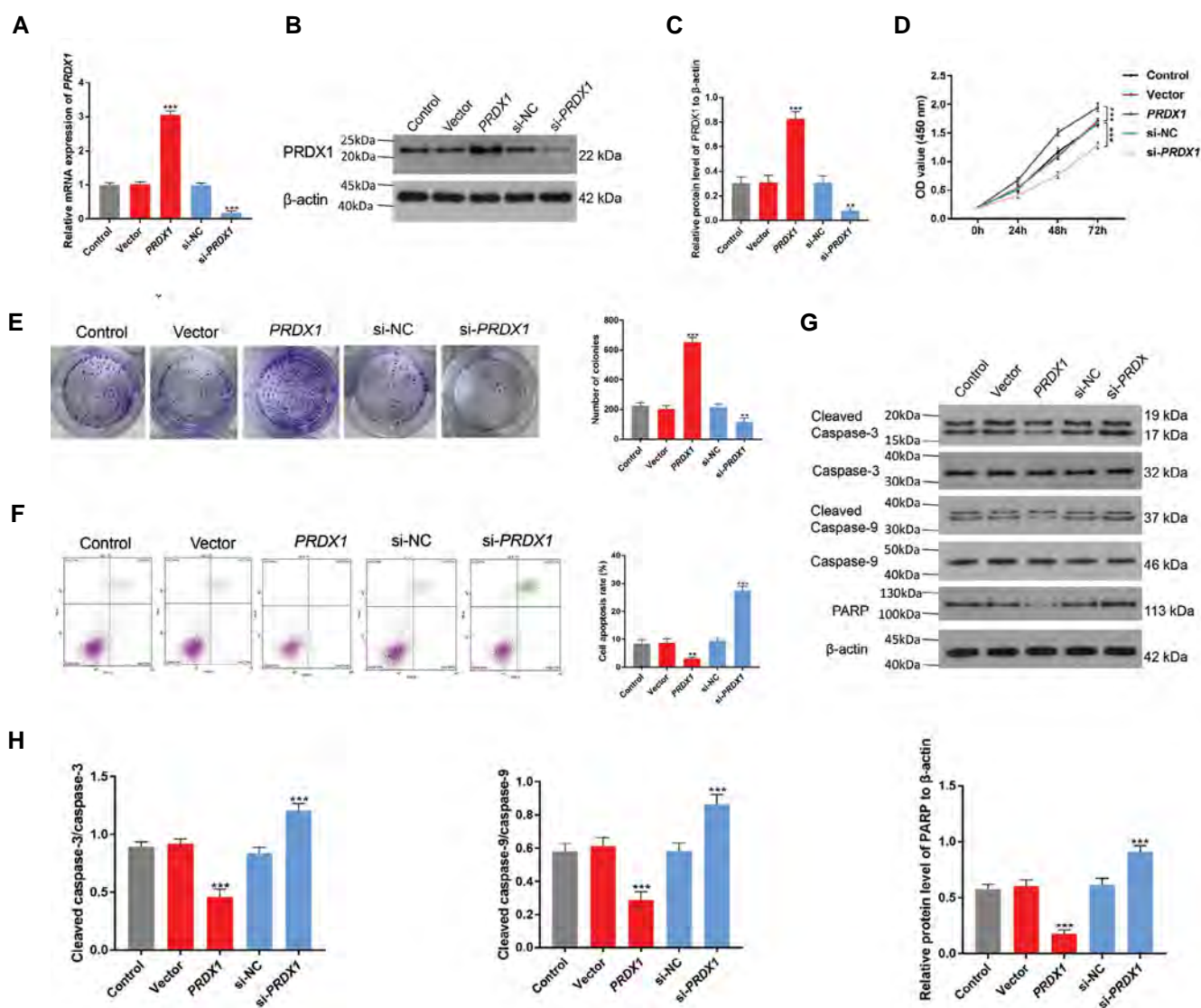


**Fig.2:** *PRDX1* knock-down induced cell death via apoptosis in HCC cells. **A.** Significant increase of *PRDX1* mRNA expression level when overexpressed in hepatoma cells. **B.** Western blot showed that *PRDX1* overexpression enhanced expression level of *PRDX1*, while knock-down of this gene substantially reduced the expression. **C.** Quantification of the protein levels. **D.** CCK-8 assay showed a significant reduction in the  $IC_{50}$  value of hepatoma cells. **E.** Clonal formation assay demonstrated effect of *PRDX1* expression on the proliferation of hepatoma cells. Knock-down *PRDX1* showed a significant inhibitory effect on cells proliferation. **F.** Quantification of the number of colonies. **G.** Western results showed the effect of knock-down of *PRDX1* protein on caspase proteins in hepatoma cells. **H.** Quantification of the protein levels. The experiment was repeated three times. Data represent mean  $\pm$  SEM. \*,  $P < 0.01$ , and \*\*\*,  $P < 0.001$ .

### PRDX1 knock-down induced apoptosis via Bax activation

PRDX1 mediated apoptosis in hepatoma cells was unknown. We wanted to explore effect of PRDX1 in hepatoma cells. We found that PRDX1 overexpression significantly increased Bcl-2 expression, while knock-down of this gene showed a significant reduction of Bcl-2 and enhanced Bax expression (Fig.3A), suggesting an apoptotic condition. Mitochondrial function is essential which is required for normal cellular metabolism. Mitochondrial fragmentation is associated with increased fission (16). Next, we assessed mitochondrial morphology

using mitotracker, whether or not PRDX1 regulate mitochondrial morphology. We found that PRDX1 knock-down significantly produced mitochondrial fragmentation (Fig.3B). All of these cellular events are closely associated with each other. These results indicated that higher expression of Bax may induce apoptosis via dysregulating mitochondrial membrane potential and induced fragmentation. While increased mitochondrial fragmentation and expression of Bax suggested a favorable condition of cellular death. Taken together, these results implied that PRDX1 played a crucial role in inducing cell death of hepatoma cells via regulating Bcl-2 and Bax (Fig.3A).

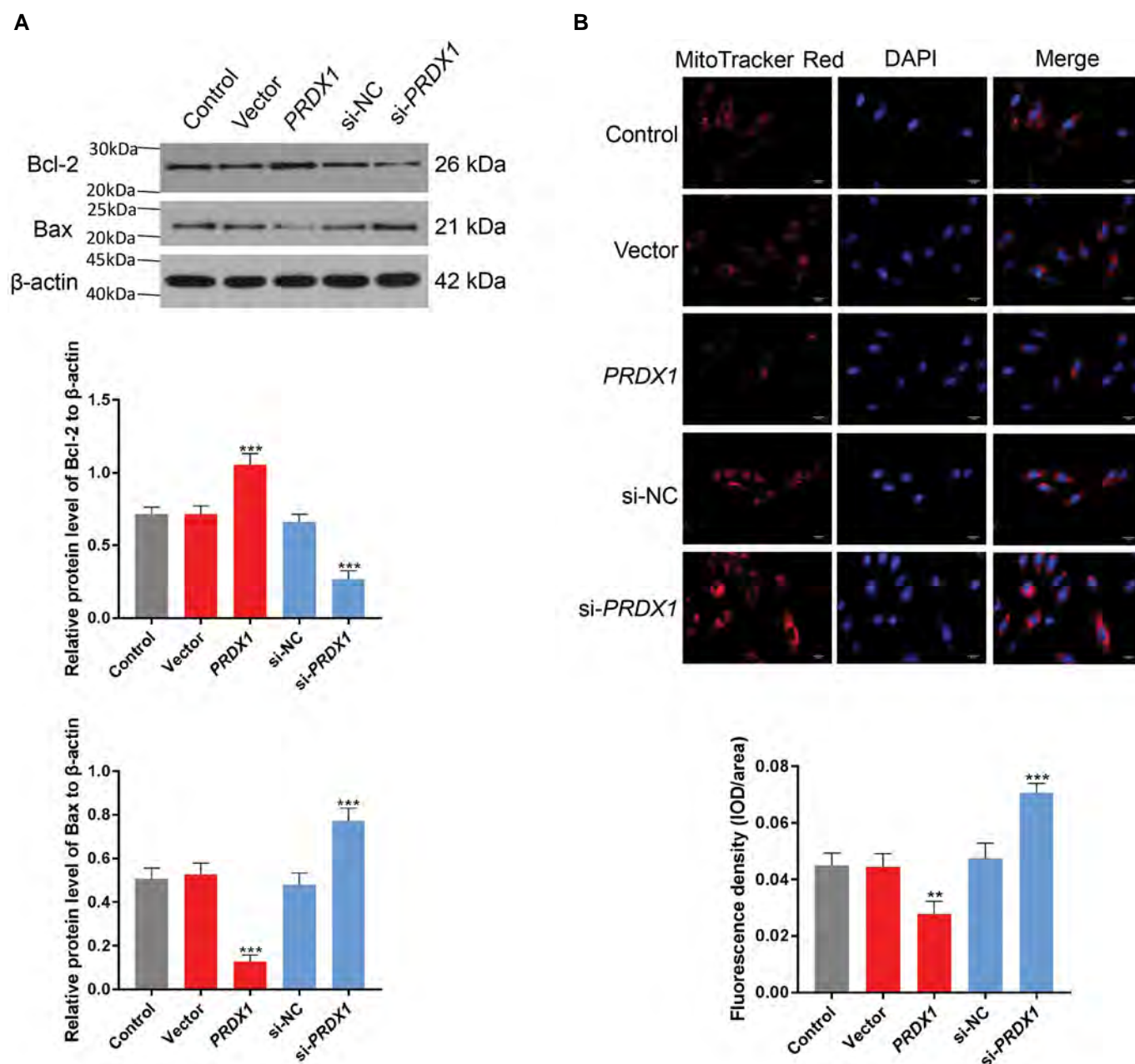


**Fig.3:** PRDX1 knock-down reduced mitochondrial transmembrane potential in HCC cells. **A.** Western blot results depicted that PRDX1 knock-down substantially reduced expression of Bcl-2 and increased Bax expression. The lower bottom showed quantifications of protein levels. **B.** Mitotracker red assay was used to see the effect of si-PRDX1 expression on mitochondrial morphology of hepatoma cells. PRDX1 knock-down induced significantly increased filamentous mitochondrial morphology, assessed by fluorescent intensity. Representative graphs show quantifications. The experiment was repeated three times. Data represent mean  $\pm$  SEM. \*\*,  $P < 0.01$ , and \*\*\*,  $P < 0.001$ .

**PRDX1 knock-down induces apoptosis via activation of mitochondrial fission**

Next, we assessed expression level of proteins which are crucial for mitochondrial fission, whether or not accumulation of these proteins regulate mitochondrial fragmentation (Fig.3B). We found that silencing *PRDX1* greatly enhanced expression of Drp1, Fis1 and Dyn2 proteins, reflecting the abnormal function of mitochondria and initiation of apoptosis process. Inhibition of GTPase activity of Drp1 by dominant-negative protein (Drp1K38A) has been shown to delay cell death (17). They demonstrated that overexpression of hFis1 induced apoptosis, suggesting a role of mitochondrial fission in apoptosis. Next, to investigate effect of *PRDX1* knock-down on mitochondrial fission machinery, we found that expression of Drp1, Fis1 and Dyn2 were significantly activated (Fig.4A), proposing mitochondrial fragmentation and apoptosis conditions.

These results suggested that *PRDX1* knock-down had a significant role in regulating critical molecules of mitochondrial fission and apoptosis.

Reduction of Bcl-2 in *PRDX1* knocked-down cells (Fig.3B) reflected release of cytochrome c, followed by activation of downstream caspase signaling. Therefore, we checked expression of cytochrome c, Apaf-1 and BH3-only proteins (Bim) to confirm its correlation with *PRDX1* knock-down (Fig.4B). Silencing *PRDX1* led to the loss of Bcl-2 and activated Bim protein, which further induced Bax protein activation. Bax further released cytochrome c from mitochondria for the induction of apoptotic proteins. Taken together, these data suggested that knock-down of *PRDX1* facilitated mitochondrial fission and activated caspase proteins, i.e. release of cytochrome c, Bim and Apaf-1, to induce death of hepatoma cells.

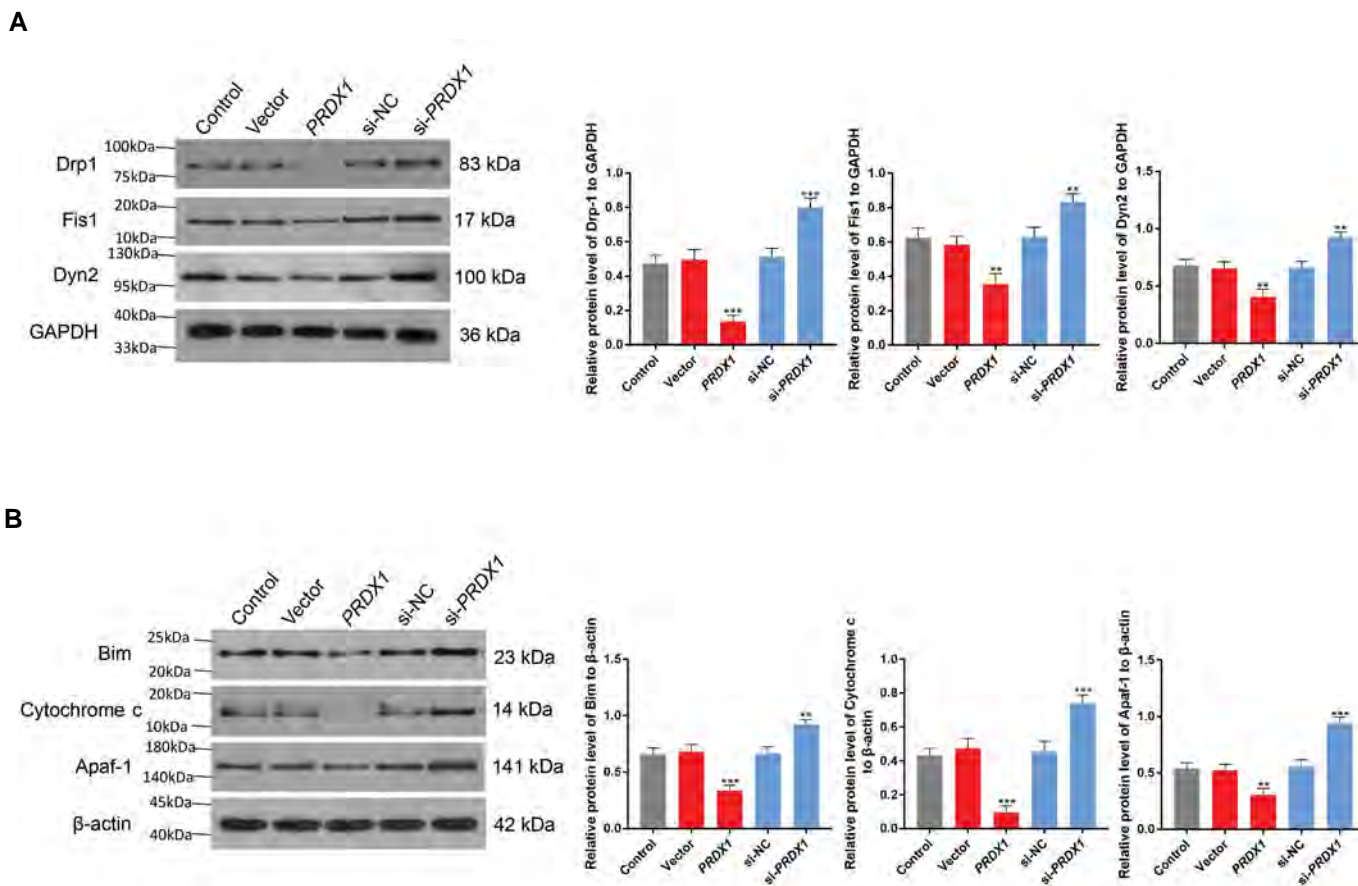


**Fig.4:** Effect of *PRDX1* knock-down on apoptosis and mitochondrial fission machinery of HCC cells. **A.** Western results showed that knock-down of *PRDX1* significantly enhanced expression of Drp1, Fis1 and Dyn2 in hepatoma cells. **B.** Images and graphs showed that overexpression of *PRDX1* decreased apoptotic proteins (Bim, cytochrome C and Apaf-1) expression level, while knock-down of this gene significantly enhanced expression of caspase proteins. The right panel shows quantifications of protein levels. The experiment was repeated three times. Data represent mean ± SEM. \*\*, P<0.01, and \*\*\*, P<0.001.

## Discussion

In this study, we explored effect of silencing *PRDX1* in hepatoma cells. Several studies showed that *PRDX1* is upregulated in different types of cancer, including lung adenocarcinoma (19, 20), soft tissue sarcoma (2) and prostate cancer (14, 21). However, cellular role of *PRDX1* in liver cells remains to be understood. Sun et al. analyzed RNA sequences from the TCGA database and reported that *PRDX1* mRNA expression level was increased 1.3 fold in the malignant compared to the control tissues (15). We tested *PRDX1* expression and found an increased expression of *PRDX1* in different HCC cell lines, which is in line with the other studies and suggested a vital role in cellular proliferation. We found relatively higher *PRDX1* mRNA and protein expression levels in HepG2 cells.

There are studies which reported role of *PRDX1* in cellular proliferation. Gong et al. (22) demonstrated that *PRDX1* regulated proliferation of esophageal squamous cell carcinoma. Lu et al. (4) reported upregulation level of *PRDX1* in cervical cancer and found that *PRDX1* enhanced proliferation, migration and invasion by inhibiting apoptosis. Next, we were interested to explore association between *PRDX1* and hepatoma cells. We found that knock-down of *PRDX1* significantly decreased the IC50 value of hepatoma cells, suggesting that knock-down of *PRDX1* possessed great anti-tumor activity. We assessed proliferation effect by clonal formation assay and found that *PRDX1* overexpression significantly enhanced proliferation of the hepatoma compared to control cells, while knock-down of this gene showed significant inhibitory effects and reduced proliferation of cells, suggesting an important role of *PRDX1* silencing in hepatoma cells. Next, we were interested to explore molecular mechanism of cell death. We asked question whether silencing *PRDX1* is associated with caspase activation? We found that knock-down of *PRDX1* induced cell death via activation of active and cleaved caspase-3 and caspase-9 proteins, which further executed apoptotic process, leading to cell death.

PARP-1 has multiple functions, involved in DNA repair, cell death and transcriptions of some essential genes involved in inflammatory processes (6). It is a well-known substrate of caspase proteins (7, 23). Caspase-3 cleaves PARP-1 upon activation and prevents PARP-1 from repairing the damage (8, 24). Our results showed that knock-down of *PRDX1* increased PARP-1 expression, suggesting depletion of NAD<sup>+</sup> levels, thereby induced cellular death.

Bcl-2, as an essential protein, is a member of the Bcl-2 family, which act as a negative regulator of apoptosis. Moreover, Bcl-2 has shown to be protective and Bax up-regulation has pro-apoptotic role (25, 26). Several evidences reported that Bcl-2 regulate cytochrome c and therefore prevented activation of apoptotic genes (27, 28). Overactivation of Bcl-2 inhibited release of cytochrome c and initiation of apoptosis (29). Lu et al. (4) found that *PRDX1* overexpression increased Bcl-2

expression, while down-regulated Bax expression. This is in line with our findings, representing that *PRDX1* overexpression significantly increased Bcl-2 expression, while knock-down of this gene showed a significant reduction of Bcl-2 and enhanced Bax expression in hepatoma cells, suggesting a vital role of *PRDX1* knock-down in cancerous cells. Once cytochrome c is released in the cytosol, cytosolic cytochrome c further mediates apoptosis-protease activating factor 1 (Apaf-1) to induce activation of the other caspase proteins (30). Researchers reported the role of Bax protein in facilitating release of cytochrome c from mitochondria to induce apoptosis process (31, 32). While, the other studies demonstrated that Bim protein directly activated Bax protein. This may suggest that BIM protein plays an indirect role by antagonizing Bcl-2 proteins, thereby allowing Bax activation to proceed (33, 34). In our study, we found that silencing *PRDX1* led to the loss of Bcl-2 and activated Bim protein which further induced activation of Bax protein. We showed that Bax further released cytochrome c from mitochondria to induce apoptotic proteins, suggesting a significant role of *PRDX1* knock-down in apoptosis. Researchers reported the role of *PRDX1* and found that overexpression of *PRDX1* enhanced Bcl-2 expression, while at the same time down-regulated Bax expression (4). Our findings showed that *PRDX1* overexpression significantly increased Bcl-2 expression, while knock-down of this gene enhanced Bax expression in hepatoma cells. This is consistent with studies previously reported in different cell lines.

Next, we asked question whether *PRDX1* has any role in regulating mitochondrial fission proteins of HCC cells. Drp1, Fis1 and Dyn2 played a role as fission mediators (35). The mitochondrial fission machinery played a vital role in mitochondrial function. Disruption in fission machinery led to the abnormal division of mitochondrial membrane. It was required to produced new mitochondria and maintained quality control of mitochondria (36). Lee et al. (37) found that down-regulation of Drp1 and Fis1 inhibited apoptosis. While in another study, James et al. showed that overexpression of hFis1 may induce apoptosis, suggesting a possible role of mitochondrial fission in apoptosis in yeast cells (18). There are other studies demonstrating the role of Drp1 and Fis1. Thus, they have been shown to inhibit mitochondrial fission and prevent apoptosis (38). In our findings, we analyzed that *PRDX1* knock-down significantly activated mitochondrial fission proteins (Drp1, Fis1 and Dyn2), which may suggest its role in inducing apoptosis. We also showed that mitochondrial fission, induced by silencing *PRDX1*, resulted in mitochondrial fragmentation. These results suggested a significant role of silencing *PRDX1* on mitochondrial fragmentation and fission associated proteins, thereby leading to apoptosis conditions.

## Conclusion

A little attention has been given to study effect of *PRDX1* on live cancer via inhibiting mitochondrial apoptosis

pathway. We reported that *PRDX1* acted via Bcl-2 to inhibit cell death and apoptosis in hepatoma cells. Furthermore, silencing *PRDX1* simulated apoptosis pathways by activating Bax protein, which facilitated release of cytochrome c from the mitochondria followed by activation of the other related apoptotic proteins to induce cell death. Future studies targeting *PRDX1* inhibitors are required, which may act as a therapeutic candidate for the treatment of liver cancer.

## Acknowledgments

There is no financial support and conflict of interest in this study.

## Authors' Contributions

H.h.S., X.I.J.; Contributed to conception and design. H.h.S.; Were responsible for overall supervision, and drafted the manuscript. H.h.S., X.I.J., Y.I.L., H.J., X.h.Y.; Contributed to all experimental works, data and statistical analyses and interpretation of data. All authors read and approved the final manuscript.

## References

- Ding C, X Fan, G Wu. Peroxiredoxin 1 - an antioxidant enzyme in cancer. *J Cell Mol Med.* 2017; 21(1): 193-202.
- Takahashi A, Nakayama R, Ishibashi N, Doi A, Ichinohe R, Ikuyo Y, et al. Analysis of gene expression profiles of soft tissue sarcoma using a combination of knowledge-based filtering with integration of multiple statistics. *PLoS One.* 2014; 9(9): e106801.
- Fang Y, He J, Janssen HLA, Wu J, Dong L, Shen XZ. Peroxiredoxin 1, restraining cell migration and invasion, is involved in hepatocellular carcinoma recurrence. *J Dig Dis.* 2018; 19(3): 155-169.
- Lu E, Hu X, Pan C, Chen J, Xu Y, Zhu X. Up-regulation of peroxiredoxin-1 promotes cell proliferation and metastasis and inhibits apoptosis in cervical cancer. *J Cancer.* 2020; 11(5): 1170-1181.
- Galluzzi L, Joza N, Tasdemir E, Maiuri MC, Hengartner M, Abrams JM, et al. No death without life: vital functions of apoptotic effectors. *Cell Death Differ.* 2008; 15(7): 1113-1123.
- Yoo L, Hong S, Shin KS, Kang SJ. PARP-1 regulates the expression of caspase-11. *Biochem Biophys Res Commun.* 2011; 408(3): 489-93.
- Chaitanya GV, Steven AJ, Babu PP. PARP-1 cleavage fragments: signatures of cell-death proteases in neurodegeneration. *Cell Commun Signal.* 2010; 8: 31.
- Decker P, Muller S. Modulating poly (ADP-ribose) polymerase activity: potential for the prevention and therapy of pathogenic situations involving DNA damage and oxidative stress. *Curr Pharm Biotechnol.* 2002; 3(3): 275-283.
- Huang Q, Zhan L, Cao H, Li J, Lyu Y, Guo X, et al. Increased mitochondrial fission promotes autophagy and hepatocellular carcinoma cell survival through the ROS-modulated coordinated regulation of the NFKB and TP53 pathways. *Autophagy.* 2016; 12(6): 999-1014.
- Moeschel K, Beck A, Weigert C, Lammers R, Kalbacher H, Voelter W, et al. Protein kinase C-zeta-induced phosphorylation of Ser318 in insulin receptor substrate-1 (IRS-1) attenuates the interaction with the insulin receptor and the tyrosine phosphorylation of IRS-1. *J Biol Chem.* 2004; 279(24): 25157-25163.
- Harwig MC, Viana MP, Egnor JM, Harwig JJ, Widlansky ME, Rafelski SM, et al. Methods for imaging mammalian mitochondrial morphology: a prospective on MitoGraph. *Anal Biochem.* 2018; 552: 81-99.
- Kim HJ, Chae HZ, Kim YJ, Kim YH, Hwang TS, Park EM, et al. Preferential elevation of Prx I and Trx expression in lung cancer cells following hypoxia and in human lung cancer tissues. *Cell Biol Toxicol.* 2003; 19(5): 285-298.
- Chang JW, Jeon HB, Lee JH, Yoo JS, Chun JS, Kim JH, et al. Augmented expression of peroxiredoxin I in lung cancer. *Biochem Biophys Res Commun.* 2001; 289(2): 507-512.
- Riddell JR, Bshara W, Moser MT, Sperryak JA, Foster BA, Gollnick SO. Peroxiredoxin 1 controls prostate cancer growth through Toll-like receptor 4-dependent regulation of tumor vasculature. *Cancer Res.* 2011; 71(5): 1637-1646.
- Sun YL, Cai JQ, Liu F, Bi XY, Zhou LP, Zhao XH. Aberrant expression of peroxiredoxin 1 and its clinical implications in liver cancer. *World J Gastroenterol.* 2015; 21(38): 10840-10852.
- Karbowski M, Lee YJ, Gaume B, Jeong SY, Frank S, Nechushtan A, et al. Spatial and temporal association of Bax with mitochondrial fission sites, Drp1, and Mfn2 during apoptosis. *J Cell Biol.* 2002; 159(6): 931-938.
- Frank S, Gaume B, Bergmann-Leitner ES, Leitner WW, Robert EG, Catez F, et al. The role of dynamin-related protein 1, a mediator of mitochondrial fission, in apoptosis. *Dev Cell.* 2001; 1(4): 515-525.
- James DI, Parone PA, Mattenberger Y, Martinou JC. hFis1, a novel component of the mammalian mitochondrial fission machinery. *J Biol Chem.* 2003; 278(38): 36373-36379.
- Li R, Wang H, Bekele BN, Yin Z, Caraway NP, Katz RL, et al. Identification of putative oncogenes in lung adenocarcinoma by a comprehensive functional genomic approach. *Oncogene.* 2006; 25(18): 2628-2635.
- Wright CM, Larsen JE, Hayward NK, Martins MU, Tan ME, Davidson MR, et al. ADAM28: a potential oncogene involved in asbestos-related lung adenocarcinomas. *Genes Chromosomes Cancer.* 2010; 49(8): 688-698.
- Basu A, Banerjee H, Rojas H, Martinez SR, Roy S, Jia Z, et al. Differential expression of peroxiredoxins in prostate cancer: consistent upregulation of PRDX3 and PRDX4. *Prostate.* 2011; 71(7): 755-765.
- Gong F, Hou G, Liu H, Zhang M. Peroxiredoxin 1 promotes tumorigenesis through regulating the activity of mTOR/p70S6K pathway in esophageal squamous cell carcinoma. *Med Oncol.* 2015; 32(2): 455.
- Zhang D, Hu X, Li J, Liu J, Baks-Te Bulte L, Wiersma M, et al. DNA damage-induced PARP1 activation confers cardiomyocyte dysfunction through NAD(+) depletion in experimental atrial fibrillation. *Nat Commun.* 2019; 10(1): 1307.
- Lazebnik YA, Kaufmann SH, Desnoyers S, Poirier GG, Earnshaw WC. Cleavage of poly(ADP-ribose) polymerase by a proteinase with properties like ICE. *Nature.* 1994; 371(6495): 346-347.
- Gaumer S, Guénal I, Brun S, Théodore L, Mignotte B. Bcl-2 and Bax mammalian regulators of apoptosis are functional in *Drosophila*. *Cell Death Differ.* 2000; 7(9): 804-814.
- Owsianowski E, Walter D, Fahrenkrog B. Negative regulation of apoptosis in yeast. *Biochim Biophys Acta.* 2008; 1783(7): 1303-1310.
- Adams JM, Cory S. The Bcl-2 apoptotic switch in cancer development and therapy. *Oncogene.* 2007; 26(9): 1324-1337.
- Chipuk JE, Green DR. How do BCL-2 proteins induce mitochondrial outer membrane permeabilization? *Trends Cell Biol.* 2008; 18(4): 157-164.
- Yang J, Liu X, Bhalla K, Kim CN, Ibrado AM, Cai J, et al. Prevention of apoptosis by Bcl-2: release of cytochrome c from mitochondria blocked. *Science.* 1997; 275(5303): 1129-1132.
- Bao Q, Shi Y. Apoptosome: a platform for the activation of initiator caspases. *Cell Death Differ.* 2007; 14(1): 56-65.
- Zhang M, Zheng J, Nussinov R, Ma B. Release of Cytochrome C from bax pores at the mitochondrial membrane. *Sci Rep.* 2017; 7(1): 2635.
- Heimlich G, McKinnon AD, Bernardo K, Brdiczka D, Reed JC, Kain R, et al. Bax-induced cytochrome c release from mitochondria depends on alpha-helices-5 and -6. *Biochem J.* 2004; 378(Pt 1): 247-255.
- Czabotar PE, Colman PM, Huang DC. Bax activation by Bim? *Cell Death Differ.* 2009; 16(9): 1187-1191.
- Kuwana T, Mackey MR, Perkins G, Ellisman MH, Latterich M, Schneider R, et al. Bid, Bax, and lipids cooperate to form supramolecular openings in the outer mitochondrial membrane. *Cell.* 2002; 111(3): 331-342.
- Okamoto K, Shaw JM. Mitochondrial morphology and dynamics in yeast and multicellular eukaryotes. *Annu Rev Genet.* 2005; 39: 503-536.
- Youle RJ, van der Bliek AM. Mitochondrial fission, fusion, and stress. *Science.* 2012; 337(6098): 1062-1065.
- Lee YJ, Jeong SY, Karbowski M, Smith CL, Youle RJ. Roles of the mammalian mitochondrial fission and fusion mediators Fis1, Drp1, and Opa1 in apoptosis. *Mol Biol Cell.* 2004; 15(11): 5001-5011.
- Kim D, Sankaramoorthy A, Roy S. Downregulation of Drp1 and Fis1 inhibits mitochondrial fission and prevents high glucose-induced apoptosis in retinal endothelial cells. *Cells.* 2020; 9(7): 1662.

# Long Non-Coding RNA *CASC2* Functions as A Tumor Suppressor in Colorectal Cancer via Modulating The *miR-18a-5p/BTG3* Pathway

Liumin Kang, M.D., Jie Sun, M.D., Jie Liu, M.D., Feng Xu, M.D., Qilin Zhu, M.D., Xiaohua Shi, M.D.\*

Department of Gastroenterology, Suzhou Science and Technology Town Hospital of Nanjing Medical University, Suzhou, Jiangsu, China

\*Corresponding Address: Department of Gastroenterology, Suzhou Science and Technology Town Hospital of Nanjing Medical University, Suzhou, Jiangsu, China  
Email: Sxh7079@163.com

Received: 08/April/2021, Accepted: 15/November/2021

## Abstract

**Objective:** Reportedly, long non-coding RNA (lncRNA) cancer susceptibility candidate 2 (*CASC2*) is involved in regulating colorectal cancer (CRC) progression. However, the function and detailed downstream mechanism of *CASC2* in CRC progression are not fully elucidated. The aim of the study was to investigate the potential function and molecular mechanism of *CASC2* in CRC progression.

**Materials and Methods:** In this experimental study, quantitative real-time polymerase chain reaction (qRT-PCR) was adopted to probe *CASC2*, microRNA-18a-5p (*miR-18a-5p*) and B cell translocation gene 3 (*BTG3*) mRNA expression in CRC tissues and cell lines. After *CASC2* was overexpressed in Colo-678 and HCT116 cell lines, methylthiazol tetrazolium (MTT) and 5-bromo-2'-deoxyuridine (BrdU) assays were employed to examine the proliferation of CRC cells. Transwell migration and invasion assays were executed to evaluate the metastatic potential of CRC cells. The targeting relationships among *CASC2*, *miR-18a-5p* and *BTG3* were validated by dual luciferase reporter gene assay. Western blot assay was applied to examine the regulatory effects of *CASC2* and *miR-18a-5p* on *BTG3* protein expression.

**Results:** *CASC2* was decreased in CRC tissues and cell lines, and its low expression in CRC tissues was associated with larger tumor size and lymph node metastasis. *CASC2* overexpression restrained proliferative, migrative and invasive capabilities of CRC cells. *CASC2* could function as a molecular sponge for *miR-18a-5p* and repress the expression of *miR-18a-5p*. Furthermore, the inhibitory effects of *CASC2* on the malignant phenotypes of CRC cells was counteracted by *miR-18a-5p* mimics. Additionally, *CASC2* could positively regulate *BTG3* expression via suppressing *miR-18a-5p*.

**Conclusion:** *CASC2* inhibits CRC development by suppressing *miR-18a-5p* and raising *BTG3* expression.

**Keywords:** B Cell Translocation Gene 3, Colorectal Cancer, lncRNA *CASC2*, *miR-18a-5p*

Cell Journal (Yakhteh), Vol 24, No 11, November 2022, Pages: 665-672

**Citation:** Kang L, Sun J, Liu J, Xu F, Zhu Q, Shi X. Long non-coding RNA *CASC2* functions as a tumor suppressor in colorectal cancer via modulating the *miR-18a-5p/BTG3* Pathway. Cell J. 2022; 24(11): 665-672. doi: 10.22074/cellj.2022.8036.

This open-access article has been published under the terms of the Creative Commons Attribution Non-Commercial 3.0 (CC BY-NC 3.0).

## Introduction

Colorectal cancer (CRC) brings about a huge health burden globally (1). In 2020, there were approximately 147,950 new cases of CRC and 53,200 deaths from CRC worldwide (2). In China, the incidence of CRC is on the rise (3). Currently, colonoscopy is the most reliable screening method for CRC screening, but it has high economic and physical burdens (4). In addition, relapse after the surgery, distant metastasis and chemoresistance contribute to the adverse prognosis of CRC patients (5). It is therefore pivotal to decipher the mechanism of CRC progression to identify potential therapy targets for treating CRC.

Long non-coding RNA (lncRNA) exceeding 200nt, is vital in imprinting, epigenetic regulation, transcription and translation regulation (6). Through modulating gene expression and the function of proteins, lncRNAs participate in regulating diverse biological processes (7). In these years, some lncRNAs emerge as either oncogenes or tumor suppressors in diverse cancers (8, 9). Notably, the expression of lncRNA cancer susceptibility candidate 2 (*CASC2*) is reduced in pancreatic cancer and

oral squamous cell carcinoma (10, 11). Importantly, it is reported that *CASC2* can play a tumor suppressive role in CRC through sponging *miR-18a* (12). However, the mechanism of action of *CASC2* in CRC still awaits more investigation.

As reported, lncRNA can serve as a competing endogenous RNA (ceRNA) to regulate targeted gene expression via sponging microRNA (miRNA) (13). Besides, miRNA dysregulation is a feature of CRC (14, 15). However, the lncRNA-miRNA network in CRC is still partly covered and requires further research. *miR-18a-5p* has been confirmed to be a promoter in many cancers including CRC (16). However, the interaction mechanism between *CASC2* and *miR-18a-5p* in CRC has not been clarified.

B cell translocation gene 3 (*BTG3*) belongs to B-cell translocation gene / Transducer of ERBB2 (BTG/TOB) family. *BTG3* is a crucial participant in regulating cell proliferation, differentiation and apoptosis (17, 18). It has been reported that *BTG3* overexpression suppresses the malignancy of CRC cells through regulating Wnt/ $\beta$ -

catenin signaling (19). But the hidden role and mechanism of *BTG3* relevant to the progression of CRC are inconclusive. Here we focused on the role and mechanism of *CASC2* in CRC. We investigated the regulatory effects of the *CASC2/miR-18a-5p/BTG3* axis on the proliferative, migrative and invasive abilities of CRC cells.

## Materials and Methods

### Tissue samples

In this experimental study, this work was endorsed by the Suzhou Science and Technology Town Hospital of Nanjing Medical University's Ethics Committee (20190712-006) and all experiments were performed according to "Declaration of Helsinki". Specifically, all subjects provided written informed consent. 65 pairs of cancerous tissues and adjacent non-cancerous tissues were available from CRC patients in the Suzhou Science and Technology Town Hospital of Nanjing Medical University. All samples were kept in liquid nitrogen immediately at  $-196^{\circ}\text{C}$  after the surgery.

### Cell culture and transfection

In this experimental study, the Type Culture Collection of Chinese Academy of Sciences (Shanghai, China) was the supplier of CRC cell lines HCT116, SW620, LoVo. Colo-678 cells were provided by Honsun Biological Technology Co., Ltd. (Shanghai, China). Normal human colorectal mucosal cell line FHC was acquired from American Type Culture Collection (ATCC). Notably, cells were cultured in RPMI-1640 medium (Gibco, Grand Island, NY, USA) with 10% fetal bovine serum (FBS, Invitrogen, Shanghai, China), 100 U/mL penicillin, and 100  $\mu\text{g}/\text{mL}$  streptomycin (Invitrogen, Carlsbad, CA, USA) in 5%  $\text{CO}_2$  at  $37^{\circ}\text{C}$ . *MiR-18a-5p* mimics (*miR-18a-5p*), and the mimics negative control (miR-NC) were available from GenePharma (Shanghai, China). *CASC2* sequences with full length were inserted into pcDNA3.0 plasmid to construct *CASC2* overexpression plasmid. Empty pcDNA3.0 vector was adopted as negative control (NC). Lipofectamine<sup>TM</sup> 3000 (Invitrogen, Carlsbad, CA, USA) was employed for transfections as protocols.

### Quantitative real-time polymerase chain reaction

Total RNA of tissues and cells isolated by TRIzol reagent (Invitrogen, Carlsbad, CA, USA) were reversely transcribed into complementary DNA (cDNA) by a PrimeScript<sup>TM</sup> RT Reagent kit (Invitrogen, Carlsbad, CA, USA). Next, qRT-PCR was conducted with SYBR<sup>®</sup> Premix-Ex-Taq<sup>TM</sup> (Takara, Tokyo, Japan) on the ABI PRISM 7000 Fluorescent Quantitative PCR System. The data were analyzed with  $2^{-\Delta\Delta\text{Ct}}$  method, with Glyceraldehyde 3-phosphate dehydrogenase (*GAPDH*) and *U6* as the endogenous references. The sequences of the primers are:

*CASC2*-

F: 5'-GCACATTGGACGGTGTTC-3'  
R: 5'-CCCAGTCCTTCACAGGTCAC-3'

*miR-18a-5p*-

F: 5'-TCCGAGATAGACGTGATCTA-3'  
R: 5'-GTGCAGGGTCCGAGGT-3'

*BTG3*-

F: 5'-ATGAAGAAAATGAAATTGCTG-3'  
R: 5'-TTAGTGAGGTGCTAACATGTG-3'

*GAPDH*-

F: 5'-GTCAACGGATTTGGTCGTATTG-3'  
R: 5'-CCGTTCTCAGCCATGTAGTT-3'

*U6*-

F: 5'-CTCGCTTCGGCAGCAC-3'  
R: 5'-AACGCTTCACGAATTTGCGT-3'

### Subcellular fractionation analysis

Cytoplasmic and nuclear RNA were isolated and extracted from Colo-678 and HCT116 cells by the Cytoplasmic and Nuclear RNA Purification Kit (Norgen, Belmont, CA, USA). Then, the expression of *CASC2* in the cytoplasm and nucleus of Colo-678 and HCT116 cells was investigated by qRT-PCR, with *GAPDH* as a cytoplasmic control and *U6* as a nuclear control.

### Methylthiazol tetrazolium (MTT) assay

Transfected Colo-678 and HCT116 cells were inoculated into 96-well plates ( $3 \times 10^3$  cells/well). The cells were cultured for different times. At different time points, 20  $\mu\text{L}$  of MTT solution (5 mg/mL, Sigma-Aldrich, St. Louis, MO, USA) was dripped into each well, and then the cells were incubated for 4 hours at room temperature. Next, the medium was discarded, and 150  $\mu\text{L}$  of DMSO (Sigma-Aldrich, St. Louis, MO, USA) was loaded into each well to dissolve the formazan. Finally, a microplate reader (Bio-Rad Laboratories, Hercules, CA, USA) was used for measuring the absorbance of the cells at 570 nm.

### 5-bromo-2'-deoxyuridine (BrdU) assay

The viability of transfected cells was examined by a BrdU incorporation assay kit (Wuhan AmyJet Scientific Inc. Wuhan, China). Briefly, Colo-678 and HCT116 cells in different groups were respectively plated into a 96-well plate ( $1 \times 10^3$  cells/well). Next, 10  $\mu\text{L}$  of BrdU solution was loaded into each well. Subsequently, 4% paraformaldehyde was added into each well to fix the cells. After the DNA was denatured, anti-BrdU antibody (Abcam, Cambridge, UK) was loaded into each well and cells were subsequently incubated at  $4^{\circ}\text{C}$  overnight. Cells were thoroughly washed by phosphate buffered solution (PBS), and cell nuclei were counterstained by Hoechst 33258 staining solution (Beyotime Institute of Biotechnology, Haimen, China) at ambient temperature for 30 minutes. Immersed in PBS again, cells were accordingly observed under a fluorescent microscope (Olympus BX51, Tokyo, Japan). The number of cells was counted using Image J. The percentage of BrdU positive

cells = the number of red fluorescent cells/the number of blue fluorescent cells  $\times$  100%.

### Transwell assay

Transwell assays were accomplished with Transwell chambers (pore size: 8  $\mu$ m; Corning, NY, USA). In the invasion assay, the filter was specifically covered with a layer of Matrigel (30  $\mu$ g/well; BD, San Jose, CA, USA); in the migration assay, Matrigel was not used. For each well,  $1 \times 10^5$  cells suspended in serum-free medium was loaded into the upper chamber, with 700  $\mu$ L of medium containing 20% FBS in the lower chamber as a chemoattractant. Next, cells were cultured for 36 hours, and then cells on the upper surface of the filter were wiped off, and those on the lower were subsequently fixed with ethanol and stained with 0.2% crystal violet solution. Subsequently, the cells were meticulously observed and photographed under an inverted microscope (Nikon TE2000-S, Tokyo, Japan). Specifically, the number of stained cells after migration or invasion was counted with the Image J software.

### Dual-luciferase reporter gene assay

Through StarBase software, we found putative binding sites between *miR-18a-5p* and *CASC2* or *BTG2*. Also, bioinformatics analysis predicted a binding site between *miR-18a-5p* and *CASC2*. Then the wild type (WT) and mutant type (MUT) predicted binding sequences of *CASC2* were subsequently synthesized and cloned into pmirGLO vector (Promega, Madison, WI, USA) to construct *CASC2*-WT and *CASC2*-MUT reporter plasmids. Next, the CRC cells were co-transfected with *CASC2*-WT or *CASC2*-MUT and *miR-18a-5p* or miR-NC. 48 hours later, the relative luciferase activity of the cells in each group was examined by the dual-luciferase assay system (Promega). The targeting relationship between *miR-18a-5p* and *BTG3* was validated in the same way.

### RNA immunoprecipitation assay

RNA immunoprecipitation (RIP) assay was accomplished employing the Magna RIP RNA-binding protein immunoprecipitation kit (Millipore, Billerica, MA, USA). Colo-678 and HCT116 cells ( $2 \times 10^7$  cells/mL) were collected and subsequently lysed in RIPA buffer containing a protease inhibitor cocktail and RNase inhibitor. Notably, cell lysates were specifically incubated with magnetic beads containing immunoglobulin G antibody (IgG, ab172730, Abcam, Cambridge, UK) or argonaute-2 antibody (Ago2, ab186733, Abcam, Cambridge, UK) at 4°C overnight. The samples were accordingly incubated with proteinase K along with shaking at 55°C. Subsequently, the immunoprecipitated RNA was isolated. Ultimately, the enrichment of *CASC2* and *miR-18a-5p* was probed by qRT-PCR. Specifically, the group without antibody was the positive control (Input), the group with IgG antibody was the negative control (anti-IgG), and the group with Ago2 antibody was the experimental one (anti-Ago2).

### Western blot

CRC cells harvested were lysed in RIPA lysis buffer (Pierce, Rockford, IL, USA) on ice for 30 minutes to extract the total protein. Notably, the total protein in each sample was respectively quantified by a BCA Protein Assay Kit (Beyotime Institute of Biotechnology, Haimen, China). Then the protein samples were subjected to 10% sodium dodecyl sulfate-polyacrylamide gel electrophoresis, and transferred to polyvinylidene fluoride (PVDF) membranes (Millipore), which was blocked with 5% skimmed milk for 2 hours at 37°C and incubated with primary antibodies against *BTG3* (1:1000, ab197399, Abcam, Cambridge, UK) or *GAPDH* (1:1000, ab181602, Abcam) overnight at 4°C. Next, the membranes were rinsed three times with Tris-buffered saline containing Tween-20 (TBST) and subsequently incubated with horseradish peroxidase (HRP)-conjugated secondary antibody for 1 hours at ambient temperature. At last, the enhanced chemiluminescence kit (Amersham Pharmacia Biotech, Little Chalfont, UK) was adopted for observing the protein band. *GAPDH* was utilized as the endogenous reference.

### Statistical analysis

The analysis was fulfilled by SPSS 17.0 statistical software (SPSS Inc., Chicago, IL, USA). Each experiment was independently replicated 3 times, with data expressed as mean  $\pm$  standard deviation (SD). The Kolmogorov-Smirnov test was used to the for normality and equal variance of the data. For data that were skewed distributed, comparisons between two groups were performed by the Mann-Whitney test. For normally distributed data, comparisons between two groups, among multiple groups were respectively accomplished by *t* test and one-way analysis of variance. Overall survival analysis was operated with Kaplan-Meier plots and log rank tests. Pearson's correlation analysis was wielded to delve into the relationships among *CASC2*, *miR-18a-5p* and *BTG3* mRNA. Chi-square ( $\chi^2$ ) test was executed to analyze the relations between *CASC2* expressions and the clinicopathological features of CRC patients.  $P < 0.05$  denoted meaningful difference.

## Results

### *CASC2* expression characteristics in CRC and its clinical significance

In the beginning, we evaluated *CASC2* expression characteristics in cancer tissues and tissues adjacent to cancer from 65 patients with CRC by qRT-PCR. As against normal tissues, *CASC2* expression in CRC tissues was remarkably down-regulated (Fig.1A). qRT-PCR was also employed to detect *CASC2* expressions in human normal colon epithelial cell line (FHC cells) and 4 human CRC cell lines (Colo-678, HCT116, SW620, and LoVo cells). It was found that compared with FHC cells, *CASC2* expression in all 4 CRC cell lines was down-regulated (Fig.1B). Subsequently, we analyzed the subcellular

distribution of *CASC2* and observed that *CASC2* was mainly located in the cytoplasm of CRC cells (Fig.1C). Chi-square test was used to analyze the relations between *CASC2* expressions and the clinicopathological indicators of CRC patients, and the results highlighted that *CASC2* low expression was in close association with the larger

tumor size and lymph node metastasis of the patients (Table 1). Besides, Kaplan-Meier analysis indicated that low expression of *CASC2* was associated with poor overall survival of CRC patients (Fig.1D). These findings implied that *CASC2* could probably participate in repressing tumor progression in CRC.

**Table 1:** Correlations between *CASC2* expression and multiple clinicopathological characteristics in colorectal cancer patients

Characteristics	Number (n=65)	<i>CASC2</i> expression		$\chi^2$	P value
		Low (n=33)	High (n=32)		
Age (Y)				0.7753	0.3785
<60	35	16	19		
≥60	30	17	13		
Gender				0.1641	0.6854
Male	39	19	20		
Female	26	14	12		
Tumor grade				0.1269	0.7216
I-II	27	13	14		
III-IV	38	20	18		
Tumor size (cm)				6.9350	0.0085**
<5	26	8	18		
≥5	39	25	14		
Smoking history				0.7392	0.3899
Yes	38	21	17		
No	27	12	15		
Lymph node metastasis				4.5241	0.0334*
Present	39	24	15		
Absent	26	9	17		
Differentiation				3.4529	0.0631
Well/moderate	29	11	18		
Poor	36	22	14		

\*, P<0.05 and \*\*, P<0.01.

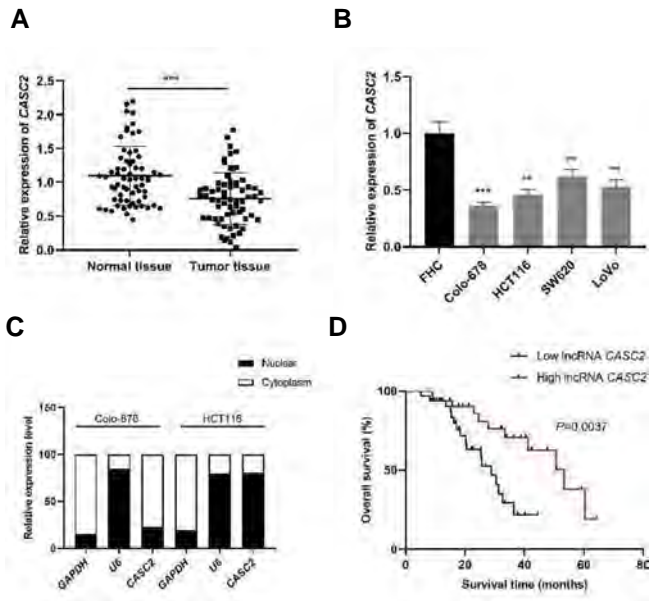


**Fig.1:** *CASC2* was down-regulated in CRC tissues and cells. **A.** qRT-PCR was used to detect the expression of *CASC2* in CRC tissues and adjacent normal tissues (n=65). **B.** qRT-PCR was adopted to detect the expression of *CASC2* in normal colorectal mucosal cell line (FHC) and CRC cell lines (Colo-678, HCT116, SW620, LoVo cells). **C.** Subcellular fractionation assay was used to measure the expression of *CASC2*, *GAPDH* and *U6* in the nuclei and cytoplasm of Colo-678 and HCT116 cells. **D.** Kaplan-Meier analysis showed a correlation between *CASC2* expression and overall survival of CRC patients. Data are represented as the mean  $\pm$  SD (n=3). \*\*, P<0.01, \*\*\*, P<0.001, CRC; Colorectal cancer, and qRT-PCR; Quantitative real-time polymerase chain reaction.

### *CASC2* overexpression impeded the malignant progression of CRC cells

To work out the biological function of *CASC2* in CRC cells, we transfected *CASC2* overexpression plasmids into Colo-678 and HCT-116 cells to construct cell models with *CASC2* overexpression (Fig.2A). MTT, BrdU and Transwell assays revealed that in comparison with the control group, *CASC2* overexpression greatly inhibited the proliferative, migrative and invasive abilities of Colo-678 and HCT-116 cells (Fig.2B-E).

### *CASC2* directly targeted *miR-18a-5p* in CRC cells

To expound the downstream mechanism of *CASC2*, bioinformatics analysis was performed, and a binding site between *CASC2* and *miR-18a-5p* was predicted (Fig.3A). Besides, *miR-18a-5p* expressions in 65 pairs of CRC tissues and tissues adjacent to cancer were then evaluated by qRT-PCR. As against normal tissues adjacent to cancer, *miR-18a-5p* was observed to be highly expressed in CRC tissue (Fig.3B). Additionally, *miR-18a-5p* expression was inhibited in Colo-678 and HCT116 cells with *CASC2* overexpression (Fig.3C). Besides, we observed a negative correlation between *CASC2* and *miR-185-5p* expression in CRC tissue (Fig.3D). In addition, dual-luciferase reporter

gene assay revealed that *miR-18a-5p* mimics could demonstrably restrain the luciferase activity of wild-type *CASC2* reporter, but make no difference on that of mutant *CASC2* reporter (Fig.3E). RIP assay highlighted that *CASC2* and *miR-18a-5p* were significantly enriched in anti-Ago2 group of Colo-678 and HCT116 cells (Fig.3F). Collectively, *CASC2* could target *miR-18a-5p* and regulate its expression negatively.

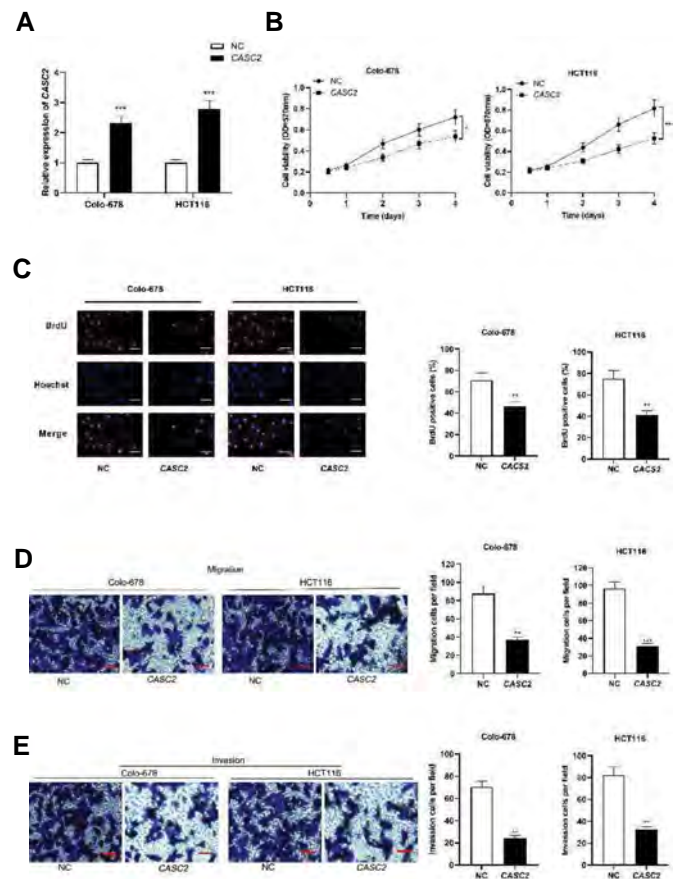


**Fig.2:** *CASC2* overexpression inhibited CRC cell proliferation, migration and invasion. **A.** qRT-PCR was used to detect the expression of *CASC2* in Colo-678 and HCT116 cells transfected with the *CASC2* overexpression plasmid. **B.** **C.** MTT and BrdU assays were employed to detect the proliferation of CRC cells with *CASC2* overexpression (scale bar: 100  $\mu$ m). **D.** **E.** Transwell assay was used to detect the migration and invasion of CRC cells with *CASC2* overexpression (scale bar: 250  $\mu$ m). The data were analyzed by independent samples t test or one-way ANOVA. Data are represented as the mean  $\pm$  SD (n=3). \*, P<0.05, \*\*, P<0.01, \*\*\*, P<0.001, NC; Negative control, CRC; Colorectal cancer, qRT-PCR; Quantitative real-time polymerase chain reaction, MTT; Methylthiazol tetrazolium, and BrdU; 5-bromo-2'-deoxyuridine.

### *MiR-18a-5p* counteracted the biological functions of *CASC2* in CRC cells

To expound the role of *CASC2/miR-18a-5p* axis in CRC, *miR-18a-5p* mimics was transfected into Colo-678 and HCT116 cells with *CASC2* overexpression.

qRT-PCR showed that the transfection of *miR-18a-5p* mimics reversed the decline of *miR-18a-5p* expression caused by *CASC2* overexpression (Fig.4A). Next, MTT assay, wound healing assay and transwell assay revealed that *miR-18a-5p* restoration counteracted the inhibiting impacts of *CASC2* overexpression on the proliferative, migrative and invasive abilities of Colo-678 and HCT116 cells (Fig.4B-E). These results implied that *CASC2* inhibited the progression of CRC cells via targeting *miR-18a-5p*.

with FHC cells, *BTG3* protein expression was declined in CRC cell lines (Fig.5E). Transfection of *miR-18a-5p* mimics reduced *BTG3* mRNA and protein expressions in CRC cells; *CASC2* overexpression induced the up-regulation of *BTG3* in CRC cells, and this effect could be diminished by *miR-18a-5p* overexpression (Fig.5F, G). Notably, *BTG3* mRNA expression was in negative correlation with *miR-18a-5p* in CRC tissue (Fig.5H), but in positive correlation with *CASC2* expression (Fig.5I). The aforementioned results confirmed that *BTG3* was a downstream target of *miR-18a-5p*, and its expression was negatively modulated by *miR-18a-5p* and positively modulated by *CASC2*.

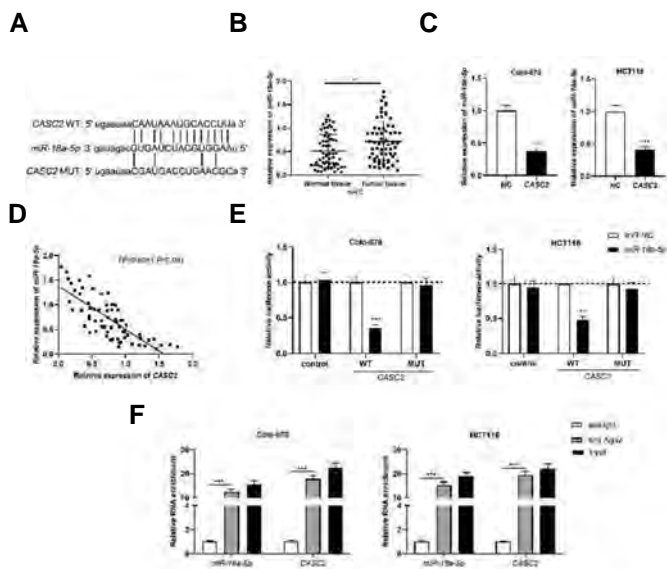


**Fig.3:** MiR-18a-5p was the target of CASC2 in CRC. **A.** StarBase software (<http://starbase.sysu.edu.cn/>) predicted a binding site between *CASC2* and *miR-18a-5p*. **B.** qRT-PCR was used to detect the expression of *miR-18a-5p* in CRC tissues and adjacent normal tissues (n=65). **C.** qRT-PCR was used to detect the expression of *miR-18a-5p* in CRC cells with *CASC2* overexpression. **D.** Pearson's correlation analysis was adopted to analyze the correlation between *CASC2* expression and *miR-18a-5p* expression in CRC tissue samples. **E.** Dual-luciferase reporter gene assay was employed to verify the targeting relationship between *miR-18a-5p* and *CASC2*. **F.** The interaction between *CASC2* and *miR-18a-5p* in Colo-678 and HCT116 cells was detected by RIP assay. The data were analyzed by Mann-Whitney test, one-way ANOVA or independent samples *t*-test. Data are represented as the mean  $\pm$  SD (n=3). \*\*, P<0.01, \*\*\*, P<0.001, CRC; Colorectal cancer, qRT-PCR; Quantitative real-time polymerase chain reaction, and RIP; RNA immunoprecipitation.

### BTG3 was the target of miR-18a-5p

Next, we searched the targets of *miR-18a-5p* using the StarBase database, and the results showed that *miR-18a-5p* could probably bind to *BTG3* 3'-UTR (Fig.5A). Dual-luciferase reporter gene assay indicated that the transfection of *miR-18a-5p* mimics dramatically repressed the luciferase activity of wild-type *BTG3* reporter but could not repress that of the mutant type *BTG3* reporter (Fig.5B). qRT-PCR revealed that *BTG3* mRNA expression was markedly reduced in CRC tissues and cells (Fig.5C, D). Additionally, western blot assay showed that in comparison

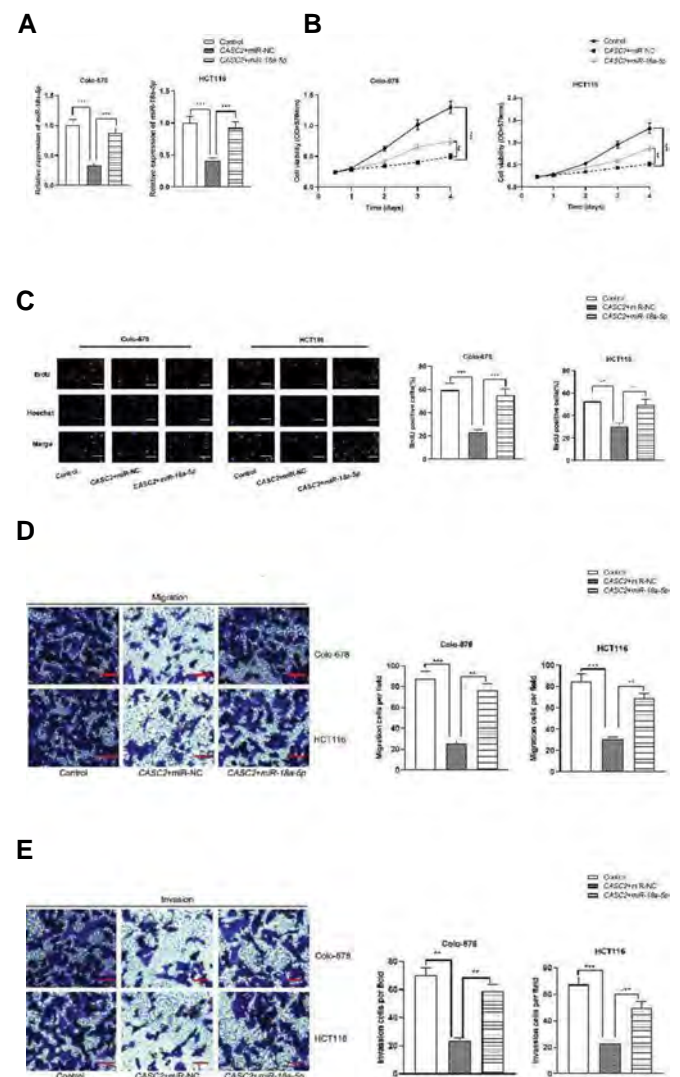


**Fig.4:** MiR-18a-5p partially reversed the inhibitory effects of CASC2 on CRC cells. **A.** *miR-18a-5p* mimics were transfected into Colo-678 cells and HCT116 cells with *CASC2* overexpression, and the expression of *miR-18a-5p* in CRC cells was detected by qRT-PCR. **B, C.** MTT assay and BrdU assay were used to detect the proliferation of Colo-678 and HCT116 cells after the transfection (scale bar: 100  $\mu$ m). **D, E.** Transwell assay was used to detect the migration and invasion of Colo-678 and HCT116 cells after the transfection (scale bar: 250  $\mu$ m). Data are represented as the mean  $\pm$  SD (n=3). The data were analyzed by one-way ANOVA. \*\*, P<0.01, \*\*\*, P<0.001, CRC; Colorectal cancer, qRT-PCR; Quantitative real-time polymerase chain reaction, MTT; Methylthiazol tetrazolium, and BrdU; 5-bromo-2'-deoxyuridine.

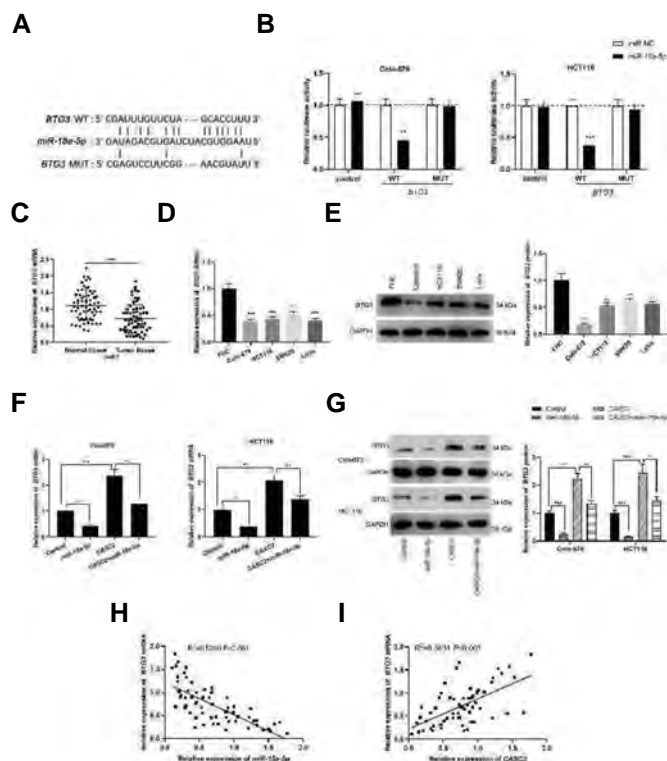


**Fig. 5:** *BTG3* was a target of *miR-18a-5p* in CRC. **A.** StarBase software (<http://starbase.sysu.edu.cn/>) predicted a binding site between *BTG3* 3'UTR and *miR-18a-5p*. Other potential targets of *miR-18a-5p* predicted on the StarBase website were detailed in Table S1 (See Supplementary Online Information at [www.celljournal.org](http://www.celljournal.org)). **B.** Dual-luciferase reporter gene assay was used to verify the targeting relationship between *miR-18a-5p* and *BTG3*. **C.** qRT-PCR was used to detect the expression of *BTG3* mRNA in CRC tissues and adjacent normal tissues (n=65). **D.** The expression of *BTG3* mRNA in normal colorectal mucosal cell line (FHC) and CRC cell lines (Colo-678, HCT116, SW620, LoVo cells) was detected by qRT-PCR. **E.** Western blot assay was used to detect the expression of *BTG3* protein in CRC cell lines (Colo-678, HCT116, SW620, LoVo cells) and FHC cells. The original blot images were provided in Figures S1, S2 (See Supplementary Online Information at [www.celljournal.org](http://www.celljournal.org)). **F, G.** qRT-PCR and western blot assays were used to detect the expression of *BTG3* mRNA and protein in CRC cells transfected with *miR-18a-5p* mimic, *CASC2* overexpression plasmid or co-transfected with *miR-18a-5p* and *CASC2*, respectively. The original blot images were provided in Figure S3 (See Supplementary Online Information at [www.celljournal.org](http://www.celljournal.org)). **H, I.** Pearson's correlation analysis was used to detect the correlations between *BTG3* mRNA and *miR-18a-5p*, or *BTG3* mRNA and *CASC2* expression in CRC tissues. Data are represented as the mean  $\pm$  SD (n=3). The data were analyzed by Mann-Whitney test or one-way ANOVA. \*\*, P<0.01, \*\*\*, P<0.001, CRC; Colorectal cancer, and qRT-PCR; Quantitative real-time polymerase chain reaction.

## Discussion

In recent years, multiple lncRNAs have been identified as a potential biomarkers and therapy targets for CRC prognosis and treatment (20). As reported, *CASC2* is frequently dysregulated in diverse cancers and modulates a wide range of biological processes (21-23). For instance, *CASC2* up-regulation inhibits the viability and metastasis of breast cancer cells by inhibiting the TGF- $\beta$  signaling pathway (21); *CASC2* inhibits the malignant biological processes of hepatocellular carcinoma cells through the MAPK signaling pathway (23). Here, we validated that *CASC2* expression was reduced in CRC tissues and cell lines and demonstrated that *CASC2* low expression was associated with the unfavorable clinicopathological indexes; functionally, we also demonstrated that *CASC2*

overexpression can suppress the malignant phenotypes of CRC cells. Our findings are consistent with the previous reports (12).

Reportedly, lncRNA can interact with miRNA as a molecular sponge of miRNA, thereby regulating the expression of the target genes of miRNA (24, 25). Besides, some studies have revealed several target miRNAs of *CASC2* in cancer. For example, in hepatocellular carcinoma, *CASC2* inhibits cell viability and induces apoptosis via modulating *miR-24-3p* (26). In addition, *CASC2* inhibits the tumorigenesis of hepatocellular carcinoma, melanoma, nasopharyngeal carcinoma and other malignant tumors through sponging *miR-18a-5p* (27-29). However, there are few reports about the target the miRNA of *CASC2* in CRC. Here, we confirmed that *miR-18a-5p* was a direct target of *CASC2* in CRC cells.

As reported, *miR-18a-5p* is pivotal in the pathogenesis of many human diseases including cancers. For example, *miR-18a-5p* accelerates osteosarcoma cell migration and invasion via directly targeting *IRF2* (30); in renal cell carcinoma, *miR-18a-5p* up-regulation can promote cancer cells proliferation, migration, invasion and inhibit apoptosis (31). The present work proved that *miR-18a-5p* expression level was elevated in CRC tissues, which is consistent with previous reports (16). Additionally, we focused on the interactions between *CASC2* and *miR-18a-5p* in CRC. Our research proved that *miR-18a-5p* was a direct target of *CASC2*, and *CASC2* could negatively modulate *miR-18a-5p* expression. Moreover, up-regulation of *miR-18a-5p* could counteract the inhibitory effect of *CASC2* overexpression on the proliferative, migrative and invasive abilities of CRC cells.

To further understand the downstream mechanism of *CASC2*, we focused on studying the downstream target of *miR-18a-5p*. Interestingly, a hidden binding site between *miR-18a-5p* and *BTG3* was revealed by searching the StarBase database. Reportedly, *BTG3* is an important participant in regulating cell growth, differentiation, migration, and DNA damage repair (32, 33). In gastric cancer, *BTG3* down-regulation facilitates the proliferative, migrative and invasive abilities of gastric cancer cells (18). *BTG3* overexpression represses the multiplication and invasion of epithelial ovarian cancer cells via modulating AKT/GSK3 $\beta$ / $\beta$ -Catenin signaling (34). In this work, we validated that *BTG3* was weakly expressed in CRC tissues and cells. Besides, we confirmed for the first time that there was a targeting relation between *miR-18a-5p* and *BTG3* in CRC cells. Moreover, we reported that *CASC2* could positively regulate *BTG3* expression, probably via suppressing *miR-18a-5p*. Collectively, *CASC2*, *miR-18a-5p* and *BTG3* could form a ceRNA network to regulate the CRC development.

## Conclusion

According to our findings, *CASC2* expression is reduced in CRC tissues and cell lines. In addition, *CASC2* can

repress the proliferative, migrative and invasive abilities of CRC cells via targeting *miR-18a-5p* and increasing *BTG3* expression. This work provides a novel mechanism to explain the progression of CRC cells, and restoration of *CASC2* may be a novel therapy strategy for CRC treatment.

## Acknowledgments

The data used to support the findings of this study are available from the corresponding author upon request. There is no financial support and conflict of interest in this study.

## Authors' Contributions

X.H.S.; Conceive and experiments design. L.M.K., J.S., J.L.; Experiments performing. F.X., Q.L.Z.; Data analysis. L.M.K., X.H.S.; Manuscript writing. All authors read and approved the final manuscript.

## References

- Shang A, Wang X, Gu C, Liu W, Sun J, Zeng B, et al. Exosomal miR-183-5p promotes angiogenesis in colorectal cancer by regulation of FOXO1. *Aging (Albany NY)*. 2020; 12.
- Siegel RL, Miller KD, Goding Sauer A, Fedewa SA, Butterly LF, Anderson JC, et al. Colorectal cancer statistics, 2020. *CA Cancer J Clin*. 2020; 70(3): 145-164.
- Keum N, Giovannucci E. Global burden of colorectal cancer: emerging trends, risk factors and prevention strategies. *Nat Rev Gastroenterol Hepatol*. 2019; 16(12): 713-732.
- Kim SY, Kim HS, Park HJ. Adverse events related to colonoscopy: Global trends and future challenges. *World J Gastroenterol*. 2019; 25(2): 190-204.
- Liu Q, Li A, Wang L, He W, Zhao L, Wu C, et al. Stomatin-like protein 2 promotes tumor cell survival by activating the JAK2-STAT3-PIM1 pathway, suggesting a novel therapy in CRC. *Mol Ther Oncolytics*. 2020; 17: 169-179.
- Wang X, Yu B, Jin Q, Zhang J, Yan B, Yang L, et al. Regulation of laryngeal squamous cell cancer progression by the lncRNA RP11-159K7.2/miR-206/DNMT3A axis. *J Cell Mol Med*. 2020; 24(12): 6781-6795.
- Kotake Y, Nakagawa T, Kitagawa K, Suzuki S, Liu N, Kitagawa M, et al. Long non-coding RNA ANRIL is required for the PRC2 recruitment to and silencing of p15(INK4B) tumor suppressor gene. *Oncogene*. 2011; 30(16): 1956-1962.
- Li Y, Xu K, Xu K, Chen S, Cao Y, Zhan H. Roles of identified long noncoding RNA in diabetic nephropathy. *J Diabetes Res*. 2019; 2019: 5383010.
- Ni Y, Li C, Bo C, Zhang B, Liu Y, Bai X, et al. LncRNA EGOT regulates the proliferation and apoptosis of colorectal cancer by miR-33b-5p/CROT axis. *Biosci Rep*. 2020; BSR20193893.
- Xu DF, Wang LS, Zhou JH. Long non-coding RNA CASC2 suppresses pancreatic cancer cell growth and progression by regulating the miR-24/MUC6 axis. *Int J Oncol*. 2020; 56(2): 494-507.
- Xing HB, Qiu HM, Li Y, Dong PF, Zhu XM. Long noncoding RNA CASC2 alleviates the growth, migration and invasion of oral squamous cell carcinoma via downregulating CDK1. *Eur Rev Med Pharmacol Sci*. 2019; 23(11): 4777-4783.
- Huang G, Wu X, Li S, Xu X, Zhu H, Chen X. The long noncoding RNA CASC2 functions as a competing endogenous RNA by sponging miR-18a in colorectal cancer. *Sci Rep*. 2016; 6: 26524.
- Feng L, Lin T, Che H, Wang X. Long noncoding RNA DANCR knockdown inhibits proliferation, migration and invasion of glioma by regulating miR-135a-5p/BMI1. *Cancer Cell Int*. 2020; 20: 53.
- Liu R, Shen L, Lin C, He J, Wang Q, Qi Z, et al. MiR-1587 regulates DNA damage repair and the radiosensitivity of CRC cells via targeting LIG4. *Dose Response*. 2020; 18(2): 1559325820936906.
- Xu Y, Zhong YD, Zhao XX. MiR-548b suppresses proliferative capacity of colorectal cancer by binding WNT2. *Eur Rev Med Pharmacol Sci*. 2020; 24(20): 10535-10541.
- Yin SL, Xiao F, Liu YF, Chen H, Guo GC. Long non-coding RNA FENDRR restrains the aggressiveness of CRC via regulating miR-18a-5p/ING4 axis. *J Cell Biochem*. 2020; 121(8-9): 3973-3985.
- Matsuda S, Rouault J, Magaud J, Berthet C. In search of a function for the TIS21/PC3/BTG1/TOB family. *FEBS Lett*. 2001; 497(2-3): 67-72.
- Ren XL, Zhu XH, Li XM, Li YL, Wang JM, Wu PX, et al. Down-regulation of BTG3 promotes cell proliferation, migration and invasion and predicts survival in gastric cancer. *J Cancer Res Clin Oncol*. 2015; 141(3): 397-405.
- Mao D, Qiao L, Lu H, Feng Y. B-cell translocation gene 3 over-expression inhibits proliferation and invasion of colorectal cancer SW480 cells via Wnt/ $\beta$ -catenin signaling pathway. *Neoplasma*. 2016; 63(5): 705-716.
- Li T, Wang B, Zhang L, Cui M, Sun B. Silencing of long noncoding RNA LINC00346 inhibits the tumorigenesis of colorectal cancer through targeting MicroRNA-148b. *Onco Targets Ther*. 2020; 13: 3247-3257.
- Zhang Y, Zhu M, Sun Y, Li W, Wang Y, Yu W. Upregulation of lncRNA CASC2 suppresses cell proliferation and metastasis of breast cancer via inactivation of the TGF- $\beta$  signaling pathway. *Oncol Res*. 2019; 27(3): 379-387.
- Xue Z, Zhu X, Teng Y. Long non-coding RNA CASC2 inhibits progression and predicts favorable prognosis in epithelial ovarian cancer. *Mol Med Rep*. 2018; 18(6): 5173-5181.
- Gan Y, Han N, He X, Yu J, Zhang M, Zhou Y, et al. Long non-coding RNA CASC2 regulates cell biological behaviour through the MAPK signalling pathway in hepatocellular carcinoma. *Tumour Biol*. 2017; 39(6): 1010428317706229.
- Wang L, Cho KB, Li Y, Tao G, Xie Z, Guo B. Long noncoding RNA (lncRNA)-mediated competing endogenous RNA networks provide novel potential biomarkers and therapeutic targets for colorectal cancer. *Int J Mol Sci*. 2019; 20(22): 5758.
- Matboli M, Shafei AE, Ali MA, El-Din Ahmed TS, Naser M, Abdel-Rahman T, et al. Role of extracellular lncRNA-SNHG14/miRNA-3940-5p/NAP12 mRNA in colorectal cancer. *Arch Physiol Biochem*. 2019; 9(1): 1-7.
- Fan JC, Zeng F, Le YG, Xin L. LncRNA CASC2 inhibited the viability and induced the apoptosis of hepatocellular carcinoma cells through regulating miR-24-3p. *J Cell Biochem*. 2018; 119(8): 6391-6397.
- Liu QY, Gao LY, Xu L, Zhang XL, Zhang LJ, Gong XL, et al. CASC2 inhibits the growth, migration, and invasion of thyroid cancer cells through sponging miR-18a-5p/FIH1 axis. *Kaohsiung J Med Sci*. 2021; 37(4): 268-275.
- Zhang Y, Qian W, Feng F, Cao Q, Li Y, Hou Y, et al. Upregulated lncRNA CASC2 may inhibit malignant melanoma development through regulating miR-18a-5p/RUNX1. *Oncol Res*. 2019; 27(3): 371-377.
- Miao WJ, Yuan DJ, Zhang GZ, Liu Q, Ma HM, Jin QQ. lncRNA CASC2/miR-18a-5p axis regulates the malignant potential of nasopharyngeal carcinoma by targeting RBBP8. *Oncol Rep*. 2019; 41(3): 1797-1806.
- Lu C, Peng K, Guo H, Ren X, Hu S, Cai Y, et al. miR-18a-5p promotes cell invasion and migration of osteosarcoma by directly targeting IRF2. *Oncol Lett*. 2018; 16(3): 3150-3156.
- Zhou L, Li Z, Pan X, Lai Y, Quan J, Zhao L, et al. Identification of miR-18a-5p as an oncogene and prognostic biomarker in RCC. *Am J Transl Res*. 2018; 10(6): 1874-1886.
- Winkler GS. The mammalian anti-proliferative BTG/Tob protein family. *J Cell Physiol*. 2010; 222(1): 66-72.
- Du Y, Liu P, Zang W, Wang Y, Chen X, Li M, et al. BTG3 upregulation induces cell apoptosis and suppresses invasion in esophageal adenocarcinoma. *Mol Cell Biochem*. 2015; 404(1-2): 31-38.
- An Q, Zhou Y, Han C, Zhou Y, Li F, Li D. BTG3 Overexpression suppresses the proliferation and invasion in epithelial ovarian cancer cell by regulating AKT/GSK3 $\beta$ / $\beta$ -Catenin signaling. *Reprod Sci*. 2017; 24(10): 1462-1468.

# MiR-140-3p Ameliorates The Inflammatory Response of Airway Smooth Muscle Cells by Targeting HMGB1 to Regulate The JAK2/STAT3 Signaling Pathway

Jun Meng, M.D.<sup>1#</sup>, Yingxia Zou, M.D.<sup>2#</sup>, Li Hou, M.D.<sup>3#</sup>, Limin He, M.D.<sup>4</sup>, Yuanjuan Liu, M.D.<sup>4,5</sup>, Menghan Cao, M.D.<sup>4</sup>,  
Chunjie Wang, M.D.<sup>3\*</sup>, Junying Du, M.D.<sup>2\*</sup>

1. Maternity School, Yuhuangding Hospital, Yantai, Shandong Province, China  
2. Children's Health Clinic, Yuhuangding Hospital, Yantai, Shandong Province, China  
3. Department of Gynecology and Obstetrics, Yuhuangding Hospital, Yantai, Shandong Province, China  
4. Department of Respiratory Medicine, Penglai Second People's Hospital, Penglai, Shandong Province, China  
5. Department of Respiratory Medicine, The Second Hospital of Shandong University, Jinan, Shandong Province, China

\*Corresponding Addresses: Department of Gynecology and Obstetrics, Yuhuangding Hospital, Yantai, Shandong Province, China  
Children's Health Clinic, Yuhuangding Hospital, Yantai, Shandong Province, China  
Emails: [ujju86586@163.com](mailto:ujju86586@163.com), [xyuu60667@163.com](mailto:xyuu60667@163.com)

# These authors contributed equally to this work.

Received: 11/May/2021, Accepted: 30/May/2022

## Abstract

**Objective:** The growth and migration of airway smooth muscle cells (ASMCs) are dysregulated in asthma. MicroRNAs (miRNAs) are associated with the pathogenesis of many diseases including asthma. Instead, the function of *miR-140-3p* in ASMCs' dysregulation in asthma remains inconclusive. This study aimed to explore the role and mechanism of *miR-140-3p* in ASMCs' dysregulation.

**Materials and Methods:** In this experimental study, ASMCs were stimulated with platelet-derived growth factor (PDGF)-BB to construct an asthma cell model *in vitro*. *MiR-140-3p* expression level in the plasma of 50 asthmatic patients and 50 healthy volunteers was measured with quantitative real-time polymerase chain reaction (qRT-PCR). Besides, the enzyme-linked immunosorbent assay (ELISA) was applied to detect the contents of interleukin (IL) -1 $\beta$ , IL-6, and tumor necrosis factor- $\alpha$  (TNF- $\alpha$ ) in the cell culture supernatant of ASMCs. Additionally, CCK-8 and transwell assays were adopted to probe the multiplication and migration of ASMCs. In addition, the western blot was employed to examine *HMGB1*, *JAK2*, and *STAT3* protein expressions in ASMCs after *miR-140-3p* and *HMGB1* were selectively regulated.

**Results:** *miR-140-3p* expression was declined in asthmatic patients' plasma and ASMCs stimulated by PDGF-BB. Upregulating *miR-140-3p* suppressed the viability and migration of the cells and alleviated the inflammatory response while inhibiting *miR-140-3p* showed opposite effects. Additionally, *HMGB1* was testified as the target of *miR-140-3p*. *HMGB1* overexpression could reverse the impact of *miR-140-3p* upregulation on the inflammatory response of ASMCs stimulated by PDGF-BB. *MiR-140-3p* could repress the activation of *JAK2/STAT3* via suppressing *HMGB1*.

**Conclusion:** In ASMCs, *miR-140-3p* can inhibit the *JAK2/STAT3* signaling pathway by targeting *HMGB1*, thus ameliorating airway inflammation and remodeling in the pathogenesis of asthma.

**Keywords:** Asthma, *HMGB1*, *JAK2/STAT3*, *miR-140-3p*

Cell Journal (Yakhteh), Vol 24, No 11, November 2022, Pages: 673-680

**Citation:** Meng J, Zou Y, Hou L, He L, Liu Y, Cao M, Wang Ch, Du J. MiR-140-3p ameliorates the inflammatory response of airway smooth muscle cells by targeting HMGB1 to regulate the JAK2/STAT3 signaling pathway. 2022; 24(11): 673-680. doi: 10.22074/cellj.2022.8067.

This open-access article has been published under the terms of the Creative Commons Attribution Non-Commercial 3.0 (CC BY-NC 3.0).

## Introduction

Bronchial asthma is a prevalent chronic respiratory inflammatory disease, featuring airway inflammation, airway remodeling, and hyper responsiveness. It's been shown that various cells (eosinophils, T cells, neutrophils, mast cells, and airway epithelial cells, etc.) and inflammatory mediators are involved in its pathogenesis (1, 2). It is estimated that 5% of adults and 10% of children suffer from asthma (3, 4). The anti-inflammatory drugs and bronchodilators can effectively control airway inflammation and hyperresponsiveness respectively; however the current treatments are not enough to reverse airway remodeling. Reportedly, the abnormal proliferation and migration of airway smooth muscle cells (ASMCs) are pivotal in airway

remodeling (5). Specifically, platelet-derived growth factor BB (PDGF-BB) can promote the multiplication and migration of ASMCs, thus aggravating airway remodeling in asthma (6).

MicroRNAs (miRNAs) are single-stranded non-coding RNAs with about 19-22nt in length, which inhibit the translation process via binding with the 3'- untranslated region (3'-UTR) of mRNAs (7, 8). More and more evidence has shown that miRNAs are vital in modulating the phenotype of ASMCs in the pathogenesis of asthma (9). Up to now, many miRNAs including *miR-200a*, *miR-142*, and *miR-485* have been reported to be implicated in the regulation of multiplication and migration of ASMCs (10-12). In addition, *miR-140-3p* is declined in human bronchial smooth muscle cells which are

stimulated by interleukin (IL)-13 (13). Instead, how *miR-140-3p* modulates the dysfunction of ASMCs in asthma is indeterminate.

High mobility group box 1 (*HMGB1*), is known as a non-histone chromosome binding protein with a highly conserved structure (14). It is reported that *HMGB1* is an important inflammatory mediator, which is related to immune diseases, malignancies, and other diseases (15). *HMGB1* is also a pivotal regulator in airway inflammation and remodeling in asthma (16). The aim of this study was to investigate the regulatory effects of *miR-140-3p* on the proliferation, migration, and inflammatory response of ASMCs after PDGF-BB stimulation and to explore the interplay between *miR-140-3p* and *HMGB1*. This study revealed a new molecular mechanism in the process of asthma exacerbation and suggested a new theoretical foundation for its treatment.

## Materials and Methods

### Clinical samples

This experimental study, with the written informed consent of all patients, healthy volunteers, or guardians of participants, was endorsed by the Ethics Committee of Linyi Central Hospital (2017-0041). Experiments involving human tissue were performed according to the Declaration of Helsinki. Blood samples of 50 patients with acute asthma treated in Linyi Central Hospital from March 2018 to June 2019 were collected. Blood samples of 50 healthy volunteers were used as the negative control. The patients were selected by simple random sampling. Blood samples were collected by vacuum blood collection tubes containing ethylene diamine tetra acetic acid (EDTA) and centrifuged at 1600×g for 15 minutes at 4°C to obtain supernatant and at 16000×g for another 10 minutes at 4°C to separate plasma. Ultimately, the separated plasma was stored at -80°C for the subsequent analysis. 50 patients with acute exacerbation asthma, were included 32 males and 18 females, with a mean age of (35.8 ± 8.76) years. Inclusion criteria were A. Meeting the diagnostic criteria of the Global Initiative for Asthma (GINA) guidelines (2016) (17); B. Being in the acute exacerbation phase, C. Age ≥16 years old. Exclusion criteria: A. Any active severe infections, B. Any presence of malignant hematological diseases or tumors, and C. Recent treatment with corticosteroids, immunosuppressants, and immunomodulators. The enrolled controls were healthy individuals who underwent physical examination in our hospital during the same period, including 27 males and 23 females with a mean age of (36.7 ± 3.12) years. Inclusion criteria were: A. Normal lung function, B. No history of asthma or other allergic diseases, C. No infections within 4 weeks, and D. Age ≥16 years. Exclusion criteria: A. Those with autoimmune diseases, hematologic diseases, severe infections, and malignancies, B. Pregnant or lactating women, and C. A recent history of leukotriene receptor

antagonists as well as glucocorticoid use.

### Cell culture and cell transfection

In this experimental study, human ASMCs were available from the Cell Bank of the Chinese Academy of Sciences (Shanghai, China). Subsequently, cells were cultivated in DMEM (Corning, Manassas, VA, USA) containing 10% fetal bovine serum (FBS), 100 U/mL penicillin, and 100 µg/mL streptomycin (Thermo Fisher Scientific, MA, USA) in 5% CO<sub>2</sub> at 37°C. When cells reached 90% confluence, subculture was carried out. ASMCs were treated with different concentration of PDGF-BB (0, 1, 10, 20, 40, 60 mg/mL, R&D Systems, Minneapolis, MN, USA) for different times (1-48 hours) to construct the *in vitro* model of asthma.

*MiR-140-3p* mimics (*miR-140-3p*), mimic negative control (miR-NC), *miR-140-3p* inhibitors (*miR-140-3p-in*), inhibitor negative control (miR-in), pcDNA3.0-*HMGB1* (*HMGB1*) and empty vector pcDNA3.0 were available from RiboBio (Guangzhou, China). Subsequently, ASMCs were transferred into a 24-well cell plate at 3×10<sup>5</sup> cells/well, and cultured at 37°C in 5% CO<sub>2</sub> for 24 hours, and then the cells were transfected by Lipofectamine 2000 (Invitrogen, Carlsbad, CA, USA).

### Quantitative real-time polymerase chain reaction

Total RNA was extracted from plasma and cells by TRIzol reagent (Invitrogen, Carlsbad, CA, USA). Total RNA was reverse transcribed into cDNA by TaqMan microRNA Reverse Transcription Kit (Applied Biosystems, Foster City, CA, USA) and PrimeScript RT Kit (Takara, Dalian, China). According to the manufacturer's protocol, qRT-PCR was conducted on ABI 7300 system (Applied Biosystems, Foster City, CA, USA) with an SYBR Green PCR Master Mix kit (Thermo Fisher Scientific, Carlsbad, CA, USA), with *U6* or *β-actin* as the endogenous control. Ultimately, the relative expressions were estimated by the 2<sup>-ΔΔCt</sup> method. The primer sequences are detailed in Table 1.

Table 1: Primer sequences

Gene	Primer sequences (5'-3')
<i>miR-140-3p</i>	F: GCGCGTACCACAGGGTAGAA
	R: AGTGCAGGGTCCGAGGTATT
<i>U6</i>	F: CTCGCTTCGGCAGCACATATACTA
	R: ACGAATTTGCGTGTTCATCCTTGC
<i>HMGB1</i>	F: AGCTGCTAGCGCCTAGCGAT
	R: CCCGTCTGATAGCGCATTCTGT
<i>β-actin</i>	F: CGTGCGTGACATTAAAGAG
	R: TTGCCGATAGTGATGACCT

### Enzyme-linked immunosorbent assay

Cells and the medium were collected after 48 hours of continuous culture, and then the cells were under centrifuged at 1000×g for 10 minutes at 4°C to collect the supernatant. ELISA kits (Shanghai Xitang Biotechnology Co, Ltd, Shanghai, China) were adopted to detect the contents of interleukin-1 $\beta$  (IL-1 $\beta$ ), IL-6, and tumor necrosis factor- $\alpha$  (TNF- $\alpha$ ), respectively, according to the manufacturer's instructions.

### Cell proliferation assay

Cell counting kit 8 (CCK-8; Dojindo, Kumamoto, Japan) was adopted to estimate the proliferative capability of ASMCs. Cells were transferred into a 96-well plate ( $1 \times 10^3$  cells/well) and cultured at 37°C for 12 hours, and then 10  $\mu$ L of CCK-8 solution was added to each well. After incubation of cells for 1 hour, the absorbance was detected at 450nm wavelength by a spectrophotometer reader (Bio-Rad, Hercules, CA, USA). With the same method, the absorbance of the cells was examined at the 24<sup>th</sup>, 48<sup>th</sup>, 72<sup>nd</sup>, and 96<sup>th</sup> hours, respectively. After that, the proliferation curve was plotted.

### 5-bromo-2'-deoxyuridine (BrdU) assay

Cell proliferation was also probed by a BrdU kit (Sigma-Aldrich, Louis, MO, USA). Briefly, the cells were transferred into 96-well plates and incubated with BrdU labeling reagent for 2 hours at 37°C. Next, the cells were incubated with FixDenat solution for 30 minutes at ambient temperature. Subsequently, the cells were incubated with the anti-BrdU antibody for 90 minutes in the dark. Thereafter the nucleus was stained with DAPI staining solution for 10 minutes. Subsequently, the ASMCs were washed with phosphate buffered saline (PBS, Beyotime Biotechnology, China) and observed under a fluorescence microscope.

### Transwell assay

Cell migration was examined with the transwell chamber (24-well insert, 8- $\mu$ m pore size, Corning Costar, Cambridge, MA, USA). Briefly,  $1 \times 10^5$  cells resuspended in 200  $\mu$ L of serum-free medium were transferred into the upper compartment, with the lower compartment filled with a medium containing 20% FBS. Twenty-four hours later, the ASMCs that failed to migrate were removed from the upper membrane surface with cotton swabs, and the migrating cells fixed in methanol were stained with 0.1% crystal violet. Cells were rinsed in tap water, dried, and then photographed under an optical microscope. Image J software was used for counting the cells.

### Dual-luciferase reporter assay

Wild-type (WT) and mutant (MUT) sequences of

*HMGB1* were subcloned into psi-CHECK2 luciferase reporter vector (Promega, Madison, WI, USA), and *HMGB1*-WT or *HMGB1*-MUT reporter vectors were constructed, respectively. Then luciferase reporter vector and *miR-140-3p* or miR-NC were co-transfected into ASMCs by Lipofectamine 2000 (Invitrogen, Carlsbad, CA, USA). Forty-eight hours later, the luciferase activity was examined by a dual luciferase analysis system (Promega) as manufacturer's instructions.

### Western blot

Total proteins in ASMCs were extracted with RIPA lysis buffer (Solarbio, Beijing, China), and their concentration was quantified by a BCA protein detection kit (Solarbio, Beijing, China). An equal amount of protein samples (20  $\mu$ g per group) was separated by SDS-PAGE and transferred to a polyvinylidene fluoride membrane (Millipore, Bedford, MA, USA), which was then blocked with 5% skimmed milk for 1 hour. The membrane was firstly incubated with the primary antibody at 4°C overnight, and then with the secondary antibody, goat anti-rabbit IgG H&L (Abcam, ab6721, 1: 3000) at 37°C for 1 hour. Ultimately, the bands were developed with the enhanced chemiluminescence reagent (Pierce Biotechnology, Rockford, IL, USA). The primary antibodies were: anti-*HMGB1* (1: 1000, ab79823), anti-p-*JAK2* (1: 1000, #8082), anti-p-*STAT3* (1: 1000, #9145), anti-*JAK2* (1: 1000, #3230), anti-*STAT3* (1: 1000, #12640) and anti- $\beta$ -*actin* (1: 1000, ab6276). Among them, anti-*HMGB1* antibody and anti- $\beta$ -*actin* antibody were bought from Abcam (Shanghai, China); anti-p-*JAK2* antibody, anti-p-*STAT3* antibody, anti-*JAK2* antibody, and anti-*STAT3* antibody were all purchased from Cell Signaling Technology (Cell Signaling Technology, Danvers, MA, USA).

### Statistical analysis

SPSS 21.0 statistical software (SPSS Inc., Chicago, IL, USA) was applied for statistical analysis, with data shown as mean  $\pm$  standard deviation. Accordingly, the differences between the two groups were analyzed by student's t test. Besides, one-way ANOVA followed by Tukey post-hoc test was executed for comparing the data of more than two groups.  $P < 0.05$  indicated the statistical significance.

### Results

#### *miR-140-3p* expression is declined in plasma of asthmatic patients and ASMCs stimulated by PDGF-BB

First, we evaluated *miR-140-3p* expression levels in the plasma of 50 asthmatic patients and 50 healthy volunteers by qRT-PCR and observed that *miR-140-3p* expressions in the plasma of asthmatic patients were remarkably

lower than that of healthy individuals (Fig.1A). qRT-PCR also suggested that PDGF-BB inhibited *miR-140-3p* expression in ASMCs dose- and time-dependently (Fig.1B, C). The half-inhibitory concentration (IC<sub>50</sub>) value of PDGF-BB-induced *miR-140-3p* expression inhibition was about 22.37 ng/mL (Fig.1B). 24 hours of PDGF-BB treatment, were reduced *miR-140-3p* expression to less than 50% in ASMCs (Fig.1C). So, in the subsequent experiments, ASMCs were treated with 20 ng/mL PDGF-BB for 24 hours as the *in vitro* asthma model. It was found that compared with ASMCs in the control group, IL-1β, IL-6, and TNF-α levels in the asthma cell model were up-regulated (Fig.1D).

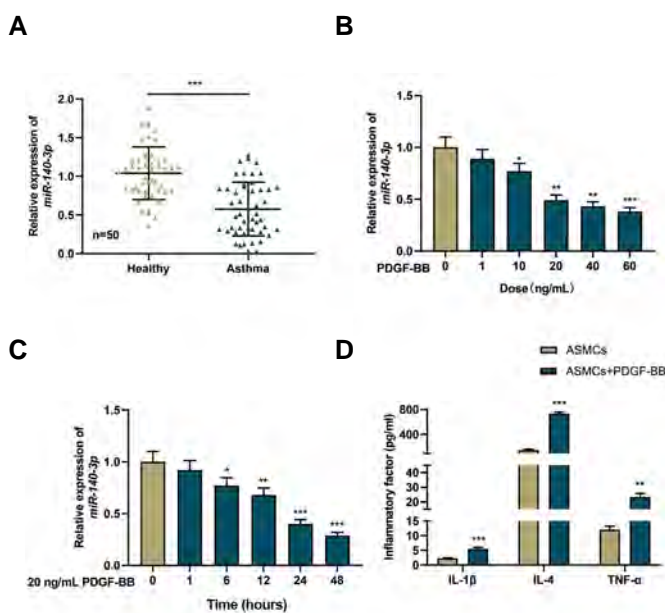


**Fig.1:** *miR-140-3p* is lowly expressed in plasma of asthmatic patients and ASMCs treated with PDGF-BB. **A.** The expression of *miR-140-3p* in plasma of asthmatic patients and healthy volunteers was detected by qRT-PCR. **B.** qRT-PCR was used to detect the relative expression of *miR-140-3p* after treating ASMCs with different concentrations (0, 1, 10, 20, 40, 60 ng/mL) of PDGF-BB for 24 hours. **C.** qRT-PCR was used to detect the relative expression of *miR-140-3p* after treating ASMCs with 20 ng/mL PDGF-BB for different time (1, 6, 12, 24, 48 hours). **D.** ELISA was used to detect the levels of IL-1β, IL-6 and TNF-α in the supernatant of ASMCs after treatment with 20 ng/mL PDGF-BB for 24 hours. Data are expressed as mean ± standard deviation (n=3). \*, P<0.05, \*\*, P<0.01, \*\*\*, P<0.001, ASMCs; Airway smooth muscle cells, qRT-PCR; Quantitative real-time polymerase chain reaction, PDGF-BB; Platelet-derived growth factor, ELISA; Enzyme-linked immunosorbent assay, IL-1β; Interleukin-1β, and TNF-α; tumor necrosis factor-α.

**MiR-140-3p restrains the multiplication and migration of PDGF-BB-induced ASMCs**

To study the biological function of *miR-140-3p* in the pathogenesis of asthma, we transfected miR-NC, *miR-140-3p* mimics, miR-in or *miR-140-3p* inhibitors into ASMCs, and successfully established the cell model of *miR-140-3p* overexpression or inhibition (Fig.2A). CCK-8, BrdU and transwell assays showed that overexpression of *miR-140-3p* significantly attenuated the promotion of PDGF-BB-induced proliferation and migration of

ASMCs, while *miR-140-3p* inhibitor exerted the opposite effect (Fig.2B-F).

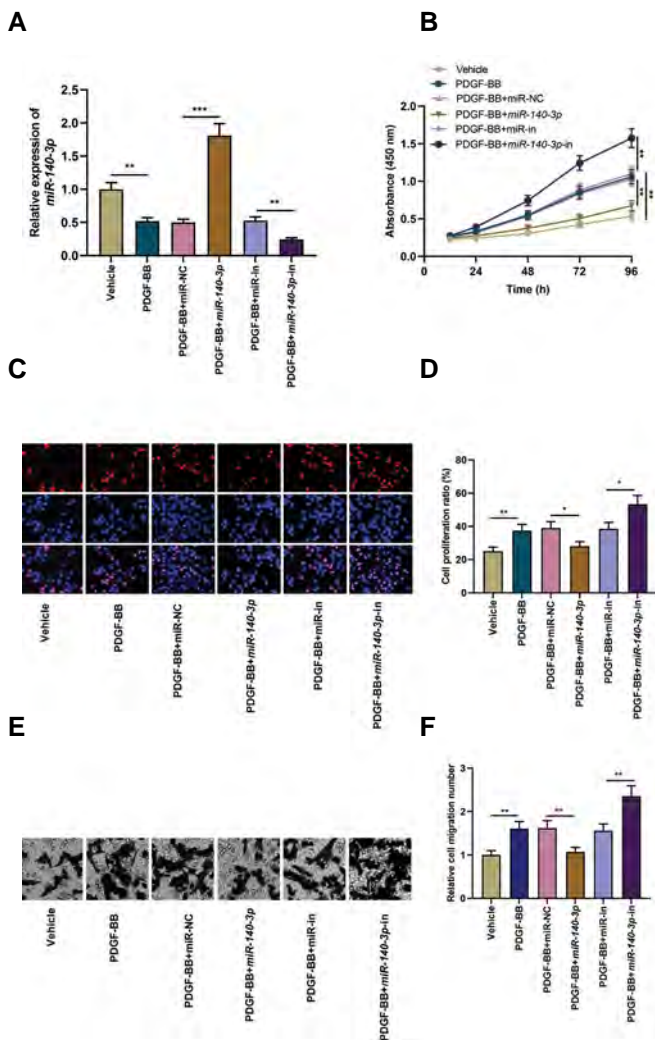


**Fig.2:** The effects of *miR-140-3p* on proliferation and migration of ASMCs induced by PDGF-BB. **A.** *miR-140-3p* mimics or inhibitors were transfected into ASMCs stimulated by 20 ng/mL PDGF-BB, and the expression of *miR-140-3p* was detected by qRT-PCR. **B.** CCK-8 assay, **C, D.** BrdU assay, and **E, F.** Transwell assay were used to detect the proliferation and migration of ASMCs stimulated by 20 ng/mL PDGF-BB after transfection. Data are expressed as mean ± standard deviation (n=3) (scale bar: C: 250 μm, E: 100 μm). \*, P<0.05, \*\*, P<0.01, \*\*\*, P<0.001, ASMCs; Airway smooth muscle cells, PDGF-BB; Platelet-derived growth factor, qRT-PCR; Quantitative real-time polymerase chain reaction, CCK-8; Cell counting kit 8, and BrdU; 5-bromo-2'-deoxyuridine.

**MiR-140-3p represses the inflammatory response of PDGF-BB-treated ASMCs**

Next, we performed ELISA and found that compared with the PDGF-BB+miR-NC group, the contents of IL-1β, IL-6, and TNF-α in the supernatant of ASMCs were markedly decreased subsequent to the transfection of *miR-140-3p* mimics; as against PDGF-BB+miR-in group, *miR-140-3p* inhibition restrained the production of IL-1β, IL-6, and TNF-α of PDGF-BB-stimulated ASMCs (Fig.3A-C), suggesting that *miR-140-3p* may repress the inflammatory response in asthma.

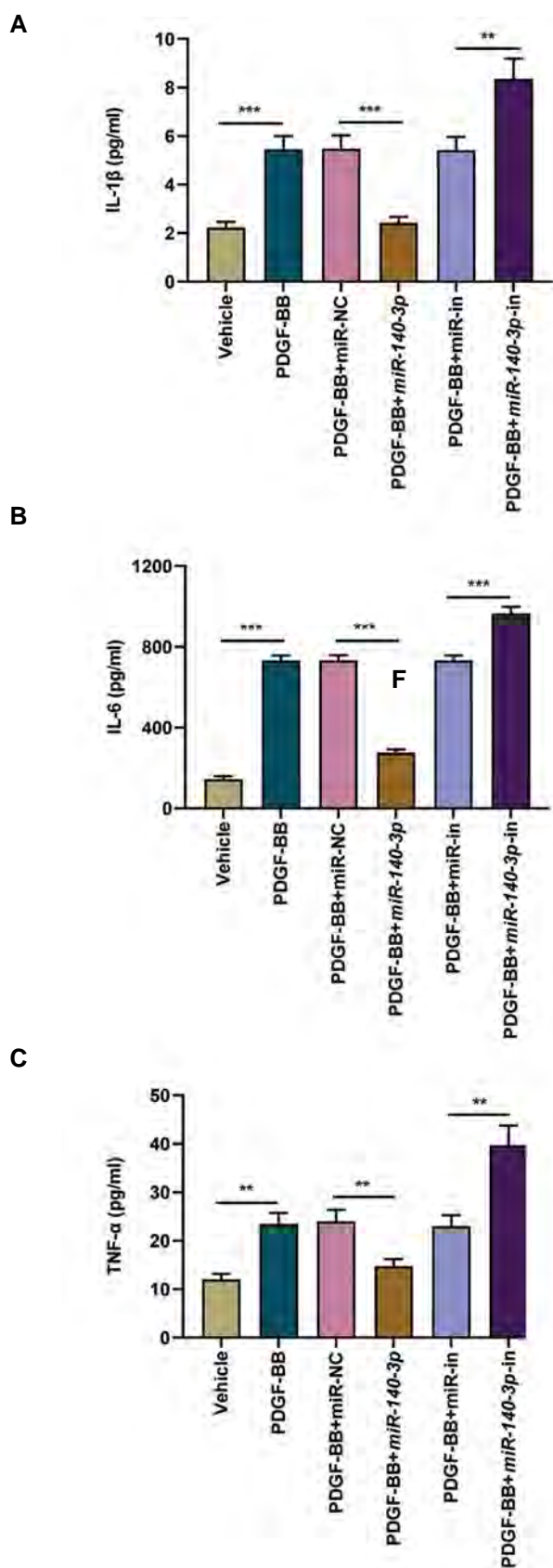


**Fig.3:** *miR-140-3p* inhibits the inflammatory reaction of ASMCs induced by PDGF-BB. ELISA was used to detect the levels of **A.** IL-1 $\beta$ , **B.** IL-6, and **C.** TNF- $\alpha$  in ASMC supernatants stimulated by 20 ng/mL PDGF-BB after transfection of *miR-140-3p* mimics or inhibitors. Data are expressed as mean  $\pm$  standard deviation (n=3). \*\*, P<0.01, \*\*\*, P<0.001, ASMCs; Airway smooth muscle cells, PDGF-BB; Platelet-derived growth factor, ELISA; Enzyme-linked immunosorbent assay, IL-1 $\beta$ ; Interleukin-1 $\beta$ , and TNF- $\alpha$ ; Tumor necrosis factor- $\alpha$ .

### *MiR-140-3p* targets *HMGB1*

We then predicted the target genes of *miR-140-3p* with the StarBase database and observed that there was a complementary binding site between *miR-140-3p* and *HMGB1* mRNA 3'-UTR (Fig.4A). Dual-luciferase reporter gene assay showed that transfection of *miR-140-3p* mimics impaired *HMGB1*-WT activity, but that of *HMGB1*-MUT was not significantly affected (Fig.4B). qRT-PCR and western blot showed that in PDGF-BB-treated ASMCs, *miR-140-3p* up-regulation restrained *HMGB1* mRNA and protein expression, while *miR-140-3p* down-regulation had the opposite effect (Fig. 4C, D). Collectively, *HMGB1* was the downstream target of *miR-140-3p* in ASMCs.

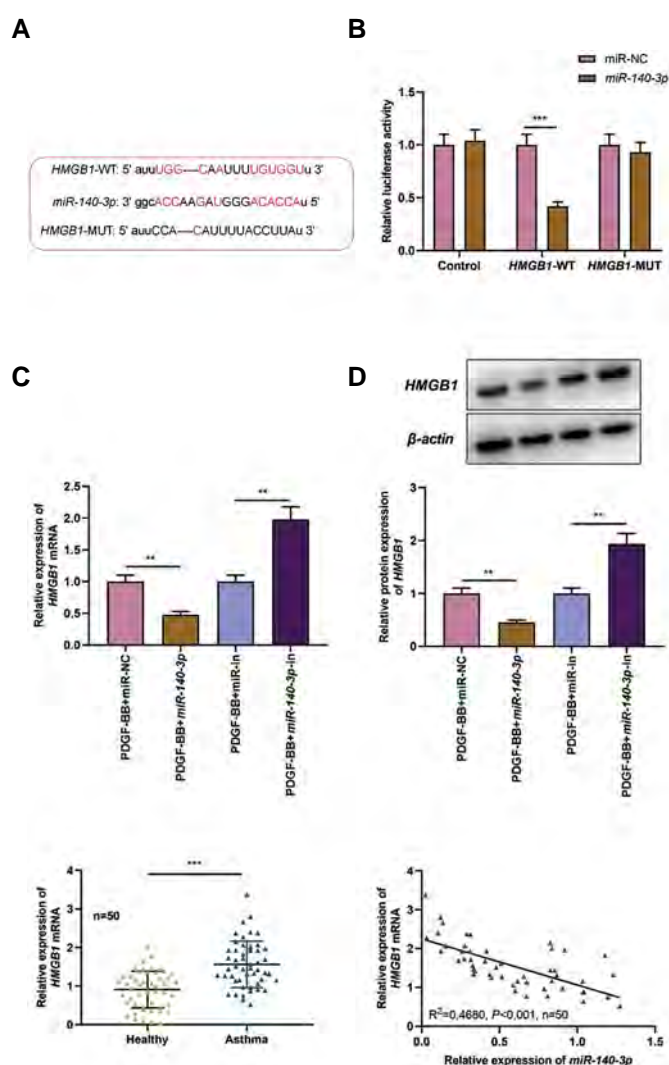


**Fig.4:** *HMGB1* is the downstream target of *miR-140-3p*. **A.** The binding sequence between *miR-140-3p* and *HMGB1* 3'-UTR. **B.** Dual-luciferase reporter gene experiment was used to verify the targeting relationship between *miR-140-3p* and *HMGB1*. **C.** qRT-PCR and **D.** Western blot were used to detect *HMGB1* mRNA and protein expression in ASMCs transfected with *miR-140-3p* mimics or inhibitors and stimulated by 20 ng/mL PDGF-BB. Data are expressed as mean  $\pm$  standard deviation (n=3). \*\*, P<0.01, \*\*\*, P<0.001, *HMGB1*; High mobility group box 1, qRT-PCR; Quantitative real-time polymerase chain reaction, ASMCs; Airway smooth muscle cells, and PDGF-BB; Platelet-derived growth factor.

### HMGB1 counteracts the impact of miR-140-3p in asthmatic ASMCS

To study the function of the miR-140-3p/HMGB1 axis in regulating the dysfunction of ASMCS, we transfected miR-140-3p mimics, HMGB1 overexpression plasmid or co-transfected miR-140-3p mimics and HMGB1 overexpression plasmids in ASMCS, respectively. qRT-PCR and western blot showed that HMGB1 overexpression enhanced HMGB1 mRNA and protein expressions in ASMCS stimulated by PDGF-BB and attenuated the impact of miR-140-3p overexpression on HMGB1 (Fig.5A, B). CCK-8, BrdU, and transwell assays indicated that HMGB1 overexpression markedly accelerated the multiplication and migration of PDGF-BB-treated ASMCS, and greatly counteracted miR-

140-3p overexpression's impacts on the growth and migration of PDGF-BB-stimulated ASMCS (Fig.5C-E). ELISA showed that compared with the PDGF-BB group, the contents of IL-1 $\beta$ , IL-6, and TNF- $\alpha$  in the PDGF-BB+HMGB1 group were up-regulated significantly; compared with those in the PDGF-BB+miR-140-3p group, these inflammatory factors in the PDGF-BB+miR-140-3p+HMGB1 group were also significantly increased (Fig.5F). Besides, Western blot showed that up-regulation of miR-140-3p repressed p-JAK2 and p-STAT3 expression levels in ASMCS, and HMGB1 overexpression significantly raised p-JAK2 and p-STAT3 expression levels, counteracting miR-140-3p overexpression's impact on p-JAK2 and p-STAT3 (Fig.5G).

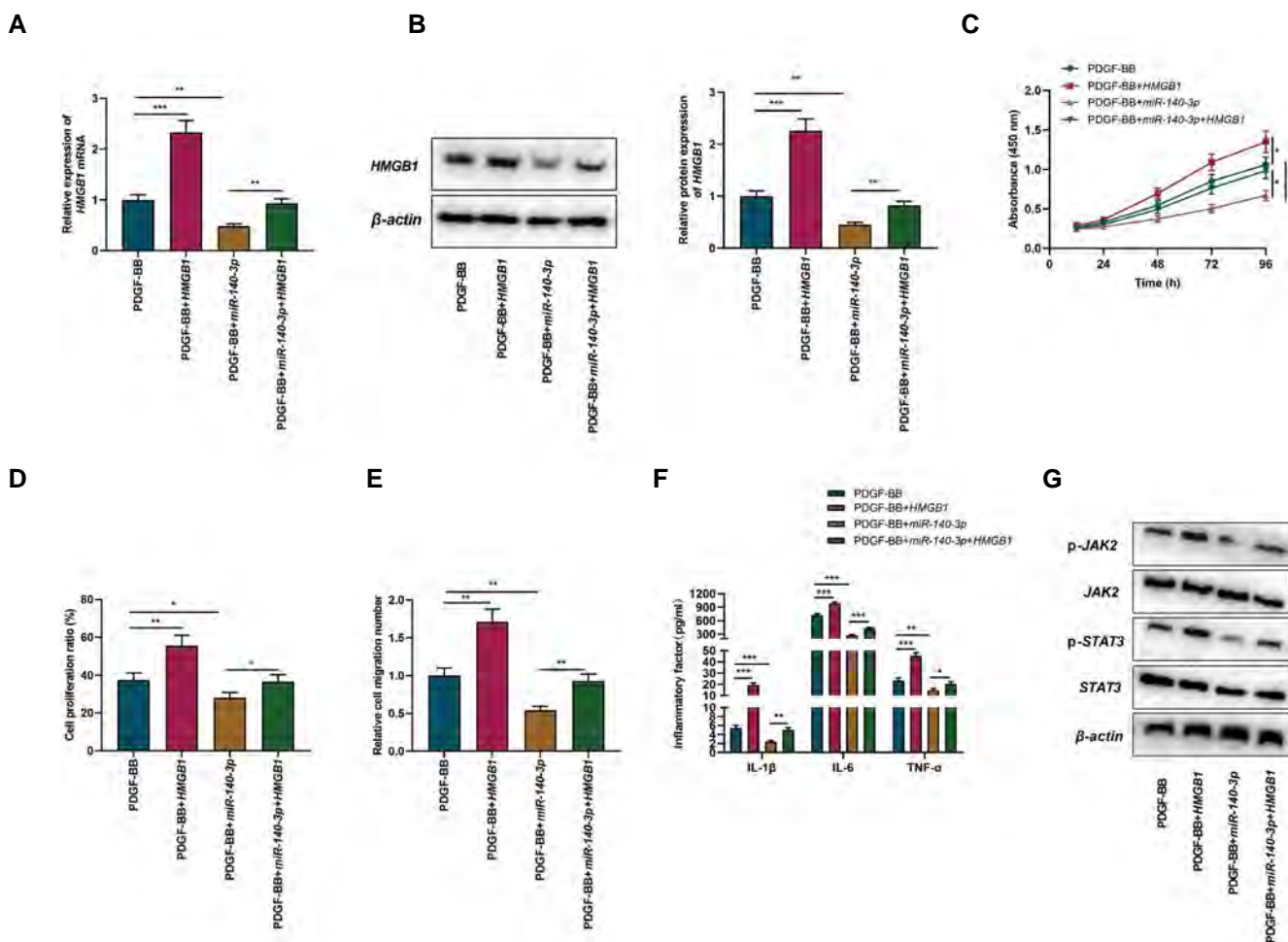


**Fig.5:** miR-140-3p targets HMGB1 through JAK2/STAT3 signaling pathway and inhibits the pathogenesis of asthma. **A.** qRT-PCR and **B.** Western blot were used to detect HMGB1 mRNA and protein expression in ASMCS stimulated with 20 ng/mL PDGF-BB after transfection with miR-140-3p mimics, HMGB1 overexpression plasmid or miR-140-3p mimics +HMGB1 overexpression. **C.** CCK-8 assay, **D.** BrdU assay, **E.** Transwell assay were used to detect the proliferation and migration of ASMCS stimulated by 20 ng/mL PDGF-BB after transfection. **F.** ELISA was used to detect the contents of IL-1 $\beta$ , IL-6, and TNF- $\alpha$  in the supernatant of ASMCS stimulated with 20 ng/mL PDGF-BB after transfection. **G.** Western blot assay was used to detect the protein expression of p-JAK2, p-STAT3, JAK2, and STAT3 in ASMCS stimulated by 20 ng/mL PDGF-BB after transfection. Data are expressed as mean  $\pm$  standard deviation (n=3). \*, P<0.05, \*\*, P<0.01, \*\*\*, P<0.001, HMGB1; High mobility group box 1, JAK2; Janus Kinase 2, STAT3; Signal transducer and activator of transcription 3, qRT-PCR; Quantitative real-time polymerase chain reaction, ASMCS; Airway smooth muscle cells, PDGF-BB; Platelet-derived growth factor, CCK-8; Cell counting kit 8, and BrdU; 5-bromo-2'-deoxyuridine, ELISA; Enzyme-linked immunosorbent assay, IL-1 $\beta$ ; Interleukin-1 $\beta$ , and TNF- $\alpha$ ; Tumor necrosis factor- $\alpha$ .

## Discussion

The abnormal growth and migration of ASMCs are crucial in the pathogenesis of respiratory diseases, like asthma (18). Many stimuli, such as growth factors, contraction agonists, inflammatory cytokines, and extracellular matrix proteins, have been reported to induce the multiplication and migration of ASMCs (19). PDGF-BB-induced growth and migration of ASMCs have been used to study the dysfunction of ASMCs in asthma *in vitro* (5). Here we observed that the stimulation of PDGF-BB markedly promoted the dysfunction of ASMCs, and when ASMCs were stimulated by PDGF-BB, the secretion of inflammatory cytokines was also significantly promoted, which is coherent with the previous studies (5, 20).

More and more evidence has shown that miRNAs exert crucial functions in regulating cell proliferation, migration, differentiation, and apoptosis, and are closely relevant to the progression of many human diseases, such as tumors, cardiovascular diseases, and asthma (21, 22). Importantly, it is reported that some miRNAs modulate the proliferation and migration of ASMCs (5, 23, 24). For example, *miR-638* expression is declined in PDGF-BB-induced ASMCs, and it suppresses the excessive growth and migration of ASMCs via pointing to *Cyclin D1* and *NOR1* (20); *miR-590-5p* represses the proliferation of ASMCs induced by PDGF via inhibiting *STAT3* (23); *miR-375* is down-regulated in ASMCs treated with PDGF, and it can block the proliferation and migration of ASMCs by targeting the *JAK2/STAT3* signaling (24). In this work, we demonstrated that the circulating *miR-140-3p* was down-regulated in the plasma of asthmatic patients. Furthermore, *miR-140-3p* expression was reduced in PDGF-BB-stimulated ASMCs, consistent with what was found in a previous study (25). Reportedly, *miR-140-3p* expression is impaired in ASMCs treated with TNF- $\alpha$ , and *miR-140-3p* can block the activation of *p38 MAPK* in ASMCs and inhibit the up-regulation of *CD38* induced by TNF- $\alpha$  (26). In addition, *miR-140-3p* inhibits PDGF-BB-induced ASMCs proliferation and promotes apoptosis by targeting *C-Myb* and *BCL-2* (25). Similarly, the present study confirmed that *miR-140-3p* up-regulation inhibited PDGF-BB-induced proliferation of ASMCs. Additionally, *miR-140-3p* up-regulation restrained the migration of ASMCs and the secretion of inflammatory cytokines induced by PDGF-BB; on the contrary, inhibition of *miR-140-3p* facilitated the growth, migration, and inflammation of ASMCs. Collectively, *miR-140-3p* could modulate the dysfunction of ASMCs in asthma.

To expound on the mechanism by which *miR-140-3p* regulates the proliferation and migration of ASMCs, we predicted the downstream targets of *miR-140-3p*. Interestingly, *HMGB1* was predicted as a target for *miR-140-3p*. Our results indicated that *miR-140-3p* could negatively modulate *HMGB1* expression in ASMCs. *HMGB1* can serve as a modulator in airway inflammation (27). Reportedly, resveratrol inhibits airway inflammation and remodeling in asthma via blocking the *HMGB1/*

*TLR4/NF- $\kappa$ B* pathway (28); cucurbitacin E can alleviate the injury and inflammation of bronchial epithelial cells induced by lipopolysaccharide via suppressing *HMGB1/TLR4/NF- $\kappa$ B* signaling (29). In a mouse model, *HMGB1* and *TLR4* depletion ameliorate asthma induced by diisononyl phthalate (DINP) (30). These studies imply that targeting *HMGB1* can probably alleviate the symptoms of asthma. In this study, we discovered that *HMGB1* overexpression promoted the viability, migration, and the activation of *JAK/STAT3* pathway of ASMCs stimulated by PDGF-BB. In addition, the effect of transfection of *miR-140-3p* mimics on the growth, migration, and inflammation of PDGF-BB-induced ASMCs could be counteracted by *HMGB1* overexpression. As reported, the abnormal activation of the *JAK/STAT3* pathway aggravates inflammatory diseases (31, 32). These findings suggest that, in the pathogenesis of asthma, the biological function of *miR-140-3p* in ASMCs is partly mediated by *HMGB1*.

## Conclusion

*miR-140-3p* expression is suppressed in asthmatic patients' plasma and ASMCs stimulated by PDGF-BB. *miR-140-3p* inhibits *JAK/STAT3* signaling activation via targeting *HMGB1*, thus blocking the growth, migration, and inflammatory response of PDGF-BB-stimulated ASMCs. Our findings highlight that the *miR-140-3p/HMGB1* axis is pivotal in regulating the pathogenesis of asthma and imply that targeting the *miR-140-3p/HMGB1* axis is a promising strategy to treat asthma.

## Acknowledgments

There is no financial support and conflict of interest in this study.

## Authors' Contributions

Y.L., C.W., J.D.; Designed the study and experiments. J.M., Y.Z., L.Ho., Y.L., M.C.; Collected clinical samples and performed the experiments. J.M., Y.Z., L.Ho., Y.L., L.He.; Conducted the data analysis. J.M., Y.Z., L.Ho., Y.L.; Drafted the manuscript. Y.L., J.M.; Reviewed and revised the manuscript. All authors read and approved the final manuscript.

## References

1. Liu G, Cooley MA, Nair PM, Donovan C, Hsu AC, Jarnicki AG, et al. Airway remodeling and inflammation in asthma are dependent on the extracellular matrix protein fibulin-1c. *J Pathol*. 2017; 243(4): 510-523.
2. Saglani S, Custovic A. Childhood asthma: advances using machine learning and mechanistic studies. *Am J Respir Crit Care Med*. 2019; 199(4): 414-422.
3. Bousquet J, Mantzouranis E, Cruz AA, Ait-Khaled N, Baena-Cagnani CE, Bleecker ER, et al. Uniform definition of asthma severity, control, and exacerbations: document presented for the World Health Organization Consultation on severe asthma. *J Allergy Clin Immunol*. 2010; 126(5): 926-938.
4. Poon AH, Hamid Q. Severe asthma: have we made progress? *Ann Am Thorac Soc*. 2016; 13 Suppl 1: S68-77.
5. Lin L, Li Q, Hao W, Zhang Y, Zhao L, Han W. Upregulation of lncRNA Malat1 induced proliferation and migration of airway smooth

- muscle cells via miR-150-eIF4E/Akt signaling. *Front Physiol.* 2019; 10: 1337.
6. Dai Y, Li Y, Cheng R, Gao J, Li Y, Lou C. TRIM37 inhibits PDGF-BB-induced proliferation and migration of airway smooth muscle cells. *Biomed Pharmacother.* 2018; 101: 24-29.
  7. Aquino-Jarquin G. Emerging role of CRISPR/Cas9 technology for MicroRNAs editing in cancer research. *Cancer Res.* 2017; 77(24): 6812-6817.
  8. Turner ML, Schnorfeil FM, Brocker T. MicroRNAs regulate dendritic cell differentiation and function. *J Immunol.* 2011; 187(8): 3911-3917.
  9. Deshpande DA, Dileepan M, Walseth TF, Subramanian S, Kannan MS. MicroRNA regulation of airway inflammation and airway smooth muscle function: relevance to asthma. *Drug Dev Res.* 2015; 76(6): 286-295.
  10. Liu Y, Miao Y, Gao X, Wang YY, Wang H, Zheng YW, et al. MicroRNA-200a affects the proliferation of airway smooth muscle cells and airway remodeling by targeting FOXC1 via the PI3K/AKT signaling pathway in ovalbumin-induced asthmatic mice. *Cell Physiol Biochem.* 2018; 50(6): 2365-2389.
  11. Wang J, Wang HS, Su ZB. MicroRNA-142 inhibits proliferation and promotes apoptosis in airway smooth muscle cells during airway remodeling in asthmatic rats via the inhibition of TGF- $\beta$  -the dependent EGFR signaling pathway. *Cell Physiol Biochem.* 2018; 47(4): 1682-1695.
  12. Wang J, Li HY, Wang HS, Su ZB. MicroRNA-485 modulates the TGF- $\beta$ / Smads signaling pathway in chronic asthmatic mice by targeting Smurf2. *Cell Physiol Biochem.* 2018; 51(2): 692-710.
  13. Chiba Y, Matsumoto M, Hanazaki M, Sakai H. Downregulation of miR-140-3p contributes to upregulation of CD38 protein in bronchial smooth muscle cells. *Int J Mol Sci.* 2020; 21(21): E7982.
  14. Goodwin GH, Johns EW. Are the high mobility group non-histone chromosomal proteins associated with 'active' chromatin? *Biochim Biophys Acta.* 1978; 519(1): 279-284.
  15. Musumeci D, Roviello GN, Montesarchio D. An overview on HMGB1 inhibitors as potential therapeutic agents in HMGB1-related pathologies. *Pharmacol Ther.* 2014; 141(3): 347-357.
  16. Imbalzano E, Quartuccio S, Di Salvo E, Crea T, Casciaro M, Gangemi S. Association between HMGB1 and asthma: a literature review. *Clin Mol Allergy.* 2017; 15: 12.
  17. Asthma Gf. Global strategy for asthma management and prevention. 2016. Available from: <http://ginasthma.org/wp-content/uploads/2016/04/GINA-2016-main-report-tracked.pdf> (11 May 2021).
  18. Liang X, Wang J, Chen W, Ma X, Wang Y, Nagao N, et al. Inhibition of airway remodeling and inflammation by isoforskolol in PDGF-induced rat ASMCs and OVA-induced rat asthma model. *Biomed Pharmacother.* 2017; 95: 275-286.
  19. Fixman ED, Stewart A, Martin JG. Basic mechanisms of development of airway structural changes in asthma. *Eur Respir J.* 2007; 29(2): 379-389.
  20. Wang H, Yao H, Yi B, Kazama K, Liu Y, Deshpande D, et al. MicroRNA-638 inhibits human airway smooth muscle cell proliferation and migration through targeting cyclin D1 and NOR1. *J Cell Physiol.* 2018; 234(1): 369-381.
  21. Shi ZG, Sun Y, Wang KS, Jia JD, Yang J, Li YN. Effects of miR-26a/miR-146a/miR-31 on airway inflammation of asthma mice and asthma children. *Eur Rev Med Pharmacol Sci.* 2019; 23(12): 5432-5440.
  22. Zhao Z, Sun W, Guo Z, Zhang J, Yu H, Liu B. Mechanisms of lncRNA/microRNA interactions in angiogenesis. *Life Sci.* 2020; 254:116900 .
  23. Shi S, Jin L, Zhang S, Li H, Zhang B, Sun M. MicroRNA-590-5p represses proliferation of human fetal airway smooth muscle cells by targeting signal transducer and activator of transcription 3. *Arch Med Sci.* 2018; 5(14 ): 1093-1101.
  24. Ji Y, Yang X, Su H. Overexpression of microRNA-375 impedes platelet-derived growth factor-induced proliferation and migration of human fetal airway smooth muscle cells by targeting Janus kinase 2. *Biomed Pharmacother.* 2018; 98: 69-75.
  25. Zhu ZR, He Q, Wu WB, Chang GQ, Yao C, Zhao Y, et al. MiR-140-3p is involved in in-stent restenosis by targeting C-Myb and BCL-2 in peripheral artery disease. *J Atheroscler Thromb.* 2018; 25(11): 1168-1181.
  26. Jude JA, Dileepan M, Subramanian S, Solway J, Panettieri RA Jr, Walseth TF, et al. miR-140-3p regulation of TNF- $\alpha$ -induced CD38 expression in human airway smooth muscle cells. *Am J Physiol Lung Cell Mol Physiol.* 2012; 303(5): L460-L468.
  27. Lv Y, Li Y, Zhang D, Zhang A, Guo W, Zhu S. HMGB1-induced asthmatic airway inflammation through GRP75-mediated enhancement of ER-mitochondrial Ca<sup>2+</sup> transfer and ROS increased. *J Cell Biochem.* 2018; 119(5): 4205-4215.
  28. Jiang H, Duan J, Xu K, Zhang W. Resveratrol protects against asthma-induced airway inflammation and remodeling by inhibiting the HMGB1/TLR4/NF- $\kappa$ B pathway. *Exp Ther Med.* 2019; 18(1): 459-466.
  29. Shang J, Liu W, Yin C, Chu H, Zhang M. Cucurbitacin E ameliorates lipopolysaccharide-evoked injury, inflammation and MU-C5AC expression in bronchial epithelial cells by restraining the HMGB1-TLR4-NF- $\kappa$ B signaling. *Mol Immunol.* 2019; 114: 571-577.
  30. Hwang YH, Lee Y, Paik MJ, Yee ST. Inhibitions of HMGB1 and TLR4 alleviate DNP-induced asthma in mice. *Toxicol Res (Camb).* 2019; 8(5): 621-629.
  31. Shi S, Liang D, Bao M, Xie Y, Xu W, Wang L, et al. Gx-50 inhibits neuroinflammation via  $\alpha$ 7 nAChR activation of the JAK2/STAT3 and PI3K/AKT pathways. *J Alzheimers Dis.* 2016; 50(3): 859-871.
  32. Liu J, Shang B, Bai J. IL-22/IL-22R1 promotes proliferation and collagen synthesis of MRC-5 cells via the JAK/STAT3 signaling pathway and regulates airway subepithelial fibrosis. *Exp Ther Med.* 2020; 20(3): 2148-2156.

# Ferulic Acid Ameliorates Cell Injuries, Cognitive and Motor Impairments in Cuprizone-Induced Demyelination Model of Multiple Sclerosis

Mojtaba Ghobadi, M.Sc.<sup>1</sup>, Babak Arji, M.Sc.<sup>2</sup>, Maryam Yadegari, Ph.D.<sup>2</sup>, Mansour Esmailidehaj, Ph.D.<sup>1</sup>, Farshad Homayouni-Moghadam, Ph.D.<sup>3</sup>, Mohammad Ebrahim Rezvani, Ph.D.<sup>1\*</sup>

1. Department of Physiology, School of Medicine, Shahid Sadoughi University of Medical Sciences, Yazd, Iran  
2. Department of Anatomical Sciences, School of Medicine, Shahid Sadoughi University of Medical Sciences, Yazd, Iran  
3. Department of Animal Biotechnology, Cell Science Research Centre, Royan Institute for Biotechnology, Isfahan, Iran

\*Corresponding Address: P.O.Box: 8915173149, Department of Physiology, School of Medicine, Shahid Sadoughi University of Medical Sciences, Yazd, Iran  
Email: me.rezvani@ssu.ac.ir

Received: 17/September/2021, Accepted: 14/February/2022

## Abstract

**Objective:** Ferulic acid (FA) is a phenolic compound that exhibits neuroprotective effects in the central nervous system (CNS). This study was conducted to evaluate the potential effects of FA on the cognitive and motor impairments in the cuprizone-induced demyelination model of multiple sclerosis (MS).

**Materials and Methods:** In this experimental study, demyelination was induced in mice by feeding them with chow containing cuprizone (CPZ) 0.2% for 6 weeks. Mice in the control group received normal chow. Mice in the CPZ+Veh, CPZ+FA10, and CPZ+FA100 groups received saline, and FA at a dose of 0, 10, or 100 mg/kg (intraperitoneal, I.P., daily) respectively. After cognitive and motor assessments, under anaesthesia, animal brains were removed for evaluating the histological, apoptosis, and molecular changes.

**Results:** The results showed that FA increased freezing behaviour in contextual ( $P<0.05$ ) and cued freezing tests ( $P<0.05$ ). FA also reduced the random arm entrance ( $P<0.01$ ) and increased spontaneous alternations into the arms of Y-maze compared to the CPZ+Veh group ( $P<0.05$ ). Time on the rotarod was improved in rats that received both doses of FA ( $P<0.01$ ). Demyelination, apoptosis, and relative mRNA expression of p53 were lower in the FA-treated groups relative to the CPZ+Veh group ( $P<0.01$ ). In addition, FA increased mRNA expression of brain-derived neurotrophic factor (*Bdnf*), *Olig2*, and *Mbp* ( $P<0.05$ ) but decreased *GFAP* mRNA expression compared to the CPZ+Veh group ( $P<0.01$ ).

**Conclusion:** The results of this study showed that FA plays a significant neuroprotective role in CPZ models of demyelination by reducing neuronal apoptosis and improving oligodendrocytes (OLs) growth and differentiation.

**Keywords:** Apoptosis, Cuprizone, Demyelination, Ferulic Acid, Oligodendrocyte

Cell Journal (Yakhteh), Vol 24, No 11, November 2022, Pages: 681-688

**Citation:** Ghobadi M, Arji B, Yadegari M, Esmailidehaj M, Homayouni-Moghadam F, Rezvani ME. Ferulic acid ameliorates cell injuries, cognitive and motor impairments in cuprizone-induced demyelination model of multiple sclerosis. 2022; 24(11): 681-688. doi: 10.22074/cellj.2022.8261.

This open-access article has been published under the terms of the Creative Commons Attribution Non-Commercial 3.0 (CC BY-NC 3.0).

## Introduction

Multiple sclerosis (MS) is one of the frequent neurological diseases characterized by chronic inflammation and demyelination in the central nervous system (CNS) (1). Demyelination of neurons in the CNS that is caused by the destruction of oligodendrocytes (OLs) leads to an abnormal interplay of glial and neural cells. This abnormality has been considered the main pathological substrate for the structural and abnormal functional consequences of MS (2). OLs are necessary for the myelination of neurons in the CNS and the normal transmission of neural signals. Also, they have a crucial role in axonal maintenance and regeneration (3). In addition to severe axonal dysfunction, apoptosis of neuronal and glial cells occurs in the CNS of patients with MS (4). Obvious demyelination and apoptotic atrophy are also observed in the corpus callosum (CC), the prefrontal cortex (PFC), the external capsule, and the hippocampus of the CNS (5). It has been demonstrated that the extensive demyelination in the CNS following

MS leads to cognitive and motor dysfunctions of the brain (6). While MS leads to several neurological disorders, optimal treatment for the disorder is yet to be discovered. Therefore, it is important to explore the potential novel neuroprotective compounds for MS therapy.

Ferulic acid (FA) is a phenolic compound widely found in vegetables, fruits, and some beverages such as coffee and beer (7). Previous studies have shown that FA has neuroprotective effects via antioxidant and anti-apoptotic mechanisms *in vitro* and *in vivo* (8), neural progenitor cell proliferation (9), differentiation of human bone marrow stromal cells into neural-like cells (10), prevention of neuronal apoptosis, acceleration of peripheral nerve regeneration, and neurogenesis (11).

There are experimental methods widely used for evaluating demyelination disorders. Cuprizone (CPZ) is a copper-chelating agent which is able to induce demyelination through the destruction of OLs. CPZ has been widely used for the induction of demyelination, and

CPZ-induced demyelination has been used as a model for the study of demyelination diseases such as MS (12). Administration of CPZ to C57BL/6 mice can induce apoptosis of mature OLs and subsequent demyelination accompanied by cognitive and motor disorders in the CC of the mice (13).

New complementary and alternative therapies that can increase OLs survival and repair the myelin sheaths are required to treat MS. Based on the present evidence for the beneficial effects of FA, we designed the study to evaluate the effect of FA on the OLs death and demyelination rate using the mouse model of CPZ-induced demyelination. The molecular and cellular mechanisms of the histological and cognitive effects of FA were targeted.

## Materials and Methods

### Chemicals

Cuprizone, Bis (cyclohexanone) oxaldihydrazone, FA (4-hydroxy-3-methoxy-cinnamic acid), Neutral Red, and Luxol- Fast blue powder were purchased from Sigma-Aldrich.co, Austria. RNA extraction kits were provided by Cinna Gen, Iran. RevertAid™ First Strand cDNA Synthesis kit was from TAKARA- BIO, Japan. Master Mix containing SYBR green DNA dye was purchased from Amplicon, Denmark, and the in-situ cell death detection kit POD (Cat no. 11 684 817 910) was obtained from Roche, Mannheim, Germany.

### Animals

All experiments were performed according to the agreement of the Animal Ethics Committee of the Yazd University of Medical Sciences (IR.SSU.MEDICINE.REC.1393.111). Male C57BL/6 mice (6-7 weeks old, 20-25 g weight) were obtained from the animal facility of Shiraz University (Shiraz, Iran). The animals were maintained in Plexiglas cages on a 12 hours light/dark cycle, controlled temperature (20-22 °C) and had free access to water and food. Every effort was taken to minimize the suffering and damage to the animals and tried to use as few animals as possible.

### Experimental protocols

In this experimental study, the animals were divided

into 4 groups of 10 mice. Group 1 (control) received standard rodent chow; the other three CPZ-treated groups received standard rodent chow mixed freshly with 0.2% CPZ for 6 weeks. Group 2 (CPZ+Veh) was treated with cuprizone and saline; group 3 (CPZ+FA10) was treated with FA at a dose of 10 mg/kg. Group 4 (CPZ+FA100) was treated with FA at a dose of 100 mg/kg. Saline or FA was administered orally once a day for 6 weeks (Table 1).

For evaluation of memory impairment and locomotor incoordination, we used the fear conditioning, Y-maze, and rotarod tests. At the end of the experiment, under anaesthesia, the brains were removed and fixed for evaluating the histological changes and apoptosis rate. Also, fresh brain tissues were used to quantify relative mRNA expressions of *Bdnf*, *Olig2*, *Gfap*, *Mbp*, and *p53* genes.

### Neurobehavioral assessments

#### Assessment of cognitive and memory impairments

##### Fear conditioning test

To determine the FA role in CPZ-induced memory impairment, we used a contextual fear conditioning test as previously described (14). On Day 1 (day of training), animals were placed into a fear conditioning chamber (Iran, Chamber: 25 × 24 × 21 cm) containing grey walls, a metal grid floor to deliver a shock, and equipped with a sound generator. The animal was first allowed to explore the chamber for 3 minutes, thereafter, presented the clicker sound for 30 seconds. At the end of the clicker sound, each animal received a foot shock (0.7 mA) at the last 2 seconds. Memory for the context (contextual memory) for each animal was determined by counting the freezing behavior, defined as the total lack of movement except for respiration. For the cued memory test, mice were placed into a novel context for 3 minutes, and after an initial 30 seconds of novel context evaluation, the same training tone was played for 3 minutes. Freezing behavior was scored over the 3 minutes testing period and data were presented as a percentage of time in the freezing over the total sampling period. Mice were habituated to the testing room for 30 minutes at the beginning of training and the test day. All tests were conducted by the same experimenter.

**Table 1:** The experimental groups and procedures

Group/Treatment	6 weeks administration	Behavioral assessments	Histological and molecular assessments
Group 1 (control)	Standard rodent chow	Motor and cognitive tests	LFB – TUNEL staining, real-time PCR
Group 2 (CPZ+Veh)	CPZ in food+Vehicle	Motor and cognitive tests	LFB – TUNEL staining, real-time PCR
Group 3 (CPZ+FA10)	CPZ in food+FA10	Motor and cognitive tests	LFB – TUNEL staining, real-time PCR
Group 4 (CPZ+FA100)	CPZ in food+FA100	Motor and cognitive tests	LFB – TUNEL staining, real-time PCR

CPZ; Cuprizone, FA; Ferulic acid, LFB-TUNEL; Luxol fast blue and TUNEL staining, and PCR; Polymerase chain reaction.

## Y-maze study

Working memory impairment was evaluated using 3 arms Y-maze apparatus. Each arm was 50 cm in length, 15 cm in height, and 10 cm in width, with equal angles (named A, B, and C). The behavioral evaluation was performed according to the previous study (15). Briefly, Mice were placed in the centre of the Y-maze and allowed to move their arms freely for 8 minutes. The total number of entrances and the number of alternations or the count of sequential entrances in the three different arms (e.g., ABC, BCA, CBA ...) were visually recorded. The percentage of alternation was calculated using the below acquisition:

$$\text{Alternation\%} = (\text{number of alternations} / \text{total number of arms entrances} - 2) \times 100.$$

## Assessment of motor coordination

### Rotarod test

The rotarod device (Borj Sanat Azma, Iran) was used to assess motor coordination and balance in the animals. The setup consists of a horizontal step ladder (2.5 cm in diameter, 38 cm in height, and a constant speed of 25 rpm). Before starting the experiment, mice were trained on the rotarod in 3 training sessions, each lasting 5 minutes for 3 days. At the end of the experiment, the performance of the mice was assessed for 5 minutes, and a fall off the rotarod within this period was recorded (16). Additionally, the number of falls and flips was counted during 300 seconds.

## Histological assessment

### Myelin staining

Luxol fast blue (LFB) staining was performed to evaluate the demyelination process in the CC. Mice were deeply anesthetized (urethane, 1 g/kg of body weight) and intracardially perfused with 100  $\mu$ l of saline followed by the same volume of formalin (10%). Brains were post-fixed in 4% paraformaldehyde for 3 days and embedded in paraffin for 24 hours. Coronal sections (6  $\mu$ m thickness) were prepared through the CC using a microtome (Leica RM2135, Germany). After dehydration with graded alcohols and clearing with xylene, the paraffinized sections were incubated overnight with 0.1% Luxol-Fast Blue and counterstained with neutral red according to the previously reported method (17). After capturing images of slides (Zeiss light microscope, 4  $\times$  objective magnification), the CC area of each slide was scored in a blinded manner by two investigators.

For the quantification of demyelination, two independent researchers in a double-blind fashion scored each region of interest and scored them from 0 to 3. A score of "0" referred to normal myelination, a score of "1" indicated demyelination of only one-third of the myelin fibers, and a score of "2" was equivalent to demyelination of two-thirds and a score of "3" referred to complete demyelination. Scores from different sections were summed up to calculate the average score for each group.

## TUNEL assay

TUNEL staining was performed to determine DNA fragmentation as an index of cell apoptosis rate. Apoptotic cells were detected using an in-situ cell death detection kit (Roche, Mannheim, Germany) as per the manufacturer's instructions. The mice brains were removed and fixed in phosphate-buffered saline (PBS, 0.1 M Sodium phosphate, 0.14 M NaCl, pH=7.4) containing 3.7% paraformaldehyde. The fixed brains were histologically processed and embedded in the paraffine. Three sections (thickness: 5  $\mu$ , interval: 30  $\mu$ ) were obtained through the CC. The sections were deparaffinised and hydrated. Thereafter, the sections were incubated with proteinase K (100  $\mu$ g/mL), washed with PBS, and treated with 3% H<sub>2</sub>O<sub>2</sub> for 10 minutes to inactivate endogenous peroxidase. Again, the sections were washed twice with PBS and incubated in the TUNEL reaction mixture for 1 hour. The tissues were rinsed and visualized using Converter-POD with 0.03% 3, 3'-diaminobenzidine (DAB). For counter-staining, the washed sections were stained with haematoxylin (DAKO, Denmark). The apoptotic cells were counted (3 windows per section/animal; 4 animals/group) and the mean value for each group was used for analysis. The percentage of apoptotic cells was calculated as TUNEL-positive cells/total numbers of cells (18).

## Quantitative real-time polymerase chain reaction

mRNA levels of *Olig2* as an OLs precursor marker, *p53* as an apoptotic regulator marker, *GFAP* as an indicative of astrogliosis, *BDNF*, and *MBP* as the markers for the survival of neurons, glial cells, and remyelination were determined using semi-quantitative real-time polymerase chain reaction (qRT-PCR). RNA of each tissue sample of CC was extracted according to the kit instruction. The efficiency and quality of RNA extraction were determined using the 260/280 ratio of optical density from each sample (Microplate reader, Epoch, England). Then, Single-strand cDNA was synthesized from 1  $\mu$ g of the extracted mRNA and finally, qRT-PCR was performed. The qPCR reaction contained 12.5  $\mu$ l of Master Mix, 10.5  $\mu$ l of purified water, 1  $\mu$ l of 10  $\mu$ M primer solution, and 1  $\mu$ l of cDNA template. All values were normalized to the hypoxanthine-guanine phosphoribosyl transferase-encoding gene (*HPRT*), a housekeeping gene with minimal variability in different experimental conditions. Finally, the  $\Delta\Delta$ Ct method was applied to compare the relative gene expression. The primers sequences are indicated in Table 2.

## Statistical analysis

Data were expressed as mean  $\pm$  SEM and analysed by statistical software GraphPad Prism 7.0 (GraphPad, Inc., USA). One-way ANOVA was used to determine the significant differences between groups and post-hoc Bonferroni or Tukey's tests as required. The P<0.05 was considered statistical significance.

**Table 2:** The primer's sequences list

Gene	Primer sequence (5'-3')
<i>p53</i>	F: TTATGTGCACGTA CTCTCTCC R: GCTGTGACTTCTTGTAGATGGC
<i>Olig2</i>	F: TTACAGACCGAGCCAACACC R: TCAACCTCCGAATGTGAATTAG
<i>Gfap</i>	F: AACCGCATCACCATTCTGT R: CAGGCTGGTTTCTCGGATCT
<i>Bdnf</i>	F: TACTTCGGTTGCATGAAGGC R: TACTGTACACACGCTCAGCTCC
<i>Mbp</i>	F: GCACGCTTTCCAAAATCTTTA R: GCCATGGGACCAGAG
<i>Hprt</i>	F: GTGATTAGCGATGATGAACCAG R: AGCAAGTCTTTCAGTCCTGTCC

## Results of cognitive evaluations

### Fear conditioning

As expected, there was not a significant difference in freezing response between experimental groups on day 1. During 120 s of the test, all animals produced a brief transient freezing-like behavior. During the fear contextual test, mice in the CPZ+Veh showed a significantly lower freezing response compared to the control group ( $P < 0.01$ ). Post-hoc analysis revealed that FA at both doses increases freezing response in the fear contextual test ( $P < 0.05$ ). During the cue test, mice in the CPZ+Veh group showed a significantly lower percentage of the freezing response compared to the control group ( $P < 0.05$ ). Also, the post-hoc analysis revealed that FA at the higher dose increased freezing response in the fear contextual test ( $P < 0.05$ ). Data are shown in Figure 1.

### Y-maze

As shown in Figure 1, the total number of random arm entries were significantly higher in CPZ+Veh group when compared to control mice ( $P < 0.01$ ). Treatment of mice with FA at both doses reduced the total number of random entries ( $P < 0.01$ ). The percentage of spontaneous alternations showed a significant decrease in the CPZ+Veh group compared to the control group ( $P < 0.05$ ), while FA treatment at both doses could significantly improve the percent of spontaneous arm alternation ( $P < 0.05$ ).

## Results of motor coordination evaluations

### Rotarod test

CPZ administration to mice in the CPZ+Veh group significantly decreased the time on the rotarod and increased the number of falls/flips from the rotarod

compared to the control group ( $P < 0.001$ ). However, treatment of mice with FA at both doses increased time on the rotarod and decreased the number of falls/flips compared with the CPZ+Veh group ( $P < 0.05$ ). Data are shown in Figure 1.

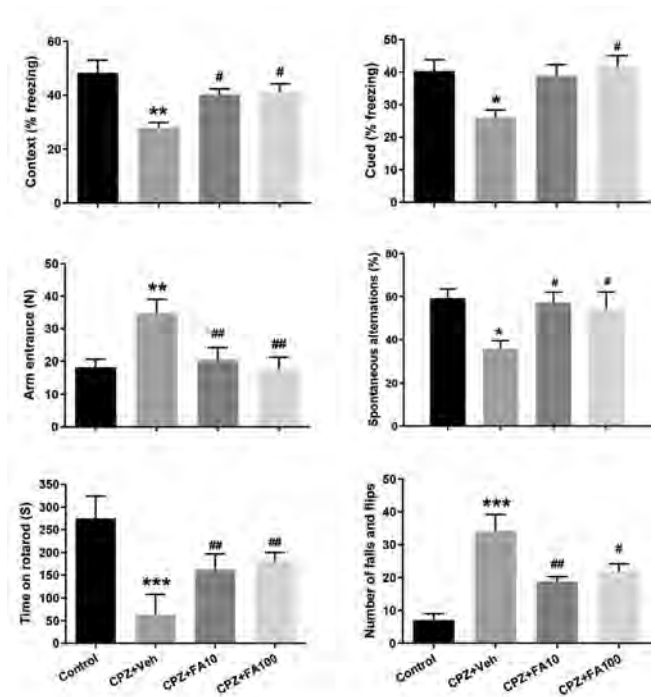


**Fig.1:** Effect of FA on cuprizone-induced impairments in cognitive function (freezing and cued behaviors in fear conditioning test, and the number of arm entries and spontaneous alternations in Y-maze) and motor coordination (time on road and the number of falling/flipping in rotarod). \*, Significant difference when compared to control group, #; Significant difference when compared to CPZ+Veh group, \*,  $P < 0.05$ , \*\*,  $P < 0.01$ , \*\*\*,  $P < 0.001$ , ##;  $P < 0.05$ , ###;  $P < 0.01$ , FA; Ferulic acid, CPZ; Cuprizone, and Veh; Vehicle. Data are mean  $\pm$  SEM.

## Histological findings

The LFB is a sensitive tissue staining method used to detect the phospholipids of CC. Qualitatively, Chronic CPZ administration led to a prominent lesion in the myelin sheath in the CC compared to the control group (Fig.2A-D). In the presence of CPZ treatment, neuroprotection of CC occurred in the FA-treated mice (Fig.2E-H) but not in vehicle-treated mice (control group). The CC of mice that received FA at a dose of 10 mg/kg showed a lesser demyelination relative to the control group. Also, this protective effect was observed in the mice treated with 100 mg/kg of FA but to a lesser extent compared to the mice treated with 10 mg/kg. Semiquantitative analysis of LFB stained cells for scoring of demyelination revealed that CPZ significantly increased demyelination in CC ( $P < 0.01$ ). FA at both doses led to a significant decrease in the CPZ-induced demyelination ( $P < 0.05$ ).

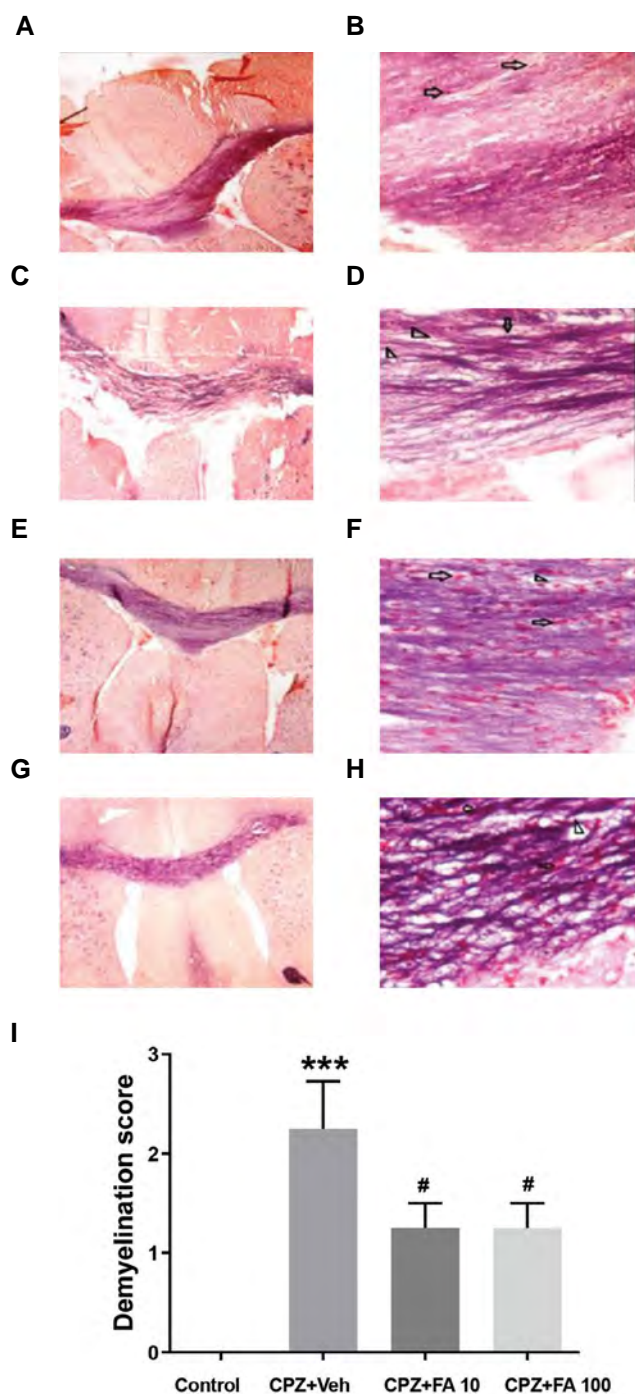


**Fig.2:** Light micrographs showing histological sections of brains from rats in CC area. Arrows and open triangles show OLs and demyelination loci respectively. **A, B.** Control group, **C, D.** CPZ+Veh group, **E, F.** CPZ+FA 10, **G, H.** CPZ+FA 100 (the right column, 40x and the left column 400x). **I.** The histogram represents demyelination scores of CC in different groups. Demyelination score data are expressed as the mean  $\pm$  SEM and analysed using one-way ANOVA followed by post hoc Turkey's test. **\*\*\*;**  $P < 0.001$ : significant difference when compared to the control group, **#;**  $P < 0.05$ : significant difference when compared to CPZ+Veh group, OLs; Oligodendrocytes, FA; Ferulic acid, CPZ; Cuprizone, and Veh; Vehicle.

### The effects of FA on apoptosis and expression of the *p53* gene in CC

As shown in Figure 3, the number of TUNEL-positive cells significantly elevated in cuprizone-treated mice compared to control rats. FA treatment at both doses decreased the number of TUNEL-positive cells in the medial region of the CC compared to the CPZ+Veh

group. The quantitative analysis revealed that the number of TUNEL-positive cells in the CPZ+Veh group was significantly more than in the control group ( $P < 0.001$ ), while FA treatment significantly reduced the number of TUNEL-positive cells ( $P < 0.01$ , Fig.2E). The mRNA level of the *p53* gene was significantly higher in the CPZ+Veh mice while it was decreased by treatment of rats with FA 10 and 100 mg/kg ( $P < 0.01$ , Fig.3F).

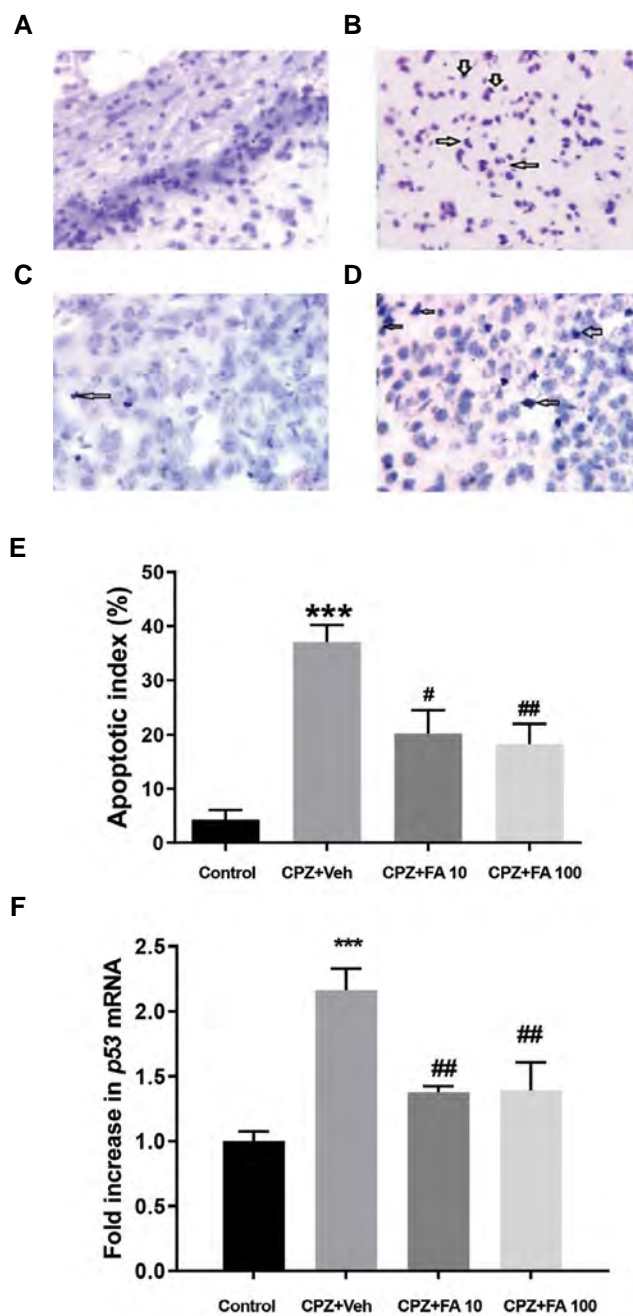


**Fig.3:** The apoptotic rate in different experimental groups light micrograph pictures (400x) of CC in experimental groups. **A.** Control group, **B.** CPZ+Veh treated group, **C.** CPZ+FA10 treated group, **D.** CPZ+FA100 treated group. The arrow indicates apoptotic cells. **E.** Quantitative analysis for calculating the ratio of TUNEL-positive cells to total cell number. **F.** The mRNA levels of *P53* relative to HPRT in the corpus callosum as determined by RT-PCR, data are expressed as the mean  $\pm$  SEM and analysed using one-way ANOVA followed by post hoc Turkey's test. **\*\*\*;**  $P < 0.001$ : significant difference when compared to the control group, **#;**  $P < 0.05$ , and **##;**  $P < 0.01$ : significant difference when compared to CPZ+Veh group. CC; Corpus callosum, CPZ; Cuprizone, Veh; Vehicle, FA; Ferulic acid, HPRT; Hypoxanthine phosphoribosyltransferase 1 and R.

**The effects of FA on gene expression of glial markers in corpus colosum**

Evaluation of mRNA gene expression in CC is shown in Figure 4. The mRNA expression level of *BDNF* in CPZ+Veh groups was significantly decreased ( $P<0.01$ ) when compared to the control group but FA at a dose of 10 mg/kg ( $P<0.01$ ) and at a dose of 100 mg/kg ( $P<0.05$ ) increased expression of *BDNF* mRNA relative to CPZ+Veh group. Relative mRNA expression of *olig2* indicated a significant decrease in CPZ+Veh group when compared to the control. However, FA at a dose of 100 mg/kg could significantly increase the mRNA expression of *Olig2* ( $P<0.01$ ). The relative mRNA expression level of *GFAP* was significantly increased in the CPZ+Veh treated mice compared to the control mice ( $P<0.001$ ) while both doses of FA could significantly decrease mRNA expression of *GFAP* compared to the CPZ+Veh group ( $P<0.01$ ). The mRNA expression level of *MBP* in the CPZ+Veh group didn't show a significant difference compared to the control group but FA at a dose of 10 mg/kg causes a significant increase in the mRNA expression level of *MBP* compared to CPZ+Veh group ( $P<0.01$ ).

(e.g. *Olig2*, *MBP*, and *BDNF*).

The CPZ model has been widely used for experimental studies on demyelination disorders and MS, and this chemical is able to cause behavioral, histological, and molecular changes such as those seen in MS (19, 20). Moreover, studies have shown that CPZ causes demyelination, apoptosis, and activation of neuroglia in the CNS (21, 22).

The results of the present study on the effect of CPZ on cognitive function are consistent with the previous studies showing that the CPZ-treated mice had higher arm entrance (13) and a lower percentage of spontaneous alternation in the Y-maze apparatus (23). Also, cognitive impairment in the contextual/cued fear conditioning tests observed in this study was similar to the previous study that indicated the CPZ-treated mice had significantly lower levels of freezing behavior than vehicle-treated mice (24).

FA is an antioxidant, found in vegetables, fruits, cereal, coffee, and beer (25). It can protect cells from oxidative stress by increasing the activity of several antioxidant enzymes and by modulating several cellular functions (26). Our results indicated that FA decreased the number of arm entries and spontaneous alternation behavior compared to CPZ+Veh mice in Y-maze tasks. Some reports indicated that FA could improve impaired cognitive function through different mechanisms (27, 28). While other few studies have shown that FA does not affect the number of arm entries or spontaneous alternation behavior (29, 30). The controversial results can be attributed to the different doses or time courses of FA administration.

CPZ could induce apoptosis in OLs, the reaction that activates microglia/macrophages and leads to the destruction of myelin sheets (31). The *p53* mRNA level expression upregulated in CC after administration of CPZ treated diet in mice (32). The *p53* as a proapoptotic protein has an essential role in OLs death so that in the transgenic animals, the *p53* gene has been knocked out, revealing no obvious apoptosis and OLs death followed by CPZ treatment (32, 33). Also, repeated treatments with pifithrin- $\alpha$ , as a *p53* inhibitor, could reduce demyelination and microglial activation (32). In this study, FA could attenuate the apoptotic rate in the CC of the mice treated with CPZ; the findings can be attributed to the *p53* inhibition by FA. These reports are also in accordance with the previous studies that showed FA is an anti-apoptotic factor that can exert its effect by suppressing caspase3 activity (34) and reducing *p53* level in the neuronal cells (35).

*Olig2* is a transcription factor that regulates neuronal and glial specifications and promotes OLs differentiation from its precursor cells, especially after cortical injury (36). The increased level of *Olig2* in the subventricular zone of CPZ-feeding mice indicates that *Olig2* is a key regulator in the period of remyelination after myelin sheet destruction (37). It has been reported that

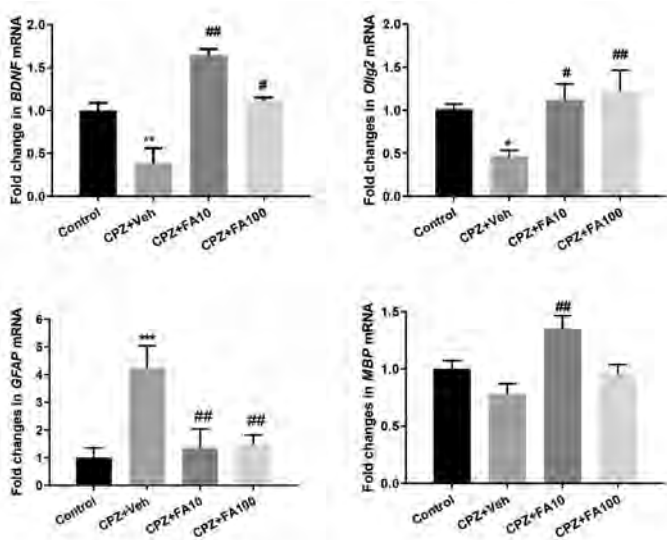


**Fig.4:** The effect of different doses of FA on mRNA expression of the genes involved in myelination. Data are expressed as the mean  $\pm$  SEM and analysed using one-way ANOVA followed by post hoc Turkey's test. \*, Significant difference when compared to the control group, #; Significant difference when compared to CPZ group, \*,  $P<0.05$ , #,  $P<0.05$ , \*\*,  $P<0.01$ , and ###;  $P<0.01$ .

**Discussion**

Our findings showed that oral administrations of FA could improve cognitive impairment and motor coordination in the CPZ model of demyelination and MS in mice. FA can also reduce CC demyelination, apoptosis, the expression of the genes involved in demyelination (*GFAP*), and increase the expression of genes involved in the myelination, neuronal, glial protection, and growth

*in vivo* and *in vitro* administrations of FA accelerate the proliferation and differentiation of neural progenitor (9) and Schwann cells (38). Indeed, our study results are in agreement with the above-mentioned evidence that implies FA could increase Olig2 mRNA expression in CC.

MBP is a major constituent of myelin sheet and its expression significantly decreased in the CC of mice treated with CPZ (21). As observed in our study, FA could increase the expression of MBP mRNA in the Schwann cells (38). The increment in myelin sheet synthesis and development of OLs may be attributed to the effect of FA on the elevation in MBP expression. Previous studies reported that FA treatment could increase the population of myelinated axons after sciatic nerve injury (11).

BDNF is a neurotrophic factor demonstrating an essential role in accelerating of OLs precursor proliferation and development (39). Also, BDNF promotes the synthesis of the protein molecules such as MBP which is a necessary base material for synthesizing myelin and thickening it. It has been reported that the level of BDNF was reduced in the CC of the mice treated with CPZ (40). We found that FA treatment could potentiate mRNA expression of BDNF in CC. It may be concluded that the part of beneficial effects of FA exert through the increase in the OLs precursor proliferation and development mediated by BDNF and MBP.

Astrogliosis, as a response to acute or chronic demyelination, was observed after different types of demyelination disorders or in animals that received a CPZ diet (39). In agreement with our findings, some studies show that FA could reduce the level of GFAP after CNS injury which indicates that it can attenuate the rate of gliosis (7).

## Conclusion

The results of the present study showed that FA improved demyelination, motor incoordination, and cognitive dysfunction in the laboratory model of MS. FA could increase myelin density and decrease the apoptotic rate in the brain affected by a CPZ. These effects are partially mediated by reducing the expression of genes involved in apoptosis and an increase in the expression of the OLs precursor proliferation and development.

## Acknowledgements

This work was supported by the deputy of research, Shahid Sadoughi University of Medical Sciences through grant No 139426. The authors declare no conflict of interest.

## Authors' Contributions

M.Gh.; Performed the induction of MS and evaluation of drug effects and data collection. B.A.; Prepared tissue samples and histological processing. M.Y.; Interpreted the histological cells for evaluation of necrotic and apoptotic

cells. M.E.; Participated in drafting and statistical analysis. F.H.-M.; Conducted to design of the study and molecular experiments and RT-qPCR analysis. M.E.R.; Participated in design of study, performed editing, and approving the final version of this paper for submission. All authors read and approved the final manuscript.

## References

- Vercellino M, Masera S, Lorenzatti M, Condello C, Merola A, Mattioli A, et al. Demyelination, inflammation, and neurodegeneration in multiple sclerosis deep gray matter. *J Neuropathol Exp Neurol*. 2009; 68(5): 489-502.
- Mi S, Hu B, Hahn K, Luo Y, Hui ES, Yuan Q, et al. LINGO-1 antagonist promotes spinal cord remyelination and axonal integrity in MOG-induced experimental autoimmune encephalomyelitis. *Nat Med*. 2007; 13(10): 1228-1233.
- Moore S, Meschkat M, Ruhwedel T, Trevisiol A, Tzvetanova ID, Battefeld A, et al. A role of oligodendrocytes in information processing. *Nat Commun*. 2020; 11(1): 5497.
- Mahad DH, Trapp BD, Lassmann H. Pathological mechanisms in progressive multiple sclerosis. *Lancet Neurol*. 2015; 14(2): 183-193.
- Treaba CA, Herranz E, Barletta VT, Mehndiratta A, Ouellette R, Sloane JA, et al. The relevance of multiple sclerosis cortical lesions on cortical thinning and their clinical impact as assessed by 7.0-T MRI. *J Neurol*. 2021; 1: 2473-2481.
- Llufriu S, Blanco Y, Martinez-Heras E, Casanova-Molla J, Gabilondo I, Sepulveda M, et al. Influence of corpus callosum damage on cognition and physical disability in multiple sclerosis: a multimodal study. *PLoS One*. 2012; 7(5): e37167.
- Mancuso C, Santangelo R. Ferulic acid: pharmacological and toxicological aspects. *Food Chem Toxicol*. 2014; 65: 185-95.
- Ren Z, Zhang R, Li Y, Li Y, Yang Z, Yang H. Ferulic acid exerts neuroprotective effects against cerebral ischemia/reperfusion-induced injury via antioxidant and anti-apoptotic mechanisms in vitro and in vivo. *Int J Mol Med*. 2017; 40(5):1444-1456.
- Srinivasan M, Sudheer AR, Menon VP. Ferulic acid: therapeutic potential through its antioxidant property. *J Clin Biochem Nutr*. 2007; 40(2): 92-100.
- Wang Y, Deng Z, Lai X, Tu W. Differentiation of human bone marrow stromal cells into neural-like cells induced by sodium ferulate in vitro. *Cell Mol Immunol*. 2005; 2(3): 225-229.
- Lee SC, Tsai CC, Yao CH, Chen YS, Wu MC. Ferulic acid enhances peripheral nerve regeneration across long gaps. *Evid Based Complement Alternat Med*. 2013; 2013: 876327.
- Praet J, Guglielmetti C, Berneman Z, Van der Linden A, Ponsaerts P. Cellular and molecular neuropathology of the cuprizone mouse model: clinical relevance for multiple sclerosis. *Neurosci Biobehav Rev*. 2014; 47: 485-505.
- Makinodan M, Yamauchi T, Tatsumi K, Okuda H, Takeda T, Kiuchi K, et al. Demyelination in the juvenile period, but not in adulthood, leads to long-lasting cognitive impairment and deficient social interaction in mice. *Prog Neuropsychopharmacol Biol Psychiatry*. 2009; 33: 978-985.
- Tomas-Roig J, Agbemenyah HY, Celarain N, Quintana E, Ramió-Torrentà L, Havemann-Reinecke U. Dose-dependent effect of cannabinoid WIN-55,212-2 on myelin repair following a demyelinating insult. *Sci Rep*. 2020; 10(1): 590.
- Xiao L, Xu H, Zhang Y, Wei Z, He J, Jiang W, et al. Quetiapine facilitates oligodendrocyte development and prevents mice from myelin breakdown and behavioral changes. *Mol Psychiatry*. 2008; 13(7): 697-708.
- Jones BJ, Roberts DJ. The quantitative measurement of motor incoordination in naive mice using an accelerating rotarod. *J Pharm Pharmacol*. 1968; 20(4): 302-304.
- Carriel V, Campos A, Alaminos M, Raimondo S, Geuna S. Staining methods for normal and regenerative myelin in the nervous system. *Methods Mol Biol*. 2017; 1560: 207-218.
- Faheem H, Mansour A, Elkordy A, Rashad S, Shebl M, Madi M, et al. Neuroprotective effects of minocycline and progesterone on white matter injury after focal cerebral ischemia. *J Clin Neurosci*. 2019; 64: 206-213.
- Matsushima GK, Morell P. The neurotoxicant, cuprizone, as a model to study demyelination and remyelination in the central nervous system. *Brain Pathol*. 2001; 11(1): 107-116.

20. Stangel M. Neurodegeneration and neuroprotection in multiple sclerosis. *Curr Pharm Des.* 2012; 18(29): 4471-4474.
21. Babbs RK, Beierle JA, Yao EJ, Kelliher JC, Medeiros AR, Anandakumar J, et al. The effect of the demyelinating agent cuprizone on binge-like eating of sweetened palatable food in female and male C57BL/6 substrains. *Appetite.* 2020; 150: 104678.
22. Bénardais K, Kotsiari A, Škuljec J, Koutsoudaki PN, Gudi V, Singh V, et al. Cuprizone [bis (cyclohexylidenehydrazide)] is selectively toxic for mature oligodendrocytes. *Neurotox res.* 2013; 24(2): 244-250.
23. Yan JJ, Jung JS, Kim TK, Hasan MA, Hong CW, Nam JS, et al. Protective effects of ferulic acid in amyloid precursor protein plus presenilin-1 transgenic mouse model of Alzheimer disease. *Biol Pharm Bull.* 2013; 36(1): 140-143.
24. Kopanitsa MV, Lehtimäki KK, Forsman M, Suhonen A, Koponen J, Piipponiemi TO, et al. Cognitive disturbances in the cuprizone model of multiple sclerosis. *Genes Brain Behav.* 2021; 20(1): e12663.
25. Zheng YZ, Zhou Y, Guo R, Fu ZM, Chen DF. Structure-antioxidant activity relationship of ferulic acid derivatives: Effect of ester groups at the end of the carbon side chain. *LWT.* 2020; 120: 108932.
26. Wang H, Sun X, Zhang N, Ji Z, Ma Z, Fu Q, et al. Ferulic acid attenuates diabetes-induced cognitive impairment in rats via regulation of PTP1B and insulin signaling pathway. *Physiol Behav.* 2017; 182: 93-100.
27. Mhillaj E, Catino S, Miceli FM, Santangelo R, Trabace L, Cuomo V, et al. Ferulic acid improves cognitive skills through the activation of the heme oxygenase system in the rat. *Mol Neurobiol.* 2018; 55(2): 905-916.
28. Mori T, Koyama N, Guillot-Sestier MV, Tan J, Town T. Ferulic acid is a nutraceutical  $\beta$ -secretase modulator that improves behavioral impairment and alzheimer-like pathology in transgenic mice. *PLoS One.* 2013; 8(2): e55774.
29. Mamiya T, Kise M, Morikawa K. Ferulic acid attenuated cognitive deficits and increase in carbonyl proteins induced by buthionine-sulfoximine in mice. *Neurosci Lett.* 2008; 430(2): 115-118.
30. Yan G, Dai Z, Shen Z, Wu R. Behavioral and neurochemical alterations in C57BL/6 mice exposed to cuprizone: An in vivo 1H-MRS STUDY at 7.0 T. *J Neurol Sci.* 2013; 333: e629.
31. Mason JL, Jones JJ, Taniike M, Morell P, Suzuki K, Matsushima GK. Mature oligodendrocyte apoptosis precedes IGF-1 production and oligodendrocyte progenitor accumulation and differentiation during demyelination /remyelination. *J Neurosci Res.* 2000; 61(3): 251-262.
32. Li J, Ghiani CA, Kim JY, Liu A, Sandoval J, DeVellis J, et al. Inhibition of p53 transcriptional activity: a potential target for future development of therapeutic strategies for primary demyelination. *J Neurosci.* 2008; 28(24): 6118-6127.
33. Hesse A, Wagner M, Held J, Brück W, Salinas-Riester G, Hao Z, et al. In toxic demyelination oligodendroglial cell death occurs early and is FAS independent. *Neurobiol Dis.* 2010; 37(2): 362-369.
34. Picone P, Nuzzo D, Di Carlo M. Ferulic acid: a natural antioxidant against oxidative stress induced by oligomeric A-beta on sea urchin embryo. *Biol Bull.* 2013; 224(1): 18-28.
35. Zhang Z, Wei T, Hou J, Li G, Yu S, Xin W. Iron-induced oxidative damage and apoptosis in cerebellar granule cells: attenuation by tetramethylpyrazine and ferulic acid. *Eur J Pharmacol.* 2003; 467(1-3): 41-47.
36. Marshall CA, Novitch BG, Goldman JE. Olig2 directs astrocyte and oligodendrocyte formation in postnatal subventricular zone cells. *J Neurosci.* 2005; 25(32): 7289-7298.
37. Chen LP, Li ZF, Ping M, Li R, Liu J, Xie XH, et al. Regulation of Olig2 during astroglial differentiation in the subventricular zone of a cuprizone-induced demyelination mouse model. *Neuroscience.* 2012; 221: 96-107.
38. Zhu X, Li K, Guo X, Wang J, Xiang Y. Schwann cell proliferation and differentiation that is induced by ferulic acid through MEK1/ERK1/2 signalling promotes peripheral nerve remyelination following crush injury in rats. *Exp Ther Med.* 2016; 12(3): 1915-1921.
39. Langhnoja J, Buch L, Pillai P. Potential role of NGF, BDNF, and their receptors in oligodendrocytes differentiation from neural stem cell: an in vitro study. *Cell Biol Int.* 2021; 45(2): 432-446.
40. Nguyen HT, Wood RJ, Prawdiuk AR, Furness SG, Xiao J, Murray SS, et al. TrkB agonist LM22A-4 increases oligodendroglial populations during myelin repair in the corpus callosum. *Front Mol Neurosci.* 2019; 12: 205.

# Human Umbilical Cord Mesenchymal Stem Cells-Derived Small Extracellular Vesicles Can Be Considered as Cell-Free Therapeutics for Angiogenesis Promotion

Somayeh Divband, M.Sc.<sup>1</sup>, Nooshin Tasharofi, Ph.D.<sup>2</sup>, Saeid Abroun, Ph.D.<sup>1</sup>, Mina Soufi Zomorrod, Ph.D.<sup>1\*</sup>

1. Department of Hematology and Cell Therapy, Faculty of Medical Sciences, Tarbiat Modares University, Tehran, Iran

2. Faculty of Pharmacy, Lorestan University of Medical Sciences, Khorramabad, Iran

\*Corresponding Address: P.O.Box: 14115-111, Department of Hematology and Cell Therapy, Faculty of Medical Sciences, Tarbiat Modares University, Tehran, Iran

Email: m.soufi@modares.ac.ir

Received: 19/September/2021, Accepted: 15/May/2022

## Abstract

**Objective:** Angiogenesis has critical roles in several physiological processes. Restoring angiogenesis in some pathological conditions such as a few vascular diseases can be a therapeutic approach to controlling this issue. Mesenchymal stem cells (MSCs) secrete specific intracellular products known as extracellular vesicles (EVs) with high therapeutic potential which compared to their source cells, do not have the limitations of cell therapy. The angiogenic effect of the human umbilical cord MSCs (hUCMSCs)-derived small EVs are evaluated in the present work. Aim of this research is to show that hUCMSCs-derived small EVs cause differentiation of genes involved in angiogenesis like *FGFR-1*, *FGF*, *VEGF*, and *VEGFR-2*.

**Materials and Methods:** In this experimental study, MSCs were isolated from the human umbilical cord, and after confirming their identities, their secreted EVs (including exosomes) were extracted by ultracentrifugation. The isolated small EVs were characterized by dynamic light scattering (DLS), transmission electron microscopy (TEM), bicinchoninic acid assay (BCA), and Western Blotting. Then, the human umbilical vein endothelial cells (HUVECs) were treated with derived small EVs for 72 hours, and the expression of the angiogenic factors including *FGFR-1*, *FGF*, *VEGF*, and *VEGFR-2* was evaluated by quantitative real-time-polymerase chain reaction (qPCR). Angiogenesis was also evaluated via a tube formation assay.

**Results:** The results demonstrated that *FGFR-1*, *FGF*, *VEGF*, and *VEGFR-2* could be elevated 2, 2, 3.5, and 2 times, respectively, in EVs treated HUVECs, and derivative EVs can encourage tube formation in HUVECs.

**Conclusion:** These findings imply that hUCMSCs-derived small EVs are valuable resources in promoting angiogenesis and are very promising in cell-free therapy.

**Keywords:** Angiogenesis, Exosome, Extracellular Vesicles, hUCMSCs, Vascular Endothelial Growth Factor

Cell Journal(yakhteh), Vol 24, No 11, November 2022, Pages: 689-696

**Citation:** Divband S, Tasharofi N, Abroun S, Soufi Zomorrod M. Human umbilical cord mesenchymal stem cells-derived small extracellular vesicles can be considered as cell-free therapeutics for angiogenesis promotion. 2022; 24(11): 689-696. doi: 10.22074/cellj.2022.8275.

This open-access article has been published under the terms of the Creative Commons Attribution Non-Commercial 3.0 (CC BY-NC 3.0).

## Introduction

The process of angiogenesis encompasses new blood vessel construction from old veins (1). Angiogenesis is a complex multi-stage process in which inactive endothelial cells are stimulated with angiogenic factors such as vascular endothelial growth factor (VEGF), fibroblast growth factor (FGF or bFGF), hepatocyte growth factor (HGF), transforming growth factor-beta (TGF- $\beta$ ), and are organized in a tubular structure (2). Among angiogenic inducing factors, VEGF and FGF are very important and well-known factors. As a crucial physiological process, angiogenesis plays a significant role in rehabilitating tissues, healing wounds, menstrual cycles, and helping in the treatment of some diseases such as cancer. Increasing angiogenesis is a therapeutic approach for people who suffer from acute ischemia (3). Angiogenesis is dependent on the exact balance between stimulation and natural inhibitors in the body. If the balance deviates from its normal state, some pathological conditions such as atherosclerosis, proliferation, and metastasis of tumors occur. On the other hand, inducing angiogenesis can be supportive in some diseases. Therefore, it is necessary to

study the mechanisms of angiogenesis and its improvement in some pathological conditions (1, 4).

Cell therapy has been considered for various kinds of diseases during the last decades, and for this purpose, different stem cells (especially mesenchymal stem cells, MSCs) were used as a promising therapeutic approach in several studies (5).

MSCs are multipotent adult non-hematopoietic stem cells (HSC) with high differentiation, proliferation, and self-renewal. These cells can be isolated from tissues with mesodermal origins, including liver, spleen, adipose tissue, thymus, umbilical cord blood, Wharton's jelly, placenta, lung, peripheral blood, dental pulp, and other tissues (6, 7). The three most important and easiest accessible sources are bone marrow, adipose tissue, and umbilical cord. Umbilical cord blood and Wharton's jelly are the most abundant sources for MSCs. MSCs from different sources are recognized with the same phenotype (spindle appearance; similar to fibroblasts) but with different functions; for example, umbilical cord MSCs have been shown to induce angiogenesis (8, 9). MSCs

are important stromal cells in the bone marrow that can feed and revitalize bone marrow (7). They have an important role in the regeneration of tissues such as bone, cartilage, fat, muscle, and tendon. These cells are also capable of differentiating into adipocytes, osteoblasts, and chondrocytes *in vitro*. Furthermore, they are capable of migrating to damaged tissues and releasing cytokines, inflammatory mediators, extracellular matrix compounds, and angiogenic and anti-fibrotic factors (6). These cells lack the major histocompatibility complex-II (MHC-II) and stimulus-assisting molecules like CD86, CD40, and CD80 (10). These features made them a good candidate for the treatment of some diseases, as they were cured by MSCs. Although there are some drawbacks to cell therapy, including safety issues, limitations of cell transplants, and graft versus host disease (GVHD) risk (11).

MSCs exert a unique function by secreting various cytokines, growth factors, microRNAs, and extracellular vesicles (EVs) (12). The EVs are spherical lipid bilayer vesicles containing biogenic substances like proteins, mRNA, and microRNA. Their average size differs from 30 nanometers to several micrometers. EVs are categorized according to their size and cell source and are comprised of exosomes, microvesicles or microparticles, apoptotic vesicles, etc (13). Exosomes, for example, belong to small EVs with a diameter of about 30-100 nanometers. They are derived from endosomes and buds from the plasma membrane with the same antigens as their cells of origin's membrane (14). Common markers between exosomes are CD9, CD81, and CD63 (tetraspanins) (15). It was shown that EVs have different functions, such as removing unwanted substances from the cells. Exosomes derived from MSCs perform similarly to MSCs, such as tissue injury regeneration, induction of angiogenesis and neurogenesis, and immune modulation. Given the specific disadvantages of cell therapies, EVs (especially exosomes), as cell products similar to their source cells, have been gaining attention as a safe alternative therapeutic approach to the paracrine function of MSCs (16).

In general, small EVs are diagnostic and prognostic biomarkers and an effective means for transmitting therapeutic agents. They can be used to diagnose and treat various inflammation, heart and metabolic diseases, neurodegenerative disorders, and malignant neoplasms (17).

With the available evidence on the benefits of using MSCs to enhance angiogenesis, we have decided to assess the effect of hUCMSCs-derived small EVs in the induction of angiogenesis *in vitro*.

## Materials and Methods

### Isolation and culture of mesenchymal stem cells from human umbilical cord

In this experimental study, The UC sample was obtained

with the personal consent of donors in Mahdijeh hospital (Tehran, Iran) after the child's birth. The applied protocols were accepted by the Ethics Committee of Tarbiat Modares University (IR.MODARES.REC.1397.237). Under sterile conditions, the umbilical cord specimen was chopped on a plate using a bistoury, and one-milliliter collagenase type II (1 mg/mL, Sigma, USA) was added and incubated for one hour at 37°C and 5% CO<sub>2</sub> until it was dissolved; it was vortexed every 15 minutes and then centrifuged at 300 g for 5 minutes. The cells (pellet) were cultured in a 75 cm<sup>2</sup> (T75) culture flask. Cell culture medium included DMEM/F12 (Bio-Idea, Iran) supplemented with 10% fetal bovine serum (FBS) (Gibco's) and 100 µl of penicillin/streptomycin (Sigma, USA). After three passages, the cells were used for further tests (18).

### Identification of mesenchymal stem cells

MSCs were identified by assessing the expression of CD31, HLA-DR, CD34, CD105, CD90, and CD73 markers with the use of flow cytometry after tagging by a fluorescent antibody (BioLegend). Briefly, cells were counted after trypsinization and suspended in 3% bovine serum albumin (1×10<sup>5</sup> cells per 100 µl). Then the desired antibodies and their control isotype were added to 100 µl of the prepared suspensions and after refrigeration for 45 minutes, they were washed with PBS, and then flow cytometry analysis was performed on the samples.

### The differentiation of mesenchymal stem cells to osteoblasts and adipocytes

The differentiation of cells into adipocytes and osteoblasts was done by adding the differentiation media and then the evaluation was done by staining with Oil-Red-O 5% and Alizarin-Red S 2% (Sigma Aldrich, USA) (2, 19). Oil-Red-O and Alizarin-Red are differential dyes that redden the color of cells when they bind to fat droplets in adipocytes or calcium sediments in osteoblasts, respectively.

For cell differentiation into osteoblasts, a medium composed of DMEM supplemented with 10% FBS, ascorbate-2-phosphate factors (0.2 mM/ml, Sigma Aldrich, USA), dexamethasone (0.1 mM, Sigma Aldrich, USA), and 10 mM beta-glycerol phosphate (Sigma Aldrich, USA) were used.

The medium for differentiating cells into adipocytes included DMEM, FBS (10%), insulin (1 µg/ml) (Sigma Aldrich, USA), dexamethasone (7-10 M, Sigma Aldrich, USA), and indomethacin (2 µM, Sigma Aldrich, USA).

The MSCs were cultured in 6 well plates after the confluency of 70%, the medium was removed entirely, and 2 ml of osteoblastic differentiation medium or adipocytic differentiation medium were added. The medium was changed twice a week for three weeks. Then staining was performed on the 21<sup>st</sup>-day.

### Isolation of small extracellular vesicles

With the current methods, exosomes can not be isolated from other kinds of EVs; for example, by ultracentrifugation, small EVs can be obtained instead of pure exosomes.

The third passage of cells was used for small EVs isolation; after achieving 40% cell confluency, the cell culture medium was changed with DMEM/F12 containing 10% exosome-free FBS (prepared by ultracentrifugation of FBS at 120,000 g for 2 hours and discarding the sediment and filtering the supernatant), and then the medium was collected when cells reached 80% density. In order to isolate small EVs, a standard method was used by ultracentrifugation.

Centrifugation was performed at 300g for 10 minutes in the first stage, and the second stage was performed at 10000g for 20 minutes to separate cells and debris. The supernatant was then filtered (0.22 Millipore filter) to separate large EVs. Then, two ultracentrifugation steps were performed at 100000g for 70 minutes at 4°C (Beckman 60 TI) to pellet the small EVs. At each stage, the sediments containing small EVs were washed with 1 ml phosphate-buffered saline (PBS, pH=7) (20).

### A quantitative and qualitative investigation of isolated extracellular vesicles protein concentration assay

The total protein concentration was determined by the Bicinchoninic Acid Assay (BCA) method. The BCA Protein Assay Kit (Biobasic, Canada) was utilized, and tests were done according to the manufacturer's protocol. The standard curve was drawn using successive dilutions of BSA protein with a certain concentration. The samples were measured by ELISA reader (BioTeK) at 562 nm and compared with the standard curve.

### Extracellular vesicles' size determination

The isolated EVs were diluted in 1 ml of PBS (pH=7) and size was examined using dynamic light scattering (DLS, Zetasizer, Malvern).

### Extracellular vesicles' morphology evaluation

The morphology and structural integrity of EVs were visualized by transmission electron microscopy (TEM, Leo 906).

### The immunodetection of extracellular vesicles by western blotting

Assessing specific markers on isolated EVs was done by western blotting.

After the separation of cellular proteins, the intended proteins can be detected with the help of specific antibodies. For the identification of EVs, tetraspanin proteins, CD9, CD63, and CD81, are the most common proteins that can be visualized by Western blotting (21).

The expression of CD63 and CD9 was evaluated in this study, as follows: EVs were lysed by lysis buffer supplemented with proteinase inhibitors to obtain the EVs' total proteins; the isolated proteins were resolved over sodium dodecyl sulfate–polyacrylamide gel electrophoresis (SDS-PAGE). Then in the blotting stage, the resolved proteins were transferred to the polyvinylidene difluoride (PVDF) membrane and treated with primary antibodies (anti-CD9 and anti-CD63 antibody) (1:1000; Santa Cruz Biotechnology, CA), followed by horseradish peroxidase (HRP)-conjugated secondary antibodies (SinaClon, Tehran, Iran). The luminescence tagged proteins were visualized using the ECL system. Beta-actin was served as the protein of control.

### Treatment of HUVEC cells with extracellular vesicles

HUVECs can be used to study the function and pathology of endothelial cells, such as angiogenesis. For evaluating the angiogenic effects of EVs, HUVECs (purchased from a stem cell research center, Tehran, Iran) were treated with EVs, and then the angiogenesis-related genes expression and angiogenesis were examined by quantitative real-time-polymerase chain reaction (qPCR) and tube formation assay, respectively.

### Investigation of the angiogenesis-related genes expression in with extracellular vesicles-treated HUVECs

About 100000 cells of fresh HUVECs were transferred to a 24-well plate and 400 µl EVs solution (equal to 50 µg/ml EVs) was added to each well and incubated for 72 hours, which is the suitable time for the entrance of EVs into the cells and gene expression. The untreated cell wells were considered as the negative control.

Changes in the expression of angiogenic genes, *VEGF*, *FGF*, *FGFR-1*, and *VEGFR-2*, were measured by real-time PCR, as follows: RNA extraction was performed by TRIzol solution (Yekta Tajhiz Azma, Iran) based on the manufacturer protocol. Next, cDNA was synthesized (Pars Tous cDNA synthesis kit, Iran). Then the cDNAs' quality was assessed by PCR, and finally, the target genes were quantified by real-time PCR using the SYBR Green master mix (Yekta tajhiz azma, Iran) and Step One Real-time PCR system (Applied Biosystems, USA). The real-time PCR results were analyzed using the  $2^{-\Delta\Delta CT}$  method and expressed as relative expression of threshold cycle (CT) value (treated groups compared to control group). Control genes (or housekeeping genes) are frequently used to normalize mRNA levels between different samples. However, the expression level of these genes may vary among tissues or cells. The cells we used were HUVECs for which the most common housekeeping gene is hypoxanthine guanine phosphoribosyl

transferase (*HPRT1*) (22). The primers used to perform the real-time PCR are summarized in Table 1.

**Table 1:** The primers used for real-time polymerase chain reaction

Gene name	Primer sequences (5'-3')	Tm (°C)
<i>VEGFA</i>	F: GCCAGCACATAGGAGAGATGAGC R: CGGCTTGTCACATTTTTCTGGT	60
<i>VEGFR-2</i>	F: ACTCTTCAAATTACTTGCAGGGG R: CTCCAGTGTCAATTCGATCAC	60
<i>bFGF</i>	F: GGCTTCTCCTGCGCATCCA R: GCTCTTAGCAGACATTGGAAGA	60
<i>HPRT1</i>	F: CCTGGCGTCGTGATTAGTG R: TCAGTCCTGTCCATAATTAGTCC	60
<i>FGFR-1</i>	F: AAACCGTATGCCGTAGC R: TCCATTATGATGCTCCAGGTG	61

### Tube formation

The angiogenic potential of EVs was assessed by a tube formation assay to see if they can form a capillary network. HUVECs, as a source of endothelial cells, were cultured in Matrigel (BD Biosciences) coated 24-well plates, and 50 µg/ml of EVs were added to sample wells; the controls remained untreated. The cell culture medium contained high-glucose DMEM supplemented with 10% FBS. Cell morphology changes were seen under an inverted microscope for 24 hours.

### Statistical analysis

All the treated and control samples were tested in triplicate. The real-time PCR results were analyzed using the  $2^{-\Delta\Delta CT}$  method and expressed as relative expression of treated groups compared to the control group. The evaluated data were shown as mean ± SD. Data were analyzed by the ANOVA statistical method using GraphPad Prism 8 software (GraphPad Software Inc, CA, USA), and a P<0.05 was considered statistically significant.

## Results

### Identification of umbilical cord-isolated mesenchymal stem cells

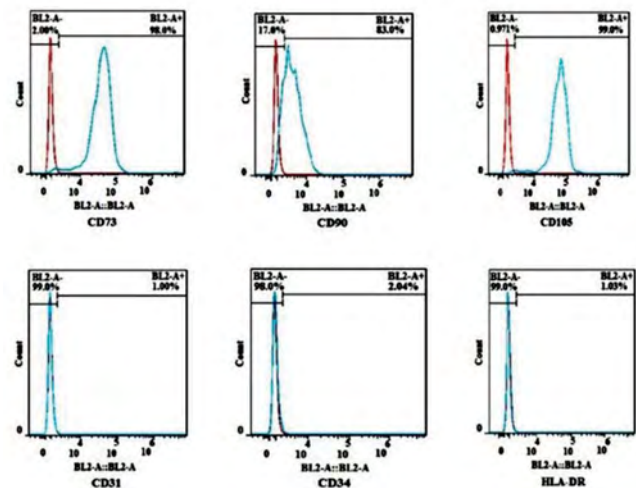
#### Evaluation of cellular immunophenotype

The data from the flow cytometry examination of human UC-derived cells are shown in Figure 1A. The tested cells were negative for HSC markers, CD342.04%) ), CD31 (1.00%), and HLA-DR (1.03%) and positive for MSC markers, CD90 (83%), CD73 (98%), and CD105 (99.0%), confirming the identification of MSCs.

### Investigation of differentiation properties

Differentiation of umbilical cord MSCs (UCMSCs) under specific differentiation media into adipocyte and osteoblast cells was assessed after 21 days using diagnostic dyes, Oil-red O and Alizarin-Red, respectively. As seen in Figure 1B, the isolated cells could be differentiated to either osteoblast or adipocyte cells in contact with the specific differentiation medium, which is characteristic of MSCs.

#### A



#### B

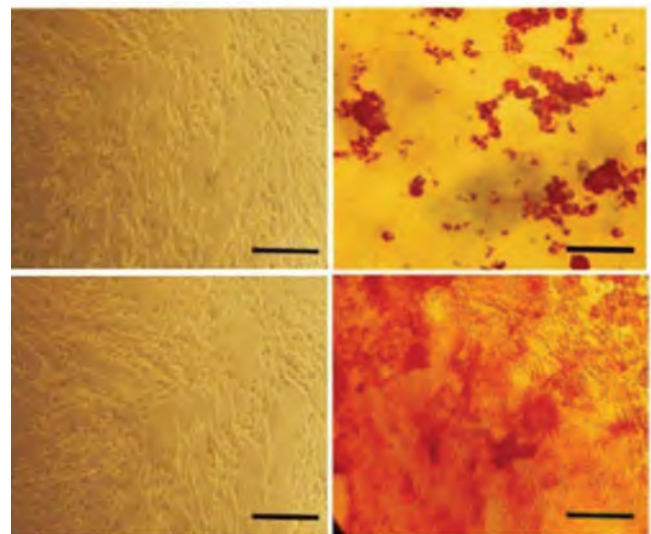


**Fig.1:** Identification of isolated cells from the human umbilical cord. **A.** Flow cytometry histograms for evaluating HSC markers, CD34, CD31, HLA-DR, and MSCs surface markers, CD73, CD99, and CD105. The cells were negative for hematopoietic and positive for MSCs markers. **B.** In the proximity of differentiation media (after 21 days), isolated UCMSCs could differentiate into adipocyte or osteoblast cells, shown in upper and lower panels, respectively. The left panels in each group are the control cells (magnification, 200X, scale bar: 50 µm). Alizarin-Red and Oil-red O were used to stain calcium-containing osteoblast and adipocytes, respectively. All the experiments were tested in triplicate. HSC; Hematopoietic stem cell, MSCs; Mesenchymal stem cells, and UCMSCs; Umbilical cord mesenchymal stem cells.

## Characterizing the extracted extracellular vesicles

### Determination of the diameter of extracellular vesicles

As shown in Figure 2A, most of the EVs populations have an average diameter of 105.7 nm. DLS Technique was used to obtain the data.

### Verification of the quality and structure of the extracellular vesicles

According to the results obtained through the TEM technique, Figure 2B shows that EVs have spherical structures, and the membrane is preserved without being damaged.

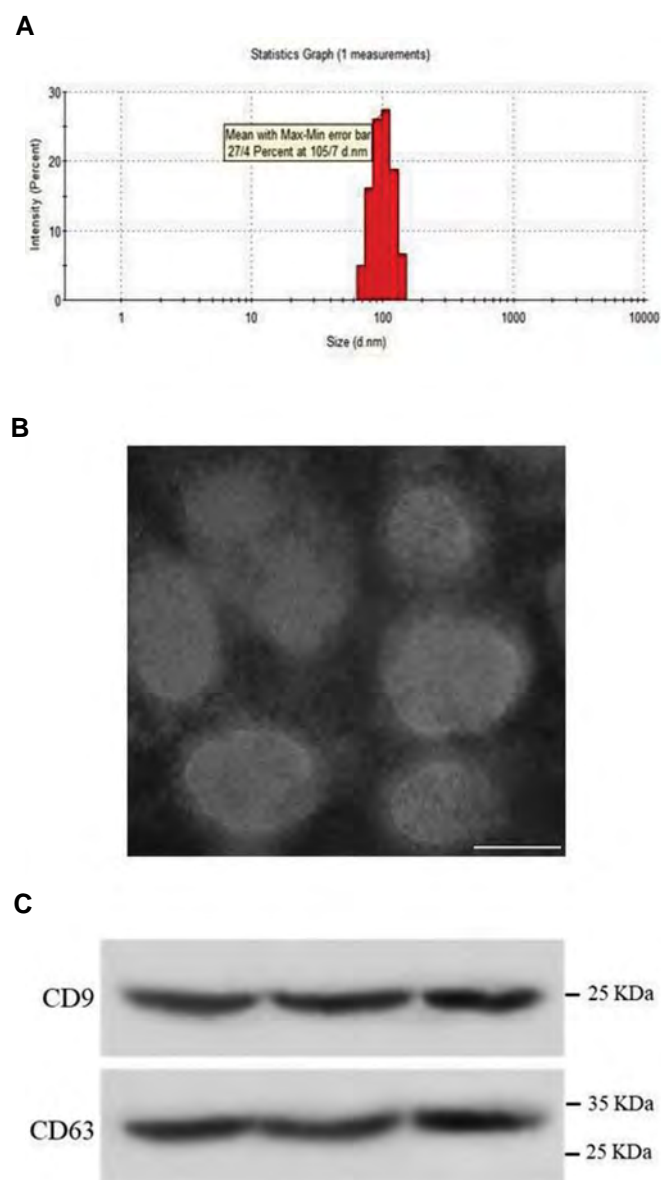


**Fig.2:** Characterization of the hUCMSC-derived EVs. **A.** Diameter of isolated EVs was measured by DLS; as shown, the majority of the EVs population has an average diameter of 105.7 nm. **B.** According to the TEM pictures the EVs have a spherical structure, and the membrane is preserved without being damaged (scale bar: 100 nm). **C.** Identification of exosomal markers, CD9 and CD63, by Western blot analysis. All the experiments were tested in triplicate. hUCMSC; Human Umbilical cord mesenchymal stem cell, EVs; Extracellular vesicles, DLS; Dynamic light scattering, and TEM; Transmission electron microscopy.

### Determination of the total protein concentration of extracellular vesicles

The BCA method measured a concentration of 203.33  $\mu\text{g/ml}$  of EVs, comparing their optical absorption with the standard curve.

### Western blotting

Western blot results (Fig.2C) showed that CD9 and CD63 (tetraspanins) were highly expressed on the surface of EVs indicating the presence of exosomes.

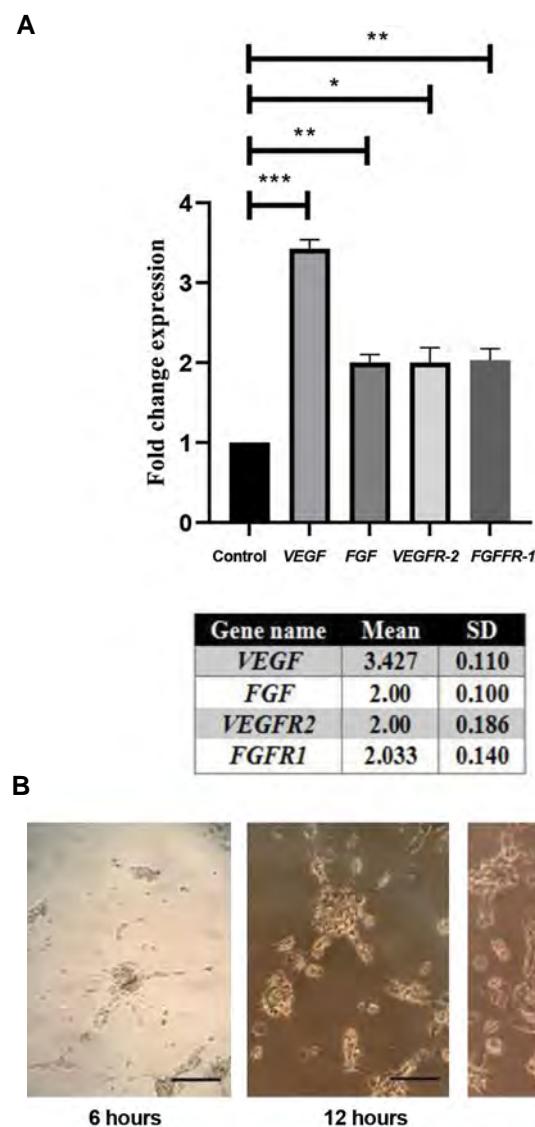


**Fig.3:** Evaluation of the angiogenic effect of the hUCMSC-derived EVs. **A.** Detection of *VEGF*, *FGF*, *FGFR-1*, and *VEGFR-2* genes expression changes compared to the control group showed that the expression of these genes in EVs-treated HUVEC cells increased significantly. Data are presented as the mean  $\pm$  SD and each group was compared with the control group; the meaningful changes are represented by asterisks (\*;  $P < 0.05$ , \*\*;  $P < 0.01$ , \*\*\*;  $P < 0.001$  and the exact numbers of P value were 0.0007 for *VEGF*, 0.0033 for *FGF*, 0.0114 for *VEGFR2*, and 0.0061 for *FGFR1*). **B.** Sequential tube formation after HUVECs treatment with EVs. Cell elongation, as well as connection to form a loop is apparent in the figure. Morphological changes in the cells were observed under the inverted microscope for 24 hours (scale bar: 50  $\mu\text{m}$ , magnification, 100x). All the experiments were tested in triplicate. hUCMSC; Human Umbilical cord mesenchymal stem cell and EVs; Extracellular vesicles.

## Angiogenic effect of extracellular vesicles

### RNA extraction and Real-time polymerase chain reaction

The expression of some critical angiogenic markers was measured in HUVECs after treating them with EVs. The qRT-PCR results were reported as relative gene expression (using the  $2^{-\Delta\Delta Ct}$  analysis method) and normalization by the housekeeping gene *HPRT1*. Data revealed that expression of *FGFR-1*, *FGF*, *VEGF*, and *VEGFR-2* genes were increased 2, 2, 3.5, and 2 fold, respectively, in treated cells compared to control groups (Fig.3A). According to these data, VEGF expression has increased more than the other genes.

### Tube formation assay

Figure 3B demonstrates the tube formation test results. Increased cell branches, elongation, and cell connections in the form of a loop are evident, confirming tube formation.

## Discussion

Angiogenesis is a vital event in the body's physiological processes during life, such as wound healing and tissue regeneration. Besides, increasing angiogenesis is highly effective in controlling many diseases, such as acute ischemia. Given the importance of angiogenesis, it can be considered a new therapeutic approach for some pathological conditions.

Although many factors increase angiogenesis, VEGF and FGF are the most critical and well-known factors (3, 23, 24).

MSCs are important as feeders of HSCs and play an important role in the regeneration of tissues by secretion of growth factors, EVs and cellular contact (7). Due to their ability to differentiate, autologous transplantation, and their unique properties, MSCs have received attention in the treatment of some diseases (25), such as bone tissue disorders (26), immune disorders (27) and cardiovascular diseases (28). Three important sources of MSCs are fat, bone marrow, and umbilical cord (7). MSCs of different sources have been shown to increase angiogenesis. Alvaro-Afonso et al. (29) examined the effect of adipose-derived MSCs (AMSCs) on diabetic foot ulcers (DFUs). Based on this study, it was concluded that AMSCs are promising for the treatment of DFUs. In another study by Zhang et al. (30), the effect of MSCs on the treatment of cardiovascular and ischemic diseases was studied. MSCs could differentiate to smooth muscle cells (SMCs) and endothelial cells (ECs) and release some factors which help cardiovascular regeneration.

A comparison of bone marrow-derived MSCs with umbilical cord MSCs by Wang et al. (31) showed that UCMSC could also induce angiogenesis and improve blood flow. It was demonstrated that UCMSCs differentiate into the three germ layers and enhance tissue repair and modulate immune responses. These cells showed a more substantial angiogenic effect than BMSCs. In these

articles, different applications of MSCs with different sources were shown; these cells have been used to stimulate angiogenesis and treat various diseases such as diabetic foot ulcers. In fact, the purpose of this study was to compare the sources of MSCs used in previous articles with the umbilical cord. The accessibility, ease of use, and comfortable extraction of MSCs make them a more suitable source as compared to previously mentioned sources for induction of angiogenesis. Other applications of MSCs are also discussed in these articles.

Considering the disadvantages of cell therapy, the idea of using a type of EVs, like exosomes, was taken into account as a new therapeutic strategy. The role of MSCs-derived exosomes was first studied in 2010 in the mouse model of myocardial ischemia/reperfusion damage, and then it was assessed in other disease models (32). EVs have different functions, such as intercellular signaling, and have unique properties in terms of concentration, appearance, and markers (13, 14). EVs also have other advantages over cell therapy, such as low immunogenicity (without MHC I, II) (33), low toxicity, facilitating the uptake of RNA and protein into damaged cells, the ability to carry large cargo, and strong protection from enzyme degradation, inherent stability and the ability to cross the blood-brain barrier (34).

Exosomes as small EVs have the same therapeutic effects on diseases as their source cells (16). There have been numerous studies on MSC-derived exosomes, which used various sources of MSCs for angiogenesis induction, and their benefits have been identified. The effect of UCMSCs-derived exosomes on acute myocardial infarction has been investigated. According to the results of such experiments, hUCMSC exosomes could protect systolic cardiac function and reduce cardiac fibrosis by protecting myocardial cells against apoptosis, which might be related to regulating Bcl-2 family gene expression and promoting angiogenesis (35). In 2016, Liang et al. (36) examined the effect of exosomes derived from adipose MSCs (adMSCs) on promoting endothelial cell angiogenesis. The researchers discovered that adMSC-derived exosomes (adMSCs-Exo) could be absorbed by endothelial cells and significantly enhance *in vitro* and *in vivo* angiogenesis. The study has also shown that adMSCs-Exo can translocate miR-125a to endothelial cells and induce angiogenesis by suppressing angiogenic inhibitor delta-like 4 (DLL4). Huang et al. (37) examined the angiogenesis and neurogenesis properties of bone marrow-derived MSCs exosomes modified with miR-126 in spinal cord injury (SCI) rats. These exosomes were used as a means of microRNA transfer for the first time. It was found that after spinal cord injury, MSC-derived exosomes (MSC-Exo) could transfer miR-126 to the affected spinal cord in rats, and exosomes containing miR-126 reduce the size of the lesion and improve function after SCI.

In this study, we used the umbilical cord (Wharton's jelly) because angiogenesis is abundant in this tissue and its other features are being easily accessible, non-invasive

harvesting, better viability, and consistent therapeutic properties (38, 39). We therefore used hUCMSCs-derived small EVs. The isolated EVs were identified. They had desirable properties, including a mean diameter of about 105 nm, the appearance of the bilayer membrane, and the presence of CD9 and CD63 markers. They were able to induce angiogenesis in HUVECs, as proved by increased expression of angiogenic genes, *FGFR-1*, *FGF*, *VEGF*, and *VEGFR-2*, and tube forming colonies. Angiogenesis is mediated mainly by VEGFA/VEGFR2 signaling. VEGFA causes endothelial proliferation, migration, and survival via activation of VEGFR2 and its downstream signal transduction pathways. VEGFA is critical for physiological and pathological processes. So VEGFA expression has been increased more (40). Analysis of tube formation images confirmed that hUCMSCs-derived EVs could induce tube branching from colonies of HUVECs.

In general, angiogenesis is a complex multi-stage process involving the activation of inactive endothelial cells, proliferation, migration, germination of endothelial cells, formation of tubular structures, maturation, and stability of newly formed buds, respectively. In this study, the signaling pathways are such that angiogenic factors are secreted by hUCMSCs-derived EVs. The secretion of these factors activates their receptors on endothelial cells (HUVEC cells) and thus begins angiogenesis. As a result, the increased expression of the desired genes compared to the control group was investigated and proven in our study. Thus, this study provided a new and useful application of hUCMSCs-derived EVs, i.e., induction of angiogenesis, which can be valuable in cell-free therapy. However, factors increasing angiogenesis are not studied in this study and need further investigation; besides, animal studies must be done to examine the potential of tumorigenesis of UCMSCs-derived exosomes.

## Conclusion

According to the present study, it has been demonstrated that hUCMSCs-derived small EVs could lead to increased expression of angiogenesis-related genes and the angiogenesis process. Based on these results and studies at the molecular level, small EVs derived from the hUCMSCs can be a good candidate for angiogenesis induction which has valuable potential as a novel cell-free medication.

## Acknowledgments

This project has been funded partially by Tarbiat Modares University, Tehran, Iran. There is no conflict of interest in this study.

## Authors' Contributions

M.S.Z., S.A.; Contributed to the conception and design. M.S.Z.; Was responsible for overall supervision. S.D.; Performed the experimental work. S.D., S.A., N.T.; Participated in data and statistical analysis, and interpretation of data. N.T.; Drafted the manuscript. All

authors read and approved the final manuscript.

## References

1. Soufi-zomorrod M, Hajifathali A, Kouhkan F, Mehdizadeh M, Rad SMAH, Soleimani M. MicroRNAs modulating angiogenesis: miR-129-1 and miR-133 act as angio-miR in HUVECs. *Tumor Biol.* 2016; 37(7): 9527-9534.
2. Komaki M, Numata Y, Morioka C, Honda I, Tooi M, Yokoyama N, et al. Exosomes of human placenta-derived mesenchymal stem cells stimulate angiogenesis. *Stem Cell Res Ther.* 2017; 8: 219.
3. Bian X, Ma K, Zhang C, Fu X. Therapeutic angiogenesis using stem cell-derived extracellular vesicles: an emerging approach for treatment of ischemic diseases. *Stem Cell Res Ther.* 2019; 10: 158.
4. Naito H, Iba T, Takakura N. Mechanisms of new blood-vessel formation and proliferative heterogeneity of endothelial cells. *Int Immunol.* 2020; 32(5): 295-305.
5. Wang S, Zhu R, Li H, Li J, Han Q, Zhao RC. Mesenchymal stem cells and immune disorders: from basic science to clinical transition. *Front Med.* 2019; 13(2): 138-151.
6. Keshkar S, Azarpira N, Ghahremani MH. Mesenchymal stem cell-derived extracellular vesicles: Novel frontiers in regenerative medicine. *Stem Cell Res Ther.* 2018; 9(1): 63.
7. Pashoutan Sarvar D, Shamsasenjan K, Akbarzadehlaleh P. Mesenchymal stem cell-derived exosomes: new opportunity in cell-free therapy. *Adv Pharm Bull.* 2016; 6(3): 293-299.
8. Brown C, McKee C, Bakshi S, Walker K, Hakman E, Halassy S, et al. Mesenchymal stem cells: Cell therapy and regeneration potential. *J Tissue Eng Regen Med.* 2019; 13(9): 1738-1755.
9. Berebichez-Fridman R, Montero-Olvera PR. Sources and clinical applications of mesenchymal stem cells state-of-the-art review. *Sultan Qaboos Univ Med J.* 2018; 18(3): e264-e277.
10. Lee M, Jeong SY, Ha J, Kim M, Jin HJ, Kwon SJ, et al. Low immunogenicity of allogeneic human umbilical cord blood-derived mesenchymal stem cells in vitro and in vivo. *Biochem Biophys Res Commun.* 2014; 446(4): 983-989.
11. Rackov G, Garcia-Romero N, Esteban-Rubio S, Carrión-Navarro J, Belda-Iniesta C, Ayuso-Sacido A. Vesicle-mediated control of cell function: The role of extracellular matrix and microenvironment. *Front Physiol.* 2018; 9: 651.
12. Park KS, Bandeira E, Shelke GV, Lässer C, Lötvall J. Enhancement of therapeutic potential of mesenchymal stem cell-derived extracellular vesicles. *Stem Cell Res Ther.* 2019; 10: 288.
13. Campanella C, Caruso Bavisotto C, Logozzi M, Marino Gammazza A, Mizzoni D, Cappello F, et al. On the choice of the extracellular vesicles for therapeutic purposes. *Int J Mol Sci.* 2019; 20(2): 236.
14. Ni YQ, Lin X, Zhan JK, Liu YS. Roles and functions of exosomal non-coding RNAs in vascular aging. *Aging Dis.* 2020; 11(1): 164-178.
15. Edgar JR. Q & A: What are exosomes, exactly? *BMC Biol.* 2016; 14: 46.
16. Cheng L, Zhang K, Wu S, Cui M, Xu T. Focus on mesenchymal stem cell-derived exosomes: Opportunities and challenges in cell-free therapy. *Stem Cells Int.* 2017; 2017: 6305295.
17. Nazimek K, Bryniarski K, Santocki M, Ptak W. Exosomes as mediators of intercellular communication: clinical implications. *Pol Arch Med Wewn.* 2015; 125(5): 370-380.
18. Mushahary D, Spittler A, Kasper C, Weber V, Charwat V. Isolation, cultivation, and characterization of human mesenchymal stem cells. *Cytom Part A.* 2018; 93(1): 19-31.
19. Riordan NH, Morales I, Fernández G, Allen N, Fearnott NE, Leckrone ME, et al. Clinical feasibility of umbilical cord tissue-derived mesenchymal stem cells in the treatment of multiple sclerosis. *J Transl Med.* 2018; 16(1): 57.
20. Zhang K, Li Z. Molecular imaging of therapeutic effect of mesenchymal stem cell-derived exosomes for hindlimb ischemia treatment. *Methods Mol Biol.* 2020; 2150: 213-225.
21. Zhang Y, Yan J, Li Z, Zheng J, Sun Q. Exosomes derived from human umbilical cord mesenchymal stem cells alleviate psoriasis-like skin inflammation. *J Interferon Cytokine Res.* 2022; 42(1): 8-18.
22. Addi T, Poitevin S, McKay N, El Mecherfi KE, Kheroua O, Jourde-Chiche N, et al. Mechanisms of tissue factor induction by the uremic toxin indole-3 acetic acid through aryl hydrocarbon receptor/nuclear factor-kappa B signaling pathway in human endothelial cells. *Arch Toxicol.* 2019; 93(1): 121-136.
23. Kishore R, Khan M. More than tiny sacks: stem cell exosomes as cell-free modality for cardiac repair. *Circ Res.* 2016; 118(2): 330-343.
24. Fallah A, Sadeghinia A, Kahroba H, Samadi A, Heidari HR, Bra-

- daran B, et al. Therapeutic targeting of angiogenesis molecular pathways in angiogenesis-dependent diseases. *Biomed Pharmacother.* 2019; 110: 775-785.
25. Lukomska B, Stanaszek L, Zuba-Surma E, Legosz P, Sarzynska S, Dreła K. Challenges and controversies in human mesenchymal stem cell therapy. *Stem Cells Int.* 2019; 2019: 9628536.
  26. Shang F, Yu Y, Liu S, Ming L, Zhang Y, Zhou Z, et al. Advancing application of mesenchymal stem cell-based bone tissue regeneration. *Bioact Mater.* 2021; 6(3): 666-683.
  27. Lee BC, Kang KS. Functional enhancement strategies for immunomodulation of mesenchymal stem cells and their therapeutic application. *Stem Cell Res Ther.* 2020; 11(1): 1-10.
  28. Teng X, Chen L, Chen W, Yang J, Yang Z, Shen Z. Mesenchymal stem cell-derived exosomes improve the microenvironment of infarcted myocardium contributing to angiogenesis and anti-inflammation. *Cell Physiol Biochem.* 2015; 37(6): 2415-2424.
  29. Álvaro-Afonso FJ, Sanz-Corbalán I, Lázaro-Martínez JL, Kakagia D, Papanas N. Adipose-derived mesenchymal stem cells in the treatment of diabetic foot ulcers: a review of preclinical and clinical studies. *Angiology.* 2020; 71(9): 853-863.
  30. Zhang C, Lin Y, Liu Q, He J, Xiang P, Wang D, et al. Growth differentiation factor 11 promotes differentiation of MSCs into endothelial-like cells for angiogenesis. *J Cell Mol Med.* 2020; 24(15): 8703-8717.
  31. Wang Z, Zheng L, Lian C, Qi Y, Li W. Human umbilical cord-derived mesenchymal stem cells relieve hind limb ischemia by promoting angiogenesis in mice. *Stem Cells Dev.* 2019; 28(20): 1384-1397.
  32. Lai RC, Arslan F, Lee MM, Sze NS, Choo A, Chen TS, et al. Exosome secreted by MSC reduces myocardial ischemia/reperfusion injury. *Stem Cell Res.* 2010; 4(3): 214-222.
  33. Zhang J, Guan J, Niu X, Hu G, Guo S, Li Q, et al. Exosomes released from human induced pluripotent stem cells-derived MSCs facilitate cutaneous wound healing by promoting collagen synthesis and angiogenesis. *J Transl Med.* 2015; 13: 49.
  34. Tian T, Zhang HX, He CP, Fan S, Zhu YL, Qi C, et al. Surface functionalized exosomes as targeted drug delivery vehicles for cerebral ischemia therapy. *Biomaterials.* 2018; 150: 137-149.
  35. Zhao Y, Sun X, Cao W, Ma J, Sun L, Qian H, et al. Exosomes derived from human umbilical cord mesenchymal stem cells relieve acute myocardial ischemic injury. *Stem Cells Int.* 2015; 2015: 761643.
  36. Liang X, Zhang L, Wang S, Han Q, Zhao RC. Exosomes secreted by mesenchymal stem cells promote endothelial cell angiogenesis by transferring miR-125a. *J Cell Sci.* 2016; 129(11): 2182-2189.
  37. Huang JH, Xu Y, Yin XM, Lin FY. Exosomes derived from miR-126-modified MSCs promote angiogenesis and neurogenesis and attenuate apoptosis after spinal cord injury in rats. *Neuroscience.* 2020; 424: 133-145.
  38. Raileanu VN, Whiteley J, Chow T, Kollara A, Mohamed A, Keating A, et al. Banking mesenchymal stromal cells from umbilical cord tissue: large sample size analysis reveals consistency between donors. *Stem Cells Transl Med.* 2019; 8(10): 1041-1054.
  39. Liu Y, Fang J, Zhang Q, Zhang X, Cao Y, Chen W, et al. Wnt10b-overexpressing umbilical cord mesenchymal stem cells promote critical size rat calvarial defect healing by enhanced osteogenesis and VEGF-mediated angiogenesis. *J Orthop Transl.* 2020; 23: 29-37.
  40. Karaman S, Leppänen VM, Alitalo K. Vascular endothelial growth factor signaling in development and disease. *Development.* 2018; 145(14): dev151019.
-

# Effect of PLGA Nanoparticle-Mediated Delivery of miRNA 503 on The Apoptosis of Ovarian Endometriosis Cells

Shahla Chaichian, M.D.<sup>1,2</sup>, Abolfazl Mehdizadeh Kashi, M.D.<sup>1</sup>, Kobra Tehermanesh, M.D.<sup>1</sup>, Vahid Pirhajati Mahabadi, Ph.D.<sup>3</sup>, Sara Minaeian, Ph.D.<sup>4</sup>, Neda Eslahi, Ph.D.<sup>5\*</sup>

1. Endometriosis Research Center, Iran University of Medical Sciences, Tehran, Iran

2. Pars Advanced and Minimally Invasive Medical Manners Research Center, Pars Hospital, Iran University of Medical Sciences, Tehran, Iran

3. Neurosciences Research Center, Iran University of Medical Sciences, Tehran, Iran

4. Antimicrobial Resistance Research Center, Institute of Immunology and Infectious Diseases, Iran University of Medical Sciences, Tehran, Iran

5. Air Pollution Research Center, Iran University of Medical Sciences, Tehran, Iran

\*Corresponding Address: P.O.Box: 354-14665, Air Pollution Research Center, Iran University of Medical Sciences, Tehran, Iran  
Email: neslahi.2@gmail.com

Received: 11/July/2022, Accepted: 29/August/2022

## Abstract

**Objective:** One of the challenges in gene therapy is the transfer of the gene to the target cell. MicroRNAs (miRNAs) regulate gene expression after transcription by binding directly to the messenger and play a vital role in cell behaviors and the pathogenesis of some diseases. This study was aimed at developing poly (lactic-co-glycolic acid) (PLGA)-based nanoparticles (NPs) for gene delivery to endometriotic cyst stromal cells (ECSCs).

**Materials and Methods:** In this experimental study, endometriosis cells were isolated from women with severe endometriosis (DIE) and digested by the enzymatic method (40 µg/ml DNAase I and 300 µg/ml collagenase type 3). PLGA-based NPs were synthesized and characterized. The size of sole PLGA NPs and PLGA/miRNA were  $60 \pm 4$  nm and  $70 \pm 5.1$  nm respectively. Poly lactic-co-glycolic-based NPs were used as vector carriers for miRNA 503 transfection in endometriosis cells. The cells were divided into the five groups of control and four doses (25, 50, 75, and 100 µm) of miRNA 503/PLGA at 12, 24, 48, and 72 hours. Viability and apoptosis were evaluated by the MTT assay and Annexin Kits. Data were analyzed by one-way analysis of variance.

**Results:** The results show that the size of PLGA/miRNA complex with dynamic light scattering (DLS) was  $70 \pm 5.1$  nm and zeta potential values of the PLGA/PEI/miRNA complexes were 27.9 mV. Based on the MTT assay results, the optimal dose of miRNA 503/PLGA was 75 µm, at which the viability of ECSCs was  $52.6\% \pm 1.2$  ( $P \leq 0.001$ ), and the optimal time was 48 hours. The apoptotic rates of ECSCs treated with PLGA/miRNA503 ( $34.75 \pm 4.9\%$ ) were significantly higher than those of ECSCs treated with PLGA alone ( $3.35 \pm 2.58\%$ ,  $P \leq 0.01$ ).

**Conclusion:** Cell death increased with increasing the concentration of miRNA; thus, it can be suggested as a treatment for endometriosis.

**Keywords:** Apoptosis, miRNA 503, Nanoparticle, Ovarian Endometriosis

Cell Journal (Yakhteh), Vol 24, No 11, November 2022, Pages: 697-704

**Citation:** Chaichian Sh, Mehdizadeh Kashi A, Tehermanesh K, Pirhajati Mahabadi V, Minaeian S, Eslahi N. Effect of PLGA nanoparticle-mediated delivery of miRNA 503 on the apoptosis of ovarian endometriosis cells. Cell J. 2022; 24(11): 697-704. doi: 10.22074/CELLJ.2022.557554.1069.

This open-access article has been published under the terms of the Creative Commons Attribution Non-Commercial 3.0 (CC BY-NC 3.0).

## Introduction

Endometriosis is an estrogen-dependent gynecological disease in which endometrial tissue is found in unusual places outside the uterus, ranging from minor lesions on other healthy pelvic organs to large endometriotic ovarian cysts. This condition changes the ovaries and causes the viscera to stick to each other, and this adhesion is the main cause of pain and infertility in these people (1). Ding et al. (2) show that the cause of estrogen sensitivity in endometriosis tissues is related to the activity of neurons. Inflammation affects the growth of the oocyte, and the unfavorable environment created by the activity of macrophages reduces the quality of the oocyte, resulting in infertility (3). There is also an endocannabinoid system in the human ovary that is effective in the neuro protection of cells and has an anti-inflammatory function through modulating cell survival and proliferation and inducing apoptosis in normal cells.

In one study a relationship between this system and

ovarian pathologies was shown (4). In endometriosis, receptors of this system are inhibited and increased cell inflammation, disease progression, and pain (5). Endometriosis is classified as a tumor disease by the World Health Organization (WHO) because it has a tumor-like structure and behaves like cancer in terms of invading other tissues. In fact, endometriosis, like cancer cells, attacks tissues, induces angiogenesis, increases the production of estrogen, impairs immune function, and causes inflammation (6). At present, the best method for the diagnosis of endometriosis and isolation of invasive tissues is laparoscopic examination with the histological confirmation of glands in removed lesions (7). Therefore, people's fear of surgery and assuming dysmenorrhea as normal delay the timely diagnosis of the disease (8).

Today, methods such as gene therapy have been used in the diagnosis and treatment of diseases. MicroRNAs (miRNAs) regulate post-transcriptional gene expression playing a crucial role in proliferation, differentiation, and

apoptosis, which are key to the diagnosis of endometriosis (9). miRNAs are involved in cell survival, proliferation, angiogenesis, and apoptosis, therefore, they are effective in the pathogenesis of endometriosis (10). In endometriosis, programmed cell death, which is called apoptosis, is reduced. Thus, endometriotic tissues develop in the abdominal and pelvic cavities. Accordingly, there is an inverse relationship between the severity of endometriosis and the rate of apoptosis (11). Viral and non-viral vectors are used for miRNAs transmission. Non-viral gene delivery vectors, such as inorganic nanoparticles (NPs) and liposomes, have been used in recent years (12).

One of the best carriers is poly (lactic-co-glycolic acid) (PLGA), which has been widely used in drug delivery because it escapes from the endo-lysosome system and keeps its contents longer. Therefore, it is also suitable for gene transfer (13). Various miRNAs have been observed in endometrial and atopic lesions (14). One of the miRNAs inhibited in endometriosis is miR-503, which is involved in endometriotic cyst stromal cells (ECSCs) cell apoptosis. miR-503 inhibits cell cycle in the G0/G1 phase and prevents cell proliferation (15). Since to date, there is no study that have been measured the effects of this nanoparticle on apoptosis of endometriosis cells, in this study we performed the effect of PLGA-micro RNA delivery on the apoptosis of stromal cells of ovarian endometrium cysts *in vitro*.

## Materials and Methods

### Sampling and culture of human endometriosis tissue

In this experimental study, ovarian endometrioma cyst walls were removed from women 30 to 40 years at Hazrat-e Rasool Hospital during laparoscopic surgery. After washing, the tissue fragments were enzymatically digested with collagenase and DNAase and incubated at 37°C with 5% CO<sub>2</sub> for 90 minutes. Then, the tissue pieces were passed through filters (45 µm) (16). Cells cultured at 37°C in a 5% CO<sub>2</sub> atmosphere in DMEM/F12 medium were supplemented with penicillin (100 U/mL), streptomycin (100 µg/mL), gentamycin (40 µg/mL), and 5% fetal bovine serum for three weeks, and the culture medium was changed every 2-3 days when they reached 80% confluency. The research was approved by the Research Ethics Committee of Iran University of Medical Sciences (IR.IUMS.REC.1397.1176).

### Immunocytochemical analysis of cultured endometriosis cells

In order to confirm the cyst wall endometrial tissue-isolated cells, immunocytochemistry was performed for CD10 markers (17). After 3 weeks, endometriosis cells were detached from the flask using trypsin/EDTA. The cells were smeared and incubated with 4% paraformaldehyde at room temperature for 10 minutes. Triton X-100 was added to the cells to make the cell membrane permeable to antibodies, then antibodies were added to the cells at appropriate concentrations in a 1:200 ratio overnight at 4°C. Also, the cells were washed

thoroughly and stained with Fluorescein isothiocyanate (FITC)-conjugated anti-mouse Ig antibodies 1:500 for 1 hour at room temperature in the dark. After a further wash, they were mounted in glycerol. CD markers were analyzed by fluorescence microscopy.

### Preparing microRNAs

miRNAs 503, including primer (sequence [5' → 3']: TAGCAGCGGGAACAGTTCTGCAG) (Fluorescent marker), were purchased from Pishgam Co. (St Kargar, Tehran, Iran), and PLGA (Resomer RG502H) with a 50:50 mole ratio of glycolic acid to lactic acid and a molecular weight of 12,000 g/mol, polyvinyl alcohol (PVA, 89 mol% hydrolyzed), Span 80, and Tween 80 were purchased from Sigma (St Louis, MO, USA).

PLGA NPs containing miRNAs were synthesized by using the water-in-oil-in-water solvent vaporization technique consisting of an organic phase and two aqueous phases in one medium (18). To stabilize the dispersed phase, a stabilizer is needed, the most commonly used of which is polyvinyl alcohol. This substance in the external aqueous phase creates a thin layer around the particles. In the organic phase, the active substance was used at the Span 80 level, and in the aqueous external phase, Tween 80 level. All the solutions were prepared in DEPC-treated water, and RNase-free media were used at all stages. To prepare the desired nano capsule, the internal aqueous phase was first obtained by creating a polyplex derived from polyethylene imine) PEI 25 (KDa and miRNA with a 3: 1 mass ratio. Polyethylene imine is capable of compressing high molecular chain genetic content that can produce NPs of appropriate size entering the cell as endocytosis. First, 0.1% solution of PEI was prepared in DEPC-treated water. A miRNA solution was also prepared using DEPC-treated water at a concentration of 100 pmol/µl. It was then combined in 80 µl of PEI solution containing 90 µg of PEI and 40 µl of miRNA containing 30 µg of miRNA, and the volume was reached to 0.5 ml by phosphate-buffered saline (PBS, Merck, USA) and incubated in a thermocycler at 37°C for 30 minutes.

To prepare the organic phase in solvent evaporation, 10 mg of PLGA was dissolved in 2 ml of organic solvent ethyl acetate. To form an initial emulsion of 0.5 ml of internal aqueous phase, 0.5 ml of Span 80 solution at a concentration of 5 mg/ml was added to the organic phase using Vertex and an ultrasonic bath. The initial water emulsion was created in the oil.

This water emulsion was then added dropwise to an oil containing 5 ml of 8% PVA and 10 mg of Tween 80 as an outer phase for 3 minutes using a probed ultrasonic device. The power of 50 watts was subjected to sonication to form a secondary emulsion. In the final step, the final dual emulsion solvent diffusion was added to 4 ml of 0.5% PVA and subjected to magnetic stirring for 4 hours until the ethyl acetate solvent was used to diffuse the external aqueous phase containing solid polymer particles. After forming the nanoparticles, they were separated twice and purified by centrifugation at 12,000 rpm for 30 minutes and also

suspended in distilled water to remove unloaded miRNA and additional surfactants in the external aqueous phase from the surface of NPs (the supernatant was investigated by dynamic light scattering to determine the separation efficiency). The nano capsules were finally dried for 24 hours and stored in a refrigerator at a temperature of 4°C for 24 hours. All of the above steps were performed with 0.5 ml distilled water without drug as internal aqueous phase (19). Poly lactic-co-glycolic (Resomer RG502H) with a 50:50 mole ratio of glycolic acid to lactic acid and a molecular weight of 12,000 g/mol, PVA (89 mol% hydrolyzed), Span 80 and Tween 80 were purchased from Sigma (St Louis, MO, USA).

### Nanoparticle characterization

Some of the dried powder of PLGA/PEI/miRNA was dispersed in 1 ml of saline phosphate buffer at pH=7.4 using an ultrasonic bath, and the zeta potential was measured using a zeta meter device. The size and morphology of the PLGA NPs and PLGA modified with PEI /miRNA complexes onto a copper sheath, carbon coated, were characterized via transmission electron microscopy (TEM). Finally, the cellular uptake of NPs was examined by TEM. For the TEM technique, ECSCs were washed with PBS, then 2.5% glutaraldehyde was used as a primary fixation for 2 hours. The cells were rinsed 2-3 times with PBS, and free glutaraldehyde was removed. Then, 1% osmium tetroxide was used as a secondary fixation for 1.5 hours. The cells were dehydrated in acetone (50%, 70%, 90%, 100%), infiltrated by resin, and finally, embedded in pure resin (Epon 812, TAAB, UK). Then, 50 nm sections were stained with uranyl acetate and lead citrate on copper grade and then imaged with TEM (LEO 906, Zeiss).

### Cytotoxicity assay

In this study, ECSCs were divided into the five groups of control and experimental groups, with cells distributed in a 96 well plate at a cell density of  $20 \times 10^3$  cells per well in the different concentrations of PLGA/miRNA (25, 50, 75, and 100  $\mu$ M) and different incubation periods (12, 24, 48, and 72 hours). We performed the MTT assay to determine the toxicity of PLGA/miRNA. To evaluate the survival rate, the cells were centrifuged and washed with PBS and incubated with 100  $\mu$ l of MTT solution (MTT tetrazolium salt 5 mg/ ml) for 3-4 hours. Finally, the cells were centrifuged, and the supernatant was removed. Next, 100  $\mu$ l of dimethyl sulfoxide (DMSO, Merck, USA) was added to the wells, and the plates were shaken for 10 minutes in a microplate shaker before observation with the ELISA reader at 570 nm. The cells were then treated with the optimum dose obtained, and survival rates compared with and without nanoparticles.

### Apoptosis evaluation

After determining the effective dose of microRNA and PLGA in cell viability, the cells were cultured with a dose of NPs and microRNA/NPs with the lowest viability for 48 hours. Then, the apoptosis rate of cells was assessed using Annexin V-FITC Apoptosis Detection Kit. That way,

500 $\mu$ l of the binding buffer was added to the cell plate. Afterward, 5  $\mu$ l of Annexin V-FITC and 5  $\mu$ l of PI at room temperature were added to the cells and incubated in foil for 10 minutes. Finally, flow cytometry was performed, and the rate of apoptosis in cells was evaluated (20).

### Transplantation of endometriosis cells to mice

In this experiment, 12 mice NMRI (n=6 in each groups) (6-8-weeks-old) with  $25 \pm 1$  g weight were divided into two groups. In the first group, cells that had only PLGA added to their culture medium were injected, and in the second group, cells treated with PLGA/miRNA were injected. The animals were kept in university laboratory's animal house. To weaken the immune system of the mice, they were treated with a single dose of 7.5 Gy  $\gamma$ -irradiation for 6 min (21). After 72 hours, cells were transplanted to the back of the thigh of the mice. The mice were anesthetized with the intra peritoneal injection of a mixture of 100 mg/kg ketamine hydrochloride 10% (Rotexmedica, Germany) and 10 mg/kg xylazine 2% (Alfasan, Holland). Then, 20  $\mu$ L of suspension, including  $2 \times 10^6$  cells at the fourth passage, was injected subcutaneously into the back of the right front limb in each group. All the mice were observed for 3 weeks.

### Statistical analysis

Data were analyzed using One-way analysis of variance (ANOVA) to compare different groups. The analysis was performed by using of SPSS, version 16 (Chicago, IL, USA). Results were expressed as mean  $\pm$  SEM, and a  $P < 0.05$  was considered significant.

## Results

### Sampling and culture of human endometriosis tissue

The stromal cells were harvested from endometriosis cell. One week after digestion and culture, size and morphology of them were similar to fibroblast cells. At the end of third week cell confluency was  $2 \times 10^5$  cells/ml. An aspect on the phase contrast microscopy of the third passage of the culture derived from an ovarian endometrioma is presented in Figure 1A, B. The cultured cells were confirmed to be positive for CD10 antigen (Fig.1C).

### Characterization of nanoparticles/miRNA complexes

The particle size and surface morphology of the NPs were examined by TEM, DLS, and Zeta potential (Fig.2A-C). PLGA NPs with a size below 100 nm are effective in gene transfer (22). In this study, the mean diameter of the sole PLGA NPs was  $60 \pm 4$  nm, whereas the size of PLGA/miRNA complex with DLS was increased to  $70 \pm 5.1$  nm. The surface charge index of NPs is determined by Zeta potential. For the endocytosis of particles into the cell, a more positive particle load leads to a stronger bond to the cell membrane surface and easier penetration to the cell. In this study, zeta potential values of the PLGA/PEI/miRNA complexes were 27.9 mV. The cellular uptake of NPs is shown by TEM (Fig.2D).

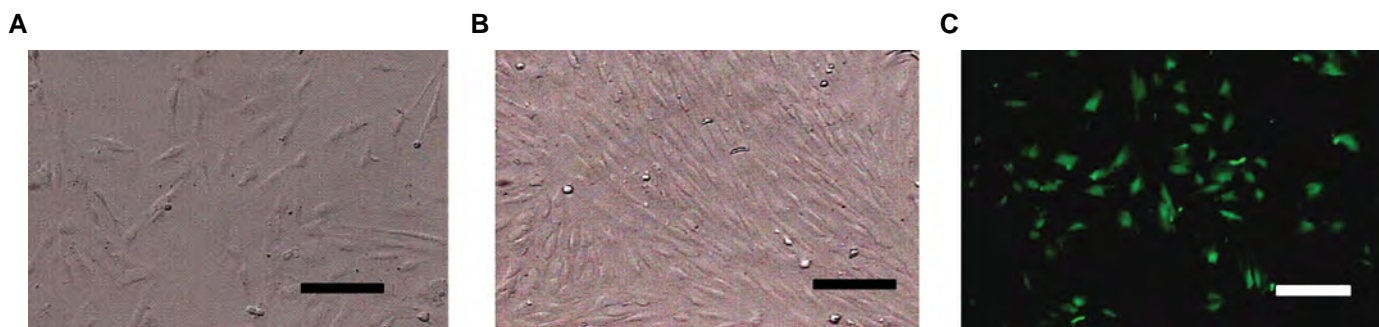


**Fig.1:** The structure of endometriosis cells in the culture medium. Size and morphology of them were similar to fibroblast cells. **A.** Endometriosis cells one week after planting, **B.** The end of the third week of culture (scale bar: 50  $\mu$ m). **C.** Immunocytochemistry of endometriosis cells with CD10 marker (scale bar: 30  $\mu$ m).

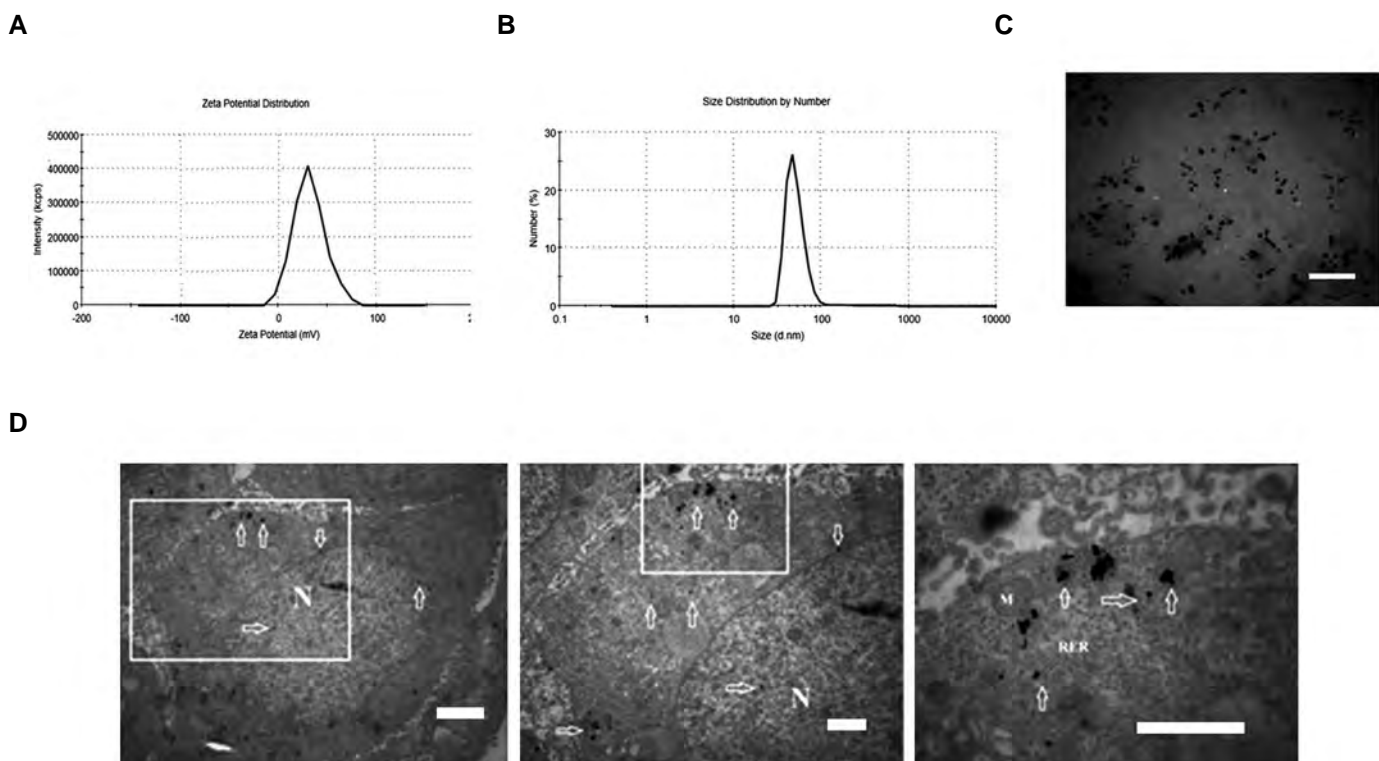


**Fig.2:** Nanoparticle evaluation tests. **A.** Zeta potential, **B.** The particle size based on the DLS test, **C.** Electron microscope image of PLGA showed spherical surface in all nanoparticles (scale bar: 500 nm), and **D.** As shown, the nanoparticles have accumulated in the nucleus and cytoplasm (scale bar: 1  $\mu$ m). DLS; Dynamic light scattering and PLGA; Poly lactic-coglycolic acid.

### Cell viability

The viability indices of cells for the control and 25, 50, 75, and 100  $\mu$ M PLGA/miRNA concentrations were 97.3%, 91.3%, 85.6%, 81.4%, and 70.2% in 12 hours, 98%, 88.4%, 80.4%, 78.8%, and 68.1% in 24 hours, and 97.3%, 70.3%, 64.2%, 52.6%, and 47.9% in 48 hours, and 98%, 66.8%, 60.3%, 49.9%, and 44.6% in 72 hours, respectively. The survival rate of stromal cells at the concentrations of 25, 50, 75, and 100  $\mu$ M PLGA/miRNA decreased compared to the control group at 12, 24, 48, and 72 hours in a time- and dose- dependent manner.

The results showed that with increasing incubation time

from 24 hours to 48 hours, the survival rate decreased, and with increasing time to 72 hours, cell survival decreased, but no significant difference was observed in this regard between 24 hours and 72 hours. Therefore, the incubation time was 48 hours. Also, in comparison with the survival rate in different doses, the survival rate decreased with increasing concentration, but as the figures shows, no significant difference was observed between 75  $\mu$ m and 100  $\mu$ m concentrations; therefore, 75  $\mu$ m doses were selected ( $P \leq 0.001$ , Fig.3). The cells were then incubated at a dose of 75  $\mu$ m of PLGA for 48 hours, and the survival rate was assessed. The cell viability rates in the control and treated groups were 98.4% and 89.9%, respectively,

which showed a significant difference in the survival of cells treated with PLGA/miRNA (Fig.4).

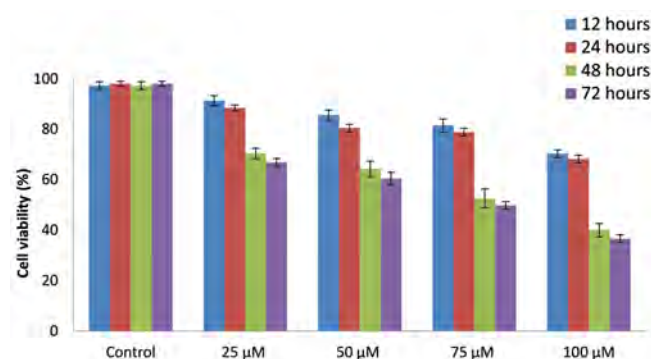


**Fig.3:** Based on MTT test, treatment with 75 μm miR-PLGA for 48 hours was selected; significant differences between groups were observed ( $P \leq 0.001$ ). MTT; (3-(4,5-dimethylthiazol-2-yl)-2,5-diphenyltetrazolium bromide and PLGA; Poly lactic-co-glycolic acid.

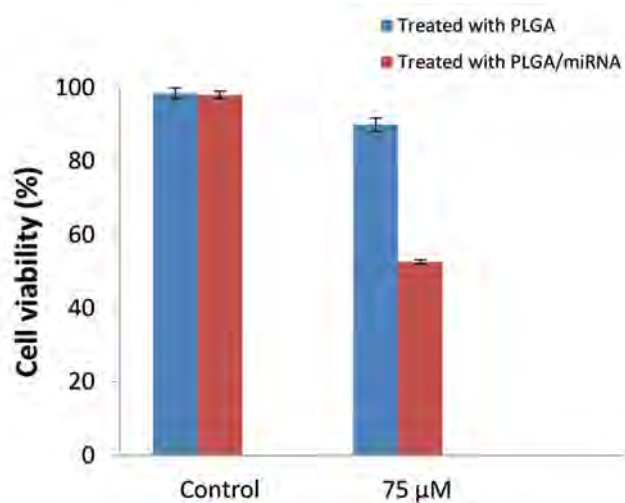


**Fig.4:** Based on MTT test, significant differences in survival rate with and without miRNA were observed ( $P \leq 0.001$ ). MTT; (3-(4,5-dimethylthiazol-2-yl)-2,5-diphenyltetrazolium bromide and PLGA; Poly lactic-co-glycolic acid.

### Apoptosis evaluation in ECSCs after treatment with PLGA/miRNA503

Apoptosis was measured using the annexin V-FITC apoptosis detection kit. The rate of apoptosis in control group was  $0.98 \pm 0.1$  (Fig.5A). The result showed that total apoptosis in ECSCs treated with PLGA miRNA503 ( $35.66 \pm 4.6\%$ ) were significantly higher than those of cells treated with PLGA ( $3.76 \pm 1.19\%$ ,  $P \leq 0.01$ , Fig.5B, C).

### The gross morphology of endometriosis lesion

The macroscopic observation of endometriosis lesions

in the two models are presented in Figure 6. In the first group, cells were treated with PLGA alone, and in the second group, they were treated with PLGA/miRNA. As shown in the figure, in the second group, the rate of cell apoptosis was higher, and tumor size was smaller. These lesions had a cystic morphology and were distinguished from the surrounding tissues.

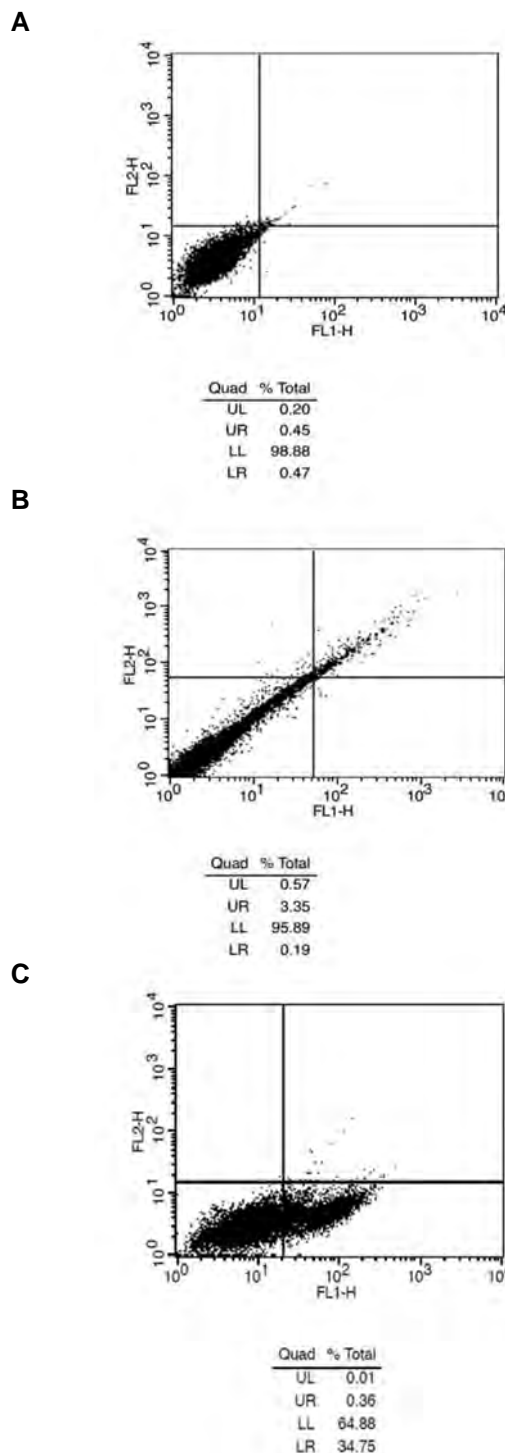


**Fig.5:** Based on the annexin assay. **A.** Flow cytometry of cells in the control group, **B.** PLGA-treated group, and **C.** PLGA/miRNA 503-treated group, result show that the apoptotic rates of the ECSCs treated with PLGA miRNA503 were significantly higher than those of cells treated with PLGA ( $P \leq 0.01$ ).

A



B



**Fig.6:** In both groups, cells was injected subcutaneously into the back of the right front limb. After 3 weeks, the endometriosis lesions in two models were shown. **A.** PLGA-treated cell injection and **B.** PLGA/miRNA503-treated cell injection.

## Discussion

Endometriosis is a benign disease of the female reproductive system, which is associated with increased angiogenesis and defects in cellular apoptosis (23) that behaves like a cancer in terms of aggressiveness (24). In one study, plant compounds with anti-inflammatory properties have been used to upturn the apoptotic effect of drugs in the treatment of cancer, and it has been observed that cell proliferation and angiogenesis were inhibited (25). Due to increase in the percentage of women with endometriosis and its common complications, including chronic pelvic pain and infertility, a non-surgical diagnosis is absolutely desirable (26). As the standard diagnostic modality for endometriosis is still laparoscopy, which carries many risks for the patient (27), a number of studies have been performed in this regard. For example, Samartzis et al. (28) used Doxycycline to inhibit the progression of endometriotic stromal cells *in vitro*.

NPs through structural mitochondrial damage are effective in causing apoptosis and cell necrosis (29). Nanomaterials in the treatment of endometriosis are

accumulation in endometriotic tissues. Chaudhury et al. (30) used cerium oxide NPs in an endometriosis-induced mouse model and observed the inhibition of angiogenesis. In another study, plant nanocomposites were used to induce apoptosis and necrosis of endometriotic stromal cells (31). NPs can be synthesized from various natural or synthetic lipids, proteins, metals, and polymers, one of the synthetic polymers used in numerous biomedical applications is PLGA (32). Poly lactic-co-glycolic NPs as drug delivery systems in antibiotic therapy, chemotherapy, and anti-inflammatory drugs have proven their potential (33). Shabani et al. (34) investigated the anticancer activity of cisplatin conjugated with PLGA NPs for elimination of mouse malignant cells from normal cell and observed that apoptosis rate of tumor cell was higher than free drug. Singh et al. (35) used the combination of doxycycline and PLGA NPs for the treatment of endometriosis and observed that angiogenesis was inhibited. Also used from letrozole and curcumin loaded-PLGA NPs for endometriosis in a mouse model. Guo et al. (36) injected endometriosis cells subcutaneously, and then the animal model was treated with two different types of NPs of different sizes (10 nm vs. 40 nm) by intravenous injection; they observed a regression of endometriosis. Li et al. (37) evaluated iron oxide NPs (15 nm) modified with hyaluronic acid in a rat model of endometriosis and reported that these NPs could accumulate in CD44 expressing tumors.

One biomarker that can be used in research is miRNAs, which raise as potent regulators of gene expression in proliferation, cell survival, and angiogenesis in some disease such as endometriosis (38). Shams et al. (19, 39) have shown that miRNAs are tumor suppressors, they used two effective miRNAs (143 and 206) to induce apoptosis in cancer cells. Hirakawa et al. (15) found that one miRNA in stromal cell of ovarian endometriosis, which inhibits cell proliferation and induction of apoptosis, is miRNA 503 that was epigenetically inhibited. Thus, we developed a PLGA-based nanoparticle polyplex with miRNA expression to induce apoptosis in endometriosis cells. Our results demonstrated that the cytotoxicity PLGA/miRNA 503 increased in ECSCs in comparison to PLGA. After the incubation of ECSCs with PLGA/miRNA 503, apoptosis evaluation was performed by using an annexin V-FITC apoptosis detection kit. The results showed that the apoptotic rates of PLGA miRNA 503 were significantly higher than those of PLGA, which is consistent with other studies (40). After the incubation of cells with PLGA miRNA and imaging by TEM, the presence of NPs in the nucleus and cytoplasm of cells was confirmed, which is in line with studies that showed that NPs with a size of 10-150 nm and surface charge of +30 – -20 mV could accumulate in endometriotic tissues (36).

## Conclusion

We reported the synthesis and characterization of PLGA/miRNA and its *in vitro* effects on the viability of ECSCs. In addition, our results demonstrated that

miRNA 503 reduced cell proliferation and progressed apoptotic rate in endometriotic cells. The obtained results support the use of the optimal dose of PLGA/miRNA as an effective approach for preventing the progression of endometriosis.

## Acknowledgments

This study was funded by a grant from Iran University of Medical Sciences (IUMS). We would like to give great thanks to the Nanotechnology Department of Iran University of Medical Sciences. The authors declare that there is no conflict of interest in this study.

## Authors' Contributions

N.E., Sh.Ch., A.M.K., K.T., V.P.-M., S.M.; Contributed to conception and design, data and statistical analysis, and interpretation of data. N.E.; Contributed to experimental work and wrote the manuscript, V.P.M.; Performed transmission electronic microscopy process. Sh.Ch.; Was responsible for overall supervision. All authors performed editing and approving the final version of this manuscript for submission, also approved the final draft.

## References

- Cranney R, Condous G, Reid S. An update on the diagnosis, surgical management, and fertility outcomes for women with endometrioma. *Acta Obstet Gynecol Scand.* 2017; 96(6): 633-643.
- Ding S, Guo X, Zhu L, Wang J, Li T, Yu Q, et al. Macrophage-derived netrin-1 contributes to endometriosis-associated pain. *Ann Transl Med.* 2021; 9(1): 29.
- Orazov MR, Radzinsky VY, Ivanov II, Khamoshina MB, Shustova VB. Oocyte quality in women with infertility associated endometriosis. *Gynecol Endocrinol.* 2019; 35 Suppl 1: 24-26.
- Ronchi A, Grauso F, Marino FZ, Quagliariello V, Maurea N, Facchini G, et al. Endocannabinoid system expression in ovarian epithelial tumors according to the dualistic model of ovarian carcinogenesis. *Eur Rev Med Pharmacol Sci.* 2021; 25(14): 4678-4686.
- Tanaka K, Mayne L, Khalil A, Baartz D, Eriksson L, Mortlock SA, et al. The role of the endocannabinoid system in aetiopathogenesis of endometriosis: a potential therapeutic target. *Eur J Obstet Gynecol Reprod Biol.* 2020; 244: 87-94.
- Guo SW. Endometriosis and ovarian cancer: potential benefits and harms of screening and risk-reducing surgery. *Fertil Steril.* 2015; 104(4): 813-830.
- Schleedoorn MJ, Nelen WL, Dunselman GA, Vermeulen N; EndoKey Group. Selection of key recommendations for the management of women with endometriosis by an international panel of patients and professionals. *Hum Reprod.* 2016; 31(6): 1208-1218.
- Mechsner S. Endometriosis: an often unrecognized pain disorder. *Schmerz.* 2016; 30(5): 477-490.
- Raja MHR, Farooqui N, Zuberi N, Ashraf M, Azhar A, Baig R, et al. Endometriosis, infertility and MicroRNA's: a review. *J Gynecol Obstet Hum Reprod.* 2021; 50(9): 102157.
- Marí-Alexandre J, Barceló-Molina M, Belmonte-López E, García-Oms J, Estellés A, Braza-Boils A, et al. Micro-RNA profile and proteins in peritoneal fluid from women with endometriosis: their relationship with sterility. *Fertil Steril.* 2018; 109(4): 675-684. e2.
- Sbracia M, Valeri C, Antonini G, Biagiotti G, Pacchiarotti A, Pacchiarotti A. Fas and Fas-ligand in eutopic and ectopic endometrium of women with endometriosis: the possible immune privilege of ectopic endometrium. *Reprod Sci.* 2016; 23(1): 81-86.
- Bai Z, Wei J, Yu C, Han X, Qin X, Zhang C, et al. Non-viral nanocarriers for intracellular delivery of microRNA therapeutics. *J Mater Chem B.* 2019; 7(8): 1209-1225.
- Ramezani M, Ebrahimian M, Hashemi M. Current strategies in the modification of PLGA-based gene delivery system. *Curr Med Chem.* 2017; 24(7): 728-739.
- Marí-Alexandre J, Sánchez-Izquierdo D, Gilabert-Estellés J, Barceló-Molina M, Braza-Boils A, Sandoval J. miRNAs regulation and its role as biomarkers in endometriosis. *Int J Mol Sci.* 2016; 17(1): 93.
- Hirakawa T, Nasu K, Abe W, Aoyagi Y, Okamoto M, Kai K, et al. miR-503, a microRNA epigenetically repressed in endometriosis, induces apoptosis and cell-cycle arrest and inhibits cell proliferation, angiogenesis, and contractility of human ovarian endometriotic stromal cells. *Hum Reprod.* 2016; 31(11): 2587-2597.
- Brueggmann D, Templeman C, Starzinski-Powitz A, Rao NP, Gayther SA, Lawrenson K. Novel three-dimensional in vitro models of ovarian endometriosis. *J Ovarian Res.* 2014; 7: 17.
- Konrad L, Kortum J, Nabham R, Gronbach J, Dietze R, Oehmke F, et al. Composition of the stroma in the human endometrium and endometriosis. *Reprod Sci.* 2018; 25(7): 1106-1115.
- Swider E, Koshkina O, Tel J, Cruz LJ, de Vries IJM, Srinivas M. Customizing poly(lactic-co-glycolic acid) particles for biomedical applications. *Acta Biomater.* 2018; 73: 38-51.
- Shams A, Shabani R, Najafi M, Karimi M, Pirhajati V, Asghari Jafarabadi M, et al. The role of MicroRNA 143 and MicroRNA 206 in the regulation of apoptosis in mouse leukemia cancer cells and spermatogonial cells. *Cell J.* 2021; 23(5): 544-551.
- Crowley LC, Marfell BJ, Scott AP, Waterhouse NJ. Quantitation of apoptosis and necrosis by annexin V binding, propidium iodide uptake, and flow cytometry. *Cold Spring Harb Protoc.* 2016; 2016(11).
- Jafarabadi M, Salehnia M, Sadafi R. Evaluation of two endometriosis models by transplantation of human endometrial tissue fragments and human endometrial mesenchymal cells. *Int J Reprod Biomed.* 2017; 15(1): 21-32.
- Rai R, Alwani S, Badea I. Polymeric nanoparticles in gene therapy: New avenues of design and optimization for delivery applications. *Polymers (Basel).* 2019; 11(4): 745.
- Delbandi AA, Mahmoudi M, Shervin A, Heidari S, Kolahdouz-Mohammadi R, Zarnani AH. Evaluation of apoptosis and angiogenesis in ectopic and eutopic stromal cells of patients with endometriosis compared to non-endometriotic controls. *BMC Womens Health.* 2020; 20(1): 3.
- Dahiya A, Sebastian A, Thomas A, George R, Thomas V, Peediacayil A. Endometriosis and malignancy: the intriguing relationship. *Int J Gynaecol Obstet.* 2021; 155(1): 72-78.
- Quagliariello V, Berretta M, Buccolo S, Iovine M, Paccone A, Cavalcanti E, et al. Polydatin reduces cardiotoxicity and enhances the anticancer effects of sunitinib by decreasing pro-oxidative stress, pro-inflammatory cytokines, and NLRP3 inflammasome expression. *Front Oncol.* 2021; 11: 680758.
- Riley KA, Benton AS, Deimling TA, Kunselman AR, Harkins GJ. Surgical excision versus ablation for superficial endometriosis-associated pain: a randomized controlled trial. *J Minim Invasive Gynecol.* 2019; 26(1): 71-77.
- Mehrdad Moghimi M, Bahram Moazzami M. Comparing the efficacy of surgery and medical therapy for pain management in endometriosis: a systematic review and meta-analysis. *Pain Physician.* 2017; 20: 185-95.
- Samartzis EP, Fink D, Stucki M, Imesch P. Doxycycline reduces MMP-2 activity and inhibits invasion of 12Z epithelial endometriotic cells as well as MMP-2 and-9 activity in primary endometriotic stromal cells in vitro. *Reprod Biol Endocrinol.* 2019; 17(1): 38.
- Eslahi N, Shakeri-Zadeh A, Ashtari K, Pirhajati-Mahabadi V, Tohidi Moghadam T, Shabani R, et al. In vitro cytotoxicity of folate-silica-gold nanorods on mouse acute lymphoblastic leukemia and spermatogonial cells. *Cell J.* 2019; 21(1): 14-26.
- Chaudhury K, Babu KN, Singh AK, Das S, Kumar A, Seal S. Mitigation of endometriosis using regenerative cerium oxide nanoparticles. *Nanomedicine.* 2013; 9(3): 439-448.
- de Almeida Borges VR, Tavares MR, da Silva JH, Tajber L, Boylan F, Ribeiro AF, et al. Development and characterization of poly(lactic-co-glycolic) acid nanoparticles loaded with copaiba oleoresin. *Pharm Dev Technol.* 2018; 23(4): 343-350.
- Chenthamara D, Subramaniam S, Ramakrishnan SG, Krish-

- naswamy S, Essa MM, Lin F-H, et al. Therapeutic efficacy of nanoparticles and routes of administration. *Biomater Res.* 2019; 23: 20.
33. Berthet M, Gauthier Y, Lacroix C, Verrier B, Monge C. Nanoparticle-based dressing: the future of wound treatment? *Trends Biotechnol.* 2017; 35(8): 770-784.
34. Shabani R, Ashjari M, Ashtari K, Izadyar F, Behnam B, Khoei S, et al. Elimination of mouse tumor cells from neonate spermatogonial cells utilizing cisplatin-entrapped folic acid-conjugated poly (lactic-co-glycolic acid) nanoparticles in vitro. *Int J Nanomedicine.* 2018; 13: 2943-2954.
35. Singh AK, Chakravarty B, Chaudhury K. Nanoparticle-assisted combinatorial therapy for effective treatment of endometriosis. *J Biomed Nanotechnol.* 2015; 11(5): 789-804.
36. Guo X, Li W, Zhou J, Hou W, Wen X, Zhang H, et al. Specific photothermal ablation therapy of endometriosis by targeting delivery of gold nanospheres. *Small.* 2017; 13(15): 1603270.
37. Li J, He Y, Sun W, Luo Y, Cai H, Pan Y, et al. Hyaluronic acid-modified hydrothermally synthesized iron oxide nanoparticles for targeted tumor MR imaging. *Biomaterials.* 2014; 35(11): 3666-3677.
38. Braza-Boïls A, Mari-Alexandre J, Gilabert J, Sánchez-Izquierdo D, España F, Estellés A, et al. MicroRNA expression profile in endometriosis: its relation to angiogenesis and fibrinolytic factors. *Hum Reprod.* 2014; 29(5): 978-988.
39. Shams A, Shabani R, Asgari H, Karimi M, Najafi M, Asghari-Jafarabadi M, et al. In vitro elimination of EL4 cancer cells from spermatogonia stem cells by miRNA-143-and 206-loaded folic acid-conjugated PLGA nanoparticles. *Nanomedicine.* 2022; 17(8): 531-545.
40. Wang F, Salvati A, Boya P. Lysosome-dependent cell death and deregulated autophagy induced by amine-modified polystyrene nanoparticles. *Open Biol.* 2018; 8(4): 170271.
-